UNIVERSITY OF SOUTHAMPTON

FACULTY OF MATHEMATICAL STUDIES

THE THEORY OF THE SCHOTTKY BARRIER SOLAR CELL

by

C.M.H. KLIMPKE

To my Parents

ACKNOWLEDGEMENTS

I am indebted to Professor P.T. Landsberg for his unfailing supervision, and continuous encouragement whilst this work was in progress.

I would like to thank Dr. J.R. Mallinson and Dr. A. Pimpale for many illuminating discussions.

My thanks also due to the other members of the solid state group, for their helpful comments.

I am grateful to the U.K. Science Research Council for a research studentship.

UNIVERSITY OF SOUTHAMPTON

ABSTRACT

FACULTY OF MATHEMATICAL STUDIES

Doctor of Philosophy

THE THEORY OF THE SCHOTTKY BARRIER SOLAR CELL

by Christopher Michael Heinz Klimpke

The theory of Schottky barrier solar cells has been investigated and the following contributions have been made.

A model of Schottky barrier solar cells with an insulating layer is described, which takes into account more accurately than has been done so far, the dependence of the barrier height on the density of interfacial states (D_S) and consequently the various potential drops in the cell. Also taken into account is the recombination traffic through the interfacial surface states. This effect is important at high values of D_S when it lowers the predicted efficiency. Recombination in the transition and bulk regions is also considered, but this does not usually have a very marked effect. Numerical results are given for an Au - SiO_2-n-type Si contact. (Chapter 2)

The effect of different meteorological conditions on Schottky barrier solar cells has been investigated. Similar results to those for p-n junction cells have been obtained, namely that although the output power density is reduced, a much higher conversion efficiency is possible when the solar cell is illuminated with diffuse radiation. (Chapter 3)

The removal of the usual assumptions regarding the quasi-Fermi levels and the depletion layer, has led us to a formalism which yields the variation with position of the quasi-Fermi levels and of the band edges. However, one interesting point is that, when the n-type S.B.S.C. is being illuminated under short circuit conditions, the reduction V_i in the potential developed across the interfacial layer is found to be negative, whereas with the device forward biased without illumination V_i is always positive (or zero when the bias voltage equals zero). (Chapers 5 & 6)

Whilst retaining the important features of the more general formalism, the usual assumptions regarding the slopes of the quasi-Fermi levels and the potential drop across the bulk region were carefully reintroduced, thereby facilitating the construction of a simplified model of a p-type S.B.S.C. Allowance for the imperfect communication between the metal and the bands of the semiconductor shows that recombination in the semiconductor's bulk and transition regions can dominate for interfacial layer thicknesses $\gtrsim 25$ Å. The results of the calculations made show that the J-V characteristics of the p-type S.B.S.C. are strongly controlled by the parameters of the interfacial layer, which in effect determine the extent of the recombination within the solar cell. The reduction V_i in the potential developed across the interfacial layer when the device is illuminated, is found to be negative for short circuit conditions, and positive at the maximum power point. (Chapter 7)

LIST OF CONTENTS

CHAPTER 1

1. Introduction

Solar cells utilizing Si homojunctions and heterojunctions with GaAs and CdS have already demonstrated the effectiveness of photovoltaics in generating electricity. If, however, photovoltaics is to emerge as a viable competitor, in the field of large scale electrical power generation, then a cost reduction of around 50 times must be achieved in the solar cells. One possibility for cost reduction lies in the method of fabricating the junction. At first sight, the idea of a simple metal semiconductor junction is quite attractive. Metal deposition methods are consistent with fast processing with high yields,with the additional advantage of requiring low substrates temperatures. This avoids degradation of the semiconductors minority carrier properties, and consequently suggests suitability to thin film and non-single crystalline semiconductor substrates.

If a metal is brought into intimate contact with a clean surface of a semiconductor, a readjustment of charge takes place in order to establish thermodynamic equilibrium and in most cases an energy band bending occurs within the semiconductor at the metal-semiconductor interface. If the metal is thin enough to be partially transparent to light whilst retaining a relatively low sheet resistivity, then some of the incident light can penetrate the metal to reach the semiconductor and a photo-current will be generated. There are three

photo-effects which can take place. Light can be absorbed in the metal and excite majority carriers over the barrier into the semiconductor (This effect is often used to determine the thermodynamic equilibrium barrier height). Long wavelength light is usually absorbed deep in the bulk region of the semiconductor, creating electron-hole pairs, the minority carriers then diffuse to the edge of the junction to be collected. Shorter wavelength light is absorbed partly in the semiconductor's depletion region and partly in the bulk semiconductor region, and very short wavelength light is absorbed almost entirely in the semiconductor's depletion region. The very high electric field in this depletion region sweeps the photogenerated carriers away before many of them recombine within the semiconductor or at the interfacial states existing at the metal semiconductor interface. A good collection efficiency for carriers generated by shortwave radiation is often observed for simple Schottky barrier solar cells, in contrast to a p-n junction solar cell where a low lifetime in the top region and a high surface recombination velocity can seriously degrade the response at short wavelengths.

The excitation of carriers from the metal into the semiconductor is a much smaller effect (see, for example, Mead 1966) than band to band excitation mechanisms in the semiconductor, and can thus be neglected for solar cell applications. In a Schottky barrier solar cell the photo-current passing through a load causes the device to be forward biased and a dark current flows in the opposite sense to the direction of the photo-current. In practice, however, intimate contact Schottky Barrier solar cells have one very large drawback in the form of a poor photo-voltage response. This effect is due to the usual thermionic emission dark current, in Schottky barrier junctions, being considerably higher than the dark currents encountered in many

homojunction and heterojunction structures. It is possible to eliminate this disadvantage, and still preserve the attractive features of these Schottky barrier solar cells. The introduction of a thin insulating interfacial layer, between the metal and the semiconductor can improve the performance of what we shall from now on, simply term the Schottky barrier solar cell.

In this type of structure the thermionic emission current can be reduced by either increasing the thermodynamic equilibrium barrier height or by decreasing the probability of majority carrier tunneling. This clearly reduces the dark thermionic emission forward current so that better conversion efficiencies and open circuit voltages are obtained. From this view point, it is probable that another current mechanism will then play a dominant role in the Schottky barrier solar cell's device characteristics. The principal disadvantage of including such an interfacial layer is that the minority carrier flow at the interface may be impeeded by its presence. This flow of minority carriers constitutes the bulk of the photo-generated current, therefore careful optimization of the thickness of the interfacial layer is required. In recent work (e.g. Fonash 1975a) the importance of the electrostatics of interfacial layers in Schottky barriers has been studied. When the Schottky barrier solar cell with an insulating interfacial layer is delivering power at an output voltage V say, a certain part of this voltage is developed across the interfacial layer. It was suggested that this effect also served to increase the open circuit voltage. The effect of interfacial surface states, at the boundary between the semiconductor and the interfacial layer was also discussed (Fonash 1975a) in terms of the interfacial voltage developed, and the thermodynamic equilibrium barrier height. The so called diode ideality factor (or n-value) was first introduced by Card and Rhoderick (1971)

to take account of the voltage developed across the interfacial layer. It has been suggested (Stirn et al 1973 and Anderson et al 1974) that the high values of n in the usual diode equation $J = J_s|\exp(eV/nkT) - 1|$ can also lead to low dark currents, even without large thermodynamic equilibrium barrier heights. This is because the function $\exp(eV/nkT)$ increases more slowly with increasing V when n is high. If the higher values of n were due to excess dark currents, it is obvious that they could not lead to increased open circuit voltages; the value of J_s would be increased in this case and consequently lower open circuit voltages would be obtained. If, on the other hand, the values of n were due to the interfacial layer and interfacial states, then the effective barrier height is increased; therefore J_s must be decreased and consequently higher open circuit voltages will result. Experimentally, it is observed that the increase in the open circuit voltage, brought about by the inclusion of an insulating interfacial layer, outweighs the decrease in the short circuit current as mentioned above.

The effects of recombination in Schottky barrier solar cells has been studied to a certain extent by Fonash (1975a) but this work only considered recombination within the bulk region of the semiconductor. More recently, however, calculations of the quantum photoelectric yield in Schottky barrier cells, without interfacial layers, have been performed by Lavagnal et al (1977). The concept of surface recombination velocities were introduced at the metal / semiconductor interface. These surface recombination velocities compete with the usual thermionic emission velocities for the carriers crossing the semiconductor metal interface. The dominant effect at the interface was the emission of photogenerated majority carriers into the metal thereby causing a reduction in the collection efficiency for strongly absorbed light. (This would therefore

seem to be an important effect for direct band gap semiconductors).

The question of the maximum attainable conversion efficiency was investigated by Pulfrey and McOuat (1974). Their model of the Schottky barrier Solar cell assumed that (a) the quantum photoelectric yield (or Quantum efficiency) was unity, (b) the reflection and resistance losses were negligible, and (c) that a metal contact of sufficiently high work function was available. On the basis of this model, they indicated that with the thermodynamic equilibrium barrier height of the order of the energy gap of the semiconductor, efficiencies above 20% are obtainable for Si and GaAs. In later work (McOuat and Pulfrey 1975) allowance for incomplete absorption and some recombination reduced their predicted efficiency to below 5% for a gold-silicon contact. Experimentally a 12% efficiency has been reported for a Cr-oxide p-type Si Single Crystal Schottky barrier solar cell with an open circuit voltage of 600 mV when illuminated by AM1 radiation(Delahoy et al 1977). Also, stable Schottky barrier solar cells (Townsend and Lillington 1977) have been fabricated from both single crystal and cast poly crystalline p-type silicon substrates, having efficiencies of 9½ and 8½% respectively. The open circuit voltages were 560 and 523 mV respectively. It is thought that the conditions under which the interfacial oxide layer is grown prove to be critical in determining both the cell's conversion efficiency and the long term stability of the structure. Similar experimental work regarding Au/n-type Si Schottky barrier solar cells has been reported (see Townsend and Lillington 1976, and Roger et al 1976). Conversion efficiencies of 7% can be infered from the experimental curves given by Townsend and Lillington 1976. Unfortunately these cells proved to be inherently unstable, in that the Au was suspected of diffusing into the silicon

substrate, thereby degrading the Schottky barrier's solar cell characteristics.

Some of the previous papers (e.g. Fonash 1975a) have made serious attempts to treat the Schottky barrier solar cell problem exactly. Those efforts have made significant contributions to the general understanding of the underlying theory. There is a need, however, to extend the theoretical understanding further. This will enable us to form a more complete picture of the roles played by the interfacial layer parameters, so that we may eventually arrive at the position of being able to forcast what is necessary to produce a 'good' Schottky barrier solar cell.

In Chapter 2, we present a theory of the Schottky barrier solar cell with an insulating interfacial layer. The more usual aspects of semiconductor theory are outlined in the earlier sections. The main features of interest are the improved expressions for the thermodynamic equilibrium barrier height and the voltage V_i developed across the interfacial layer. This model also takes account of recombination through the interfacial states, as well as recombination within the depletion layer. The semiconductor was assumed to be n-type. Results of the numerical calculations made showed that the density of interfacial states D_S and their capture cross-sections play a very dominant role in the performance of Schottky barriers as solar cells. It was found that with a low value of the density of interfacial surface states, the interfacial surface state recombination is relatively small when compared with the thermionic emission of majority carriers over the barrier. This is due to the fact that the barrier height is relatively small at low values of D_S. On the other hand, as the density of interfacial surface states is increased, the barrier height increases,

thereby reducing thermionic emission over the barrier, but the interfacial surface state recombination current eventually increases to dominate the current flow mechanisms.

Using the same model of the Schottky barrier solar cell as developed in Chapter 2, the effects of different meteorological conditions on these cells was studied in Chapter 3. Similar results to those for p - n junction cells were obtained, namely that, although the output power density is reduced, a much higher conversion efficiency is possible when the solar cell is illuminated with diffuse radiation. In this work we show how the output power P and the efficiency η^* of the Si n-type Schottky barrier solar cell depends on the diffuse component. A few improvements to the theory of Chapter 2 are required to make the theory more complete. The interfacial surface state recombination model, which was based on a generalization of the usual Shockley-Read recombination statistics by Evans and Landsberg (1963), requires improvement, to include the effect of carriers tunneling between the metal and the interfacial surface states (i.e. the interfacial surface state population model must be adapted, to include the communication between these surface states and the metal). Also the various effects of tunneling on the thermionic emission currents and on the photogenerated current should be examined in detail. If one is to assess the value of a Schottky barrier device as a solar cell, then all of the above points must be given careful consideration. The theory may be improved further by removing the usual assumptions about the quasi-Fermi levels, and by completely disregarding the concept of the depletion layer edge (i.e. depletion approximation).

In order to correct the interfacial surface state population model, a concept of a tunneling time constant was introduced. Chapter 4 deals with this tunneling phenomena by generalizing the work of

Lundstrom and Svensson (1972) to deal with the two-band problem. This generalisation was necessary to give the correct form of the tunneling time constant for tunneling between the metal and interfacial surface states near the valence band edge of the semiconductor. The W.K.B. approximation is invoked several times during subsequent discussions of the thermionic emission tunnel currents, and its use is obviously not always justifiable. The analysis could have been extended to eliminate the use of the W.K.B. approximation altogether, but as this would involve additional computational complexities it was felt that the approximation used would yield a reasonably reliable result.

Chapter 5, sets out the improved theory for the calculation of the band structure and barrier height of an n-type Schottky barrier solar cell in thermodynamic equilibrium. The assumptions outlined above have been removed. We remark, that in all our work done to date the electron and hole mobilities have been assumed to be constant throughout the semiconductor. In thermodynamic equilibrium the Fermi level is constant and after some major adjustments to the theory of the thermodynamic equilibrium barrier height in Chapter 2, due to the removal of the depletion approximation, we can formulate the equilibrium problem. Two non-linear differential equations are eventually constructed, the first equation is of the 1st order non-linear type, and expresses the barrier height as some function of semiconductor thickness. The second differential equation, however, arises from the Poisson equation, and is of the second order non-linear type. These equation together with their boundary conditions can only be solved by numerical procedures. The solution, when found, yields the form of the equilibrium band edge shape and the thermodynamic equilibrium barrier height. The effects of image force lowering have not been included in the calculations, this is also discussed in Chapter 5.

The formalism of Chapter 6, sets out to give us a more complete picture of the Schottky barrier both as a rectifying diode and as a solar cell. A much improved equation for the interfacial layer voltage was produced by again eliminating the depletion approximation and also the assumptions of quasi-Fermi levels of negligible slope in the so-called depletion layer. The assumptions that the electron quasi-Fermi level has negligible slope in the bulk region and that the potential drop across this region is negligible, have both been removed entirely. The remaining differential equations are the phenomenological current density equations, Poisson's equation, the two continuity equations (one for electrons in the semiconductors conduction band and the other for holes in the semi-conductors valence band). The boundary conditions for this system of equations are quite complex. In essence, the boundary conditions are of mixed type , thus making the problem of the Schottky barrier solar cell a two point boundary value problem. The boundary conditions covering the electron and hole current densities, at the interface between the semiconductor and the insulator, are each formed from two components. The first component is due to the thermionic emission of carriers tunneling through the insulating interfacial layer, and the second component is produced by the recombination traffic through the interfacial surface states.

Chapter 6, also presents the results of calculations made on the n-type Schottky barrier, firstly with the device forward biased without any illumination, and secondly, with the illuminated device delivering power.Among other things these solutions show us the variation of the quasi-Fermi levels with position, together with

the band edge shape. However, one very interesting point is that when the Schottky barrier solar cell is being illuminated under short circuit conditions, the interfacial voltage V_i developed across the insulator is negative, whereas before with the device forward biased without illumination V_i is always positive (or zero when the bias voltage equals zero). The reason for the change in sign of V_i is, we believe, due to the change in the occupancy of the interfacial surface states, caused by the accumulation of photo-generated carriers in the semiconductor near the interfacial layer. In fact a simple argument of electrostatics or charge conservation both point to V_i being of negative sign when the device is operating under short circuit conditions.

From the view point that negative interfacial voltages can be explained by relatively simple arguments, a simplified model of a p-type Schottky barrier solar cell is presented in Chapter 7. Whilst retaining the more important features of the formalism set out in Chapters 5 and 6, the usual assumptions regarding the quasi-Fermi levels and potential drop across the bulk region were carefully re-introduced. The resulting theory of the p-type S.B.S.C. reduces to a system of non-linear algebraic equations, with integral dependencies for surface state effects (e.g. the interfacial voltage and the electron/hole recombination rates at the interface). The numerical calculations which have been performed on the basis of this model certainly predict negative interfacial voltages at short circuit conditions. The interfacial voltage developed becomes positive for larger operating voltages of the illuminated S.B.S.C.

Results show that the parameters of the interfacial layer in effect determine the recombination throughout the solar cell. Recombination in the semiconductors bulk and space charge regions are shown to be of great importance. For some thicker interfacial layers > 25 Å

say, these recombination currents in the semiconductors depletion layer and bulk region can dominate.

Chapter 8, however, presents the conclusions of the above mentioned work, and outlines future possible research topics, which are required to make the theory more complete in several points of detail.

Finally, reasonable agreement between theory and experiment has been obtained for both the n-type and p-type Schottky barrier solar cells. Unfortunately the detailed calculations performed in Chapters 5 and 6 serve only as guide to single crystal silicon solar cells, due to the fact that the substrate thickness is of the order of a few microns. This detailed model is, however, suited best to thin film single crystal devices such as those constructed from CdS. Several new effects have been noted (e.g. negative interfacial voltages at short-circuit conditions and the fanning of the quasi-Fermi levels for the interfacial surface states) and the importance of recombination processes, both through the interfacial surface states and within the semiconductor, cannot be overemphasised.

CHAPTER 2

THE THEORY OF THE n-TYPE SCHOTTKY BARRIER SOLAR CELL

2.1 Introduction

In this chapter we will examine the effect of interfacial surface states on the barrier height and the interfacial recombination current in an n-type Schottky barrier solar cell.

Firstly, the basic theories of recombination, drift and diffusion are discussed, so that the phenomenological current density equations may be constructed. Secondly, thermionic emission effects will also be examined in part here, but will be dealt with more fully in Appendix A. We will then go on, to establish several relations between the various potentials occuring within the semi-conductor region and the interfacial layer. We shall use the fact that potential is continuous across charged interfaces in generating these expressions. The electrostatic fields and charges will then be discussed, paying particular attention to the charge on the interfacial surface states, both in and out of thermodynamic equilibrium.

The current densities flowing in a non-degenerate semiconductor containing recombination centres of one type, each of which can only trap one electron, are calculated following the method of Evans and Landsberg (1963). However, only unavoidable (i.e. band to band) recombination processes are considered in the depletion layer. The model used for the interfacial surface state recombination was due to a generalization of the results of Evans and Landsberg (1963). This model neglects the possible adaptation of the surface state occupation

probability due to the proximity of the metal. On the other hand, the transmission probability for electrons tunneling through the interfacial layer, between the metal and the semiconductors conduction band,has been assumed to be unity.

To sum up, in this chapter a theoretical model of a metal-insulator-semiconductor solar cell is developed which improves existing ones in two main respects. (a) Account is taken of recombination effects through the interfacial surface states, in the depletion layer and in the bulk region. (b) Improved relations are developed for the thermodynamic equilibrium barrier height and the potential drops in the cell. This avoids earlier approximations (see for example Fonash 1975) in which the temperature dependence in part of these expression is removed by taking values at absolute zero (Cowley & Sze 1965). The main result of (a) arises from the recombination through the interfacial states. As their density D_S is increased, other quantities being kept constant, the thermodynamic equilibrium barrier height and efficiency improve until the efficiency is dragged down by recombination, the thermodynamic equilibrium barrier height remaining almost constant. This physically clear effect has not been analysed before. The main effect of (b) is that the thermodynamic equilibrium barrier height ϕ_B rises more rapidly with D_S than on previous theories, thus yielding higher efficiencies. One therefore finds that at low D_S effect (b) dominates,in agreement with earlier results while at high D_S effect (a) dominates.

Results for a $Au - SiO_2 - Si$ n-type solar cell are presented using the numerical data summarized in table 1. We make some additional comments on the electric field dependence of the recombination coefficients and on the possible "fanning out" of the quasi-Fermi levels for interfacial surface states. This is an effect not previously discussed.

2.2 Basic background semiconductor theory

Recombination processes

The various processes of recombination fall into two distinct classes, depending on whether the electrons and holes recombine directly by band to band transitions or indirectly through intermediate localized energy levels in the energy gap of the semiconductor. Each of these processes can be characterised by an average capture cross section σ for the recombination. The average probability K that in unit time a free carrier makes the transition to a localized level or across the energy gap is given by $v_{th}\sigma$ per localized level or per free carrier of the opposite type. Measured values of this capture cross section range from 10^{-22} to $10^{-12}cm^2$. A commonly reported value for localized levels is $10^{-15}cm^2$. In direct recombination, the electrons must release an amount of energy approximately equal to the full energy gap, while an equal amount of energy must be released in two stages with transitions involving the localized levels. Three physical mechanisms have been envisaged for the energy release, they are (a) radiation of photons, (b) phonon emission, and (c) transfer to another free carrier (Auger process). For band to band recombination photon emission is usually the important energy transfer mechanism, while for recombination through the localized trapping levels phonon emission predominates.

In a transition involving a localized trapping level the transfer of energy to the lattice requires the excitation of many phonons, because even the highest phonon energy is much less than the energy which is to be transfered. Such a multi-phonon process is extremely unlikely. It has therefore been proposed that the electron cascades into the ground state of an imperfection centre via its excited

states, emitting a phonon at each stage. A similar process is suggested for hole capture by a centre.

The statistical treatment of recombination via localized trapping states, as given by Shockley and Read (1952), will be briefly outlined below. Consider a non-degenerate semi-conductor under steady excitation. The recombination centres with density N_t cm^{-3} are all assumed to be at an energy E_t in the forbidden energy gap. Each centre is capable of capturing one electron when empty and one hole when occupied by an electron, the capture probability for these processes being T_1^s and T_2^s respectively. The rate at which holes are captured by occupied localized trap states is

$$R_p = T_2^s \; p \; n_t \qquad (2.2.1)$$

where p is the hole concentration in the semiconductors valence band and n_t is the density of occupied localized trap states. Similarly the rate of capture of free electrons by empty localized states is given by

$$R_n = T_1^s \; n \; p_t \qquad (2.2.2)$$

with $p_t + n_t = N_t$, and n as the electron concentration in the semiconductors conduction band.

Simultaneously with the capture of free carriers, the bound carriers are re-emitted thermally from the localized trap states back into the bands. Thus we write the net recombination rates as

$$U_n = T_1^s \; n \; p_t - A \; n_t.1 \qquad (2.2.3)$$

and

$$U_p = T_2^s \; p \; n_t - B \; p_t.1 \qquad (2.2.4)$$

where A and B are constants. The principle of detailed balance, which states that at thermodynamic equilibrium the recombination rate must equal the thermal generation rate, is invoked.

So we have

$$A = T_1^{\,s}\, n_1 \quad \text{with} \quad n_1 = n_o\, p_{t_o}/n_{t_o} = N_c e^{-e(E_c - E_t)/kT}$$

$$\text{and} \quad B = T_2^{\,s}\, p_1 \quad \text{with} \quad p_1 = p_o\, n_{t_o}/p_{t_o} = N_v e^{e(E_v - E_t)/kT} \qquad (2.2.5)$$

where a suffix o denotes a thermodynamic equilibrium quantity. It is seen that n_1 and p_1 are equal to the electron and hole concentrations when the Fermi level is coincident with the trap energy. Under steady state conditions $U_n = U_p$ i.e. the net electron capture rate equals the net hole capture rate.

So we have the net steady state recombination rate U_t given by

$$U_t = U_n = U_p = \frac{T_1^{\,s}\, T_2^{\,s}(n\,p - n_o\,p_o)}{T_1^{\,s}(n + n_1) + T_2^{\,s}(p + p_1)}\, N_t \qquad (2.2.6)$$

Similarly the net band to band recombination rate can easily be shown to be given by

$$U_b^{\,s} = B^s\,(n\,p - n_o\,p_o) \qquad (2.2.7)$$

where B^s is the appropriate reaction constant. The superfix s has been used to denote single carrier transitions. Later, Auger effects will be considered,in which case the reaction constants will be donated by letters without the superfix.

Drift and Diffusion of excess carriers

The carrier concentrations are most often functions of position for a variety of reasons too numerous to mention here, and in addition, an external electric field is usually present. It is therefore necessary to establish relationships governing the behaviour of the carriers (i.e. electrons in the conduction band and holes in the valence band) under these conditions. When the densities are not uniform, carriers tend to diffuse from regions of high concentration to regions of low concentration. Thus a diffusion current is established along with a drift current set up by the external field. If the former is assumed to be directly proportional to the concentration gradient, we may write the hole and electron current densities as

$$\underset{\sim}{J}_h = e \mu_p p \underset{\sim}{E} - e D_p \text{ grad } p \qquad (2.2.8)$$

$$\underset{\sim}{J}_e = e \mu_n n \underset{\sim}{E} + e D_n \text{ grad } n \qquad (2.2.9)$$

Here μ_p and μ_p are the electron and hole mobilities, also n and p are respectively, the position dependent electron and hole concentrations, $\underset{\sim}{E}$ is the electric field, D_n and D_p are the diffusion constants for electrons and holes respectively, with $\underset{\sim}{J}$ $(= \underset{\sim}{J}_h + \underset{\sim}{J}_e)$ as the total current density. According to the principle of detailed balance, in the absence of external electrostatic fields and temperature gradients, the electron and hole current densities must vanish separately. When there is neither a time variation (steady state) nor a magnetic field present we may write the electrostatic field as

$$E = - \text{grad } \phi \quad , \qquad (2.2.10)$$

where ϕ is the electro-static potential. We can write this potential, in terms of the electrochemical potential $\bar{\mu}$ (which incidentally equals the Fermi energy eE_{FM}) and the chemical potential μ in thermodynamic equlibrium, as $\bar{\mu} - \mu = + e\,\phi$ for electrons and holes. (Incidentally both $\bar{\mu}$ and μ are measured on the electrons energy scale).

We shall restrict ourselves to the case for electrons in deducing the Einstein relation, however, it is simple to show that the same relation holds true for holes. Now from equations (2.2.9) and (2.2.10), the application of thermodynamic equilibrium conditions yields

$$0 = -\mu_n\, n\, \text{grad}(\bar{\mu} - \mu) + D_n\, e\, \text{grad}\, n = -\mu_n\, n\, \nabla\mu + e\, D_n \frac{\partial n}{\partial \mu}\, \nabla\mu \quad ,$$

which becomes

$$0 = \mu_n\, n + e\, D_n \frac{\partial n}{\partial \mu} \qquad \text{if} \qquad \text{grad}\,\mu \neq 0.$$

Consider the ratio $\lambda = \dfrac{e\, D_n}{\mu_n} = -\dfrac{n}{(\partial n/\partial \mu)}$, and by assuming that the semiconductor is non-degenerate (i.e. Boltzmann statistics apply) then the free electron concentration $n \alpha \exp(+ e\phi/kT)$.

Thus

$$\frac{n}{(\partial n/\partial \mu)} = -kT \quad , \quad \text{which gives} \quad e\, D_n = \mu_n\, kT. \qquad (2.2.11)$$

This is the well known Einstein relation. It will now be used to derive the phenomenological current density equations. We shall now return to non-equilibrium situations.

The action of the various current mechanisms on the carrier concentrations may conveniently be expressed by the quasi-Fermi levels

E_{Fn} and E_{Fp} for the electrons and holes. For a non-degenerate semiconductor these are defined by the relations

$$n = N_c \exp\left(e(E_{Fn} - E_c)/kT\right) \qquad (2.2.12)$$

and $$p = N_v \exp(e(E_v - E_{Fp})/kT) \quad , \qquad (2.2.13)$$

where E_c and E_v are the energies (measured in units of eV's) of the semiconductors conduction and valence band edges respectively, with

$$N_c = 2\left(2\pi\, m_e\, kT/h^2\right)^{3/2} \quad \text{and} \quad N_v = 2\left(2\pi\, m_h\, kT/h^2\right)^{3/2}. \qquad (2.2.14)$$

Here m_e , m_h are the effective masses of an electron in the semiconductors conduction band, and of a hole in the semiconductors valence band respectively. Thus, the electron and hole current densities may be written as

$$J_e = -\, e\mu_n\, n\, \text{grad}\phi + e^2 D_n\, \text{grad}\left(E_{Fn} - E_c\right)/kT \,.\, n$$

$$J_h = -\, e\mu_p\, p\, \text{grad}\phi + e^2 D_p\, \text{grad}\left(E_{Fp} - E_v\right)/kT \,.\, p$$

These equations reduce to their usual phenomenological forms when the Einstein relation is invoked. So we have,

$$J_e = e\mu_n\, n\, \text{grad}\left(E_{Fn}\right) \qquad (2.2.15)$$

and $$J_h = e\mu_p\, p\, \text{grad}\left(E_{Fp}\right) \qquad (2.2.16)$$

as the electron and hole current density equations. Notice that the electric field $\underset{\sim}{E} = -\,\text{grad}\phi$ also equals $\text{grad}(E_c)$ and $\text{grad}(E_v)$.

A discussion of semiconductor band theory will be defered until Chapter 4, where a quantum mechanical discussion of the tunneling time constant for the two band problem will be presented.

2.3 Thermionic emission in Schottky barriers.

In this section, a brief outline to the modelling of the thermionic emission of carriers over the barrier, formed at a metal semi-conductor junction (without an insulating interfacial layer), will be given . Figure 2.1 illustrates the effect of forward and reverse voltage bias on a metal n-type semiconductor junction. Here, we shall assume conditions of non-degeneracy, so that the Maxwell-Boltzmann distributions apply. Also, we shall neglect all tunnel and image-force barrier lowering effects. Electrons having energies in excess of $E_{FM} + \phi_B$, (see Figure 2.1) moving towards the interface, shall be assumed to cross this interface. This of course neglects the fraction of electrons which are reflected quantum mechanically. Appendix A is based on the Fowler-Nordheim supply function (which holds true even under degenerate conditions), with a view to examining both majority and minority carrier thermionic emission tunnel currents.

By the Maxwell distribution the average density of particles with a velocity component between u and $u + du$ in the x direction is given by

$$\bar{n}(du) = n \left(\frac{m}{2\pi kT}\right)^{\frac{1}{2}} \exp \left(-\frac{m\,u^2}{2\,kT}\right) du \qquad (2.3.1)$$

where n is the free electron concentration, and m is the mass of the electron. These electrons in the semiconductors conduction band are not moving freely, they are under the influence of a periodic potential (due to the lattice periodicity). By the application of the effective mass theorem. (see for example P.T. Landsberg (1969)),

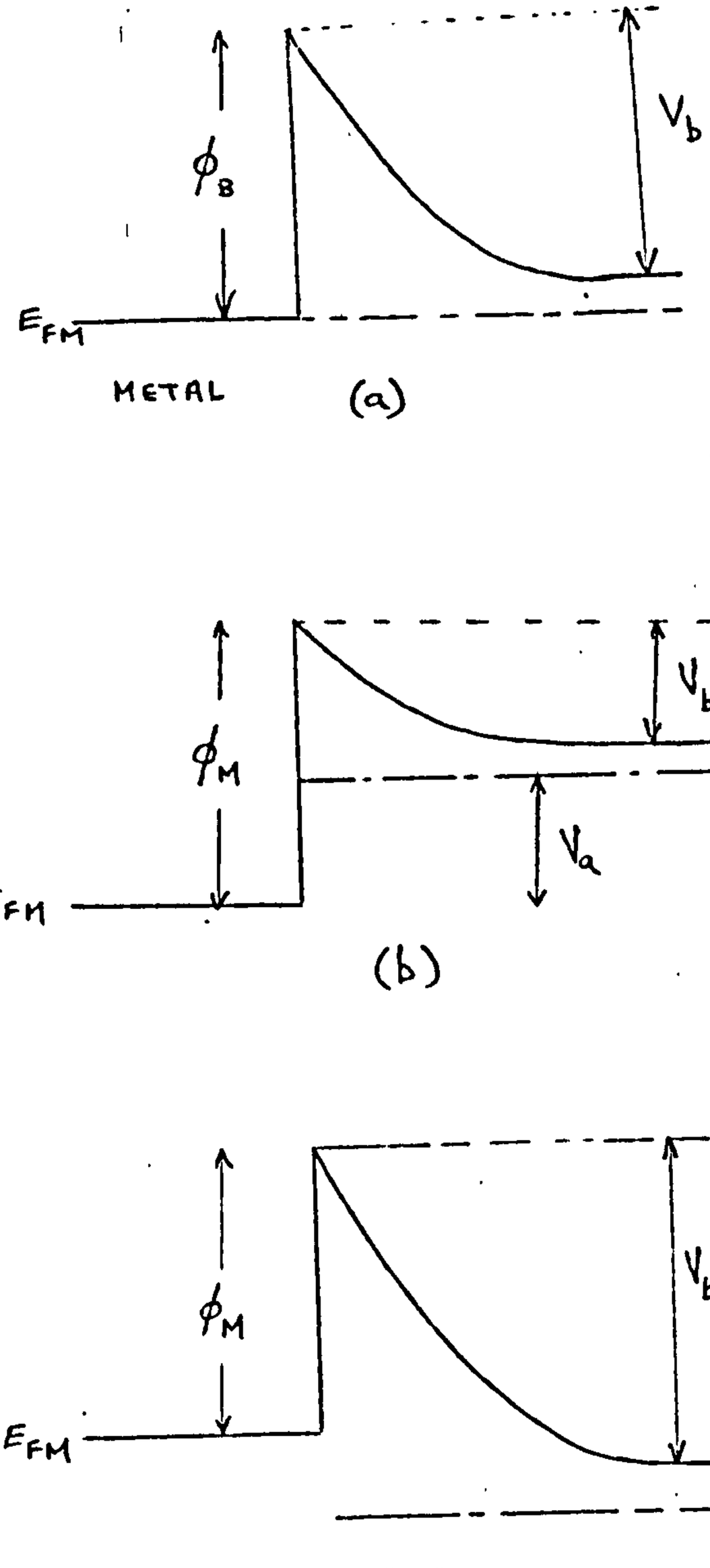

Figure 2.1 Energy diagrams for a metal semiconductor junction.

the periodic potential term occuring in the Hamiltonian can be removed at the expense of introducing the electron effective mass m_e in place of the classical mass m. So the theory of free electrons can be used to represent the theory of "nearly free" electrons by simply replacing the classical electron mass m by its "effective" counterpart.

If we assume that carrier flow is caused by thermionic emission alone (i.e. no recombination, or diffusion) then the electron current in the semiconductor's conduction band must be independent of position. It is therefore sufficient to calculate the net carrier flow in the x-direction at any point within the semiconductor. Without loss of generality we may choose this point to be deep inside the bulk region, so that in this case the free electron concentration n nearly equals the doping concentration N_D. Thus the number of electrons having kinetic energy greater than eV_D that are directed towards unit area of the junction at zero bias, is given by

$$J_o/e = N_D \int_{\left(\frac{2eV_b}{m_e}\right)^{1/2}}^{\infty} u\bar{n}(du) = \int_{\left(\frac{2eV_b}{m_e}\right)^{1/2}}^{\infty} u\, N_D \left(\frac{m_e}{2\pi kT}\right)^{\frac{1}{2}} \exp\left|-\frac{m_e u^2}{2kT}\right) du$$

$$\text{So} \quad J_o = e\, N_D \left(\frac{kT}{2\pi m_e}\right)^{\frac{1}{2}} e^{-eV_b/kT} \qquad (2.3.2)$$

where J_o is the saturation current density. If V_n is the separation between the conduction band edge and the Fermi level deep inside the semiconductor then clearly $\phi_B = V_b + V_n$ and from ordinary semiconductor theory $N_D \sim N_c \exp(-e V_n/kT)$, so that the saturation current density

may be written as

$$J_o = \left\{\frac{4\pi\ e\ m_e}{h^3}\ k^2\right\} T^2\ \exp(-\ e\ \phi_B/kT)\ , \qquad (2.3.3)$$

with $A^*(= 4\pi\ e\ m_e\ k^2/h^3)$ as the effective Richardsons constant. However, with zero applied bias the current due to emission from the semiconductor to the metal must be exactly balanced by the opposite process (i.e. emission from the metal to the semiconductor). When a forward voltage V is applied the effective barrier to carriers leaving the semiconductor reduces to $e(V_b - V)$ while the barrier to carriers leaving the metal remains unchanged. Thus under an applied forward bias V the electron flow from the semiconductor is enhanced by a factor $\exp(e\ V/kT)$. So the net current flowing is given by

$$J = J_o\ (\exp(e\ V/kT) - 1)\ . \qquad (2.3.4)$$

2.4 The electrostatics of the junction

In this section we will endeavour to establish the equations covering the various electrostatic parameters of the n-type Schottky barrier solar cell (with an insulating interfacial layer and "fast" interfacial surface states). The following assumptions will be made (a) in the depletion region $0 < x < w$ of the semiconductor the quasi-Fermi levels are taken to be of negligible slope. (b) The potential drop across the bulk semiconductor $w < x$ is regarded as negligible and the electron quasi-Fermi level has negligible slope in this region. (c) the band diagram is as shown in figure 2.2 for forward bias without illumination. A broadly x-independent light generated current must be imagined as superimposed and flowing from right to left on the diagram.

The electrostatics of the junction will now be studied under the

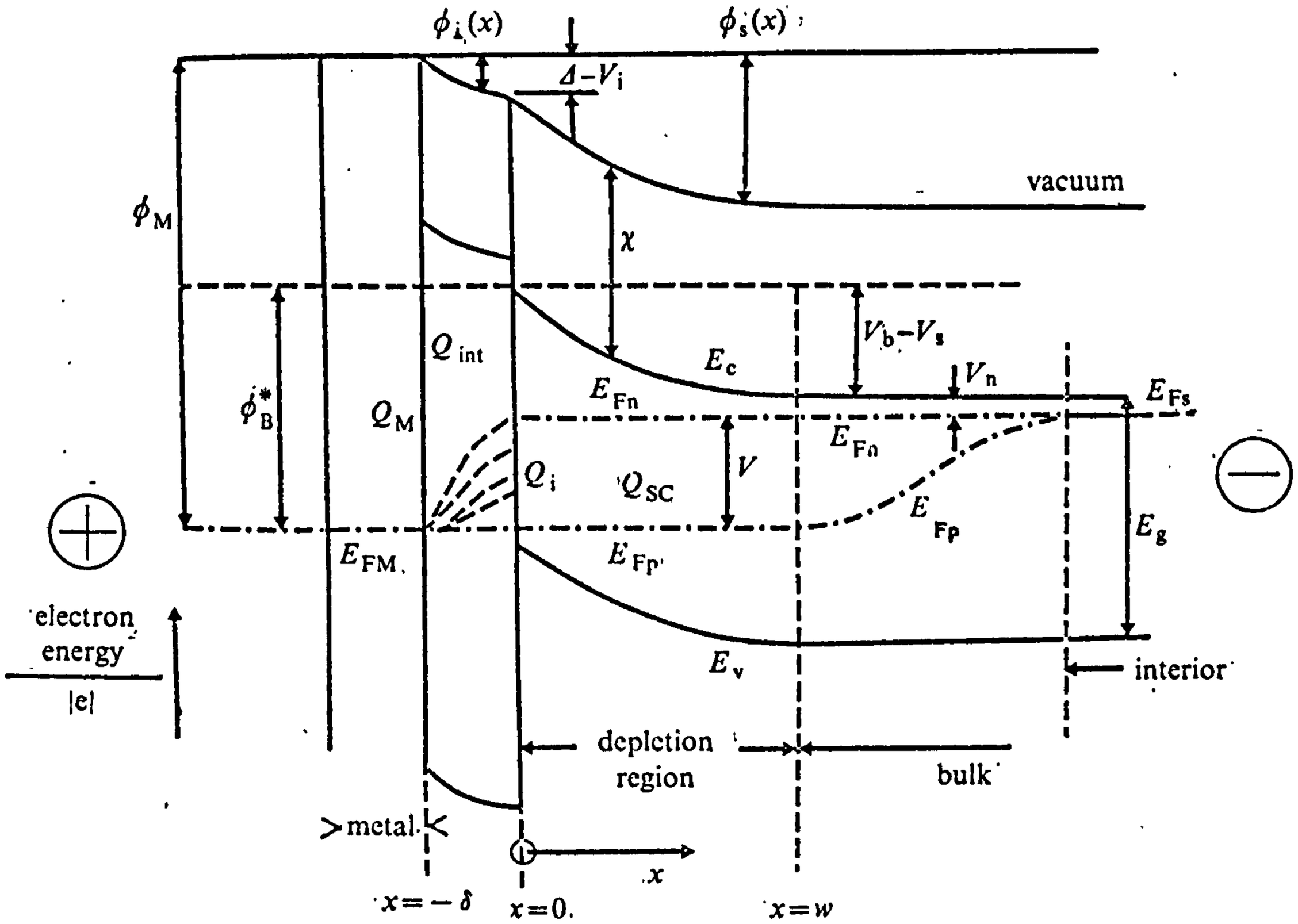

Figure 2.2 Band diagram under forward bias for a Schottky barrier solar cell with an interfacial layer.

assumptions as given above. Let D_S be the density of interfacial surface states (m^{-2} e V^{-1}) and let Q_M, Q_{int}, Q_i , Q_{sc} be the charges per unit area in the surface of the metal, interfacial layer, interfacial states and depletion layer respectively. The Fermi energy in the metal is denoted by E_{FM} , similarly we denote by E_{Fs} , the Fermi energy deep inside the semiconductor. The quantities ϕ_M and χ (measured in units of electron volts (e V)), represent the work function of the metal and the electron affinity of the semiconductor respectively.

In what follows we shall endeavour to construct various relations between the potentials in the cell. The voltage drop V across the whole cell is given by

$$V = V_i + V_s \qquad (2.4.1)$$

where V_i and V_s are the parts of the output voltage developed across the interfacial layer and the depletion layer respectively.

The Fermi level in the interior of the semiconductor (see Figure 2.2) is $E_{Fs} = E_{FM} + V = E_{Fn}$. Also $E_{Fn} - E_{Fp} = V, (0 < x < w)$, so that $E_{FM} = E_{Fp}$ for $x < w$, where w is the depletion layer thickness.

Let ϕ_B^* be the barrier height, $V_b - V_s$ the potential drop across the depletion layer, and $\Delta - V_i$ the potential drop across the interfacial layer each under illumination. Under zero illumination and applied bias $V = V_s = V_i = 0$; Δ is thus the equilibrium potential drop across the interfacial layer and ϕ_B^* becomes ϕ_B (the thermodynamic equilibrium barrier height). Using figure (2.2) we observe that

$$\phi_M = V + V_n + (V_b - V_s) + \chi + (\Delta - V_i) = V_n + V_b + \chi + \Delta \qquad (2.4.2)$$

and $$\phi_B^* = V + V_n + (V_b - V_s) = V_n + V_b + V_i (\equiv \phi_B + V_i), \qquad (2.4.3)$$

where V_n is the separation between the bottom of the conduction band and the Fermi level E_{Fs} deep inside the bulk semiconductor.

The electric fields in various regions of the Schottky barrier solar cell will be calculated from Poisson's equation in a one dimensional setting. Let $\rho(V)$ be the charge density inside the interfacial layer under bias V. The field $E_s(x)$ in the semiconductors depletion layer may be written as

$$E_s(x) = \frac{e\ N_D}{\varepsilon_s}\ (x - w) \quad , \qquad (2.4.4)$$

where the depletion approximation has been used together with the boundary condition $E_s(w) = 0$. The ionized doping concentration is N_D (here we have assumed that all donors are ionized), and ε_s is the permittivity of the semiconductor. The potential distribution $\phi_s(x)$ in the depletion layer is given by

$$\phi_s(x) = B - \frac{e\ N_D}{2\ \varepsilon_s}\ (x - w)^2 \quad , \qquad (2.4.5)$$

where B is a constant and $x \in (0,w]$. In the interfacial layer one has without approximation

$$dE_{i}/dx = \rho/\varepsilon_i \qquad (2.4.6)$$

where $E_i(x)$ is the field in the interfacial layer at position x, ε_i is the permittivity of the interfacial layer and ρ is assumed to be independent of x. Thus $E_i(x)$ is given by

$$E_i(x) = \frac{1}{\varepsilon_i}\ \left(\rho\ x - (Q_i + Q_{sc})\right) \quad , \quad x \in [-\delta, 0) \quad , \qquad (2.4.7)$$

where the boundary condition $(\underline{D}_s - \underline{D}_i).\hat{\underline{n}} = Q_i$ has been applied, with $\hat{\underline{n}}$ as the unit vector normal to the plane of the junction. $\underline{D}$ is the displacement vector, Q_i is the interfacial surface state charge density (Qm^{-2}) and $Q_{sc}(= e\ N_D w)$ is the space charge density in the depletion layer each under illumination. In order to calculate w, the depletion layer thickness, we examine the potential drop across the depletion layer. This is $V_b - V_s$, and is given under illumination by

$$V_b - V_s = -\int_o^w E_s(x)\ dx = \frac{e\ N_D}{2\ \varepsilon_s}\ w^2 . \qquad (2.4.8)$$

This yields the depletion layer thickness, which enables us to calculate the charge density Q_{sc} in the depletion layer as

$$Q_{sc} = e\ N_D\ w = \left\{2\ \varepsilon_s\ e\ N_D(V_b - V_s)\right\}^{\frac{1}{2}} \qquad (2.4.9)$$

The charge contained within the interfacial layer Q_{int} per unit area is given by

$$Q_{int} = \delta\rho \quad , \qquad (2.4.10)$$

where δ is the thickness of the interfacial layer. In thermodynamic equilibrium denoted by a suffix o, one has $V = V_s = V_i = 0$ so that

$$Q_{sco} = \left[2\ \varepsilon_s\ e\ N_D\ V_b\right]^{\frac{1}{2}} \qquad (2.4.11)$$

is the thermodynamic equilibrium space charge density. The charge Q_M per unit area on the metal/interfacial layer boundary is given by the Gauss flux theorem:

$$Q_M = - \delta\rho - Q_i - Q_{sc} = - (Q_{int} + Q_i + Q_{sc}) \qquad (2.4.12)$$

where equation (2.4.7) has been used. Notice that (2.4.12) is just the equation for the conservation of charge.

For a continuous sheet distribution of interface states $D_S(m^{-2}\ e\ V^{-1})$ we shall discuss the statistics, firstly with a view to determining the number of occupied states (so that we may eventually, derive expressions for both the thermodynamic equilibrium and the non-equilibrium interfacial surface state charge densities), and secondly, in a subsequent section we will estimate the interfacial surface state recombination current .

The number of interfacial surface states (or trap states) in the energy range $(E_t,\ E_t + dE_t)$ [measured in units of electron volts] is therefore $D_S d\ E_t$. We will consider the electron and hole trapping processes in turn, making allowances for the Auger effect.

There are three electron trapping rates (see figure 2.3) denoted by dR_1, dR_2 and dR_3. For electron transitions to an interfacial state having an energy lying within the range $(E_t,\ E_t + dE_t)$, these transition rates (or net electron trapping rates), at the interface $x = 0$, are given by

$$dR_1 = T_1{}^s{}_i(n(0)dp_t - dn_t n_1(0)), \quad dR_2 = T_1{}_i n(0)(n(0)dp_t - dn_t n_1(0))$$

$$\text{and} \qquad dR_3 = T_2{}_i p(0)\ (n(0)dp_t - n_1(0)\ dn_t), \qquad (2.4.13)$$

with $dn_t + dp_t = D_S\ dE_t$.

Here dn_t and dp_t are respectively the concentrations of occupied and unoccupied interfacial surface states within the energy range $(E_t, E_t + dE_t)$.

Similarly the hole transition rates at the interface $x = 0$ (see Figure 2.3) dR_4 , dR_5 and dR_6 are given by

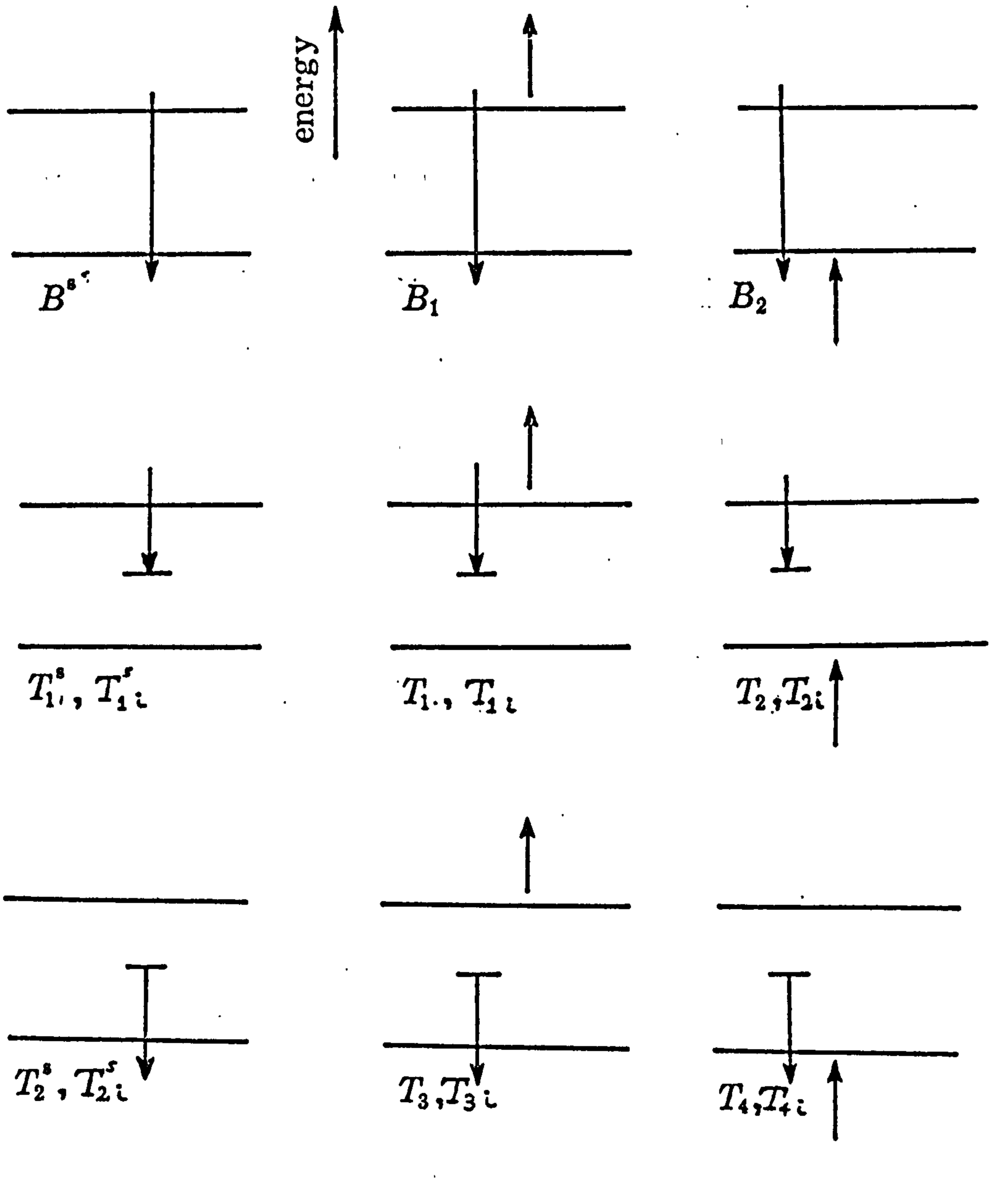

Figure 2.3 Definition of reaction constants occuring in equations (2.4.13), (2.4.14), (2.5.1) and (2.5.4). The recombination rate for the first diagram is then $B^s np$ and similarly for the remaining diagrams.

$$dR_4 = T_2^{s}{}_i(dn_t p(0) - p_1(0)dp_t), \quad dR_5 = T_{3\ i}\ n(0)\ (p(0)dn_t - p_1(0)dp_t)$$

and $dR_6 = T_{4\ i}\ p(0)\ (p(0)\ dn_t - p_1(0)\ dp_t)$ (2.4.14)

with n(0) and p(0) respectively as the electron and hole concentrations at the interface $x = 0$. When the Fermi level is at the trap energy, the thermodynamic equilibrium electron and hole concentrations at the interface $x = 0$ are represented by $n_1(0)$ and $p_1(0)$ respectively. The localized trap reaction constants, defined in figure 2.3, are denoted by letters T_i, of which the use of a superscript s indicates a single electron process, while its absence indicates an Auger process. Notice that the principle of detailed balance has been applied to each individual recombination process.

Summation of the rates (2.4.13) and (2.4.14), in turn yields the total electron and hole trapping rates dU_e^{ifr} and dU_h^{ifr} (due to the traps' communication with the bands of the semiconductor) occuring within the energy range $(E_t, E_t + dE_t)$. They are

$$dU_e^{ifr} = G\left[n(0)\ dp_t - n_1(0)\ dn_t\right]$$

$$= G\left[n(0)\ D_S\ dE_t - (n(0) + n_1(0))dn_t\right] = d(R_1 + R_2 + R_3)$$

(2.4.15)

and $dU_h^{ifr} = H\left[(p(0) + p_1(0))dn_t - p_1(0)\ D_S\ dE_t\right] = d(R_4 + R_5 + R_6)$

(2.4.16)

Here $G = T_{1i}^{s} + T_{1i}n(0) + T_{2i}p(0)$ and $H = T_{2i}^{s} + T_{3i}n(0) + T_{4i}p(0)$, and we note that all trap to trap transitions at the interface $x = 0$ have been neglected.

As we will only consider the steady state, one must have $dU_e^{ifr} = dU_h^{ifr}$ in order that the number of trapped electrons in the energy range $(E_t, E_t + dE_t)$, remains constant. Hence from (2.4.15), (2.4.16), and after a little algebra, the steady state concentration $dn_t(m^{-2})$ of trapped electrons and the steady state recombination rate dU_{ifr}, due to the interfacial surface states within the energy range $(E_t, E_t + dE_t)$, are given by

$$dn_t = \frac{\left[G\, n(0) + H\, p_1(0)\right] D_S\, d\, E_t}{G(n(0) + n_1(0)) + H(p(0) + p_1(0))} \qquad (2.4.17)$$

$$dU_{ifr} = dU_h^{ifr} = dU_e^{ifr} = \frac{\left[n(0)\ p(0) - n_i^{\,2}\right] G\, H\, D_S\, dE_t}{G(n(0) + n_1(0) + H(p(0) + p_i(0))} \quad ,$$

$$\text{with} \quad n_i^{\,2} = n_1(0)p_1(0) = n_o(0)p_o(0)$$

(2.4.18)

This work has followed that of Evans and Landsberg (1963), by simply introducing an elemental trapping level at energy E_t. The total number of occupied interfacial surface states n_t is therefore obtained by integrating (2.4.17) over all the interfacial states. Hence

$$n_t = \int_{E_v(0)}^{E_c(0)} \frac{(G\, n(0) + H\, p_1(0))D_S\, d\, E_t}{G(n(0) + n_1(0)) + H(p(0) + p_1(0))} \qquad (2.4.19)$$

$$\equiv \int_{E_v(0)}^{E_c(0)} D_S \quad f_t \quad d\, E_t \qquad (2.4.20)$$

The reaction constants T^s_{1i} , T^s_{2i} , $T_{1i}\ T_{2i}\ T_{3i}$ and T_{4i} correspond to the recombination processes dR_1, dR_4, dR_2, dR_3, dR_5 and dR_6 respectively, and will be taken to be the same for all interfacial surface states. Also, the argument given above could be generalized to the case of a non-uniform distribution of interfacial surface states and non-constant reaction coefficients, simply by making the identifications $D_S \longrightarrow D_S(E_t)$ and $T_{ji} \longrightarrow T_{ji}(E_t)$. Equation (2.4.19) neglects the possibility that electrons may tunnel through the interfacial layer into the metal from the surface states, thereby influencing their population. This process will be very important if the thickness of the layer is less than about 30 Å (see, for example, Card and Rhoderick 1971). If this is the case the population of the surface states will be determined by the metal. The non equilibrium surface state analysis presented in this chapter is therefore only applicable for comparatively thick films of thickness more than about 30 Å (however, see section 2.7, below).

When discussing the interfacial surface state charge density (Qm^{-2}) it is usual to introduce the "so called" neutral level ϕ_o such that interfacial states are donors below it and acceptors above it. Its value is measured from the valence band edge at $x = 0$. In thermodynamic equilibrium the interfacial surface state charge density is, by using (2.4.20) and denoting the equilibrium Fermi level by E_{FM},

$$Q_{io} = e\ D_S \left\{ \int_{E_{vo}(0)}^{\phi_o + E_{vo}(0)} (1 - f_{to})\ d\ E_{to} - \int_{\phi_o + E_{vo}(0)}^{E_{co}(0)} f_{to}\ dE_{to} \right\} \qquad (2.4.21)$$

where the first integral represents the charge on the donor states. [If a donor state is occupied then it has zero net charge. If, however, it is unoccupied then the donor state has a net positive charge]. The second integral represents the charge on the acceptor type states above ϕ_o. Measuring all the energies within the Schottky

barrier solar cell relative to the Fermi level in the metal, Q_{io} is then given by

$$Q_{io} = - e\, n_{to} + eD_S\phi_o = - eD_S \int_{E_{FM}+\phi_B-E_g}^{E_{FM}+\phi_B} \left[1+\exp\left(e\left(E_{to}-E_{FM}\right)/kT\right)\right]^{-1} dE_{to}$$

$$+ e\, D_s\phi_o \qquad (2.4.22)$$

$$= D_S\, kT \left\{ \ln \left\{ \frac{1+\exp(e\phi_B/kT)}{1+\exp(e(\phi_B-E_g)/kT)} \right\} - e\, E_g/kT \right\}$$

$$+ e\, D_S\phi_o \qquad (2.4.23)$$

where E_g is the energy gap of the semiconductor, measured in electron volts.

The interfacial surface state charge density Q_i, in the presence of illumination is deduced in a manner similar to that of the thermodynamic equilibrium surface state charge density. If the density of interfacial surface states is a constant, and if the reaction parameters are also constants with respect to the energy of the interfacial surface states, then once again the integrations are performed over the interfacial surface states (in their equilibrium configuration within the semiconductor's band gap). If, however, either the density of interfacial surface states D_S or the reaction constants were functions of the interfacial surface state energy, then care in evaluating the occupation integral must be taken. The reason for this is that, as the parameters $n_1(0)$ and $p_1(0)$ are known in terms of their equilibrium surface state energies, care must be exercised to ensure that the energy dependence of the density of interfacial surface states and the

reaction constants do in fact correspond to an equilibrium energy dependence measured relative to the Fermi level E_{FM} in the metal. The electron and hole concentrations, at the interface $x = 0$ when the Fermi level is at the trap energy in thermodynamic equilibrium, are denoted by $n_1(0)$ and $p_1(0)$ respectively. They are given by

$$n_1(0) = n_o(0)\exp(e(E_{to} - E_{FM})/kT), \text{ and } p_1(0) = p_o(0)\exp(e(E_{FM} - E_{to})/kT) \tag{2.4.24}$$

with $n_o(0)$ and $p_o(0)$, respectively as the <u>equilibrium</u> electron and hole concentrations at the interface $x = 0$.

Turning to the question of the interfacial surface state charge density Q_i in the presence of illumination, we have, using equations (2.4.20), (2.4.24) together with constant reaction constants and a constant interfacial state density,

$$Q_i = -e\,n_t + e\,D_S\,\phi_o = D_S\,\frac{kT}{2}$$

$$\times\left\{\ln\left\{\frac{Hp_o(0)\exp(-2e\phi_B/kT) + \exp(-e\phi_B/kT)(Gn(0) + Hp(0)) + Gn_o(0)}{Hp_o(0)\exp(2e(E_g-\phi_B)/kT) + \exp(e(E_g-\phi_B)/kT)(Gn(0)+Hp(0)) + Gn_o(0)}\right\}\right.$$

$$\left. - \frac{(G\,n(0) - H\,p(0))}{(A-B)G\,n_o(0)}\ln\left\{\frac{(\exp(e\phi_B/kT)-A)(\exp(e(\phi_B - E_g)/kT)-B)}{(\exp(e\phi_B/kT)-B)(\exp(e(\phi_B - E_g)/kT)-A)}\right\} + eD_S\phi_o\right., \tag{2.4.25}$$

$$\text{with } \left.\begin{matrix}A\\B\end{matrix}\right\} = -\frac{(G\,n(0) + H\,p(0))}{2\,G\,n_o(0)} \pm \left\{\left(\frac{G\,n(0) + H\,p(0)}{2\,G\,n_o(0)}\right)^2 - \frac{H\,p_o(0)}{G\,n_o(0)}\right\}^{\frac{1}{2}}.$$

After a little algebraic manipulation, expression (2.4.25) for the non-equilibrium charge density at the interfacial states reduces to expression

(2.4.23), when conditions of thermodynamic equilibrium are applied.

At this stage, we can establish relations covering the thermodynamic equilibrium barrier height ϕ_B, and the portion of the output voltage developed across the interfacial layer (V_i). The potential drop across the interfacial layer is given under illumination by

$$\Delta - V_i = -\int_{-\delta}^{0} E_i(x)\, dx = \frac{\rho\delta^2}{2\varepsilon_i} + (Q_i + Q_{sc})\, {}^{\delta}/_{\varepsilon_i} \quad ,$$

thus $({}^{\varepsilon i}/_{\delta})(\Delta - V_i) = \frac{1}{2}\,\delta\rho + Q_i + Q_{sc}$ (2.4.26)

becomes in equilibrium $({}^{\varepsilon i}/_{\delta})\Delta = \frac{1}{2}\,\delta\rho_o + Q_{io} + Q_{sco}$. (2.4.27)

Subtracting $-({}^{\varepsilon i}/_{\delta})V_i = \frac{1}{2}\,\delta(\rho - \rho_o) + (Q_i - Q_{io}) + (Q_{sc} - Q_{sco})$. (2.4.28)

Now from $\phi_B = \phi_M - \chi - \Delta$, (2.4.2) and $V_b + V_n = \phi_B$, (2.4.3) together with the expressions (2.4.11) and (2.4.23) for Q_{sco} and Q_{io} respectively, the thermodynamic equilibrium barrier height ϕ_B is given by the solution of

$$\phi_B = \phi_M - \chi - \frac{\delta^2}{2\varepsilon_i}\,\rho_o + \frac{D_S\delta}{\varepsilon_i}\left(e\,E_g - kT\,\ln\left\{\frac{1 + \exp(e\phi_B/kT)}{1 + \exp(e(\phi_B - E_g)/kT}\right\}\right)$$

$$- \frac{\delta e}{\varepsilon_i}\,D_S\,\phi_o - \frac{\delta}{\varepsilon_i}\sqrt{(2\varepsilon_s e\,N_D(\phi_B - V_n))} \qquad (2.4.29)$$

This is an implicit relation for ϕ_B in terms of the parameters given in Table 1, and can be solved by iteration. Relation (2.4.28) is an implicit relation for V_i.

2.5 Junction currents

In this section we shall consider a non-degenerate semiconductor containing recombination centres of one type each of which can only trap

Table 1

Data adopted for an Au - SiO_2 n-type Si Schottky barrier solar cell

parameter	numerical value	dimensions	references and notes
A^*	120	$A.cm^{-2}K^{-2}$	Pülfrey & McOuat (1974)
D_S	$0.1x10^{17} \rightarrow 0.1x10^{19}$	$m^{-2}eV^{-1}$	Lane (1968)
δ	$1 \rightarrow 2$	nm	-
$m_{e/m}$	1.1	-	Effective mass ratio for electrons*
$m_{h/m}$	0.59	-	Effective mass ratio for holes*
μ_p	425	$cm^2V^{-1}s^{-1}$	* [an asterisk refers to Sreedhar et al (1969)]
E_g	1.1	eV	*
χ	4.01	eV	*
T	300	K	-
ϕ_M	>4.12, Au 4.7	eV	Riviere (1957), Sze (1969)
ε_s	11.8 ε_o	-	} ε_o permittivity of free space
ε_i	3.9 ε_o	-	
P_{in}	0.1	Wcm^{-2}	incident power using an AM1 spectrum
N_D	3×10^{17}	cm^{-3}	-
V_n	0.11	eV	-
ρ_o	3×10^{17} e	Q cm^{-3}	-
B^S	1×10^{-11}	$cm^3\ s^{-1}$	Landsberg (1967). The smaller value $B^S \approx 10^{-15}$ (Varshni 1967) would not change the results of the present work.
B_1	1.2×10^{-32}	cm^6s^{-1}	} D. Hill and P.T. Landsberg (1976).
B_2	1.2×10^{-32}	cm^6s^{-1}	
$T^s_{1i} = T^s_{2i}$	1.12×10^{-8}	cm^3s^{-1}	from capture cross section x thermal velocity (Barret & Vapaille 1975).
$T_{1i}=T_{2i}=T_{3i}=T_{4i}$	$3.66x10^{-25}$	cm^6s^{-1}	$T_{1i}=T^s_{1i} \times (5x10^{-7})/n_i$ (Evans & Landsberg 1963).

Table 1 continued

The values of the recombination coefficients T_i are needed only in the calculations of the interfacial recombination current (see section 2.6) and the interfacial surface state charge density, and are there taken as independent of the trap energy E_t. It is hoped however, that the simplification implied by the last two lines of Table 1 will yield the correct order of magnitude of the interfacial surface state recombination current. The bulk electron concentration is

$$n_n = 2\left(\frac{2\pi\ m_e\ kT}{h^2}\right)^{3/2} \exp\left\{e\left(E_{Fs} - E_c\right)/kT\right\} = 3 \times 10^{23}\ m^{-3} \quad .$$

The bulk hole lifetime is given by

$$\frac{1}{\tau_p} = B^s\ n_n + B_1\ n_n^2,\ \tau_p = 1/\left(B^s\ n_n + B_1\ n_n^2\right) = 3.33 \times 10^{-7} s.$$

The bulk hole diffusion constant is obtained from the Einstein relation to be

$$D_p = \mu_p\ kT/e = 1.1 \times 10^{-3}\ m^2\ s^{-1}.$$

The bulk diffusion length is

$$L_p = \left(D_p\ \tau_p\right)^{\frac{1}{2}} = 1.9 \times 10^{-5} m\ .$$

one electron. The total unavoidable recombination rate U_{unav} (band to band transitions) is, following Evans and Landsberg (1963), made up of three components. The first component U_b^s is due to radiative recombination, while the second and third components U_1^a, U_2^a are due to Auger effects. With the notation of Figure 2.3, and by means of the principle of detailed balance for each individual process, the net transition rates may be determined as

$$U_b^s = B^s(n\,p - n_i^2) \quad , \quad U_1^a = B_1\,n\,(n\,p - n_i^2)$$

$$U_2^a = B_2\,p(n\,p - n_i^2) \quad ,$$

where n and p are the electron and hole concentrations in the semiconductor's conduction and valence bands respectively, at some position x inside the semiconductor. The quantity n_i^2 represents the product of the thermodynamic equilibrium electron and hole concentrations. The total unavoidable recombination rate U_{unav} is therefore given by

$$U_{unav} = U_b^s + U_1^a + U_2^a = \bar{F}(n\,p - n_i^2) \quad , \qquad (2.5.1)$$

where $\bar{F} = B^s + B_1 n + B_2 p$ and n_i is the intrinsic carrier concentration.

The steady state concentration of trapped electrons $n_t(x)$ and the total steady state avoidable recombination rate U_{avoid} (due to transitions through localized trapping levels) at any point x in the semiconductor are, by the same argument leading to equations (2.4.17,18), given as

$$n_t(x) = \frac{(\bar{G}\,n + \bar{H}\,p_1)\,N}{\bar{G}(n+n_1) + \bar{H}(p+p_1)} \qquad (2.5.2)$$

$$U_{avoid} = \frac{(n\,p - n_i^2)\,\bar{G}\,\bar{H}\,N}{\bar{G}(n+n_1) + \bar{H}(p+p_1)} \quad . \qquad (2.5.3)$$

Here, N is the concentration of trapping states (m^{-3}) at a single energy level E_t. n_1, p_1 are respectivety, the electron and hole concentrations at some position $x > 0$, when the Fermi level is at the effective trap energy in thermodynamic equilibrium. Also $\bar{G}$ and $\bar{H}$ are given by

$$\bar{G} = T_1^{s} + T_1 n + T_2 p$$
$$\bar{H} = T_2^{s} + T_3 n + T_4 p \qquad (2.5.4)$$

where once again the letter T shows that traps are involved, and the superscript s indicates single electron processes. The reaction constants represent the processes,as illustrated in Figure 2.3, which occur in the semiconductor region of the Schottky barrier solar cell.

We now seek to find the contribution to the total current due to the light induced photo-current and the recombination current within the transition region (depletion layer). By the conservation of charge (see figure 2.4) and taking the conventional current density as positive when it is flowing to the right (i.e. in the forward direction), the net recombination rate is $(U - F)$ where F is the photo-generation rate of electron-hole pairs, and U is the recombination rate (recombination minus thermal generation).

The number of excess electrons lost due to the net recombination rate in element δx is given by

$$(U - F)\delta x = \frac{1}{e}\left[J_e(x + \delta x) - J_e(x)\right] = \frac{1}{e}\frac{dJ_e(x)}{dx}\delta x$$

which gives $$e(U - F) = \frac{dJ_e(x)}{dx}, \qquad (2.5.5)$$

where $J_e(x)$ is the electron current density at position x in the semiconductor. Similarly for the hole current density $J_h(x)$

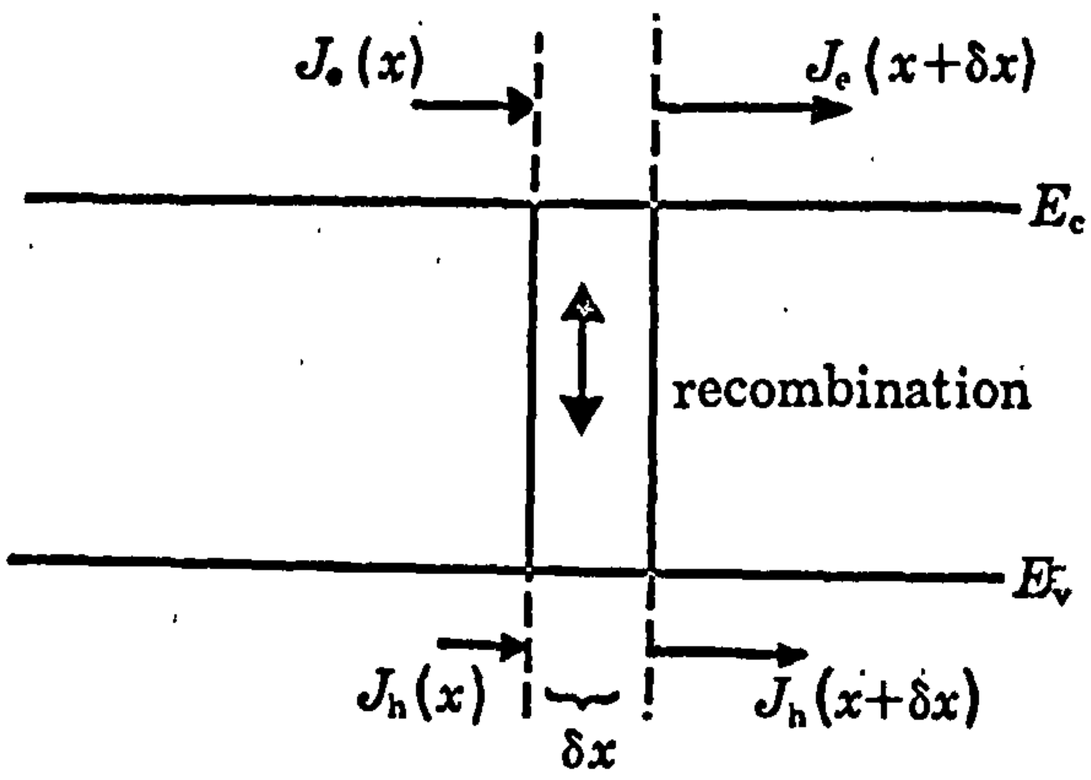

Figure 2.4 Diagram illustrating charge conservation.

$$e(U - F) = - \frac{dJ_h(x)}{dx} \quad . \qquad (2.5.6)$$

These continuity equations give $J_e(x) + J_h(x) = J$ which is independent of x.

The total current density J flowing through the junction under illumination is given by

$$J = J_e(0) + J_h(0)$$

$$= J_e(0) + J_h(w) + e \int_0^w (U - F)\, dx \; . \qquad (2.5.7)$$

Here $J_e(0)$ represents the net electron emission current density over the barrier at $x = 0$. Schottky barrier lowering effects are neglected and the transmission probability for electrons tunneling through the interfacial layer is assumed to be unity. Having made no provision for anything other than good communication between the metal and the semiconductor's valence band $(E_{FM} = E_{Fp})$, which implies that the photo-generated holes in this band move with comparative ease to the metal, thereby requiring near unit probability for the transmission of holes, it would therefore seem reasonable to assume the same for electrons communicating between the metal and the semiconductor's conduction band (i.e. the electron tunneling transmission probability is assumed to be near unity). However, in later work these assumptions are removed completely.

The assumptions regarding the quasi-Fermi levels will now be implemented. The majority carrier quasi-Fermi level E_{Fn} (in the case of the n-type Schottky barrier solar cell) is assumed to have negligible slope across both the bulk and depletion layers. Therefore the difference between the electron quasi-Fermi level and the Fermi level in the metal is close to V, the output voltage. As mentioned above, Schottky barrier lowering effects have been neglected, so that the bottom of the conduction band at

position $x = 0$ is above the Fermi level in the metal by an amount equal to ϕ_B^* $(= \phi_B + V_i)$ electron volts. Now by using results (A.9) and (A.10) of Appendix A we may identify the current density J_{ms}^e due to electrons passing from the metal to the semiconductors conduction band and the current density J_{sm}^e due to electrons passing from the semiconductors conduction band to the metal, as

$$J_{ms}^e = A^* T^2 \exp(-e(\phi_B + V_i)/kT) \qquad (2.5.8)$$

and $$J_{sm}^e = A^* T^2 \exp(-e(\phi_B - V_s)/kT) \quad , \qquad (2.5.9)$$

where A^* is the effective Richardson's constant, and T is the absolute temperature. Thus $J_e(0)$ is given by

$$J_e(0) = J_{sm}^e - J_{ms}^e \quad . \qquad (2.5.10)$$

The net hole current density at $x = w$ is given by

$$J_h(w) = - e D_p \left.\frac{dp}{dx}\right|_{x=w} \quad , \qquad (2.5.11)$$

where equation (2.2.8) has been used together with the assumption of a negligible potential drop across the bulk region of the semiconductor (i.e. $E = 0$ in the bulk). Returning now to the recombination rate at some point x in the semiconductors bulk region. It is usual to introduce the minority carrier lifetime τ_p, as a convenient means of measuring the recombination rate in the bulk region of a semiconductor.

Thus for $x > w$, $\quad U \simeq (p - p_o)/\tau_p \qquad (2.5.12)$

where $p - p_o$ is the excess minority carrier concentration.
The lifetime τ_p of the minority carriers (in this case they are holes) can be expressed in terms of the concentration of trapping states N

and the reaction constants of the recombination processes occuring within the semiconductor. If the trapping level is around the middle of the semiconductors band gap, and if a sufficiently high doping concentration is used, then for $x > w$

$$n_o \sim n >> p,\ p_1,\ n_1 \ . \qquad (2.5.13)$$

Hence by using (2.5.13) we may approximately equate the recombination rate given in equation (2.5.12) to the sum of the recombination rates U_{unav} and U_{avoid} in expressions (2.5.1) and (2.5.3) respectively. Thus we have $U_{unav} + U_{avoid} \simeq \dfrac{(p - p_o)}{\tau_p}$, which then yields, $\dfrac{1}{\tau_p} \simeq B^s n + B_1 n^2 + [T_2^s + T_3 n]N$, with τ_p as the minority carrier lifetime in the bulk region of the semiconductor. However, later in this chapter, when numerical calculations are performed we shall only consider the unavoidable recombination mechanisms, both in the depletion and bulk layers of the semiconductor .

By using the continuity equation (2.5.6) for holes in the semiconductors valence band, together with equation (2.2.8) setting the electric field E to zero in the bulk region, we construct a differential equation for the hole concentration in the valence band of the semiconductor:

$$\frac{d}{dx} J_h(x) = - e D_p \frac{d^2 p}{dx^2} = - e(U - F) \quad , \qquad (2.5.14)$$

which gives

$$\frac{d^2 p}{dx} - \frac{p - p_o}{D_p \tau_p} + \frac{F(x)}{D_p} = 0 \quad , \qquad (2.5.15)$$

as the continuity equation for holes in the semiconductors bulk region. A solution of this equation with appropriate boundary conditions yields, the hole concentration p as a function of position x inside the bulk region.

The photo-generation rate of electron-hole pairs $F(x)$ represents the number of electron-hole pairs generated per unit volume per unit time at a position x in the semiconductor. The number of photons in the wavelength range $(\lambda, \lambda + d\lambda)$, absorbed per unit time per unit area in an element δx of the semiconductor is given by

$$(\hat{\Phi}(x,\lambda) - \hat{\Phi}(x + \delta x,\lambda))\ d\lambda = -\frac{d\hat{\Phi}}{dx}(x,\lambda)\ \delta x\ d\lambda = \alpha(\lambda)\hat{\Phi}(x,\lambda)\delta x\ d\lambda\ , \quad (2.5.16)$$

where $\hat{\Phi}(x,\lambda)d\lambda$ is the photon flux $(m^{-2}\ s^{-1})$ in the wavelength range $(\lambda,\lambda + d\lambda)$ and $\alpha(\lambda)$ is the absorption coefficient for radiation of wavelength λ. By applying the boundary condition $\hat{\Phi}(x,\lambda)\Big|_{x=0} = \Phi(\lambda)$, where $\Phi(\lambda)d\lambda$ is the incident photon flux(to the semiconductor) in the wavelength range $(\lambda, \lambda + d\lambda)$, we see that equation (2.5.16) may be solved to give $\hat{\Phi}(x,\lambda)$ as

$$\hat{\Phi}(x,\lambda) = \Phi(\lambda)\ e^{-\alpha(\lambda)x}\ .$$

Hence we therefore deduce that the total photo-generation rate $F(x)(m^{-3}s^{-1})$ is given by

$$F(x) = \int_{\lambda_0}^{\lambda_1} \alpha(\lambda)\ \Phi(\lambda)\ e^{-\alpha(\lambda)x}\ d\lambda\ , \quad (2.5.17)$$

where $\lambda_0 < \lambda_1 = hc/eE_g$ indicate the useful wavelength limits for the incident solar spectrum,with h as Planck's constant and c as the velocity of light.

The net hole current density at $x = w$ is obtained by solving the differential equation (2.5.15) for p and then substituting the expression for $p(x)$ into equation (2.5.11):

$$J_h(w) = ep_o(\exp(eV/kT)-1)D_p/L_p - \int_{\lambda_0}^{\lambda_1} \frac{e\alpha(\lambda)\Phi(\lambda)L_p e^{-\alpha w}d\lambda}{1 + L_p\,\alpha} \qquad (2.5.18)$$

where $L_p\,(= (\tau_p D_p)^{\frac{1}{2}})$ is the diffusion length of holes in the valence band of the semiconductor, and the following boundary conditions have been used:

(1) $p(x) \longrightarrow p_o$ the unilluminated hole concentration far from the junction as $x \longrightarrow \infty$.

(2) $p(w) = p_o \exp(eV/kT)$ and is a consequence of assumption (a) of section 2.4.

The contribution to the current density from the depletion layer is

$$J_T^D = e\int_0^w (U - F)dx$$

$$= e\int_0^w U\,dx - \int_{\lambda_0}^{\lambda_1} e\,\Phi(\lambda)(1 - e^{-\alpha(\lambda)w})d\lambda = J_{rec}^D - J_L^{eD} \qquad (2.5.19)$$

where J_L^{eD} is the current density due to light being absorbed in the depletion layer, and J_{rec}^D is the recombination current density from both interface state recombination J_{ifr}^D and band-to-band recombination J_{unav}^D. We write

$$J_{rec}^D = J_{unav}^D + J_{ifr}^D \quad , \qquad (2.5.20)$$

which neglects the avoidable recombination current density J_{avoid}^D, due to transitions through localized trapping levels in the depletion layer. (see (2.5.3)). Thus the current density flowing through the device is given by

$$J = J_{sm}^e - J_{ms}^e + J_h(w) + J_{unav}^D + J_{ifr}^D - J_L^{eD} \qquad (2.5.21)$$

where equations (2.5.7, 10, 18, 19 and 20) have been used. Thus the total light current from (2.5.18) and (2.5.19) is

$$J_L = J_L^{eD} + \int_{\lambda_0}^{\lambda_1} \frac{e\,\alpha(\lambda)\Phi(\lambda)L_p\, e^{-\alpha w}}{1 + L_p\,\alpha}\, d\lambda = \int_{\lambda_0}^{\lambda_1} \left\{ e\Phi(\lambda) - \frac{e\Phi(\lambda)e^{-\alpha w}}{1+L_p\alpha} \right\} d\lambda \quad (2.5.22)$$

It is independent of x and depends on the forward voltage $(V_s + V_i)$ through w by equation (2.4.8). Thus the current density under illumination can be written as

$$J = J_{fwd} - J_L \quad (2.5.23)$$

where J_{fwd} (the dark forward current density) is given by

$$J_{fwd} = J_{sm}^e - J_{ms}^e + J_h^o + J_{unav}^D + J_{ifr}^D \quad . \quad (2.5.24)$$

The bulk recombination current J_h^o is the first term in equation (2.5.18), i.e.

$$J_h^o = e\, p_o(\exp(e\, V/kT) - 1)\, D_{p/L_p} \quad . \quad (2.5.25)$$

It turns out that for the case studied numerically later $J_{sm}^e + J_{ifr}^D$ dominate in (2.5.24). Recombination in the transition region J_{unav}^D and the bulk region J_h^o are never important. Even when the interfacial recombination current density J_{ifr}^D is small because D_S is small, its recombination traffic is not taken over by $J_h^o + J_{unav}^D$. Instead the barrier height decreases and the emission current J_{sm}^e increases to dominate in (2.5.24). It is perhaps, worthwhile to mention that in the context of <u>this</u> model of an n-type Schottky barrier solar cell, unit photo-quantum efficiency has been assumed in the depletion layer. i.e. Each and every photon of light, absorbed in the depletion layer of the

semiconductor, produces one carrier which is collected as photocurrent. This assumption is made on the grounds that, within the depletion layer the high electric field present, "sweeps" the photo-generated carriers out of this region before many of them can recombine. However, this is not the case in the bulk region of the semiconductor. Here the carriers are assumed to move by diffusion and not due to an electric field. One would therefore expect many of these photo generated carriers to recombine before they are collected as photo-current. This is borne out by equation (2.5.18), where the second term, due to the absorption of light in the bulk region, is clearly dependent on the hole diffusion length L_p which is simply related to the minority carrier lifetime τ_p (of the holes in the n-type bulk region).

2.6 Recombination currents.

In this section we develop analytical expressions for the current densities due to, (1) unavoidable recombination processes in the semiconductors depletion layer, and (2) interfacial surface state recombination at the interface $x = 0$.

The current density due to unavoidable recombination processes occuring within the depletion leayer of the semiconductor is given by

$$J^D_{unav} = e \int_0^w U_{unav} \, dx \qquad (2.6.1)$$

with U_{unav} from (2.5.1).

The electron concentration n in the semiconductors conduction band and the hole concentration p in the semiconductors valence bands, are given by equations (2.2.12) and (2.2.13) to be

$$n = N_c \exp(e(E_{Fn} - E_c)/kT)$$

and $$p = N_v \exp(e(E_v - E_{Fp})/kT) \quad ,$$

for a non-degenerate semiconductor.

If we use the potential distribution $\phi_s(x)$ from (2.4.5)

$$E_{Fn} - E_c = -\left\{V_n + \frac{e\,N_D}{2\,\varepsilon_s}(x - w)^2\right\} \qquad (2.6.2)$$

and $$E_{Fp} - E_v = E_g - \frac{e\,N_D}{2\,\varepsilon_s}(x - w)^2 - V_n - V \qquad (2.6.3)$$

in the depletion layer. Thus n and p become for $x \in [0,w]$

$$n(x,V) = N_c \exp\left(-e\left(V_n + \frac{e\,N_D}{2\,\varepsilon_s}(x - w)^2\right)/kT\right) \qquad (2.6.4)$$

and $$p(x,V) = N_v \exp\left(e\left\{\frac{e\,N_D}{2\,\varepsilon_s}(x - w)^2 + V_n + V - E_g\right\}/kT\right) . \qquad (2.6.5)$$

The equilibrium electron and hole concentrations, n_o and p_o at the edge of the depletion layer adjoining the bulk are given by

$$n_o = n(w,V) = N_c \exp(-e\,V_n/kT) = n(w,0) \qquad (2.6.6)$$

and $$p_o = p(w,0) = N_v \exp(e(V_n - E_g)/kT) , \qquad (2.6.7)$$

which gives $$n_i^2 = n_o\,p_o = N_c\,N_v \exp(-e\,E_g/kT) , \qquad (2.6.8)$$

where n_i is the intrinsic carrier concentration.

Thus the unavoidable recombination current density J^D_{unav} in the semi-conductors depletion layer is given by

$$J^D_{unav} = e\int_0^w (B^s + n\,B_1 + p\,B_2)(np - n_i^2)\,dx ,$$

which becomes, after a little manipulation,

$$J^D_{unav} = e\,N_c\,N_v(e^{\eta} - 1)\,e^{-\eta_g}\left(w\,B^s + B_1\,e^{-\phi_n}\,I_1 + B_2\,N_v\,e^{\phi_n+\eta-\eta_g}\,I_2\right), \qquad (2.6.9)$$

where $\phi_n = e\ V_n/kT$, $\eta_g = e\ E_g/kT$, $\eta = e\ V/kT$

$$I_1 = \int_0^w e^{-\Lambda(x - w)^2}\ dx \quad \text{and} \quad I_2 = \int_0^w e^{\Lambda(x - w)^2}\ dx$$

with $$\Lambda = \frac{e^2\ N_D}{2\varepsilon_s kT} \ .$$

The interfacial surface state recombination rate R_{ifr} will be calculated here, under the same assumptions as used before. Namely that, all trap to trap transitions at the interface $x = 0$ have been neglected, a constant distribution of interfacial surface states (trap states) over the semiconductors band gap has been assumed, together with constant reaction constants with respect to the energy of the surface trap states. Thus the total recombination rate through the interfacial surface states (at $x = 0$) is given by

$$R_{ifr} = \int d\ U_{ifr} = \int_{E_v(0)}^{E_c(0)} \frac{(n(0)p(0) - n_i^2)\ G\ H\ D_S\ dE_t}{G(n(0) + n_1(0)) + H(p(0) + p_1(0))} , \quad (2.6.10)$$

from equation (2.4.18) with $n_1(0)$ and $p_1(0)$ (given by (2.4.24)) as the thermodynamic equilibrium electron and hole concentrations, at the interface $x = 0$, when the Fermi level is at the trap energy.

The total recombination rate through the traps at the interface $x = 0$, neglecting trap to trap transitions, is therefore given by

$$R_{ifr} = (n(0)p(0) - n_i^2)\ \frac{H\ D_S\ kT}{n_o(0)e(A-B)}\ \ln\left\{\frac{(\exp(e\phi_B/kT)-A)\,(\exp(e(\phi_B-E_g)/kT)-A)}{(\exp(e\phi_B/kT)-B)\,(\exp(e(\phi_B-E_g)/kT)-B)}\right\}$$

(2.6.11)

where A and B are as given in section (2.4). The contribution to the total current density from the interfacial surface state recombination

may be written as

$$J^{D}_{ifr} = e\, R_{ifr} \,. \qquad (2.6.12)$$

It must be stressed, however, that in all of the interfacial state recombination statistics performed in this chapter, the influence of the metal on the interfacial surface state population, and hence on the recombiantion rate R_{ifr}, has been neglected. Anyway this does not seem to cause any problems for the cases studied numerically in the next section. In any case this omission will be rectified later in subsequent chapters.

2.7 Results

Some results of this theory are presented in figures 2.5 - 2.9. They were calculated for an Au - SiO_2 - n-type Si Schottky barrier solar cell by assuming that a total potential V is developed by the cell and that the parameters of table 1 are given. This enables the charge densities (Qm^{-2}) Q_{sco} and Q_{io} to be calculated. It has been assumed that the charge density $\rho(Qm^{-3})$ in the interfacial layer remains unchanged when the solar cell is operating, so that $\rho = \rho_o$ in all of the numerical calculations. Also the charge densities Q_{sc} and Q_i per unit area can be calculated in terms of the interfacial voltage V_i. Thus equations (2.4.11), (2.4.23), (2.4.9) and (2.4.25) when used in conjunction with equation (2.4.28), gives the value of the interfacial voltage V_i, as the solution of this implicit relation. Both the thermodynamic equilibrium barrier height ϕ_B and the interfacial voltage V_i are calculated using iterative procedures. Turning to the neutral level ϕ_o, this is assumed independent of illumination and output voltage, and has been estimated to lie at about 0.30 ± 0.36 eV for an Au n-type Silicon junction (Cowley and Sze 1965). It has been taken as zero for the present calculation. A positive value of ϕ_o would

however reduce the efficiencies, because as ϕ_o increases the thermodynamic equilibrium barrier height decreases, therefore causing an increase in the net thermionic emission current $(J^e_{sm} - J^e_{ms})$, which consequently leads to higher dark forward currents.

Returning now to the numerical algorithm, we next calculate the total current density J from (2.5.23), using (2.5.8), (2.5.9), (2.5.22), (2.5.24), (2.5.25), (2.6.9) and (2.6.12). The recombination parameters (or reaction constants) B^s, B_1, B_2 are needed for J^D_{unav}. For the current density J^D_{ifr}, we require the recombination data G, H, A and B. They are calculated via the reaction constants T^s_{1i}, T_{1i}, T_{2i}, T^s_{2i}, T_{3i}, T_{4i} and knowledge of the electron and hole concentrations at the interface $x = 0$, (see equations (2.6.4) and (2.6.5)). The conversion efficiency $V|J|/P_{in}$, where P_{in} is the incident power density, can then be maximised from the usual current density-voltage plots.

In figure 2.5 the maximum conversion efficiency η^* is plotted against the metal work function ϕ_M. For high interfacial surface state densities the variable metal work function has little effect on the maximum conversion efficiency. This is because at high interfacial surface state densities D_S the thermodynamic equilibrium barrier height is not greatly increased with an increase of metal work function. Conversely, with lower interfacial surface state densities the equilibrium barrier height readily increases with an increase of metal work function, so the maximum conversion efficiency fluctuates more rapidly. Also, with the lower values of the interfacial surface state density there is a smaller loss due to the interfacial state recombination current density J^D_{ifr}, therefore the maximum attainable efficiencies are improved as shown for high work function metals.

Turning now to figure 2.6 the maximum conversion efficiency is plotted as a function of the interfacial surface state density. Here, the thickness

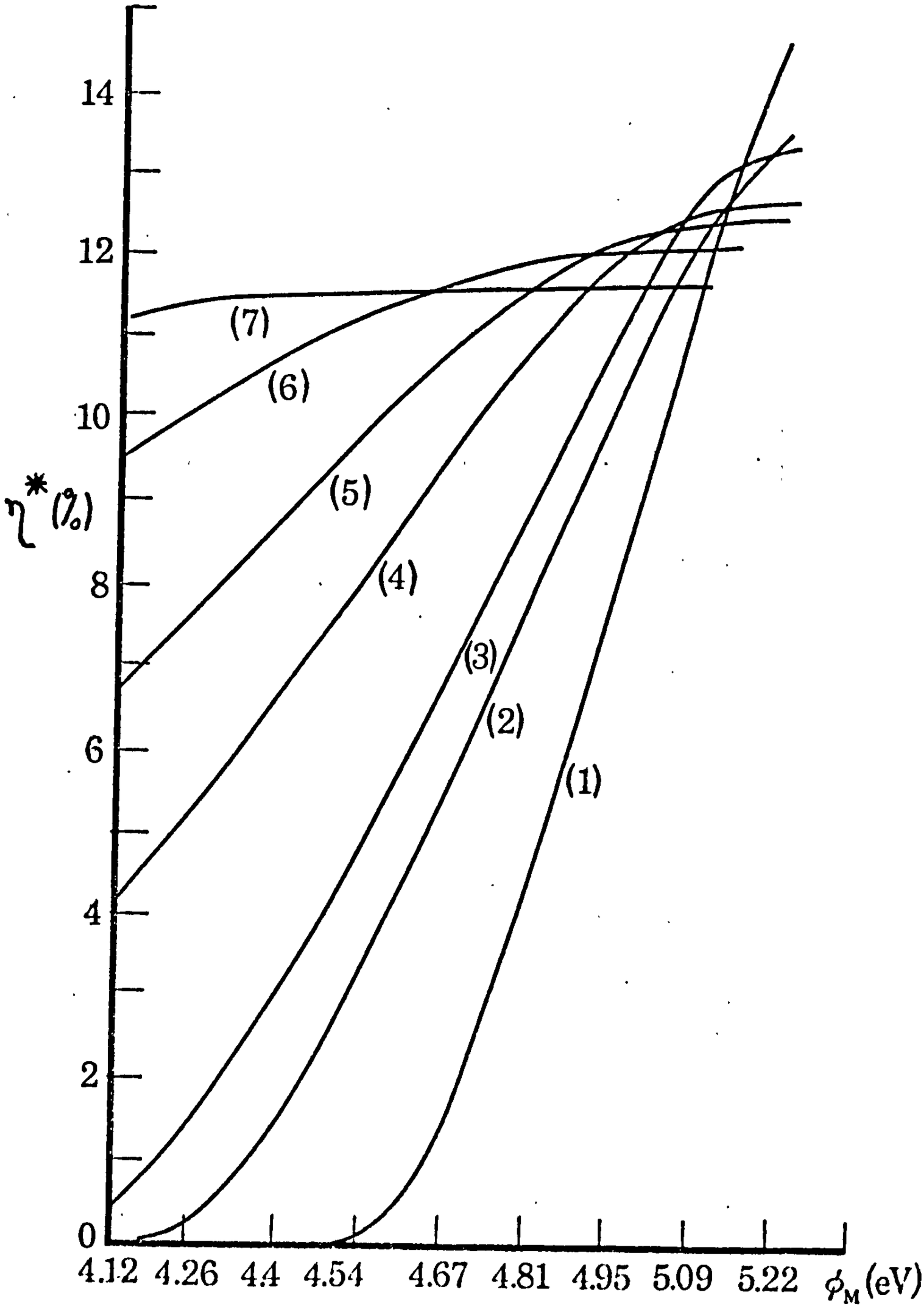

Figure 2.5 The maximum conversion efficiency η^* as a function of metal work function ϕ_M for various interfacial state densities D_S. The parameters of table 1 have been used together with $\delta = 19$ Å.

(1) $D_S = 0.1 \times 10^{17}\ m^{-2}\ eV^{-1}$, (2) $D_S = 0.7 \times 10^{17}\ m^{-2}\ eV^{-1}$,

(3) $D_S = 0.1 \times 10^{18}\ m^{-2}\ eV^{-1}$, (4) $D_S = 0.2 \times 10^{18}\ m^{-2}\ eV^{-1}$,

(5) $D_S = 0.3 \times 10^{18}\ m^{-2}\ eV^{-1}$, (6) $D_S = 0.5 \times 10^{18}\ m^{-2}\ eV^{-1}$,

(7) $D_S = 0.9 \times 10^{18}\ m^{-2}\ eV^{-1}$.

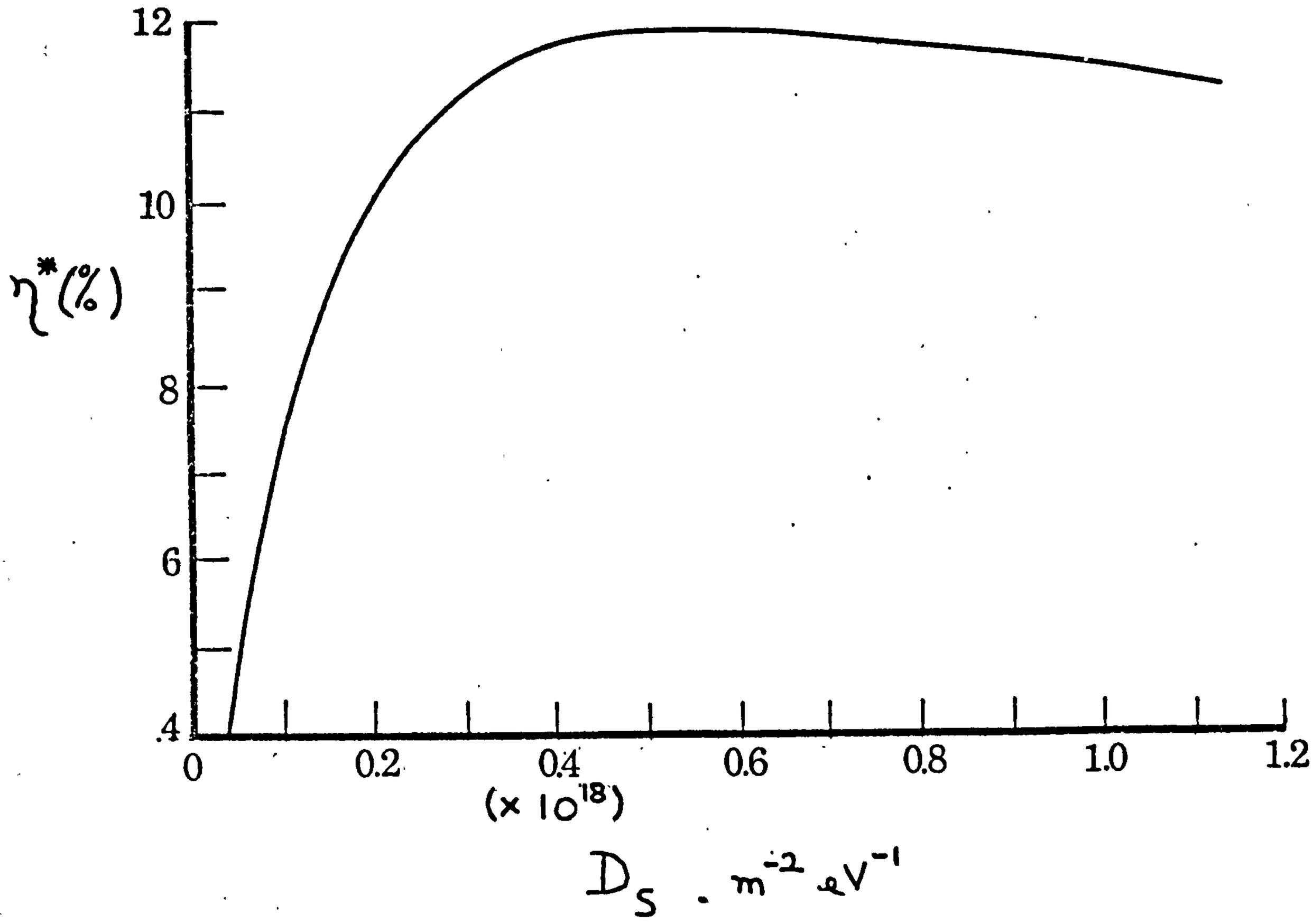

Figure 2.6 The maximum conversion efficiency η^* as a function of interfacial state density D_S. The parameters of table 1 have been used together with $\delta = 19$ Å and $\phi_M = 4.70$ eV (gold).

δ of the insulating interfacial layer and the metal work-function are held constant. The increase in the maximum conversion efficiency with increasing, but low, density of interfacial surface states (ca. 10^{17}) is caused by the rapid increase in the thermodynamic equilibrium barrier height ϕ_B, which in turn makes electron emission over the Schottky barrier more difficult. At such low values of the interfacial state density D_S the recombination traffic across the interface has a marginal effect. If the density of the interfacial surface states is increased, the advantage of an increase in the thermodynamic equilibrium barrier height is eventually out-weighed by the increasing contribution from the interfacial surface state recombination current density. At this point the maximum conversion efficiency η^* begins to fall off. The maximum value of η^* as D_S is varied, but δ and ϕ_M are kept fixed, is denoted by η^{**}(the maximum attainable conversion efficiency).

The current density-voltage characteristics of n-type Schottky barrier solars cells, are given in figure 2.7 for various interface parameters. The increase with the density of interfacial surface states D_S of the open-circuit voltage and power output is attributed to the increase in the thermodynamic equilibrium barrier height ϕ_B with increasing, but low, density of interfacial surface states. At these densities D_S the interfacial recombination current density has little effect on the overall characteristics. However, as the density of the interfacial surface states is increased beyond some critical density the recombination processes increase to dominate the J - V characteristics, thus causing a reduction in the open circuit voltage and power output of the Schottky barrier solar cell. The maximum attainable conversion efficiency η^{**} increases with δ in the range between 10 and 20$\mathring{A}$. The current density-voltage characteristic corresponding to an interfacial layer thickness of 19$\mathring{A}$,

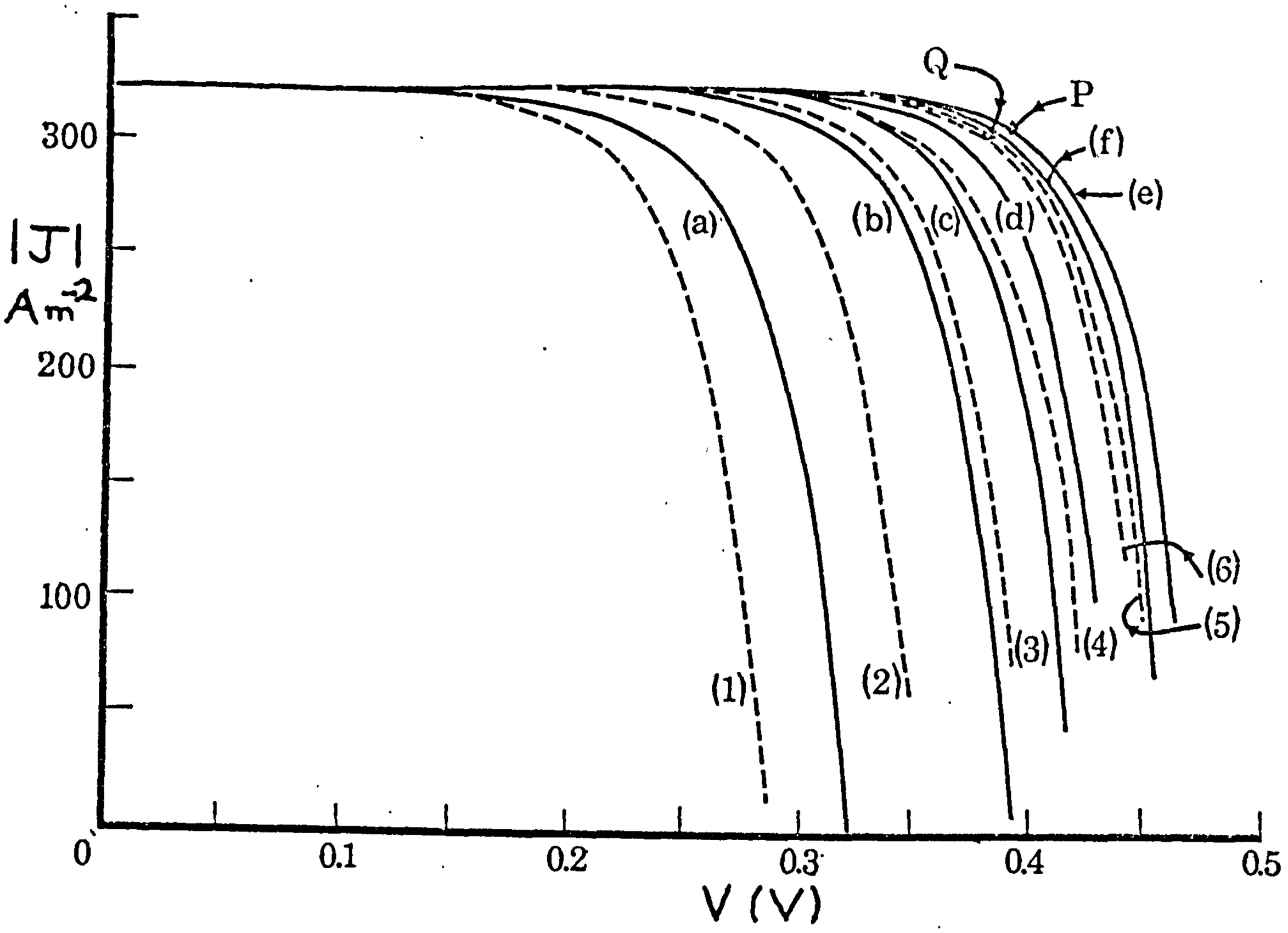

Figure 2.7 The current density-voltage characteristics for various interface state densities $D_S(m^{-2}\ eV^{-1})$. The parameters of table 1 have been used together with $\delta = 19$ Å (full lines), $\delta = 10$ Å (dashed lines), and $\phi_M = 4.70$ eV (gold).

(a) $D_S = 0.1 \times 10^{18}\ m^{-2}\ eV^{-1}$ (b) $D_S = 0.18 \times 10^{18}\ m^{-2}\ eV^{-1}$

(c) $D_S = 0.23 \times 10^{18}\ m^{-2}\ eV^{-1}$ (d) $D_S = 0.28 \times 10^{18}\ m^{-2}\ eV^{-1}$

(e) $D_S = 0.51 \times 10^{18}\ m^{-2}\ eV^{-1}$ (f) $D_S = 0.9 \times 10^{18}\ m^{-2}\ eV^{-1}$.

For $\delta = 19$ Å the maximum attainable conversion efficiency is 11.9% and occurs at point P.

(1) $D_S = 0.11 \times 10^{18}\ m^{-2}\ eV^{-1}$, (2) $D_S = 0.2 \times 10^{18}\ m^{-2}\ eV^{-1}$,

(3) $D_S = 0.3 \times 10^{18}\ m^{-2}\ eV^{-1}$, (4) $D_S = 0.4 \times 10^{18}\ m^{-2}\ eV^{-1}$,

(5) $D_S = 0.64 \times 10^{18}\ m^{-2}\ eV^{-1}$, (6) $D_S = 0.9 \times 10^{18}\ m^{-2}\ eV^{-1}$.

For $\delta = 10$ Å the maximum attainable conversion efficiency is 11.4% at point Q.

together with the density of interfacial surface states at about $0.23 \times 10^{18}\ m^{-2}\ eV^{-1}$ (curve c , of figure 2.7), agrees well with observed experimental data (Lillington and Townsend 1976) after adjusting the transmission coefficient (for light passing through the gold film) to 77% and the series resistance (by the use of an equivalent circuit) to ca. 1.5Ω for a cell of area 1 cm^2. A detailed analysis of equivalent circuits has been given by Hovel (1975).

From figure 2.8, one sees that the present theory, does not lead to a linear relationship between the voltage V_s developed in the semiconductor and the total output voltage V. In fact, when the output voltage V is relatively low, the interfacial surface state population is controlled by the minority carriers (i.e. holes in this case). Thus for small operating voltages the minority carriers tend to be in "equilibrium" with the surface states. However, the minority carriers, as mentioned earlier (see section (2.5)), communicate easily with the metal. Hence it is clear that for small operating voltages V, the interfacial surface states are approximately governed by the metal Fermi level. This is expected for thinner oxide layers (see, for example Fonash 1975a). As the output voltage V is increased, then it is seen from figure 2.8 that $V_i (= V - V_s)$ increases with V. This is expected because as V is increased, the concentration of majority carriers (electrons) at the interface x = 0 increases, thus causing the surface state population to become less influenced by the minority carriers.

An argument, based on the conservation of charge (see for example (2.4.28) with $\rho = \rho_o$) in the Schottky barrier solar cell will be used to illustrate the above point. With a cell output voltage $V > 0$ and by assuming $\rho = \rho_o$ say, then from equations (2.4.9) and (2.4.11), the change in the space charge density (within the semiconductor) $Q_{sc} - Q_{sco}$

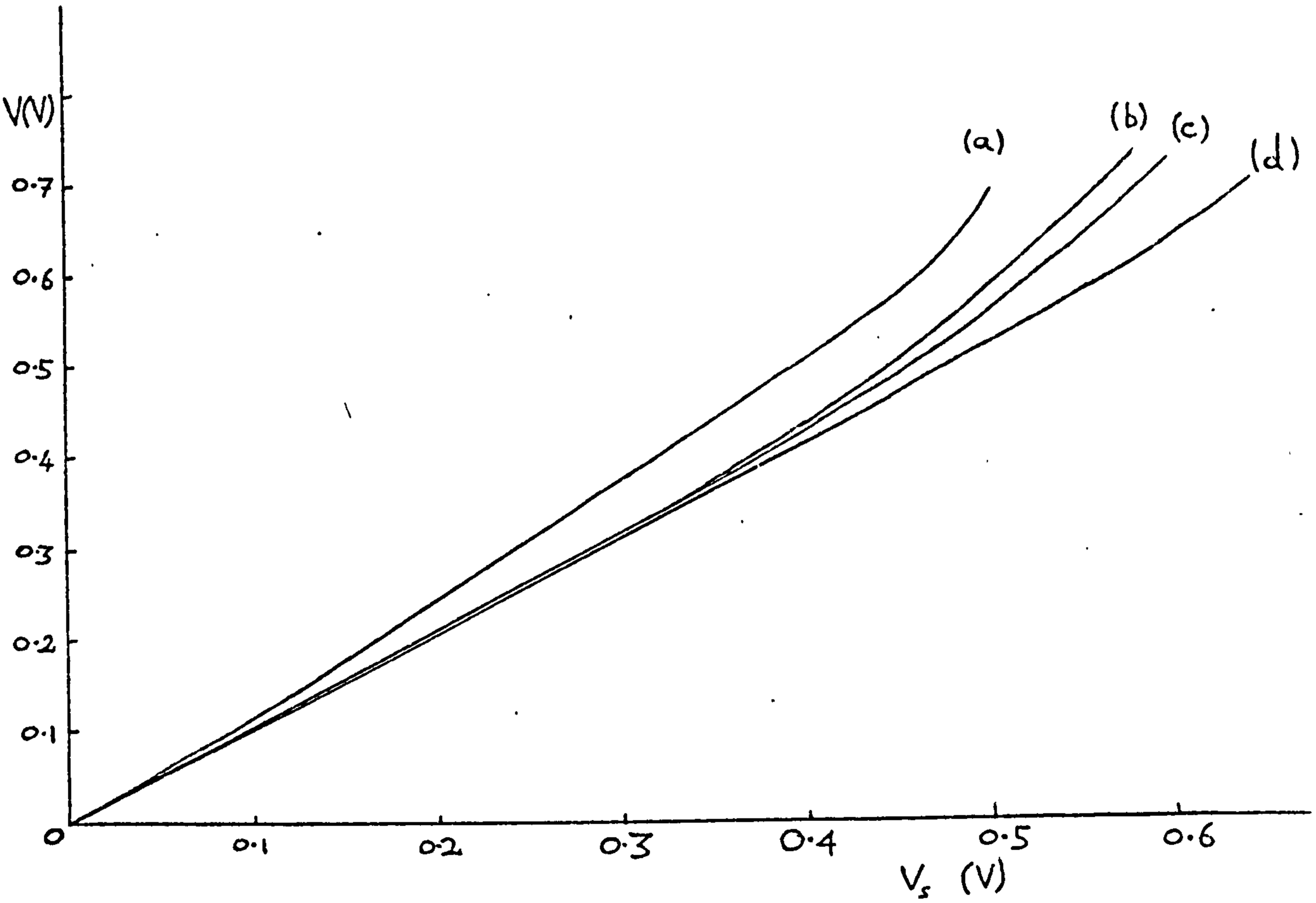

Figure 2.8 The voltage V_s developed in the semiconductor as a function of the total output voltage V for various interfacial surface state densities $D_S(m^{-2}\ eV^{-1})$. The parameters of table 1 have been used together with $\delta = 19\ \text{Å}$ and $\phi_M = 4.7$ eV (gold)

(a) $D_S = 10^{16}\ m^{-2}\ eV^{-1}$ (b) $D_S = 0.9 \times 10^{17}\ m^{-2}\ eV^{-1}$.

(c) $D_S = 0.11 \times 10^{18}\ m^{-2}\ eV^{-1}$. (d) $D_S = 0.2 \times 10^{18}\ m^{-2}\ eV^{-1}$

becomes a negative quantity. Similarly the change in the interfacial state charge density $Q_i - Q_{io}$ is also negative, this is due to the quasi Fermi levels of the interfacial surface states rising above that of the metal (see section 8 below). Now by appealing to equation (2.4.28) or by using the Gauss flux theorem in conjunction with the increase in charge on the surface of the metal, we find that the interfacial voltage V_i is positive (if $\rho = \rho_o$). Further to this we have found that the barrier height $\phi_B^* (= \phi_B + V_i)$ for oxide thickness $< 20\mathring{A}$ tends to remain constant within 10% as the load is changed, all other variables being kept constant. This reinforces the statement above, that the interfacial surface states are approximately governed by the metal Fermi level. Although the analysis presented in this chapter is only applicable to oxide thicknesses $\gtrsim 30\mathring{A}$, as noted in connection with (2.4.19) and (2.6.12), in view of the above discussion it is hoped therefore that our numerical results in this chapter are reasonably reliable.

In figure 2.9, one observes that the present theory leads to a more rapid rise in the thermodynamic equilibrium barrier height ϕ_B as a function of $D_S(m^{-2}\ eV^{-1})$ than does previous work (see, for example, Fonash 1975a). This difference is due to the removal of the temperature dependence in the expression for the thermodynamic equilibrium interfacial surface state charge density Q_{io}, by taking values at the absolute zero. With this procedure one obtains, for the interfacial surface state charge density Q_{io} at thermodynamic equilibrium

$$Q_{io} = -e(E_g - \phi_B)\, D_S + e\, D_S\, \phi_o \quad . \qquad (2.7.1)$$

Substitution of this expression for Q_{io} into equation (2.4.27) would effectively yield a quadratic equation in $(\phi_B - V_n)^{\frac{1}{2}}$. Solution of this equation gives the thermodynamic equilibrium barrier height equation corresponding to the previous work.

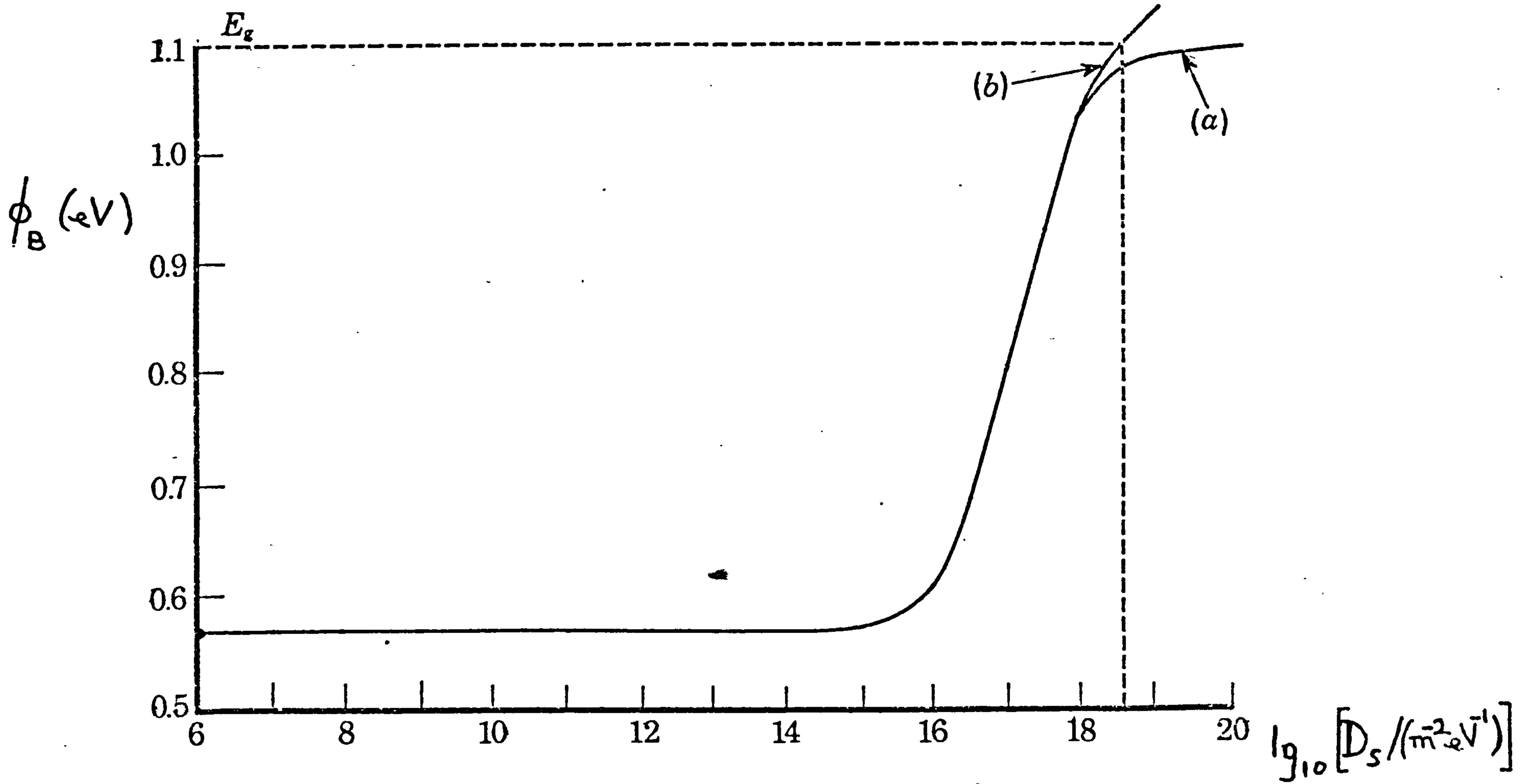

Figure 2.9 The thermodynamic equilibrium barrier height as a function of interfacial state density. (a) According to Cowley and Sze (1965) with their $\phi_o = 0$. (b) According to the present theory. The parameters of table 1 have been used together with $\delta = 19$ Å.

However by (2.4.29) it can be seen that, with the neutral level ϕ_o set to zero, the thermodynamic equilibrium barrier height can attain its maximum value which is E_g (the semiconductors energy gap), when the density of interfacial surface states D_S reaches its maximum reasonable value D_{SC} say. From figure 2.9 this value is $D_{SC1} = 0.37 \times 10^{19}\ m^{-2}\ eV^{-1}$. We will now give a separate estimate to the value of D_{SC}.

Since single crystal silicon possesses the diamond structure, with lattice constant. $a = 5.42\ \mathring{A}$, we will find that for a (1,1,1) cleavage plane, the number of lattice sites is $4/(\sqrt{3}\ a^2)$ per square metre. Silicon has a tendency to form tetrahedral covalent bonds, which facilitates the formation of the diamond type structure. The lattice is cubic face centred with side of length $a(= 5.42\ A^o)$ with additional atoms at $(\frac{1}{4}, \frac{1}{4}, \frac{3}{4})a$; $(\frac{3}{4},\frac{3}{4},\frac{3}{4})a$; $(\frac{3}{4}, \frac{1}{4}, \frac{1}{4})a$; $(\frac{1}{4}, \frac{3}{4}, \frac{1}{4})a$ (see figure 2.10a). Now, consider a projection of the lattice structure shown in figure 2.10a, down a cube diagonal (i.e. a view of a (1,1,1) face). The heights of the atoms are marked in twelfths of the lattice diagonal in figure 2.10b. The net's side length b is given by

$$b = {}^{a}/_{2} \cdot \sqrt{2} = a/\sqrt{2} \quad . \qquad (2.7.2)$$

This net fills 2-space completely and there is one distinct lattice site per net at a particular height. The area of the net is given by

$$2\ {}^{1}/_{2} \cdot b^2 \sin {}^{\pi}/_{3} = a^2\ \frac{\sqrt{3}}{4} \qquad (2.7.3)$$

Therefore the number of lattice sites per unit area on a (1,1,1) cleavage plane is given by $4/(\sqrt{3}\ a^2)$.

Now,if we assume that the maximum number of dangling bonds is nearly equal to the number of lattice sites (i.e. nearly a complete miss-match), and further to this if we also assume that each dangling bond gives rise

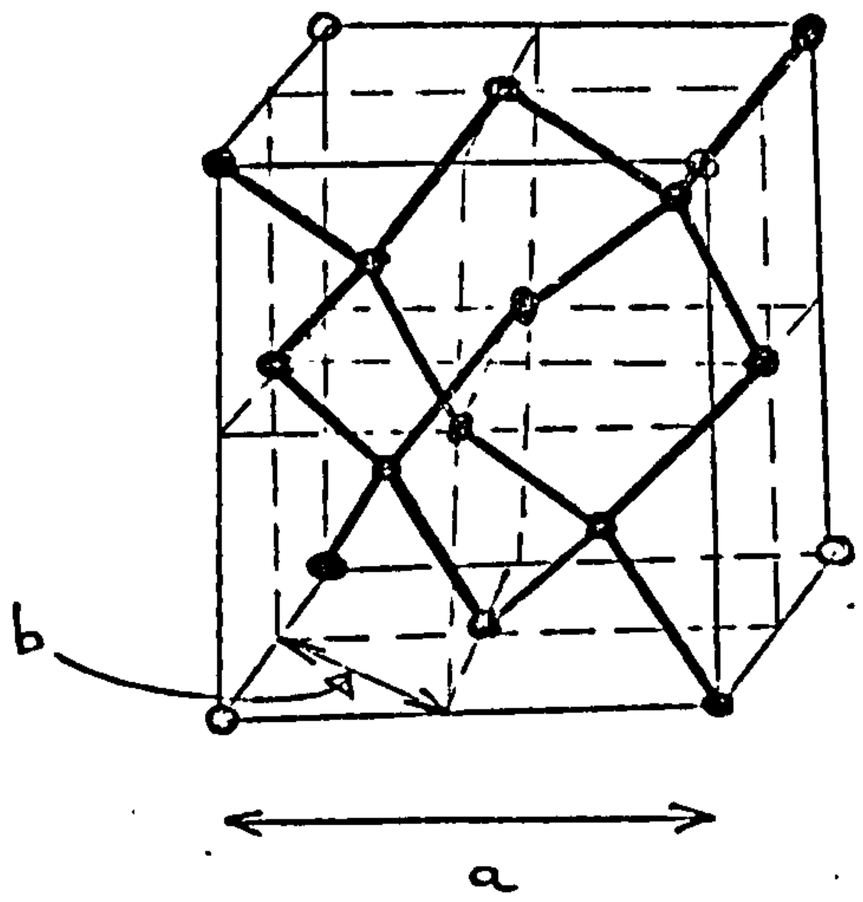

(a)

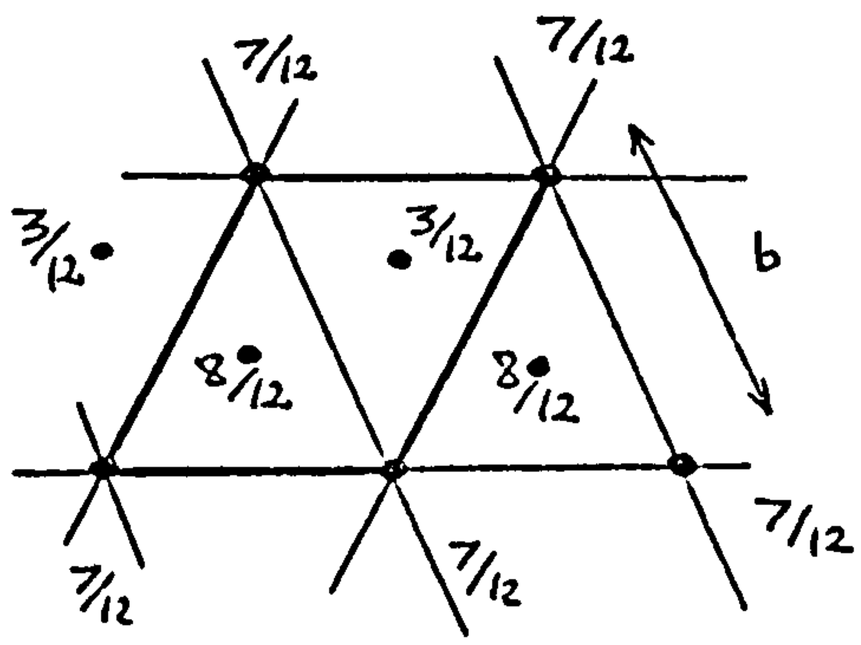

(b)

Figure 2.10 Structure of single crystal Si (a) Perspective view of the unit cell, with positions of atomic centres. Also shown are the interatomic bonds. (b) Projection down a cube body diagonal; the heights of the atoms are marked in twelfths of the cube diagonal.

to an interfacial surface state, then the maximum number of interfacial surface states is given by

$$E_g D_S \lesssim 4/(\sqrt{3}\, a^2) \qquad (2.7.4)$$

where it has been assumed that the interfacial surface states are distributed evenly over the energy gap of the semiconductor with density $D_S(m^{-2}\ eV^{-1})$. Hence with a practically complete lattice mismatch between the Si and the SiO_2, one would expect the maximum value of D_S to be given by

$$D_{SC2} = \frac{4}{\sqrt{3}\, a^2}\ \frac{1}{E_g} \approx 0.71 \times 10^{19}\ m^{-2}\ eV^{-1}\ . \qquad (2.7.5)$$

One would expect D_{SC2} to be larger than D_{SC1} because a complete lattice mismatch is not physically possible. In fact D_{SC1} and D_{SC2} are too large to have been realised experimently so far. Figure 2.9 shows that an upper limit at $D_S \approx 10^{17}\ m^{-2}\ eV^{-1}$ limits the thermodynamic equilibrium barrier height ϕ_B to ca. 0.8 eV.

2.8 Discussion

In this section we shall briefly examine the effect of the reaction constants's variation with electric field, and will then go on to discuss the quasi-Fermi level distribution for the interfacial surface states.

The variation of the reaction constants with electric field is for interaction with accoustic phonons usually of the form (D.J. Hill 1976)

$$B_i(E_s) = B_i(0)\ \exp\left\{E_s^2 \,/\, \bar{E}_c^2\right\}\ , \qquad (2.8.1)$$

where $\bar{E}_c^2 = \frac{24(kT)^3}{\hbar^2 e^2}\left(\frac{1}{m_e} + \frac{1}{m_h}\right)^{-1}$ is a critical electric field,

$E_s(x)$ is the electric field at any point x in the semiconductor, m_e and m_h are the effective masses of an electron in the conduction band and a hole in the valence band of the semiconductor respectively. Since

the magnitude of $\frac{1}{w}\int_0^w \exp\left\{E_s(x)^2/\bar{E}_c^2\right\} dx \simeq 1$, we conclude that for a M-O-S junction the effect that the field has upon the recombination currents is minimal when the device is delivering maximum power. Further study of this effect may be desirable as other expressions for $\bar{E}_c$ are available in the literature (e.g. Bonch-Bruevich 1965).

Turning now to the quasi-Fermi level distribution for interfacial surface states at $x = 0$, we will derive an expression giving the quasi-Fermi level F_t for any particular surface state relative to the Fermi level E_{FM} in the metal. Now from equation (2.4.17) one has

$$dn_t = \frac{G\,n(0) + H\,p_1(0)}{G(n(0) + n_1(0)) + H(p(0) + p_1(0))} D_S\, d\,E_t = f_t\, D_S\, dE_t, \quad (2.8.2)$$

as the number of occupied interfacial surface states in the energy range $(E_t, E_t + dE_t)$. Here E_t is measured in eV's and f_t is the interfacial surface state occupation probability, whose quasi-Fermi level will be denoted by F_t, so that we may write

$$\frac{1 - f_t}{f_t} = \exp(e(E_t - F_t)/kT) = \frac{G\,n_1(0) + H\,p(0)}{G\,n(0) + H\,p_1(0)} . \quad (2.8.3)$$

By multiplying (2.8.3) throughout by $\exp(e(E_{FM} - E_{to})/kT)$ where E_{FM} is the thermodynamic equilibrium Fermi level, and by using (2.4.24) we then obtain

$$E_t - E_{to} + E_{FM} - F_t = \frac{kT}{e} \ln\left\{\frac{Gn_o(0) + Hp(0)\exp(e(E_{FM} - E_{to})/kT)}{Gn(0) + Hp_o(0)\exp(e(E_{FM} - E_{to})/kT)}\right\}, \quad (2.8.4)$$

where E_{to} and E_t are the interfacial surface state energies in and out of thermodynamic equilibrium respectively. Now as we are measuring all energies relative to the metal, then obviously (see, for example figure 2.2) $E_t = E_{to} + V_i$, where V_i is the portion of output voltage

developed across the interfacial layer. Thus the difference between the equilibrium metal Fermi level and the quasi-Fermi level for interfacial states at energy E_{to} (eV) is given by

$$E_{FM} - F_t = \frac{kT}{e} \ln\left\{\frac{Gn_o(0) + Hp(0)\exp(e(E_{FM} - E_{to})/kT)}{Gn(0) + Hp_o(0)\exp(e(E_{FM} - E_{to})/kT)}\right\} - V_i \qquad (2.8.4)$$

There are three special cases.

(a) Thermodynamic equilibrium: $n(0) = n_o(0)$, $p(0) = p_o(0)$, $V_i = 0$

This gives $E_{FM} = F_t$

(b) $E_{to} >> E_{FM}$: gives the result that

$$E_{FM} - F_t \approx \frac{kT}{e} \ln\left\{\frac{n_o(0)}{n(0)}\right\} - V_i \quad .$$

Now with $n_o(0) = N_c \exp(-e\,\phi_B/kT)$ and $n(0) = N_c \exp(-e(\phi_B + V_i - V)kT)$ from (2.6.4) and (2.4.8), the difference between the interfacial surface state quasi-Fermi level and the metal Fermi level is given by

$$E_{FM} - F_t \approx V_i - V - V_i \quad \text{i.e.} \quad F_t \approx E_{FM} + V = E_{Fs} \quad .$$

Thus interfacial surface states of high energy are in good communication with the semiconductor.

(c) Similarly if $E_{to} << E_{FM}$ then $F_t \approx E_{FM}$ showing that interfacial surface states, of low energy, are in good communication with the metal.

The quasi-Fermi levels for the interface states "fan out" between E_{Fn} and E_{FM}. Perhaps this may be connected by means of the Poisson equation to the charge density ρ inside the interfacial layer. The effect of varying the thickness δ has been investigated by other workers cited

in the literature, but we shall return to study the effects of varying the thickness δ, on the recombination and tunneling currents in later chapters.

Among effects omitted in the above theory we note:

(a) The photogenerated current density J_L has been calculated on the basis employed by previous workers (e.g. Fonash 1975a). Thus holes and electrons are generated in the depletion layer and tend to move to the left and right respectively on figure 2.2 without recombination giving J_L^{eD}. The remaining photons generate carriers in the bulk region which are subject to recombination (second term in (2.5.18)). The corresponding result without recombination is obtained if L_p is imagined to become very large. The reduction of the light current due to a non-unit probability of tunneling between the metal and the semiconductor valence band has not been included. This causes J_L and hence $(-J > 0)$ to be over-estimated in (2.5.24).

(b) Another cause of an over-estimate of $-J(> 0$ when delivering power) arises from an underestimate of J_{sm}^e due to the neglect of image force lowering of the potential near $x = 0$. The effect of image force lowering on J_{ms}^e is likely to be rather small.

(c) Opposing the above two effects is an under-estimate of $-J(> 0)$. This arises from the fact that electrons with energy in excess of $E_{FM} + \phi_B^*$ have all been assumed to tunnel from the semiconductor to the metal in accordance with (2.5.9), while electrons with less energy have been assumed to participate in interfacial state recombination (2.6.12) in accordance with their concentration. In fact both mechanisms are open to all these electrons; the net effect is expected to be a reduction in J_{sm}^e, i.e. an increase in $-J$ (the positive current flowing when the Schottky barrier solar cell is delivering power). A more detailed discussion of the validity of this model of an n-type Schottky barrier solar cell will be defered until the end of the next chapter.

CHAPTER 3

METEOROLOGICAL EFFECTS ON SCHOTTKY BARRIER SOLAR CELLS AND THE VALIDITY OF ASSUMPTIONS MADE

3.1 Introduction

In this chapter the effect of different meteorological conditions on Schottky barrier solar cell outputs have been investigated, using a model for an n-type solar cell. This model is basically that developed in chapter 2. The effect of different meteorological conditions on the output of a typical p-n junction solar cell has been studied extensively by Mallinson and Landsberg (1977). For this purpose they considered a whole range of super-positions of (100-d)% direct and d% diffuse radiation. They found for example that the optimum energy gap $E_g(d)$ depends on the parameter d. One can also find how a solar cell of given energy gap, and given other semi-conductor parameters, reacts to different conditions d by considering the power output P(d) and efficiency η (d). In chapter 2 we made a study of an n-type Schottky barrier solar cell. In this we showed how the characteristics of an n-type Schottky barrier solar cell are affected by interfacial surface state recombination.

We wish to draw these two strands together here and show, using the theory of chapter 2, how the output power P and the efficiency η^* of a Si n-type Schottky barrier solar cell depends on the diffuse component. In figures 3.1 and 3.2 we show the spectral

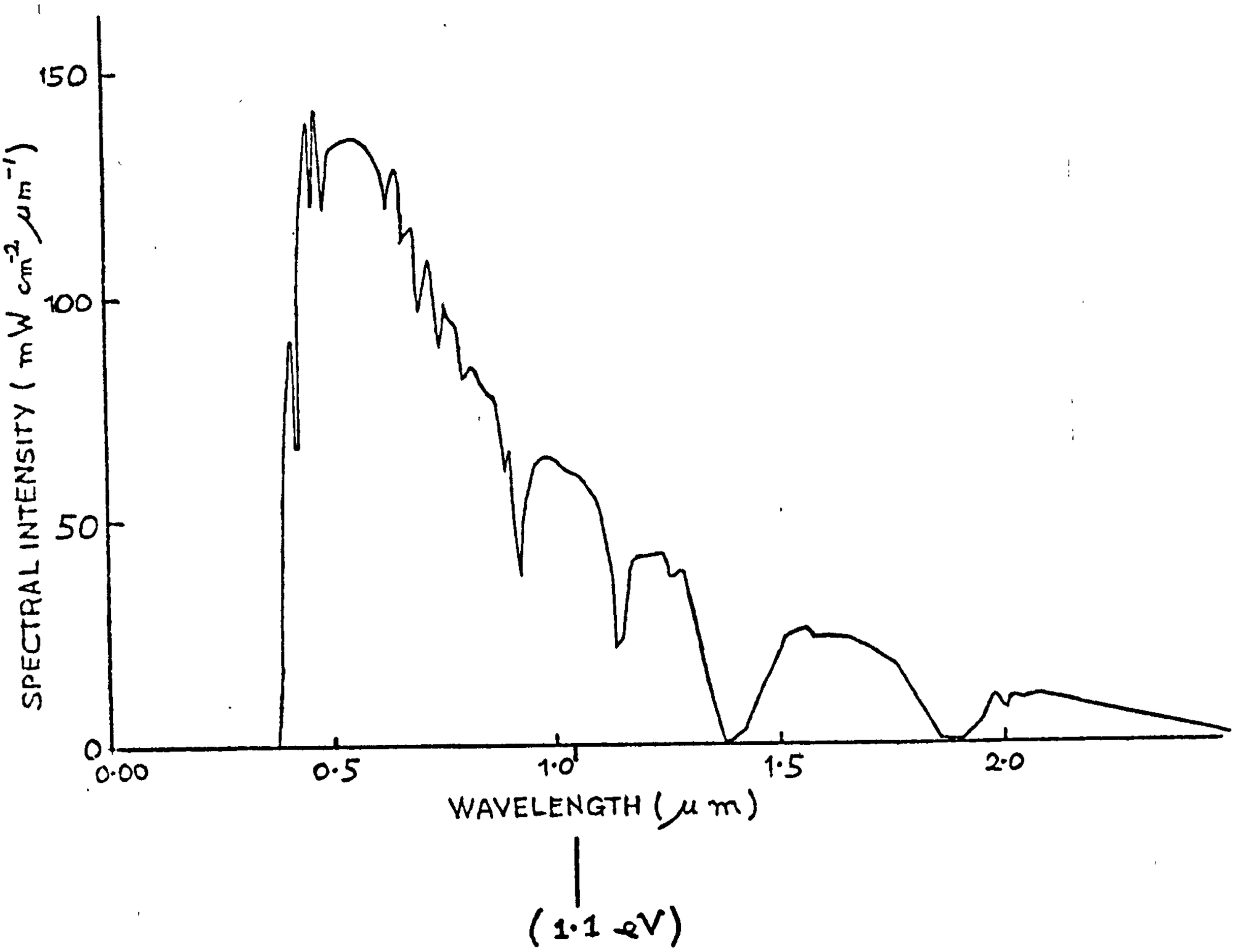

Figure 3.1 Spectral energy distribution as a function of wavelength for direct solar radiation on Earth's surface with sun vertically overhead on a clear day AM1 (87.2 mW cm^{-2}).

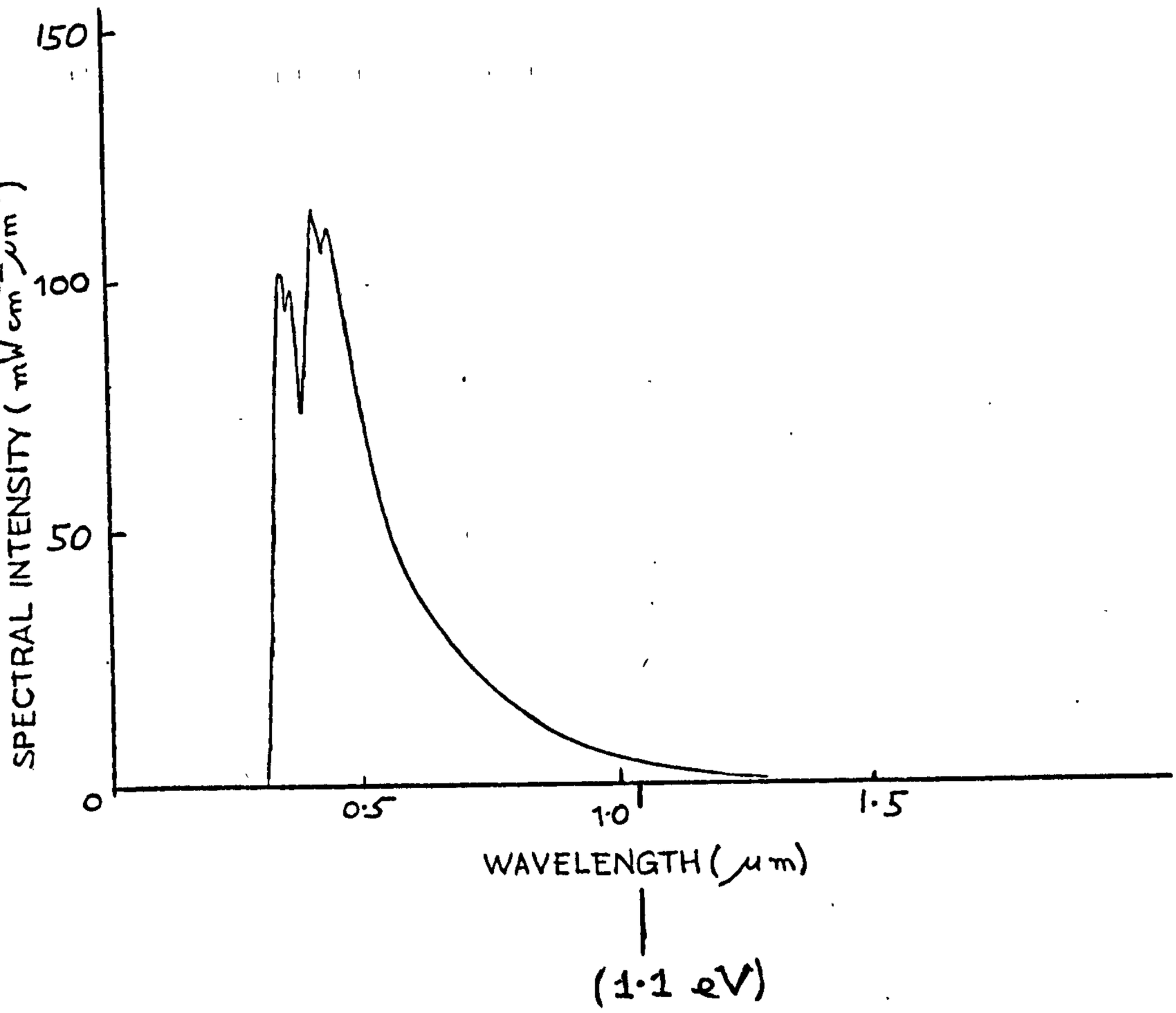

Figure 3.2 Spectral energy distribution as a function of wavelength for diffuse radiation on Earth's surface on a cloudy day (30 mW cm^{-2}).

curves which underlie the analysis. They are based on the spectra of figure 4 of Mallinson and Landsberg (1977). Similar results to those for p-n junction cells were obtained namely that, although the output power density is reduced, a much higher conversion efficiency is possible when the solar cell is illuminated with diffuse radiation.

A few improvements to the basic theory are required to make the theory more complete. The interfacial surface state recombination model should be improved to include the effect of carriers tunneling from the metal, through the interfacial layer, into the interfacial surface states. This together with the effects of tunneling, on the thermionic emission currents, and on the photo-generated current will be briefly outlined later in this chapter. Finally, we present a discussion of the validity of the various assumptions made so far.

3.2 Meteorological effects on S.B.S.C's

By applying a diffuse radiation spectrum of incident power density P_{in} (=30mW cm^{-2}) to an n-type silicon Schottky barrier solar cell, and by using the formalism developed in chapter 2, we have obtained a set of results similar to those presented earlier. Owing to the nature of the diffuse spectrum (see figure 3.2) and in the light of the discussion given by Mallinson and Landsberg (1977), one would expect an increase in the conversion efficiency relative to direct radiation.

Although the conversion efficiency increases when a change from direct to diffuse illumination is made, it is clear that the output

power will be much reduced. At first sight, this drop in output power would simply seem to be caused by the decrease in the incident power density, as the spectrum changes from that of direct radiation to one of diffuse radiation. Indeed this is the case, but then we might ask "why does the conversion efficiency tend to increase when the solar cell is illuminated with diffuse radiation instead of direct radiation?" The answer to this question is really quite simple. Forget for the moment, the reduction in the conversion efficiency η^* with decreasing incident power density P_{in} of a particular radiation spectrum. For a device comprising silicon as the photosensitive material, the absorption edge occurs at a wavelength $\lambda_1 = hc/eE_g$, which corresponds to the largest wavelength a photon can have if it is ever to produce a useful electron - hole pair. Now, turning to figures 3.1 and 3.2 we observe that for the direct spectrum, the number of photons incident per unit time having energies less than 1.1 electron volts represents a non-negligible fraction of the total photon flux. On the other hand however, in the case of a diffuse spectrum, nearly all the incident photons are available to generate useful electron-hole pairs. This indicates that a diffuse spectrum enables one to make better use of the radiation. Therefore one expects an increase in the conversion efficiency as the incident spectrum is changed from one of direct to another of diffuse radiation.

Returning now, to the question of the reduction in the conversion efficiency η^* due to a decrease in the incident power density P_{in} of <u>any particular</u> radiation spectrum, we see that this reduction of η^* can be attributed to one basic effect. It is, though somewhat indirectly, the linear reduction of the photo-generated current density J_L with decreasing incident power density.

The open circuit voltage is then slightly decreased, following the reduction in the photo-generated current density J_L [The usual diode equation $J = J_o (\exp (eV/kT) -1) -J_L$, may be used to <u>illustrate</u> this argument for the slight reduction in the conversion efficiency due to a reduction in the incident power density, of a particular radiation spectrum.] It is easily shown that, on one-hand the conversion efficiency increases as a transition from direct to diffuse radiation is made (keeping P_{in} constant) while on the other-hand as the incident power density P_{in} (of a particular radiation spectrum) is reduced the conversion efficiency reduces slightly also. The net effect, is an increase in the overall conversion efficiency as the incident spectrum changes from direct radiation of a high power density, to diffuse radiation of a lower power density.

For the sake of making a meaningful comparison between the diffuse and direct spectra, we compare the J-V characteristics, for any set of Schottky barrier solar cell parameters (e.g., density of interfacial states D_S m^{-2} eV^{-1} and δ the thickness of the insulating interfacial layer) when the incident power densities for the two spectra are the same. It should be noted however that the diode equation given above does not accurately predict the J-V characteristics of an n-type Schottky barrier solar cell with an insulating interfacial layer. This is due to the facts that firstly, the photo-generated current J_L is dependent to a certain extent on the output voltage of the Schottky barrier solar cell. Secondly, the saturation current dens ity J_o will in general be a function of V_i, the portion of the output voltage developped across the interfacial layer, which in turn depends on the output

voltage V. This shows that the standard formula $J = J_o \times (\exp(eV/kT) - 1) - J_L$ which shifts the characteristics by the light current J_L, is not valid.

Using the theory of Chapter 2 for the Au-SiO_2- n-type Si Schottky barrier solar cell together with the parameters of table 1, the only exception being the nature of the incident spectra, we will compare two sets of results. These two sets will be calculated by using a direct spectrum for one, and a diffuse spectrum for the other, both spectra will have an incident power density of 30mW cm^{-2} so that a meaningful comparison can be made.

Figure 3.3 indicates that both the open circuit voltages, and the short-circuit currents are increased for the J-V characteristics obtained from the diffuse spectrum. This shows that more efficient use may be made of a diffuse radiation spectrum than of a direct one (see, for example, Mallinson and Landsberg 1977) Also, in figure 3.3 the increase with the interfacial surface state density D_S (m^{-2} eV^{-1}) of the open-circuit voltage and power output are both due to the increase in the thermodynamic equilibrium barrier height with an increasing density of interfacial surface states D_S. With a low value of the density of interfacial surface states, the contribution to the total current density from the interfacial surface state recombination is negligible. As this interfacial surface state density is increased, the interfacial recombination current density increases to dominate the J-V characteristics, thus causing a reduction in the power output and open-circuit voltage. The J-V characteristics corresponding to diffuse radiation vary in much the same way as the J-V characteristics corresponding to direct radiation, when changes in the interfacial layer parameters (such as the density

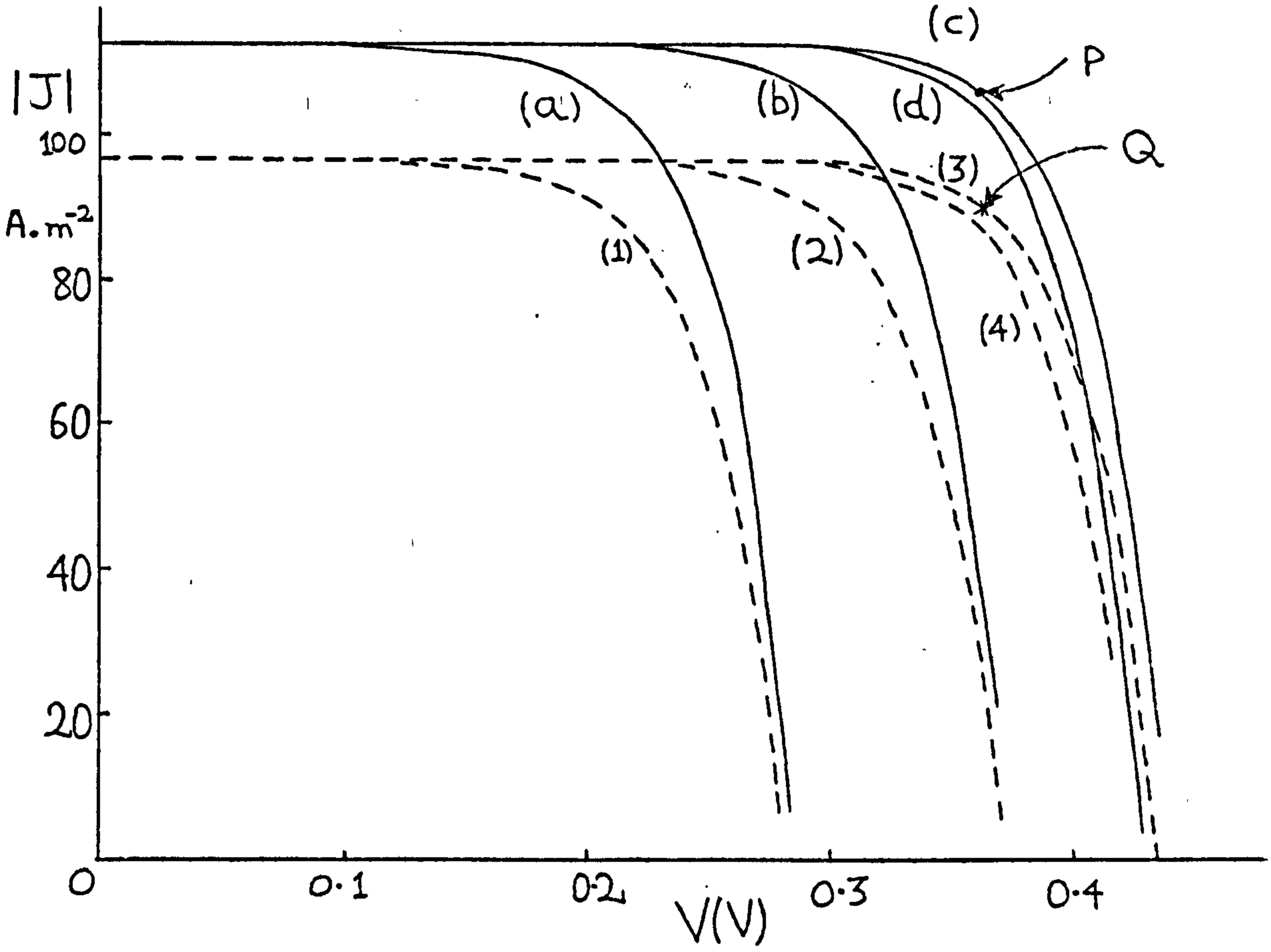

Figure 3.3 The current density-voltage characteristics for various interface state densities D_S m^{-2} eV^{-1}. The parameters of Table 1 have been used together with $\delta = 19$ Å and $\phi_M = 4.70$ (Au) for incident spectra of power (30 mW cm^{-2}). The direct spectrum gives characteristics represented by dashed lines whose maximum attainable conversion efficiency is 10.9% and occurs at point Q. For the diffuse spectrum the maximum attainable conversion efficiency is 12.9% and occurs at point P (full lines).

(1) $D_S = 0.1 \times 10^{18}$ m^{-2} eV^{-1}, (2) $D_S = 0.2 \times 10^{18}$ m^{-2} eV^{-1},

(3) $D_S = 0.5 \times 10^{18}$ m^{-2} eV^{-1}, (4) $D_S = 0.1 \times 10^{19}$ m^{-2} eV^{-1},

(á) $D_S = 0.1 \times 10^{18}$ m^{-2} eV^{-1}, (b) $D_S = 0.2 \times 10^{18}$ m^{-2} eV^{-1},

(c) $D_S = 0.5 \times 10^{18}$ m^{-2} eV^{-1}, (d) $D_S = 0.1 \times 10^{19}$ m^{-2} eV^{-1}.

of interfacial surface states) are made.

In figure 3.4, the increase in conversion efficiency with increasing, but low, density of interfacial surface states D_S ($\sim 10^{17} m^{-2}\ eV^{-1}$) is caused by the rapid increase in the thermodynamic equilibrium barrier height, which in turn attenuates the electron thermionic emission current density. As this density of interfacial surface states is increased the interfacial recombination current density turns from a low order, to a higher order effect which then dominates the current flow mechanisms. At this stage, the advantage of an increase in the thermodynamic equilibrium barrier height, is outweighed by the increasing contribution from the interfacial recombination current density, and the maximum conversion efficiency η^* falls off.

With the interfacial layer thickness δ at the lower of the two values we observe that the thermodynamic equilibrium barrier height increases less rapidly with D_S, than it does for δ at the higher value. This is due to the fact that the thermodynamic equilibrium barrier height tends to become relatively less dependent on the interfacial surface state density D_S, when the insulating interfacial layer becomes as thin as $10\mathring{A}$. Therefore with δ at its lower value ($10\mathring{A}$) we see that the thermionic emission current density J^e_{sm} remains larger than it would for $\delta = 19\mathring{A}$, when the density of interfacial surface states is being held constant. However, the interfacial surface state recombination current density is not greatly affected by a small change in the thermodynamic equilibrium barrier height (see equation 2.5.12), so we therefore expect, and indeed we observe from figure 3.4, that the interfacial

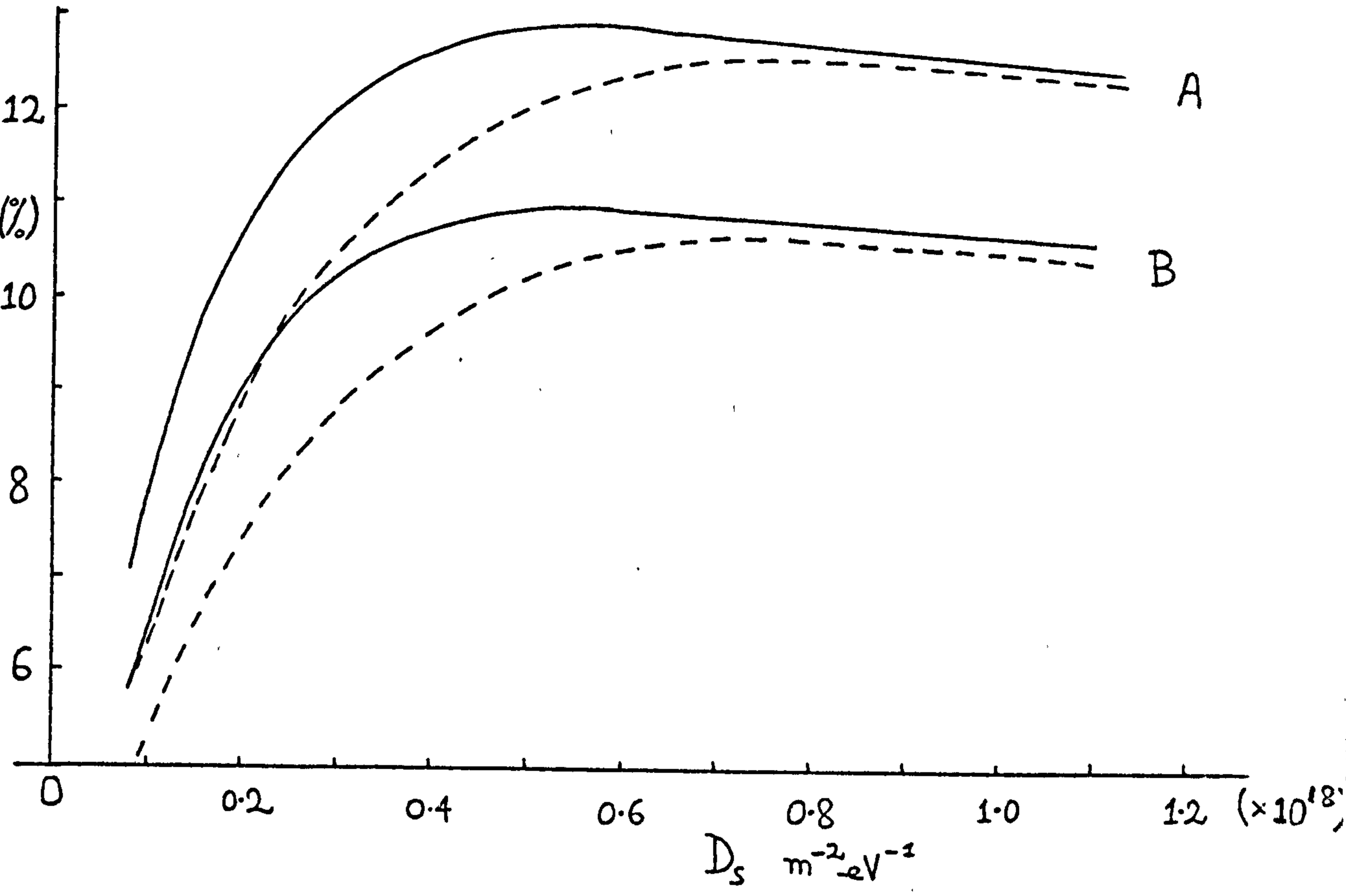

Figure 3.4 The maximum conversion efficiency as a function of interfacial state density D_S. The parameters of Table 1 have been used together with ϕ_M = 4.70 eV (Au) and δ = 19 Å (full lines), δ = 10 Å (dashed lines). An incident power density of 30 mW cm^{-2} has been used and efficiencies for diffuse spectra have been labelled A while those for the direct spectra have been labelled B.

surface state recombination acts in a manner virtually irrespective of interfacial layer thickness. Thus the maximum attainable conversion efficiency increases with interfacial layer thickness within the range between 10 and 20 $\mathring{A}$. Again it is observed that for an n-type silicon Schottky barrier solar cell, the efficiency is enhanced when the cell is illuminated with diffuse radiation of power equivalent to that of the direct spectrum used formerly.

Turning now to figure 3.5, we observe that at high interfacial surface state densities D_S the variable metal-work function has a very small affect on the maximum conversion efficiency η^*. This is because at high interfacial surface state densities, the barrier height is only slightly increased with an increase of metal work function. Conversely with lower interfacial surface state densities the barrier height increases rapidly with metal work function ϕ_M. Also there is less interfacial surface state recombination with the lower values of D_S (m^{-2} eV^{-1}) so that the maximum attainable conversion efficiencies are improved as shown. Here again we observe that higher conversion efficiencies are possible when the solar cell is illuminated with diffuse, instead of direct radiation.

To sum up, the effect of the direct as against the diffuse spectra has been exhibited in figures 3.3 to 3.5. The obvious disadvantage of diffuse radiation is its low intensity. However the diffuse spectrum being more compact, enables one to make better use of this radiation. In the graphs we have standardised on one incident power density (30mW cm^{-2}), thus shielding the results from the first disadvantage. This must be borne in mind when studying the figures. As expected from the remarks made earlier, for given incident power the output power is greater for

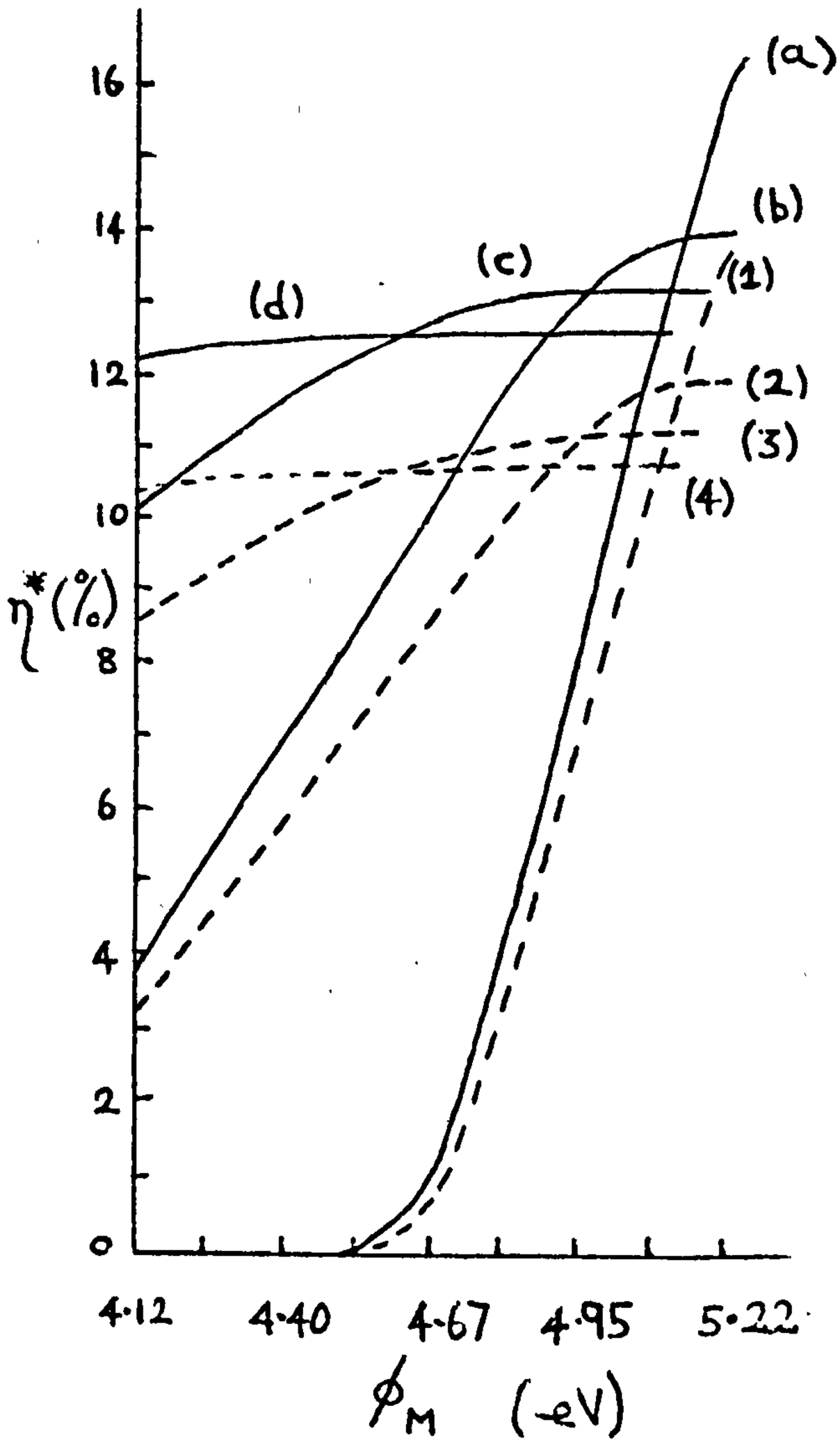

Figure 3.5 The maximum conversion efficiency as a function of metal work function ϕ_M for various interface state densities D_S. The parameters of Table 1 have been used together with $\delta = 19$ Å, and incident spectra, direct (dashed lines), diffuse (full lines), both of power 30 mW cm^{-2}

(1) and (a) $D_S = 0.1 \times 10^{17}$ m^{-2} eV^{-1}

(2), (b) $D_S = 0.2 \times 10^{18}$ m^{-2} eV^{-1}

(3), (c) $D_S = 0.5 \times 10^{18}$ m^{-2} eV^{-1}

(4), (d) $D_S = 0.9 \times 10^{18}$ m^{-2} eV^{-1}

diffuse radiation. Apart from this (expected) conclusion, one observes that the efficiency depends on cell parameters in much the same way for both incident spectra. It is possible that the substrate thickness could have a bearing on all these calculations. The extra complications involved by introducing a finite substrate thickness would not be difficult to deal with, but in the light of there being many simplifications inherent in this model it was felt that such a refinement would not greatly enhance the state of present knowledge.

3.3 The Short-comings of the theory.

Probably, one of the most serious oversights of the theory developed in chapter 2, was the neglect of any direct communication between the interfacial surface states and the metal. According to Card and Rhoderick (1972), the interfacial surface states tend to equilibrate with the metal when $\delta \lesssim 20\text{Å}$ and consequently the direct communication between the surface states and the metal will be important. This omission will however, be rectified in the later chapters. In order to achieve this goal without introducing a single quasi-Fermi level for the interfacial surface states (see, for example Fonash 1975a), we will introduce the tunneling time constant. This will enable us to take full account of the influence the metal's proximity has upon the interfacial surface state population. The tunneling time constant is a function of both the interfacial surface state energy, although this turns out to be rather a weak dependence, and the interfacial layer thickness δ. Physically, the tunneling time constant represents the average time a carrier, at some interfacial surface state energy, takes to tunnel through the interfacial layer. The two band model of the tunneling time constant mentioned in the

introduction will be developed in chapter 4, and the revised interfacial surface state occupation model will be presented early in chapter 6. We would expect the interfacial surface state population to be strongly controlled by the metal Fermi level when the interfacial layer is extremely thin. Conversely for thick interfacial layers we would expect the population of the interfacial surface states to be controlled almost completely by the carriers at the interface x = o, in accordance with (2.4.19).

The neglect of the attenuation of both the thermionic emission and the photo-generated current densities due to tunneling through the interfacial layer have caused both $(J^e_{sm} - J^e_{ms})$ and J_L to be overestimated in (2.5.24). Even though the tunneling barrier is approximately rectangular, thereby indicating that the W.K.B.approximation may in fact never be valid, it is commonly invoked to give some indication of the tunneling attenuation to be expected.

We now turn to the assumptions regarding the potential drop across the bulk region, and the variation of the quasi-Fermi levels within the so called depletion layer. The potential drop across the bulk region may well be virtually insignificant for finite substrate thicknesses. Also, the electric field in the bulk region is usually assumed to be approximately constant. In fact the potential drop across the bulk region will be of the order $L.J/(en\mu_n)$ volts, for an n-type substrate with J as the current density, L as the thickness of the semi-conductor region, n as the electron concentration in the bulk region and μ_n as the electrons mobility. For small L and large n and μ_n the potential drop across the bulk will be negligible when compared with the potential drop across the so called depletion layer.

However, for an 'infinite' substrate thickness, the above relation would certainly predict an 'infinite' potential drop across the bulk region. To overcome this apparent absurdity we shall, when referring to an 'infinite' bulk region, mean that the bulk region is very much thicker than the depletion layer, such that near the back contact the electron and hole concentrations vary only very slightly with position. Also, the bulk thickness L must be sufficiently low, so that the order of the potential drop across the bulk region $LJ/(en\mu n)$,remains small compared with the potential drop across the depletion layer, and yet, the substrate must be of sufficient thickness to ensure that nearly all of the useful radiation is absorbed in accordance with (2.5.22). In practice such a compromise is easily found.

In all of our work we have assumed a constant doping profile. This essentially means that the majority carrier quasi-Fermi level in the bulk region remains approximately parallel to the band edge. The assumptions regarding the quasi-Fermi levels in the 'so called' depletion layer (see section 2.4) may not be completely valid, especially when the Schottky barrier is operating under illumination. In particular these assumptions are likely to become increasingly unreliable for the case of strong illumination, i.e., when drastic changes in the magnitudes of the electron and hole current densities occur over small distances close to the interface $x = 0$ (Note that the greater part of the radiation spectrum will usually be absorbed in the depletion layer in accordance with equation (2.5.17)).

The theory previously developed in chapter 2 depends strongly on the depletion approximation: which assumes that all the free carriers are "stripped out" of the depletion layer by the high

electric field present, so that the volume charge density is just eN_D (instead of $e(p - n + N_D)$) in the depletion layer, and zero ($0 = e(p-n+N_D)$) in the bulk region. Apart from the obvious falseness of this assumption for the case of moderate forward bias (where the carrier concentrations can often approach or sometimes even exceed the doping concentration N_D i.e. inversion layer conditions), we shall, in due course show that the usual concept of the depletion layer edge leads to a contradiction. Therefore we will deduce that the volume charge density is non-zero everywhere in the semi-conducting region, except perhaps at an ohmic contact where the volume charge density may actually equal zero at one point x only. The last remark to be made before going on to discuss the volume charge density, is that in all of the above work we have assumed that all the donor states are completely ionized. This assumption, among the others outlined above, will be removed entirely within the context of the formalism developed later in chapters 5 and 6.

3.4 The examination of the volume charge density within the semiconductor.

In this section we shall examine the so called bulk region of the semiconductor when a total steady current density J is flowing. According to the depletion approximation, we shall set the volume charge density $\rho(x)$ equal to zero everywhere in the bulk region, then by Poissons equation we deduce that the electric field E in the bulk region is a constant with respect to position. Without loss of generality we shall restrict ourselves to the case of an n-type bulk region. For the minority carriers (holes in the n-type bulk) we can rewrite the continuity equation as

$$D_p \frac{d^2p}{dx^2} - \mu_p E \frac{dp}{dx} - \frac{p-p_o}{\tau_p} + \alpha\Phi e^{-\alpha x} = 0, \qquad (3.4.1)$$

by using equations (2.5.6), (2.2.8) and (2.5.17) for monochromatic radiation. The general solution of this equation is easily found to be

$$(p - p_o) = A \exp(X_1 x) + B \exp(X_2 x) - \frac{\alpha \Phi \exp(-\alpha x)}{\{\alpha^2 + \alpha\mu_p E/D_p - 1/L^2{}_p\}} \qquad (3.4.2)$$

$$\text{with } X_1, X_2 = \frac{\mu_p E}{2D_p} \pm \sqrt{\left\{\left(\frac{\mu_p E}{2D_p}\right)^2 + \frac{1}{L_p^2}\right\}} \in \mathbb{R} \quad . \qquad (3.4.3)$$

Clearly the constants of integration A and B would be fixed by the usual boundary conditions at the ohmic contact, and at the edge of the depletion layer. Suppose that the ohmic contact occurs at position x = L and the edge of the depletion layer is at x = w. We therefore write the boundary conditions as

(1) $p = p_o$ at $x = L$, (This corresponds to an infinite back wall surface recombination velocity).

(2) $p - p_o = p^*$ at $x = w$, where p^* is the excess concentration of holes at the edge of the depletion layer and will in general be a function of illumination and output voltage.

Application of these two boundary conditions yields for A and B, the expression

$$\begin{pmatrix} A \\ B \end{pmatrix} = \frac{1}{e^{(X_1 w + X_2 L)} - e^{(X_2 w + X_1 L)}} \begin{pmatrix} e^{X_2 L} & -e^{X_2 w} \\ -e^{X_1 L} & -e^{X_1 w} \end{pmatrix} \begin{pmatrix} p^* + Ce^{-\alpha w} \\ Ce^{-\alpha L} \end{pmatrix} \qquad (3.4.4)$$

$$\text{with } C = \frac{\alpha\Phi}{\{\alpha^2 + \alpha\mu_p E/D_p - \frac{1}{L^2{}_p}\}} \quad .$$

As mentioned earlier (in section 3.3), we assume that L (the total thickness of the substrate) is large enough to allow the quasi-Fermi levels E_{Fn} and E_{Fp} to come together gradually as they approach the back surface (i.e. the ohmic contact), see figure 3.6. We may therefore take the slopes of the electron and hole quasi-Fermi levels to be equal to that of the band edge near the ohmic contact, by assuming a constant ionized doping profile. Hence the total current density J flowing through the device is given by

$$J = e(n_o\mu_n + p_o\mu_p)\,E = \sigma E, \qquad (3.4.5)$$

where n_o and p_o are respectively, the equilibrium electron and hole concentrations near the ohmic contact. For our purpose we shall assume that at an ohmic contact the carrier concentrations take their respective bulk equilibrium values, however see below. Further we may express the electric field E (Vm^{-1}) as

$$E = \frac{J}{e(n_o\mu_n + p_o\mu_p)}, \begin{cases} <o \text{ if the n-type S.B.S.C is delivering power.} \\ >o \text{ if the n-type S.B.S.C is absorbing power.} \end{cases} \qquad (3.4.6)$$

If a p-type substrate were used in the same configuration as that described for the n-type Schottky barrier solar cell, then the inequalities above would be reversed.

The important basic assumptions made so far are that the donors are fully ionized, the electron and hole mobilities (μ_n and μ_p respectively) are constant with respect to position, and the volume charge density is zero in the bulk region of the semiconductor. Firstly, the volume charge density ρ (x) having been set to zero gives

$$\rho(x) = p - n + N_D = 0 \quad \text{and} \quad \frac{dn}{dx} = \frac{dp}{dx} \qquad (3.4.7)$$

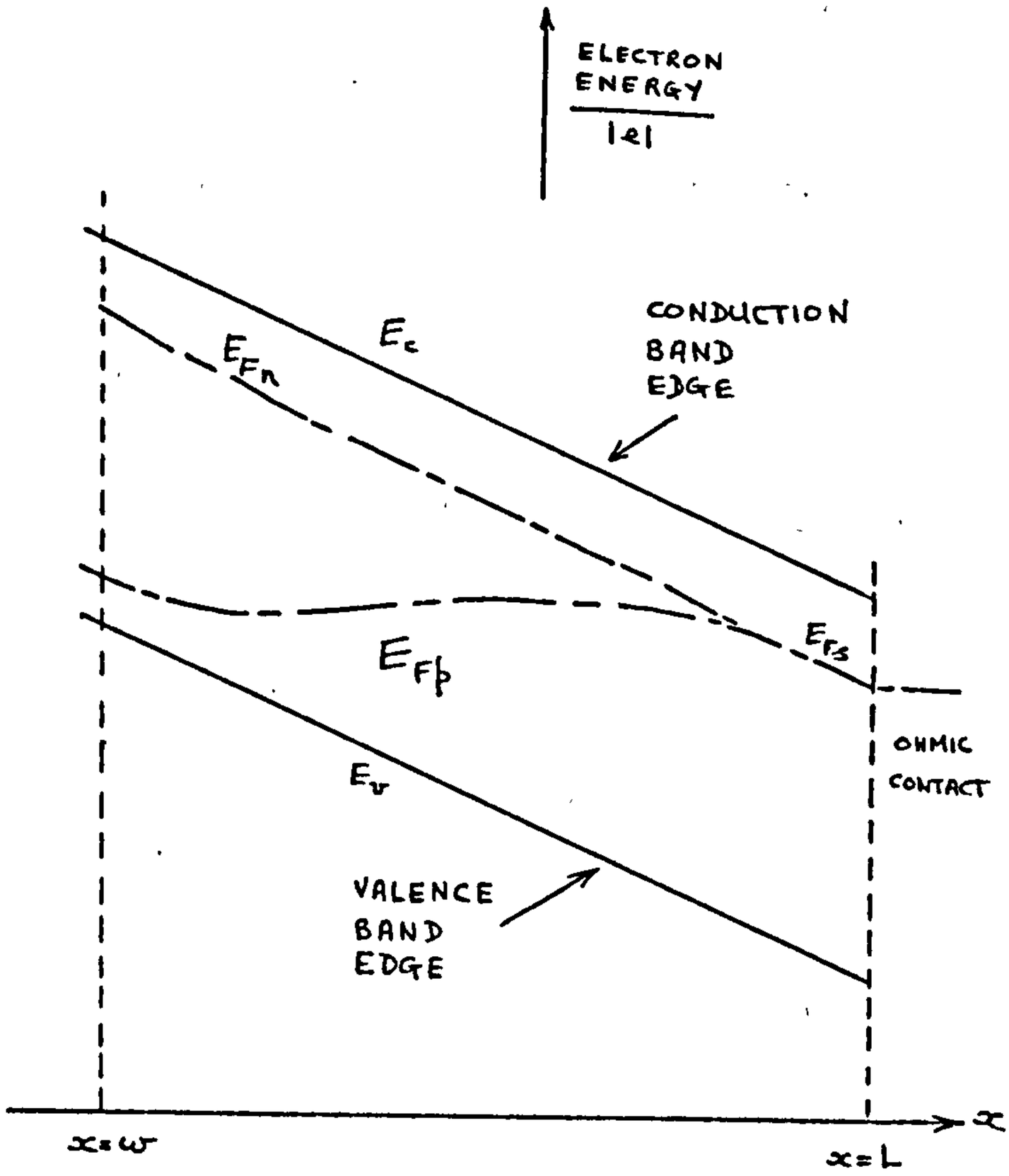

Figure 3.6 Diagram illustrating an ohmic contact to an n-type semiconductor. The edge of the depletion layer is at $x = w$ while the ohmic contact is at $x = L$.

by the assumption of a constant and fully ionized doping profile. Secondly, application of equations (2.2.8) and (2.2.9) together with (3.4.7) gives the total current density J as

$$J = e\left\{ (D_n - D_p)\frac{dp(x)}{dx} + \mu_p\, pE + \mu_n\,(p + N_D)\,E \right\} \qquad (3.4.8)$$

$$= e\left\{ (D_n - D_p)\frac{dp(x)}{dx} + pE\,(\mu_p + \mu_n) - \mu_n\, N_D\, E \right\}, \quad x\varepsilon[w,L]$$

From equation (3.4.6) we observe that, for some value J of the total current density, the electric field E is fixed, and furthermore E is held at this fixed value throughout the bulk region according to Poisson's equation $\frac{dE}{dx} = \rho(x)$, with $\rho(x) = 0$. Substitution of (3.4.2) for the variation of the hole concentration with position in the bulk region, into equation (3.4.8) yields an expression for the total current density J in terms of the multipliers $\exp(X_1 x)$, $\exp(X_2 x)$ and $\exp(-\alpha x)$. Now remembering that the total current density J must be independent of position x, and by also observing that the multipliers $\exp(X_1 x)$, $\exp(X_2 x)$ and $\exp(-\alpha x)$ are linearly independent as $(X_1 \neq X_2) \neq \alpha$, then the coefficient of each multiplier must be zero. Thus we have

$$X_1\,(D_n - D_p) + E\,(\mu_n + \mu_p) = 0,$$

$$X_2\,(D_n - D_p) + E\,(\mu_n + \mu_p) = 0,$$

and $$\alpha\,(D_n - D_p) + E\,(\mu_n + \mu_p) = 0.$$

for linear independence, when $x\varepsilon\ [w,L]$. As E, μ_n and μ_p are constants with respect to position we have found a contradiction. Therefore the original postulate was incorrect, and we deduce that the volume space charge density is not zero everywhere in the bulk region of the semiconductor.

An ohmic contact is one which supplies a reservoir of carriers to enter the bulk material as needed. Usually the energy bands bend downwards at an ohmic contact to an n-type semi-conductor, and conversely they bend upwards at an ohmic contact to a p-type semi-conductor. The space charge so produced, in the vicinity of the ohmic contact, is of opposite sign to the space charge near the Schottky barrier. It is therefore clear that the volume charge density ρ (x) changes its sign as we move from one contact to another, or at least ρ (x) tends towards zero as the ohmic contact is approached from within the semiconductor, if we have the special case of no band bending near the ohmic contact. [This can be achieved theoretically by choosing a metal (for the ohmic contact) whose work function is the same as the work function of the bulk semiconductor]. The main properties of an ohmic contact (for the present discussion) are that (a) it can always supply more carriers than the bulk material can carry under given applied potential, and (b) it produces an insignificant amount of energy band bending in the vicinity of the ohmic contact. An ohmic contact, therefore, cannot give any photo-emission current because the number of carriers which the metal supplies to the semiconductor is already more than the material can carry, and no increase in the current density results if still more carriers are supplied by photoexcitation.

To sum up, we have found that the volume space charge density $\rho(x)$ is not zero everywhere in the bulk region of the S.B.S.C. To all intents and purposes $\rho(x)$ may be taken as zero only at the ohmic contact (of course a fuller treatment would certainly consider the accumulation region produced in the bulk semiconductor near the ohmic contact) if the accumulation region so produced is negligibly small. The formalism developed in chapters 5 and 6 use this assumption. The generalization of this more general formalism to consider the ohmic contact more precisely is a relatively simple task, but in view of the complexity of this formalism, this effect has not been given serious attention. Again, it is emphasised that the concept of a depletion layer edge, based on the usual assumptions of a zero volume charge density $\rho(x)$ in the bulk region and non-zero $\rho(x)$ in the region of the Schottky barrier (depletion layer), turns out to be contradictory. Therefore the formalism of chapters 5 and 6 will not use any notion of two distinct regions. The volume charge density will be allowed to vary continuously from zero to some positive value near the rectifying contact in case of an n-type Schottky barrier solar cell.

Here we have outlined all of the major assumptions made so far. We have discussed their validity; some assumptions i.e. constant mobilities w.r.t. position, seem at first sight to be reasonable, while others such as the depletion approximation and the assumed quasi-Fermi levels of negligible slope within the so called depletion layer may not be so profound. To this end the formalism of chapters 5 and 6 will set out to give a description of the Schottky barrier solar cell without the need to appeal to any of these weakly founded assumptions.

CHAPTER 4

THE INTERFACIAL SURFACE STATE TUNNEL TIME CONSTANT

4.1 Introduction

As mentioned before in Chapter 3, there is a serious defect in the already existing theory of Chapter 2. This was the neglect of any direct communication between the interfacial surface states and the metal. This oversight will be corrected in Chapter 6, but first the concept of a tunneling time must be introduced. Physically, the tunneling time constant represents the mean time a carrier (at some interfacial surface state energy) takes to tunnel through the insulating interfacial layer. With this tunneling time constant, we will, in Chapter 6, develop the theory of the statistics of the interfacial surface states to include the effects of direct communication between these surface states and the metal. Only in this way, can we take account of the effect the metals proximity has upon the interfacial surface state population, and the interfacial surface state recombination currents. Of course, there will be an extra current path, due to the direct tunneling of carriers to and from the interfacial surface states. This will mean that the recombination rates involving the semiconductors conduction and valence bands will no longer be equal in steady state situations, however see Chapter 6 below.

The work of Lundström and Svensson (1972) will be generalized in this chapter, to deal with the two band problem. This generalisation is necessary to give the correct form of the tunneling time constant, for tunneling between the metal and interfacial surface states near the

valence band edge of the semiconductor. For an n-type Schottky barrier solar cell this would be very important because interfacial surface states near the valence band edge may carry part of the photo-generated current. The photo-generated holes would tend to build up in the semiconductor's valence band adjacent to the insulating interfacial layer, consequently some of these holes will tunnel from the semiconductor's valence band directly into the metal, while the others will recombine at the surface states with either electrons from the semiconductor's conduction band or electrons tunneling from the metal to the interfacial surface states. The latter process represents an additional useful current path, while the recombination of the photogenerated holes with electrons from the semiconductor's conduction band, at the interfacial surface states, represents a loss mechanism. The above comments apply to an n-type Schottky barrier solar cell, similar statements may be made for a p-type Schottky barrier solar cell.

Before going on to perform this generalization, some basic theory of semiconductor band structure, crystal momentum and effective masses is presented. The golden rule of transition probabilities is then established using perturbation theory. After this we will study the tunneling of electrons between the conduction band of a metal and a trap (interfacial surface state) in the band gap of an insulator. The trap is characterised by a δ-function potential in three dimensions. The direct tunneling probability for a metal conduction band electron to the ground state of a trap located at a distance δ from the metal surface is derived using Bardeen's method (see for example Kane (1969)). Then on similar lines we will study the tunneling of holes between the conduction band of the metal and an interfacial surface state in the insulator. This trap is also characterised by a δ-function potential in 3-D at a distance

δ from the metal surface. Eventually we will construct the expression for the net transition rate due to both electron and hole tunneling between the metal's conduction band and an interfacial surface state. This immediately gives us an expression for the net tunneling time constant. Incidentally, it turns out that the net tunneling time constant has rather a weak dependence on the energy of the interfacial surface state.

4.2 Band Structure , Crystal Momentum and Effective Mass.

In a crystal lattice there exists a periodic potential due to the systematically arranged array of atomic sites. This periodic potential gives rise to bands of allowed and forbidden energies in a solid. The exact form of the Energy band $E_n(\underline{k})$ curves depends in some detail on the actual three dimensional crystal structure (see for example Landsberg 1969). The appropriate wave function for an electron in a periodic potential is a Bloch function $\psi_{nk}(\underline{r})$: a plane wave $e^{i\underline{k}.\underline{r}}$ modulated by a periodic function $u_{n\underline{k}}(\underline{r})$ with the periodicity of the crystal. The square of the amplitude of such a Bloch wave function is the same at points in the crystal separated by a lattice vector $\underline{R}$. The wavefunction itself differs at two such points only by the appropriate phase factor. Since the form of the Bloch function is not affected if $\underline{k}$ (the wave vector which is related to the energy and the momentum) is increased by a reciprocal lattice vector $\underline{K}$, it is possible to describe all the energy bands within a basic range of $\underline{k}$ values, called the basic Brillouin zone. A state specified by some general wave vector $\underline{k}$ can be specified by a band number n and the reduced wave vector lying in the basic Brillouin zone. Also it is known that the function $E_n(\underline{k})$ always has zero slope at the edges of the allowed bands.

The crystal momentum $\hbar\underline{k}$ represents the motion of a perfectly free electron. As the energy of the electron in the crystal increases (the

particle thereby becoming more nearly "free") the values of $\underline{k}$ in general (near the middle of the allowed band) approximate those of the free particle momentum divided by $\hbar$. It is clear that these conclusions must hold no matter what form the periodic potential takes, see McKelvey (1966). To make the distinction between the actual momentum and the crystal momentum, we must note that due to the presence of the periodic lattice potential, the true <u>instantaneous</u> momentum of an electron is not a constant of the motion and is not directly calculable by the methods of quantum mechanics, except as an average value (in the form of the velocity of a Bloch electron).

The time dependent Bloch functions $\psi_{n\underline{k}}(\underline{r},t)$ are obtained by multiplying the time independent ones $\psi_{nk}(\underline{r})$ by a factor $\exp\left[-\,i\,E_n(\underline{k})t/\hbar\right]$, as usual. Hence $\psi_{n\underline{k}}(\underline{r},t)$ is given by

$$\psi_{n\underline{k}}(\underline{r},t) = \psi_{n\underline{k}}(\underline{r})\; e^{-iE_n(\underline{k})t/\hbar} \qquad (4.2.1)$$

A wave packet $\psi(\underline{r},t)$ of Bloch functions (of a band n) with amplitude function $a(\underline{k})$ can be used to represent a Bloch electron in the state $(n,\underline{k})$. This wave packet may be written as

$$\psi(\underline{r},t) = \int_{\Omega'} a(\underline{k})\; \psi_{n\underline{k}}\;(\underline{r},t)\; d\underline{k} \qquad , \qquad (4.2.2)$$

where Ω' represents the volume of the unit cell in the reciprocal lattice (or the basic Brillouin zone). In general the wave packet will have a strong maximum at some wave vector $\underline{k}_m$ say, so that we may expand $E_n(\underline{k})$ as

$$E_n(\underline{k}) = E_n(\underline{k}_m) + \underline{\xi}.\nabla_{\underline{k}}\left[E_n(\underline{k})\right]_{\underline{k}=\underline{k}_m} + \ldots\ldots \qquad , \qquad (4.2.3)$$

where $\underline{\xi} = \underline{k} - \underline{k}_m$. Now if we assume that $u_{n\underline{k}}(r)$ varies sufficiently slowly with $\underline{k}$ so that it can be taken out of the integral and by also assuming $\underline{\xi}$ is small for all important $\underline{k}$, then $\psi(\underline{r},t)$ is given by

$$\psi(\underline{r},t) = u_{n\underline{k}_m} e^{i\left[\underline{k}_m \cdot \underline{r} - E_n(\underline{k}_m)\, t/\hbar\right]} \int_{\Omega'} a(\underline{k}) e^{i\left[\underline{r} - \nabla_{\underline{k}} E_n(\underline{k})\Big|_{\underline{k}_m} t/\hbar\right] \cdot \underline{\xi}} d\underline{k}$$

$$= \psi_{n\underline{k}_m}(\underline{r},t) \cdot A \quad , \tag{4.2.4}$$

where A is the wave packets amplitude and thus determines the group behaviour. The amplitude A varies more slowly than $\psi_{n\underline{k}_m}(\underline{r},t)$ and therefore the wave packet has constant amplitude at points $\underline{r}$ satisfying $\underline{r} - \nabla_k E_n(\underline{k})\Big|_{\underline{k}_m} t/\hbar = \text{constant}$.

Hence the group velocity is given by

$$\dot{\underline{r}} = \hbar^{-1} \left[\nabla_{\underline{k}} E_n(\underline{k})\right]\Big|_{\underline{k}_m} . \tag{4.2.5}$$

We will associate this velocity with that of the Bloch electron. Therefore the velocity of a Bloch electron in the state $(n,\underline{k})$ is given by

$$V_{n\underline{k}} = \hbar^{-1} \nabla_{\underline{k}} E_n(\underline{k}) \quad . \tag{4.2.6}$$

The electrical conductivity of a material with a partially filled conduction band can be conveniently described in terms of the current associated with the electrons in that band. Thus the current density obtained when a small voltage is applied is given by

$$J = -n e \bar{v} = -\frac{e}{V} \sum_i v_i \quad , \tag{4.2.7}$$

where n is the electron concentration in the band, $\bar{v}$ is the average electron velocity, v_i is the velocity of an electron labeled by a suffix i, and finally V is the volume of the crystal.

If, however, the band is nearly full except for a few empty states near the top of the allcwed band, the current density equation can then be expressed in another way

$$J = -\frac{e}{V}\sum_i v_i = -\frac{e}{V}\left\{\sum_j v_j - \sum_k v_k\right\} = \frac{e}{V}\sum_k v_k \qquad (4.2.8)$$

Here i represents the sum over <u>all velocity states occupied</u> by electrons, the sum over j represents the sum over <u>all</u> the velocity states in the band and the sum over k represents the sum over <u>all unoccupied</u> velocity states. Owing to the symmetry of the $E_n(\underline{k})$ curves about the energy axis, we see that for every state of positive velocity $\frac{1}{\hbar}\nabla_{\underline{k}}E_n(\underline{k})$ corresponding to a point of positive slope, there exists a state corresponding to a negative velocity of equal magnitude (a point with negative slope). Therefore the sum $\sum_j v_j$, for <u>all</u> the velocity states in a band must be zero. It is possible to consider the conductivity in a nearly full band in terms of the motion of equivalent particles with a positive charge; these equivalent particles are called holes. A hole is associated with an unoccupied electronic state and must not be confused with a vacancy, an empty atomic or ionic state. Hole energies are measured in an opposite sense to electron energies, because electrons and holes, having charges of equal magnitude but opposite in sign, are both subject to the same electrostatic potential in an allowed band.

Figure 4.1 shows an energy band curve represented both on an electron energy scale $E_n(\underline{k})$ with respect to an electron wave vector $\underline{k}$ and on a hole energy scale $E_h(\underline{k}')$ with respect ot the hole wave vector $\underline{k}'$. Let $\underline{k}_1$ and $\underline{k}_1'$ be respectively the electron and hole wavevectors representing the state P. Then we have from Figure 4.1

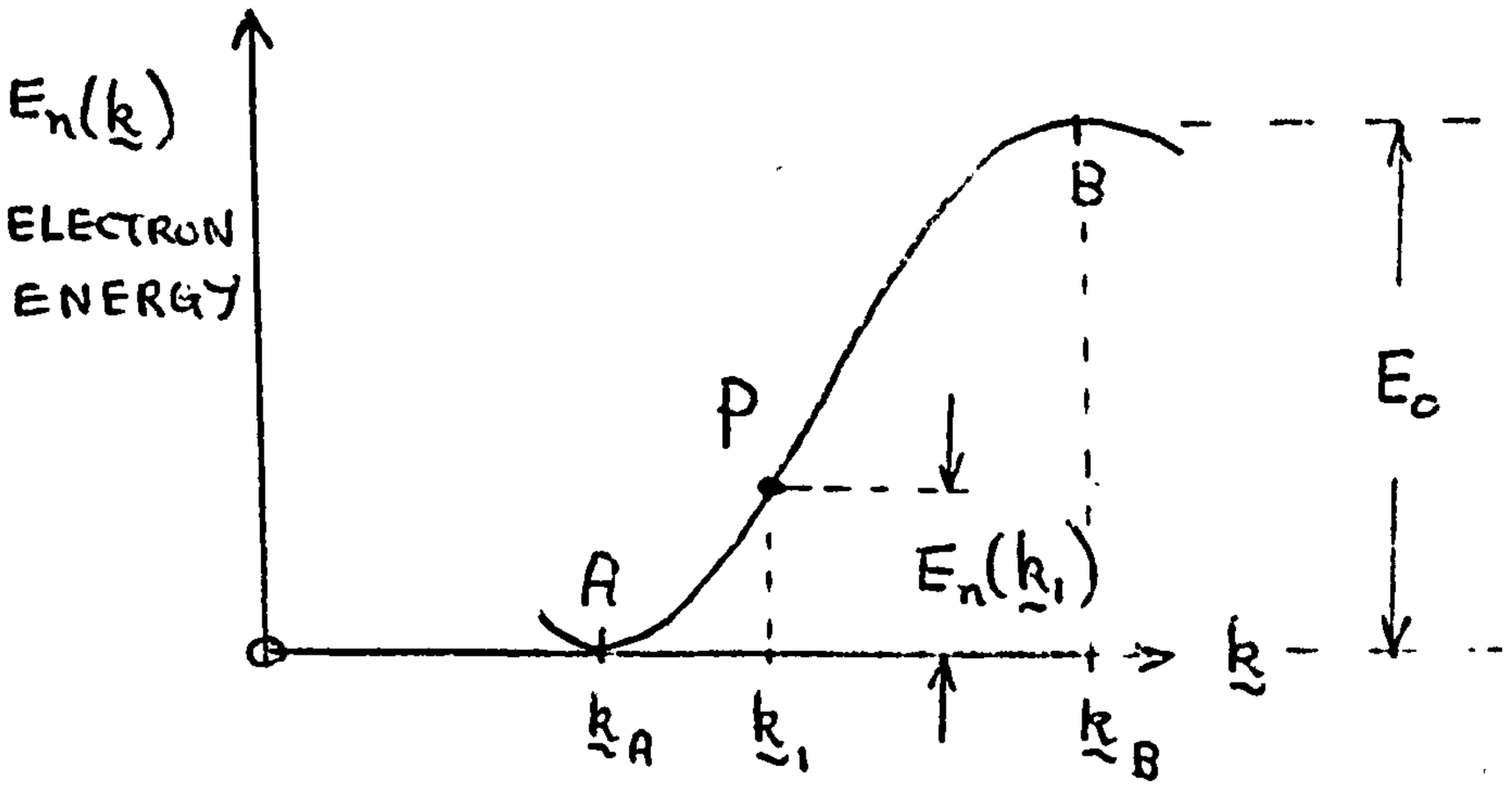

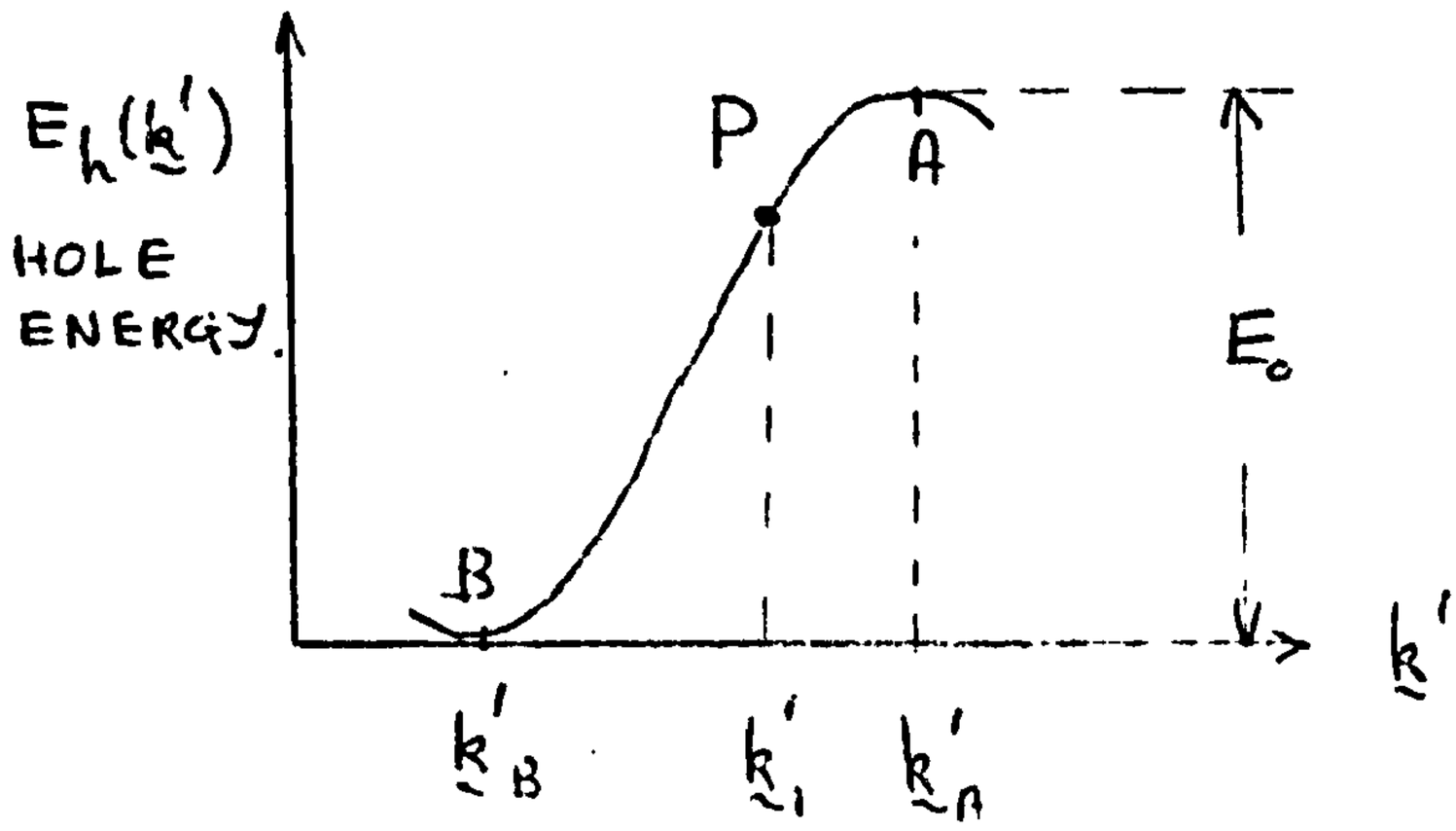

Figure 4.1 Energy band curve represented both, on the electron energy scale $E_n(\underset{\sim}{k})$ with respect to the electron wave vector $\underset{\sim}{k}$, and on the hole energy scale $E_h(\underset{\sim}{k}')$ with respect to the hole wave vector $\underset{\sim}{k}'$.

$$E_n(\underline{k}_1) + E_h(\underline{k}_1') = E_n(\underline{k}_B) = E_h(\underline{k}_A') = E_o(\text{constant}) \qquad (4.2.9)$$

and $\underline{k}_B - \underline{k}_A = \underline{k}_A' - \underline{k}_B'$.

For the sake of simplicity we shall take a common $\underline{k}$ origin at A (see figure 4.1), so that we may write $\underline{k} = -\underline{k}'$.

Now following Landsberg (1969) we may write the tensorial effective mass as

$$\left(\frac{1}{m}\right)_{ij}^{n\underline{k}} = \hbar^{-2} \frac{\partial^2 E_n(\underline{k})}{\partial k_i \, \partial k_j} \quad , \qquad (4.2.10)$$

which when used in conjunction with the expression for the acceleration $\underline{a}_{n\underline{k}}$ in terms of the accelerating force $\underline{F}$, shows that the acceleration is not always parallel to the applied force. The acceleration $\underline{a}_{n\underline{k}}$ is given in component form by

$$(\underline{a}_{n\underline{k}})_i = \sum_{j=1}^{3} \left(\frac{1}{m}\right)_{ij}^{n\underline{k}} F_j \qquad (4.2.11)$$

The tensorial effective mass of an electron at the state P is given by

$$\left(\frac{1}{m}\right)_{ij}^{n\underline{k}} = \hbar^{-2} \frac{\partial^2 E_n(\underline{k})}{\partial k_i \, \partial k_j} \quad , \qquad (4.2.12)$$

and the tensorial effective mass of a hole in the state P is given by

$$\left(\frac{1}{m}\right)_{ij}^{n\underline{k}'} = -\hbar^2 \frac{\partial^2 E_h(\underline{k}')}{\partial k_i' \, \partial k_j'} \quad . \qquad (4.2.13)$$

Using equations (4.2.12) and (4.2.13) in conjunction with (4.2.9), we observe that the effective mass of an electron in some state P, is the negative of the effective mass of a hole, if this hole were present at the state P instead of the electron.

We will now examine the velocities of electrons and holes when they occupy the state P in turn. To do this, suppose that an electric field $\underline{E}$ is imposed, then for an electron in the state P the force $\underline{F}$ is equal to $-|e|\underline{E}$ which implies that the acceleration of the electron is given by

$$(a_{n\underline{k}})_i = -|e| \sum_{j=1}^{3} \left(\frac{1}{m}\right)^{n\underline{k}}_{ij} E_j \quad , \tag{4.2.14}$$

Similarly for a hole occupying the state P, the force $\underline{F}$ is equal to $|e|\underline{E}$ which then implies that the acceleration of the hole is exactly equal to that of the electron because, as mentioned before, the effective mass of a hole at the state P is the negative of the electron's effective mass at the same state P. The velocity of an electron $v_{n\underline{k}}$ $(= \hbar^{-1}\nabla_{\underline{k}} E_n(\underline{k}))$ in the state $(n,\underline{k})$ is clearly the same as that for a hole $v^h_{n\underline{k}'}$ in the same state $(n,\underline{k}')$ i.e.

$$v^h_{n\underline{k}'} = \hbar^{-1} \nabla_{\underline{k}'} E_h(\underline{k}') = \hbar^{-1} \nabla_{\underline{k}} E_n(\underline{k}) = v_{n\underline{k}} \quad . \tag{4.2.15}$$

Therefore the current due to a band with a single unoccupied state P must be the negative of the current due to a band with a single occupied state P.

Suppose that we have a band maximum B at $\underline{k}_o$, figure 4.1 may be used if one imagines the energy axes translated to position A, then assuming spherical surfaces of constant energy in $\underline{k}$-space near $\underline{k}_o$ the electron band energy is given by

$$E_n(\underline{k}) = E_n(k_o) + \frac{\hbar^2}{2m_j} (\underline{k} - \underline{k}_o)^2 \quad , \tag{4.2.16}$$

where $m_j < 0$ is the scalar effective mass of an electron near a band maximum. The electron velocity near an electron band maximum B would then be given by

$$\underline{v}_{n\underline{k}} = \frac{1}{\hbar} \nabla_{\underline{k}} E_n(\underline{k}) = \frac{\hbar}{m_j} (\underline{k} - \underline{k}_o) \quad , \qquad (4.2.17)$$

which gives the Bloch electron momentum as $\hbar(\underline{k} - \underline{k}_o)$. Similarly the hole momentum may be found as $\bar{h}(\underline{k}' - (-\underline{k}_o))$ near a hole band minimum B (see Figure 4.1). Remembering now that the wave vector $\underline{k}'$ for a hole state must be the negative of the $\underline{k}$ of the missing electron state, we deduce that the hole momentum near the point B is $\bar{h}(\underline{k}_o - \underline{k})$. Therefore the momentum of a hole is the negative of the missing electron's momentum in the state near the electron band maximum. Note that the crystal momentum is just $\hbar\underline{k}$.

4.3 The Golden Rule of Transition Probabilities

The Golden rule of transition probabilities is a very well known result, its derivation has been presented to clarify the exposition. In this section time dependent perturbation theory will be used to determine the transition probability per unit time. We assume that the Hamiltonian of the system can be written in the form $H = H_o + H'$, where H' represents a perturbing term which is small compared with H_o. H' does not contain the time explicitly. H_o is the unperturbed Hamiltonian with eigen values E_n and normalised eigen functions ψ_n, therefore we have

$$H_o \psi_n = E_n \psi_n \quad . \qquad (4.3.1)$$

The solution ψ of the actual Schrodinger equation:

$$i\hbar \frac{\partial \psi}{\partial t} = H\psi = (H_o + H')\psi \quad , \qquad (4.3.2)$$

can be written as a series of the eigen functions of H_o because the eigen functions ψ_n form a complete orthonormal set. So we may write the wave function ψ in the following form

$$\psi = \sum_n b_n(t)\, \psi_n\, e^{-iE_n t/\hbar} \quad , \qquad (4.3.3)$$

where $b_n(t)$ has the physical significance that if we measure the energy of the unperturbed system at time t, the probability of finding the eigen value E_n is given by $|b_n(t)|^2$. Note that for this purpose it is necessary to switch off the purturbation H' at the time t. By substituting the expression for the wave function ψ, equation (4.3.3), into the Schrödinger equation (4.3.2) we have

$$\sum_r \left\{\dot{b}_r - \frac{i}{\hbar} E_r\, b_r\right\} \psi_r\, e^{-iE_r t/\hbar} = -\frac{i}{\hbar}(H_o + H') \sum_s b_s \psi_s\, e^{-iE_s t/\hbar}$$

$$= -\sum_s \left\{ {}^{i}/_{\hbar}\, E_s b_s\, \psi_s\, e^{-iE_s t/\hbar} + \frac{i}{\hbar}\, H' b_s \psi_s\, e^{-iE_s t/\hbar}\right\} . \qquad (4.3.4)$$

This therefore reduces to give

$$\sum_r \dot{b}_r\, \psi_r\, e^{-iE_r t/\hbar} = -\sum_s \frac{i}{\hbar} H'\, b_s\, \psi_s\, e^{-iE_s t/\hbar} \qquad (4.3.5)$$

Pre-multiplying equation (4.3.5) by $\psi_n^*\, e^{iE_n t/\hbar}$ and by integrating over all of real space, we obtain for $\dot{b}_n(t)$

$$i\hbar\, \dot{b}_n(t) = \sum_s b_s(t)\, H'_{ns}\, e^{-i(E_s - E_n)t/\hbar} \quad , \qquad (4.3.6)$$

where

$$H'_{ns} = \int_{\text{all space}} \psi_n^*\, H'\, \psi_s\, d^3\underline{r} \quad . \qquad (4.3.7)$$

We require a solution of equation (4.3.6) subject to specific initial conditions at the time $t = 0$. It is convenient to choose

these initial conditions such that, at time $t = 0$, the system is found in a definite unperturbed state E_{n_o} say. Therefore, by the remarks made earlier about the probability $|b_n(t)|^2$ we see that, at time $t = 0$,

$$b_n(0) = 0, \text{ for all } n \text{ except } n_o \text{ in which case } b_{n_o}(0) = 1. \quad (4.3.8)$$

This simply indicates that the probability of finding the <u>initial</u> system in an unperturbed state $E_n (\neq E_{n_o})$ is zero, while the probability of finding the <u>initial</u> system in the state E_{n_o} is unity.

Owing to the perturbation H' (which will be switched on at time $t = 0$) transitions to other states n take place, and after a time t the probability that a transition to a state E_n has occurred is equal to $|b_n(t)|^2$. If, however, H' is small when compared to H_o and if we choose the time t to <u>be not too long</u>, then the transition probabilities are also likely to be small. This enables us to deduce an approximate solution to equation (4.3.6). For a small perturbing time t, equations (4.3.8) will approximately hold true. Now by substituting (4.3.8) into equation (4.3.6) one finds that $\dot{b}_n(t)$ is given by

$$\dot{b}_n(t) = -\frac{i}{\hbar} H'_{nn_o} b_{n_o} e^{-i(E_{n_o}-E_n)t/\hbar} \quad (4.3.9)$$

which when integrated subject to the boundary conditions (4.3.8) yields:

$$b_n(t) = \frac{1}{E_{n_o} - E_n} H'_{nn_o} \left(e^{-i(E_{n_o} - E_n)t/\hbar} - 1 \right), \quad n \neq n_o, \quad (4.3.10)$$

and

$$b_{n_o}(t) = e^{-iH'_{n_o n_o} t/\hbar} . \quad (4.3.11)$$

Therefore the probability of finding the state E_n at time t is

given by

$$|b_n(t)|^2 = 2\left(\frac{|H'_{n\,n_o}|}{E_{n_o} - E_n}\right)^2 (1 - \cos((E_{n_o} - E_n)t/\hbar)) \quad . \qquad (4.3.12)$$

Although we only require the direct transition probability from the initial state to the final state, we shall, for the sake of completeness examine transitions via intermediate states.

In many cases the matrix elements H'_{nn_o}, for the transition from an initial state n_o to a final state n, vanish. If this is the case then the method of approximation has to be refined. We shall assume the existance of intermediate states n' for which $H'_{nn'}$ as well as $H_{n'n_o}$ are different from zero. Using a slightly improved approximation to the one used earlier, we shall again use equations (4.3.8) to a more limited extent. On the R.H.S. of equation (4.3.6) we equate to zero all $b_m(t)$ except for $b_{n'}$ and b_{n_o}. Again b_{n_o} will be equated to unity.

If the perturbing time t is small then by using equation (4.3.6) $\dot{b}_n(t)$ and $\dot{b}_{n'}(t)$ are given by

$$i\hbar\,\dot{b}_{n'} = H'_{n'n_o}\, e^{-i(E_{n_o} - E_{n'})t/\hbar} \qquad (4.3.13)$$

and

$$i\hbar\,\dot{b}_n = \sum_{n'} H'_{nn'}\, b_{n'}(t)\, e^{-i(E_{n'} - E_n)t/\hbar} \qquad (4.3.14)$$

After a little manipulation $b_n(t)$ is given by

$$b_n(t) = \sum_{n'} \frac{H'_{n\,n'}\, H'_{n'\,n_o}}{E_{n_o} - E_{n'}} \left\{ \frac{e^{-i(E_{n_o} - E_n)t/\hbar} - 1}{E_{n_o} - E_n} - \frac{e^{-i(E_{n'} - E_n)t/\hbar} - 1}{E_{n'} - E_n} \right\} ,$$

(4.3.15)

The probability of a transition from the initial state n_o to a final state n, via some intermediate states n', is given by

$$|b_n(t)|^2 = \frac{2|H'|^2}{(E_{n_o} - E_n)^2} (1 - \cos(E_{n_o} - E_n)t/\hbar + \text{terms containing } (E_n, -E_n))$$

with
$$|H'| = \left| \sum_{n'} \frac{H'_{n\,n'}\, H'_{n'\,n_o}}{E_{n_o} - E_{n'}} \right| \quad . \qquad (4.3.16)$$

We shall assume that in the neighbourhood of the final state n there are a large number of states with the same physical properties, and that $\left(\frac{dN}{dE}\right)dE$ represents the number of these states with energies between E and $E + dE$. The perturbation term of the Hamiltonian H' will in general depend only on the physical properties of the final state. However, we are <u>not</u> interested in finding the probability that the system is in only one state n, after a time t, but rather in <u>any one</u> of these unperturbed states. This probability is obtained from the product of equation (4.3.12) for direct transitions, or (4.3.16) for transitions involving intermediate states, with the number of states $\left(\frac{dN}{dE}\right)dE$ within the energy range $(E, E + dE)$ and finally integrating over a small energy interval ΔE. Because of the assumed large number of states, with the same physical properties, in the neighbourhood of the final state we shall approximate the descrete spectrum of states by a continuum. We therefore make the identifications that E_n will be represented by E, while E_{n_o} will be represented by E_o. Thus the probability of finding the system in any one of the unperturbed states, after a perturbation time t, will be given by integrals of the form

$$\int_{\Delta E} f(E) \frac{(1 - \cos(E_o - E)t/\hbar)}{(E_o - E)^2}\, dE \quad , \qquad (4.3.17)$$

In order to proceed we shall interpret $\dfrac{1 - \cos(E_o - E)t/\hbar}{(E_o - E)^2}$,

which has a strong maximum at $E = E_o$, as a δ-function. To this end, put $x = (E - E_o)t/\hbar$ and examine the integral given by

$$\int_{-\infty}^{\infty} \frac{1 - \cos(E_o - E)t/\hbar}{(E_o - E)^2}\, dE = \frac{t}{\hbar}\int_{-\infty}^{\infty} \frac{1 - \cos x}{x^2}\, dx = \frac{t}{\hbar}\,\pi \qquad (4.3.18)$$

here elementary complex integration techniques have been employed to evaluate the second integral. So, having introduced the δ-function in place of $\dfrac{1 - \cos(E_o - E)t/\hbar}{(E_o - E)^2}$, expression (4.3.17) reduces to

$$t\,\pi\, f(E_o) / \hbar \quad . \qquad (4.3.19)$$

The probability is appreciable only when the energy of the final state is equal to the energy of the initial state. Thus if t is not too long, the transition probability is proportional to t . We can therefore define a transition probability per unit time p_{E_o} , which according to equations (4.3.12), (4.3.15) and (4.3.19) is given by

$$p_{E_o} = \frac{1}{t}\int_{\Delta E} |b_n(t)|^2 \left(\frac{dN}{dE}\right) dE = \frac{2\pi}{\hbar}\left(\frac{dN}{dE}\right)_{E_o} |H'(E_o)|^2 \qquad (4.3.20)$$

where $H'(E_o) = H'_{n\, n_o}$ if a direct transition from n_o to n is possible,

or $H'(E_o) = \sum_{n'} \dfrac{H_{n\, n'}\, H_{n'\, n_o}}{E_{n_o} - E_{n'}}$, if the transition occurs only by passing through the intermediate states n'.

In the next section we shall develop the theory of electron and hole tunneling from the metal to traps at the interfacial layer/semiconductor interface. For this purpose we shall only consider direct

transitions between a state in the metal and the ground state of a trap located at a distance δ from the metal surface. For a direct transition between an initial state n_o and a final state n the matrix element $H'_{n\,n_o}$ (i.e. the matrix element for a tunnel transition) can be written (see, for example Kane 1969) as

$$H'(E_o) = H'_{n\,n_o} = \int_{\text{All space}} \psi_n^* \, H' \, \psi_{n_o} \, d^3\underline{r}$$

$$= \int_{\text{All space}} \psi_n^* \, (H - E_{n_o}) \, \psi_{n_o} \, d^3\underline{r} \quad , \qquad (4.3.21)$$

where $H = H_o + H'$ and $H_o\psi_n = E_n\psi_n$ have been used. Therefore the transition probability per unit time is given by

$$p_{E_o} = \frac{2\pi}{\hbar} \left(\frac{dN}{dE}\right)_{E_o} \left| \int_{\text{All space}} \psi_n^* \, (H - E_{n_o}) \, \psi_{n_o} \, d^3\underline{r} \right|^2 \quad . \qquad (4.3.22)$$

This result is known as the golden rule of transition probabilities. $\hbar$ is Planck's constant divided by 2π and $\left(\frac{dN}{dE}\right)_E$ represents the density of states at the energy E_o.

4.4 Tunneling to interfacial surface states.

At the interfacial layer/semiconductor boundary of a Schottky barrier type structure, there may exist one or more trap energy levels (interfacial surface states). A direct injection of charged carriers from the metal to the interfacial surface states may also occur. The purpose of this section is, firstly to investigate the tunneling of

electrons between the metal and the interfacial trap states, at a distance δ from the metal surface (see figure 4.2a), and then secondly, to investigate the tunneling of holes between the metal and the interfacial surface states. At this stage we will construct the net tunneling time constant. Here, we have derived the tunneling time constant from first principals, without introducing phenomenological surface state tunneling capture cross sections as proposed by Freeman and Dahlke 1970.

The tunneling of electrons between the conduction band of a metal and a trap in an insulator will now be studied. As mentioned earlier, the trap is characterised by a δ-function potential in three dimensions. The direct tunneling probability of a metal conduction band electron to the ground state of a trap located at a distance δ from the metal is derived following Lundstrom and Svensson (1972). Figure 4.2a illustrates the potential energy diagram appropriate to the electron tunneling problem. The matrix element for a tunnel transition, using Bardeen's approach (see Kane 1969), may be written as

$$H'_{r\ell} = \int_{\text{all space}} \psi_r^* \, (H - E_\ell) \, \psi_\ell \, d^3\underline{r} \quad , \qquad (4.4.1)$$

where H is the correct Hamiltonian and E_ℓ is the energy of the electron in the metal. The wave functions ψ_ℓ and ψ_r characterise an electron, of energy E_ℓ (measured from the bottom of the metal's conduction band on the electron energy scale), in the metal and a trapped electron respectively. ψ_ℓ and ψ_r are calculated using the two approximate potential energy diagrams (figures 4.2(b) and (c)). Thus in determining ψ_ℓ we neglect the presence of the δ-function

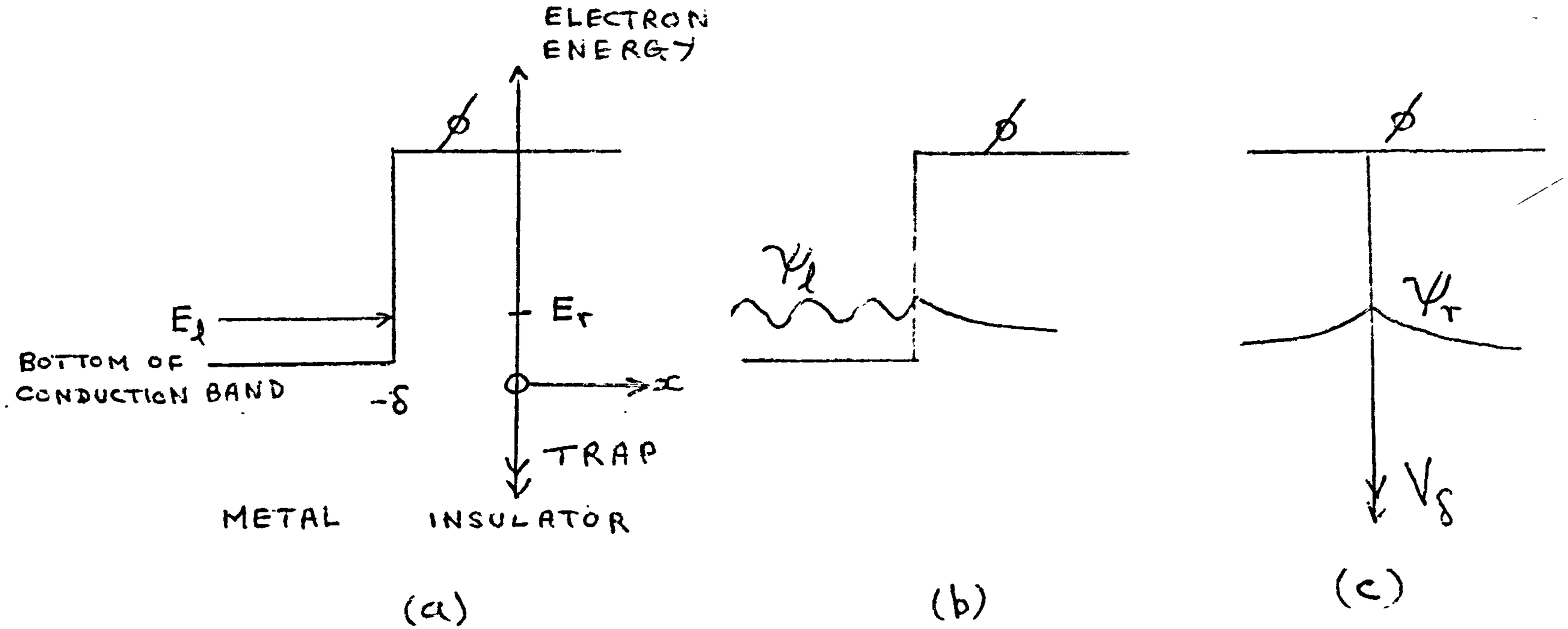

Figure 4.2

(a) Energy diagram for the electron tunnel process. V_δ characterises a three dimensional δ-function trap. E_ℓ and E_r are the total energies for a conduction band-electron and a trapped electron respectively. ϕ is the height of the electron potential barrier between the metal and the insulator.

(b) Potential energy diagram used in the calculation of the wave function, ψ_ℓ.

(c) Potential energy diagram used in the calculation of the "trap" wave function, ψ_r.

trap, and similarly in determining ψ_r we neglect the presence of the metal. Now $(H - E_\ell)\psi_\ell$ is zero everywhere except at the δ-function potential. Therefore the matrix element for a tunnel transition is given by

$$H'_{r\ell} = \int_{\text{all space}} \psi_r^* V_\delta \psi_\ell \delta(\underline{r}) \, d^3\underline{r} \quad , \qquad (4.4.2)$$

where V_δ is the strength of the δ-function potential. In order that we may evaluate the matrix element (4.4.2), we first need to find expressions for the metal and trap wave functions. The time independent Schrodinger equation in the metal is, using figure 4.2b, given by

$$(H - E_\ell)\psi_\ell = \left(-\frac{\hbar^2}{2m_\ell} \nabla^2 - E_\ell\right) \psi_\ell = 0 \quad , \qquad (4.4.3)$$

where m_ℓ is the effective mass of an electron in the metal. Therefore the electron wave function in the metal is given by

$$\psi_\ell(\underline{r}) = A \exp(i k_x x + i k_y y + i k_z z) + B \exp(-i k_x x + i k_y y + i k_z z) \, , \qquad (4.4.4)$$

with $x \leqslant -\delta$ and $k_x^2 + k_y^2 + k_z^2 = 2 m_\ell E_\ell/\hbar^2$. The first term of (4.4.4) represents the wave incident to the insulating layer $x \geqslant -\delta$, while the second term represents the wave reflected from the insulating layer. Because the reflection occurs only in the x-direction, the components of the wave vector in the y and z directions remain the same.

The wave function of an electron in the insulator's forbidden energy gap is, using fig. 4.2b, given by the solution to Schrodinger's equation

$$(H - E_\ell)\psi_\ell = \left(-\frac{\hbar^2}{2m_r}\nabla^2 - (E_\ell - \phi)\right)\psi_\ell = 0 \quad , \qquad (4.4.5)$$

where m_r is the effective mass of an electron in the insulators forbidden energy gap, and ϕ is the height of the electron potential barrier between the metal and the insulator. Thus the electron's wave function in the insulating layers forbidden region is given by

$$\psi_\ell = C e^{ik_y y + i k_z z - H_1(x + \delta)} \quad , \text{ with } x \geq -\delta, \qquad (4.4.6)$$

where we have neglected the presence of the trap according to figure 4.2b, and H_1 is given by

$$H_1^2 = \mathcal{H}^2 + k_y^2 + k_z^2 \text{ , with } \mathcal{H}^2 = \frac{2m_r}{\hbar^2}(\phi - E_\ell) \qquad (4.4.7)$$

ψ_ℓ in this case represents the "transmitted" wave function(in the insulating region there is no reflected wave). Again no potential barrier was present in either the y or z directions, so the components of the wave vector in the y and z directions remain unaltered. Equivalently, the components of the wave vector in the y and z directions are seen to remain unaltered due to the fact that $\frac{\partial\psi_\ell}{\partial x}$, $\frac{\partial\psi_\ell}{\partial y}$ and $\frac{\partial\psi_\ell}{\partial z}$ are all continuous at $x = -\delta$. Also, the metal wavefunction ψ_ℓ is continuous at $x = -\delta$. These boundary conditions enable us to find two relations between the constants of integration A, B and C in equations (4.4.4) and (4.4.6). The wave function ψ_ℓ must be normalised to fix the remaining constant of integration, thus

$$1 = \int_{\text{All space}} \psi_\ell^* \psi_\ell \, d^3\underline{r} = \int_{\text{Metal}} \psi_\ell^* \psi_\ell \, d^3r + \int_{\text{Insulator}} \psi_\ell^* \psi_\ell \, d^3\underline{r} \, ,$$

(4.4.8)

This expression represents the sum of the probabilities that the electron is in (a) the metal and, (b) in the insulating layer. Because the probability of the electron being in the insulating layer is small, we shall normalise the metal wave function as follows.

$$1 \approx \int_{\text{Metal}} \psi_\ell^* \psi_\ell \, d^3\underline{r} \approx \int_{\text{Metal}} (A^*A + B^*B) \, d^3\underline{r} \quad , \qquad (4.4.9)$$

where the neglected terms in this expansion, being harmonic, give a small contribution to the total integral. Using the relations between the constants of integration in conjunction with (4.4.9), $|C|$ is given by

$$|C| = \left(\frac{2 k_x^2}{H_1^2 + k_x^2} \right)^{\frac{1}{2}} L^{-3/2} \quad ,$$

where L^3 is the volume of the metal. Therefore the metal wave function for an electron(from the metal) in the forbidden energy gap of the insulator, is given by

$$\psi_\ell = L^{-3/2} \left(\frac{2 k_x^2}{H_1^2 + k_x^2} \right)^{\frac{1}{2}} \exp \left[ik_y y + ik_z z - H_1(x + \delta) \right] \quad , \qquad (4.4.10)$$

for $x \geq - \delta$.

The trap electron wave function is calculated by ignoring the presence of the metal (see figure 4.2c). Then in the insulator, with $r \neq 0$, the Schrodinger equation is given in its spherically symmetric form by

$$- \frac{\hbar^2}{2m_r} \frac{1}{r^2} \frac{d}{dr} (r^2 d\psi_{r/dr}) + \phi \psi_r = E_r \psi_r \quad , \qquad (4.4.11)$$

where E_r is the energy of the electron in the insulator. In fact, following the discussion of section 4.3, we shall take E_r equal to E_ℓ. Thus signifying that tunneling is appreciable only when the energy of the initial state equals the energy of the final state (i.e. direct tunneling at constant energy). Now, equation (4.4.11) may be rewritten as

$$\frac{d^2\psi_r}{dr^2} + \frac{2}{r}\frac{d\psi_r}{dr} - \mathcal{H}^2\psi_r = 0, \quad \text{with } \mathcal{H} \text{ as given in (4.4.7).}$$

Because the electron is in the insulators forbidden energy gap, the electron wave function must decay as we move away from the δ-function trap. Therefore ψ_r tends towards zero as r tends towards infinity. A solution to the above differential equation with its boundary condition gives the result that

$$\psi_r = D\frac{e^{-\mathcal{H}r}}{r} .$$

The constant D is determined by the normalization of ψ_r : $\int_{\text{All space}} \psi_r^* \psi_r \, d^3\underline{r} = 1$. Therefore the trap electron wave function is given by

$$\psi_r = \left(\mathcal{H}/2\pi\right)^{\frac{1}{2}} \frac{\exp(-\mathcal{H}r)}{r} . \qquad (4.4.12)$$

We note that although $\psi_r \longrightarrow \infty$ as $r \longrightarrow 0$, we have a limited probability density $4\pi r^2 \psi_r^* \psi_r$, for all r .

For a spherical system we put $d^3\underline{r} = r^2 \sin\theta \, d\theta \, d\phi \, dr$ and furthermore if the system is spherically symmetric $d^3\underline{r}$ may be replaced by

$4\pi\ r^2\ dr$ and then the integration may be performed over the r coordinate instead of all space coordinates.

The strength of the δ-function potential is obtained from the Schrodinger equation. Multiplying the spherically symmetric Schrodinger equation by $4\pi\ r^2$ we obtain

$$4\pi\ r^2 \left\{ -\frac{\hbar^2}{2m_r}\ \frac{1}{r^2}\ \frac{d}{dr}\ \left[\frac{r^2 d\psi_r}{dr}\right] + \left[\phi + V_\delta\ \delta(r)\right]\psi_r \right\} = 4\pi\ r^2\ E_r\psi_r\ , \quad (4.4.13)$$

We shall integrate this equation between $r = 0$ and $r = \varepsilon$ and then let ε tend towards zero. Before we proceed, a few important properties will be introduced. The dirac δ-function $\delta(r)$, in spherical coordinates, is defined by

$$1 = \int_{\text{All space}} \delta(\underline{r})\ d^3\underline{r} = \int_{r=0}^{r=\infty} 4\pi\ r^2\ \delta(r)\ dr. \quad (4.4.14)$$

Also, if we consider a three-dimensional square potential well with a radius a and a depth V, as representing the δ-function trap, when $a \longrightarrow 0$, then following Merzbacher 1961, we would find that the ground state wave function inside the well is approximately given by $\sin(kr)/r$. Hence we shall assume that, for the trap electron wave function ψ_r, $\left[\frac{r^2 d\psi_r}{dr}\right]_0 = 0$. Now returning to the derivation of the δ-function potential's strength we have

$$-\frac{\hbar^2 4\pi}{2m_r} \int_0^\varepsilon \frac{d}{dr}\ (r^2\ \frac{d\psi_r}{dr})dr + 4\pi \int_0^\varepsilon r^2(\phi - E_r)\psi_r dr + V_\delta\ \psi_r(0) = 0\ , \quad (4.4.15)$$

by integrating equation (4.4.13) between $r = 0$ and $r = \varepsilon$. Using equation (4.4.12) for the trap electron wavefunction together with the three-dimensional square well representation of the δ-function potential, and taking the limit as ε tends towards zero, V_δ is then given by

$$V_\delta \psi_r(0) = \frac{\hbar^2}{2m_r} \cdot 4\pi \lim_{\varepsilon \to 0} \left\{ \left| \frac{r^2 d\psi_r}{dr} \right|_{r=\varepsilon} \right\} = - \frac{\hbar^2}{m_r} (2\pi \mathcal{H})^{\frac{1}{2}} . \qquad (4.4.16)$$

The modulus squared of the matrix element for an electron tunnel transition $H'_{r\ell}$, using equations (4.4.2), (4.4.10) and (4.4.16), is given by

$$\left| H'_{r\ell} \right|^2 = \int_{\text{All space}} \psi_r^* V_\delta \psi_\ell \, \delta(\underline{r}) \, d^3\underline{r} \cdot \int_{\text{All space}} \psi_\ell^* V_\delta \psi_r \, \delta(\underline{r}) \, d^3\underline{r}$$

$$= \frac{4\pi \hbar^4}{m_r^2 L^3} \cdot \frac{\mathcal{H} k_x^2}{H_1^2 + k_x^2} \exp(-2 H_1 \delta) \quad . \qquad (4.4.17)$$

Eventually, we will apply the golden rule of transition probabilities to this electron tunneling problem, but first we must find the density of states in the metal, at an energy E_ℓ, with longitudinal wave vector components k_x.

It is a well known fact that there are 2 states (allowing for spin) in a volume $\left(\frac{2\pi}{L}\right)^3$ of $\underline{k}$ space, see for example Landsberg (1969). Therefore the density of states per unit volume of $\underline{k}$ space is $2(L/2\pi)^3$. Hence the number of states in an element $d^3\underline{k}$ of $\underline{k}$-space is given by

$$2\left(L/2\pi\right)^3 d^3\underline{k} = 2\left(\frac{L}{2\pi}\right)^3 \frac{d^3\underline{p}}{\hbar^3} = 2L^3 \frac{d^3\underline{p}}{h^3} . \qquad (4.4.18)$$

This gives $\frac{2}{h^3}\,dp$ as the number of states having momenta within the range $(p,\ p + dp)$, in unit volume of the metal. Let $\left.\frac{dN}{dE}\right|_{E_\ell}$ be the density of states at an energy E_ℓ with transverse momenta of constant magnitude $\left|\hbar k_{11}\right|$, where $k_{11}^2 = k_y^2 + k_z^2$. Therefore the number of states at constant k_{11} in the energy range (E, E + dE) is given by

$$\frac{dN}{dE} \cdot dE = 2\left(\frac{L}{2\pi}\right)^3 \cdot 2\pi\, k_{11}\, dk_{11}\, dk_x = 4\pi\left(\frac{L}{2\pi}\right)^3 k_{11}\, dk_{11}\, d\left(\frac{2m_\ell E}{\hbar^2} - k_{11}^2\right)^{\frac{1}{2}}$$

$$= \frac{2\pi\, m_\ell}{\hbar^2\, k_x}\left(\frac{L}{2\pi}\right)^3 dk_{11}^2\, dE \quad , \tag{4.4.19}$$

where the relation $k_x^2 + k_{11}^2 = 2\, m_\ell E/\hbar^2$ has been used. The density of states in the metal, with an energy of E_ℓ and with transverse momenta of constant magnitude $\left|\hbar k_{11}\right|$, is therefore given by

$$\left.\frac{dN}{dE}\right|_{E_\ell} = \frac{2\pi\, m_\ell}{\hbar^2\, k_x}\left(\frac{L}{2\pi}\right)^3 d\, k_{11}^2 \quad . \tag{4.4.20}$$

Generally speaking $k_{11} << \mathcal{H}$ (this is usually observed from $k_x^2 + k_{11}^2 = \frac{2m_\ell E_\ell}{\hbar^2} << \frac{2m_r}{\hbar^2}(\phi - E_\ell)$) and so we can expand the argument of the exponential factor in equation (4.4.17) as

$$2H_1\delta = 2\delta(\mathcal{H}^2 + k_{11}^2)^{\frac{1}{2}} = 2\delta\mathcal{H}\left(1 + \frac{k_{11}^2}{\mathcal{H}^2}\right)^{\frac{1}{2}} \approx 2\delta\mathcal{H}\left(1 + \frac{k_{11}^2}{2\mathcal{H}^2} \ldots.\right) \quad , \tag{4.4.21}$$

For a direct transition, the golden rule of transition probabilities gives the probability per unit time that an electron of energy E_ℓ with constant $\left|k_{11}\right|\left(= \sqrt{k_{xy}^2 + k_z^2}\right)$ tunnels from the metal to the trap. Hence the total probability P_e per unit time of electron tunneling at the energy E_ℓ is obtained integrating over all the allowed values of k_{11}

(magnitude of the transverse wave vector), and is given by

$$P_e = \int_{k_{11}=0}^{k_o} \frac{4\hbar\, m_\ell}{m_r^{\,2}} \frac{\mathcal{H}}{\mathcal{H}^2 + k_o^{\,2}} e^{-2\mathcal{H}\delta} \cdot (k_o^{\,2} - k_{11}^{\,2})\, e^{-k_{11}^{\,2}\delta/\mathcal{H}}\, k_{11}\, d\, k_{11} \,, \tag{4.4.22}$$

where equations (4.3.22), (4.4.7), (4.4.17), (4.4.20) and (4.4.21) have been used together with $k_o^{\,2} = \frac{2m_\ell E_\ell}{\hbar^2} = k_{11}^2 + k_x^{\,2}$ and $H_1^{\,2} + k_x^{\,2} = \mathcal{H}^2 + k_o^{\,2}$. After a little manipulation the probability P_e per unit time of electron tunneling may be written as

$$P_e = \frac{2\hbar\, m_\ell}{m_r^{\,2}} \frac{\mathcal{H}^2 k_o/\delta}{\mathcal{H}^2 + k_o^{\,2}} \exp(-2\mathcal{H}\delta) \left\{ 1 - \left(\frac{\mathcal{H}}{\delta k_o^{\,2}} \right)^{\frac{1}{2}} D\left[\left[\frac{\delta k_o^{\,2}}{\mathcal{H}} \right]^{\frac{1}{2}} \right] \right\} \,, \tag{4.4.23}$$

where $D(x)$ is Dawsons integral, which is given by

$$D(x) = e^{-x^2} \int_0^x e^{t^2}\, dt \quad . \tag{4.4.24}$$

The electron tunneling time constant τ_e may now be deduced from equation (4.4.23). It is given by $\tau_e \equiv 1/p_e$, and can be written in the form

$$\tau_e = \tau_{oe} \exp(2\mathcal{H}\delta) \,, \tag{4.4.25}$$

where

$$\tau_{oe} = \frac{m_r^{\,2}}{2\hbar\, m_\ell} \frac{\mathcal{H}^2 + k_o^{\,2}}{\mathcal{H}^2 k_o} \frac{\delta}{1 - (\mathcal{H}/\delta k_o^{\,2})^{\frac{1}{2}} D\left[\left(\delta k_o^{\,2}/\mathcal{H} \right)^{\frac{1}{2}} \right]} \tag{4.4.26}$$

This expression for the tunneling time constant is alright as far as it goes, but when dealing with an n-type Schottky barrier solar cell it will be necessary to allow for a spectrum of interfacial trap states.

Expression (4.4.25) however, does have a serious drawback. At the interfacial trap states near the valence band edge of the semiconductor, the tunneling time constant as predicted by equation (4.4.25) fails to allow sufficient communication between these states, of low electronic energy, and the metal. This would therefore result in the loss of a useful current path in the case of the n-type Schottky barrier solar cell, and would also cause the interfacial surface state population to be less strongly controlled by the metal Fermi level. It is for these reasons, that the tunneling (mathematically) of a hole from the metal to an interfacial surface state is considered. In this, we shall determine the tunneling time constant for holes communicating between the metal and the δ-function trap state.

The direct tunneling probability of a metal conduction band hole to the ground state of a trap located at a distance δ from the metal is derived. Figure 4.3a illustrates the appropriate potential energy diagram for this problem. The matrix element for a hole tunnel transition, from (4.3.21), is given by

$$H'^{h}_{r\ell} = \int_{\text{all space}} \psi^{h*}_{r} \, (H - E_h) \, \psi^{h}_{\ell} \, d^3\underline{r} \qquad (4.4.27)$$

where H is the correct Hamiltonian, and E_h is the energy of the hole on the hole energy scale. ψ^{h}_{ℓ} and ψ^{h}_{r} represent the wave-functions of a hole in the conduction band of the metal and a trapped hole respectively. They are calculated using the potential energy diagrams detailed in figures 4.3 (b) and (c). Thus as before, in the electron tunneling problem, we neglect the presence of the δ-function trap when calculating the wave function in the metal and correspondingly we neglect the presence of the metal when determining the hole trap wave-

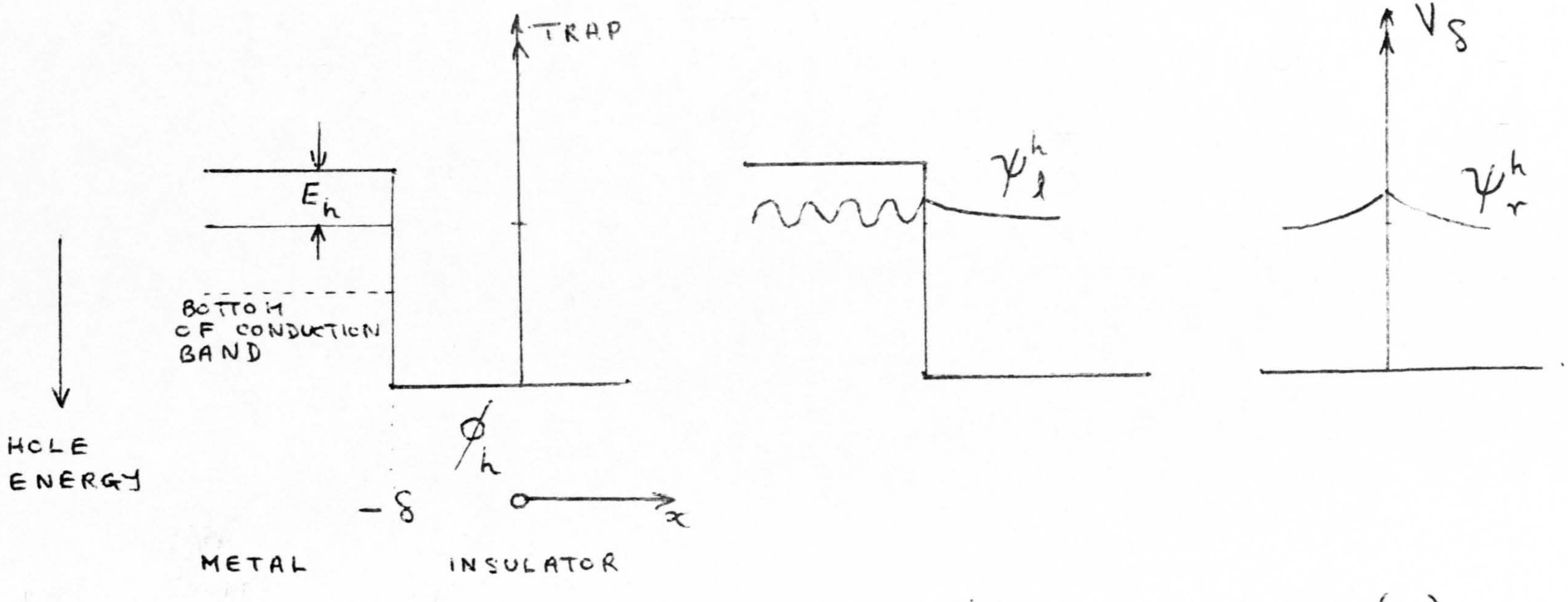

Figure 4.3

(a) Energy diagram for the hole tunnel process. V_δ^h characterises a three-dimensional δ-function trap. E_h is the total energy for both a conduction band hole and a trapped hole. ϕ_h is the height of the hole potential barrier between the metal and the insulator.

(b) Potential energy diagram used in the calculation of the 'metal' hole wave function, ψ_ℓ^h. (c) Potential energy diagram used in the calculation of the 'trap' hole wave function, ψ_r^h.

function. The matrix element for a hole tunnel transition $H'^{h}_{r\ell}$, from (4.3.21), is given by

$$H'^{h}_{r\ell} = \int_{\text{all space}} \psi^{h*}_{r} \; V^{h}_{\delta} \; \psi^{h}_{\ell} \; \delta(\underline{r}) \; d^{3}\underline{r} \quad , \qquad (4.4.28)$$

because $(H - E_h)\psi^h_\ell = 0$ everywhere except at the δ-function potential, whose strength is denoted by V^h_δ .

The hole wave function in the metal will now be determined. It will be assumed that the hole is near a hole band maximum (i.e. near an electron band minimum)in the metal. Then the wave function of a hole near a hole band maximum would be given by the solution to the Schrodinger equation

$$H \psi^{h}_{\ell} = E_{h} \psi^{h}_{\ell} \quad . \qquad (4.4.29)$$

Suppose we have a hole band maximum at $\underline{k}' = 0$ (this is ensured if we redfine the $\underline{k}'$ origin to be at A in figure 4.1, however see section 4.2), then assuming spherical surfaces of constant energy in $\underline{k}'$ -space near $\underline{k}' = \underline{0}$, the hole band energy is given by

$$E_h(\underline{k}') = E_h(\underline{0}) + \frac{\hbar^2}{2 m^h_\ell} \underline{k}'^2 \quad , \qquad (4.4.30)$$

where m^h_ℓ is the effective mass of a hole near the hole band maximum at the hole energy level E_h (see figure 4.3a). If the hole energy $E_h (= E_h(\underline{k}'))$ corresponds to the same energy level as E_ℓ (the electron energy) then we see from equation (4.2.12) and (4.2.13), that $m^h_\ell = - m_\ell < 0$.

Now by equation (4.2.9) and by using the identification $\underline{k}' = - \underline{k}$ (i.e. the hole wavevector is the negative of the electron wave vector), together with the fact that $E_n(\underline{k})$ is periodic in the reciprocal lattice, we have ψ^h_ℓ given by

$$-\frac{\hbar^2}{2m_\ell}(-i\underset{\sim}{\nabla})^2\,\psi_\ell^h = \left[E_h(\underline{k}') - E_h(\underline{O})\right]\psi_\ell^h\,, = \left[E_h - E_h(O)\right]\psi_\ell^h \qquad (4.4.31)$$

where the Wannier theorem (see Landsberg 1969) has been applied. Therefore the wave function for holes with wave vector $\underline{k}'$ near the hole band maximum is given by

$$\psi_\ell^h = A\,e^{+ik_x'x + i\underline{k}_y'y + ik_z'z} + B\,e^{-ik_x'x + ik_y'y + k_z'z}\,, \qquad (4.4.32)$$

where $k_x'^2 + k_y'^2 + k_z'^2 = \frac{2m_\ell}{\hbar^2}\left[E_h(O) - E_h\right] = \frac{2m_\ell E_\ell}{\hbar^2} > O$. Now by making the identification $\underline{k}' = -\underline{k}$ once again, we see that the wave function for holes at wave vector $\underline{k}$ is the same as the electron wave function at the electron wave vector $-\underline{k}$. Thus equation (4.4.32) may be re-written as

$$\psi_\ell^h = A\,e^{-ik_x x - ik_y y - ik_z z} + B\,e^{+ik_x x - ik_y y - ik_z z} \qquad (4.4.33)$$

with $x \leqslant -\delta$. A and B are the constants of integration.

The wave function representing a hole in the insulators forbidden energy gap is, using figure 4.3b, given by the solution of

$$\left(\frac{\hbar^2\,\underset{\sim}{\nabla}^2}{2m_r^h} + \left(E_h - \phi_h\right)\right)\psi_\ell^h = O\,, \qquad (4.4.34)$$

which gives ψ_ℓ^h, for $x \geqslant -\delta$, as

$$\psi_\ell^h = C\exp\left(-\bar{H}_1(x+\delta) - ik_y y - ik_z z\right)\,,$$

with $$\bar{H}_1^2 - k_y^2 - k_z^2 = \frac{2m_r^h}{\hbar^2}(\phi_h - E_h) = \bar{H}^2\,, \qquad (4.4.35)$$

where m_r^h is the effective mass of a hole in the insulators forbidden

energy gap, and ϕ_h is the hole potential barrier between the metal and the insulator. Here, the presence of the trap has been neglected according to figure 4.3(b). After the application of boundary conditions similar to those used in the electron tunnel time problem, and by using the same assumptions and techniques developed for the normalisation of the metal wave function, the wave-function of a hole at an energy E_h (on the hole energy scale) in the insulators forbidden band is given by

$$\psi_{\ell}^{h} = L^{-3/2} \left(\frac{2 k_x^2}{\bar{H}_1 + k_x^2} \right)^{\frac{1}{2}} \exp\left[-ik_y y - ik_z z - \bar{H}_1 (x + \delta) \right] , \quad (4.4.36)$$

for $x \geq -\delta$.

The hole trap wave function ψ_r^h is found in an analogous way to that used for the determination of the electron wave-function. This wave-function is calculated by ignoring the presence of the metal (see figure 4.3(c)). Thus in the insulator, with $r \neq 0$, the appropriate spherically symmetric Schrodinger equation is given by

$$-\frac{\hbar^2}{2m_r^h} \frac{1}{r^2} \frac{d}{dr} \left(r^2 \frac{d\psi_{\ell}^h}{dr} \right) + \phi_h \psi_r^h = E_h \psi_r^h . \quad (4.4.37)$$

Therefore the hole trap wave function for $r \neq 0$ is given as

$$\psi_r^h = (\bar{H}/2\pi)^{\frac{1}{2}} \frac{1}{r} \exp(-\bar{H} r) . \quad (4.4.38)$$

Also the strength of the hole δ-function potential is found, using assumptions analogous to those of the electron tunneling problem, to be given by

$$V_\delta^h \psi_r^h (0) = -\left(\hbar^2 / m_r^h \right) (2\pi \bar{H})^{\frac{1}{2}} . \quad (4.4.39)$$

The modulus squared of the matrix element for a hole tunnel transition

is, from (4.4.28), (4.4.36) and (4.4.39), given by

$$\left|H'^{h}_{r\ell}\right|^2 = \int_{\text{all space}} \psi_r^{h*} \; V_\delta^h \; \psi_\ell^h \; \delta(\underline{r}) d^3\underline{r} \cdot \int_{\text{all space}} \psi_\ell^{h*} \; V_\delta^{h*} \psi_r^h \; \delta(\underline{r}) d^3\underline{r}$$

$$= \frac{4\pi \hbar^4}{m_r^{h2} L^3} \; \frac{\bar{H} \, k_x^2}{\bar{H}_1^2 + k_x^2} \; \exp(-2\bar{H}_1 \delta) \quad , \qquad (4.4.40)$$

where L^3 is the volume of the metal.

At this point we shall make a few remarks about the metal's density of states function $\left(\frac{dN}{dE}\right)$, which was introduced earlier in this section. The density of states at hole energy E_h in the metal, near a hole band maximum, is obviously exactly equal to the density of states at an electron energy E_ℓ near an electron band minimum, provided that the energies E_ℓ and E_h refer to the same energy level. From figure 4.1 and equation (4.2.9) with $E_n(\underline{k}_1) = E_\ell$, $E_h(\underline{k}'_1) = E_h$ and $E_h(\underline{k}'_A = \underline{0}) = E_h(\underline{0})$, one observes that if $E_\ell + E_h = E_h(\underline{0})$ then E_ℓ and E_h refer to the same energy level. Therefore from equation (4.4.20), the density of states in the metal with a hole energy E_h (near the hole band maximum), and with transverse momenta of constant magnitude $|\hbar k_{11}|$, is

$$\left.\frac{dN}{dE}\right|_{E_h} = \left.\frac{dN}{dE}\right|_{E_\ell} = \frac{2\pi m_\ell}{\hbar^2 k_x} \left(\frac{L}{2\pi}\right)^3 d\, k_{11}^2 \quad , \qquad (4.4.41)$$

where $(dN/dE)|_{E_h}$ represents the density of states measured on the hole energy scale, while $(dN/dE)|_{E_\ell}$ represents the density of states on the electronic energy scale. Here, m_ℓ is the electron effective mass in the metal near the electron band minimum, with k_x as the component of the electrons wave vector in the x-direction. Thus k_x and k_{11} are given by the relations

$$k_x^2 + k_{11}^2 = \frac{2m_\ell \; E_\ell}{\hbar^2} = \frac{2m_\ell}{\hbar^2}\,(E_h(\underline{0}) - E_h) \quad \text{and} \quad k_{11}^2 = k_y^2 + k_z^2 \; . \tag{4.4.42}$$

It is perhaps worthwhile mentioning that the density of states in the metal, given by equation (4.4.41), has been obtained in this form to facilitate the use of the golden rule of transition probabilities. For a constant k_{11} and E_ℓ say, the electron wave vector in the x-direction will be fixed by equation (4.4.42), also the expressions for the squares of the moduli of the matrix elements $H'_{r\ell}$ and $H'^{h}_{r\ell}$ (see equations (4.4.17) and (4.4.40)) will be fixed. If we use the density of states function given by (4.4.41) together with the golden rule of transition probabilities (4.3.22), then we can find the transition probability per unit time for holes at an electron energy E_ℓ with transverse momenta of constant magnitude $|\hbar\, k_{11}|$. The total hole transition probability P_h per unit time is then obtained by integrating over all allowed values of k_{11}.

Before we proceed to find P_h, the hole transition probability per unit time, we expand the argument of the exponential factor in equation (4.4.40) as

$$2\,\bar{H}_1\delta = 2\delta\bar{\mathcal{H}}(1 + k_{11}^2\,/\,\bar{\mathcal{H}}^2)^{\frac{1}{2}} \approx 2\,\delta\bar{\mathcal{H}}\left(1 + \frac{k_{11}^2}{2\bar{\mathcal{H}}^2}\right), \tag{4.4.43}$$

where we have used equations (4.4.35), (4.4.42) together with the fact that, generally speaking $k_{11} \ll \bar{\mathcal{H}}$.

For a direct transition, the golden rule of transition probabilities gives the probability per unit time that a hole of energy E_h on the hole energy scale (this is equivalent to an energy of E_ℓ on the electron energy scale), with constant $|k_{11}|$ tunnels to the trap from the metal. Hence the total probability P_h per unit time of hole tunneling (at the

energy E_h) is obtained by integrating over all the allowed values of k_{11}, and is given by

$$P_h = \int_{k_{11}=0}^{k_o} \frac{4\hbar\, m_\ell}{m_r^{h2}} \frac{\bar{\mathcal{H}}}{\bar{\mathcal{H}}^2 + k_o^2} e^{-2\bar{\mathcal{H}}\delta} (k_o^2 - k_{11}^2) e^{-k_{11}^2\delta/\bar{\mathcal{H}}} k_{11} dk_{11}, \qquad (4.4.44)$$

where equations (4.3.22), (4.4.35), (4.4.40), (4.4.41) and (4.4.43) have been used together with the definition $k_o^2 \equiv 2m_\ell E_\ell/\hbar^2 = k_{11}^2 + k_x^2$. After some manipulation the probability P_h of hole tunneling may be writen as

$$P_h = \frac{2\hbar\, m_\ell}{m_r^{h2}} \frac{\bar{\mathcal{H}}^2 k_o/\delta}{\bar{\mathcal{H}}^2 + k_o^2} \exp(-2\bar{\mathcal{H}}\delta) \left\{1 - \left(\frac{\bar{\mathcal{H}}}{\delta k_o^2}\right)^{\frac{1}{2}} D\left[\left(\frac{\delta k_o^2}{\bar{\mathcal{H}}}\right)^{\frac{1}{2}}\right]\right\} \qquad (4.4.45)$$

where $D(x)$ is as given in equation (4.4.24).

The hole tunneling time constant τ_h can now be deduced. It is given by $\tau_h \equiv 1/P_h$, and can be written in the form

$$\tau_h = \tau_{oh} \exp(2\bar{\mathcal{H}}\delta), \qquad (4.4.46)$$

where

$$\tau_{oh} = \frac{\delta\, m_r^{h2}}{2\hbar\, m_\ell} \frac{\bar{\mathcal{H}}^2 + k_o^2}{\bar{\mathcal{H}}^2 k_o} \left(1 - (\bar{\mathcal{H}}/\delta k_o^2)^{\frac{1}{2}} D\left[\left(\delta k_o^2/\bar{\mathcal{H}}\right)^{\frac{1}{2}}\right]\right)^{-1} \qquad (4.4.47)$$

It should be mentioned that the transition rates (transition probabilities per unit time) have been calculated on the assumptions that the states in the metal were fully occupied whilst obtaining the expression (4.4.23) for P_e, and completely unoccupied whilst obtaining the expression (4.4.45) for P_h. We will now construct the net tunnel time constant for communication between one trap state (at energy E_ℓ)

and the metal. Suppose that f_m is the occupation probability of states at energy E_ℓ in the metal, and that f_t is the occupation probability of the trap state at the energy E_ℓ, then the actual charge transition rate(from the metal to the trap state) due to electron tunneling is

$$- e\, f_m P_e (1 - f_t) + e\, f_t P_e (1 - f_m) = e\, P_e (f_t - f_m) \,, \qquad (4.4.48)$$

where the first term represents electron transitions to the trap state from the metal, while the second represents electron transitions from the trap state to the metal. Similarly, the actual charge transition rate from the metal to the trap state due to hole tunneling is given by

$$e(1 - f_m) P_h f_t - e\, f_m P_h (1 - f_t) = e\, P_h (f_t - f_m) \qquad (4.4.49)$$

Hence we can construct the total actual charge transition rate I from the sum of expressions (4.4.48) and (4.4.49), so

$$I = e(P_e + P_h)\,(f_t - f_m)$$

$$= e \left(\frac{1}{\tau_e} + \frac{1}{\tau_h} \right) (f_t - f_m) = e \frac{1}{\tau} (f_t - f_m) \,, \qquad (4.4.50)$$

$$\text{with} \qquad \frac{1}{\tau} = {}^{1}/_{\tau_e} + {}^{1}/_{\tau_h} \,. \qquad (4.4.51)$$

This equation defines the net tunnel time constant τ, in terms of equations (4.4.25) and (4.4.46) for τ_e and τ_h respectively. This result will be used later in chapters 6 and 7, to establish the correct interfacial surface state population.

CHAPTER 5

THE THERMODYNAMIC EQUILIBRIUM BARRIER HEIGHT AND BAND EDGE OF AN n-TYPE SCHOTTKY BARRIER SOLAR CELL

5.1 Introduction

The aim of this chapter is to set out an improved theory, for the calculation of (a) the variation with position of the semiconductor's band edge and (b) the barrier height, of an n-type Schottky barrier solar cell, with a finite substrate thickness, in thermodynamic equilibrium. Following the discussion, presented towards the end of the third chapter, regarding the volume charge density $\rho(x)$ in the bulk semiconductor, the depletion approximation will be dispensed with entirely.

The work presented in the second and third chapters assumed that all the donors were ionized both in and out of equilibrium. In terms of the band picture we say that the donor atoms introduce localized energy levels (donor levels) just below the bottom of the conduction band. Electrons may be thermally excited out of these donor levels into the conduction band. If the Fermi level dictating the occupation of the donor states is well below the donor levels, then almost all of the donor states will be unoccupied. This is the condition for almost complete ionization of the donors. However, if the Fermi level dictating the occupation of the donor states approaches the donor levels (to within a few kT), then we have a situation where not all of the donor states will be ionized. In an attempt to allow for this eventuallity, we have developed relations giving the concentration of ionized donor states as a fraction of the total donor state concentration.

These relations will be derived for the thermodynamic equilibrium situation, and then the corresponding relations for non-equilibrium conditions will be deduced following Evans and Landsberg (1963).

In thermodynamic equilibrium the Fermi level is constant throughout the Schottky barrier solar cell. After making appropriate adjustments to the thermodynamic equilibrium barrier height equation (as first developed in chapter 2) due to the removal of the assumptions outlined above, we shall rewrite the thermodynamic equilibrium barrier height equation, as a first order non-linear differential equation together with its corresponding boundary condition. By using this equation in conjunction with Poissons equation for the variation of the electrostatic potential and electric field with position x (in the semiconductor substrate), we establish the system of equations covering the S.B.S.C.'s thermodynamic equilibrium band edge variation with position together with the equilibrium barrier height.

This system of equations has been solved numerically and the results for an Au - SiO_2 n-type Si cell will be presented towards the end of this chapter. Lastly, we shall make some remarks concerning the image force lowering of the barrier.

5.2 The ionized doping concentration

The occupation statistics for all quantum states in a semiconductor in equlibrium can be derived from a single result of statistical mechanics, well known as the Grand canonical partition function (see Landsberg 1969). We shall consider an impurity atom or other defect in a pure crystal structure, capable of trapping up to M ($M \geq 1$) electrons. A system of r ($0 \leq r \leq M$) identical electrons is allowed to interact with the impurity atom such that, although the number of electrons and the total energy are free to fluctuate, the mean number of electrons, the mean energy and the volume, remain fixed. It is assumed that a defect having trapped r

electrons can be in a number of quantum states β (depending on r), the total energy of the defect plus its trapped electrons in the state β being $E_{r\beta}$. From Landsberg(1969) the grand canonical partition function for the defect is

$$\boxed{Z} = \sum_{r=0}^{M} \sum_{\beta} \exp\left[(r\bar{\mu} - E_{r\beta})/kT\right] = \sum_{r=0}^{M} Z_r \, e^{r\bar{\mu}/kT} \quad , \qquad (5.2.1)$$

where $$Z_r \equiv \sum_{\beta} \exp(-E_{r\beta}/kT) \quad , \qquad (5.2.2)$$

the sum being over all quantum states of a defect with r electrons. Z_r is called the partition function for a def ect with r electrons. Here $\bar{\mu}$ is the electro-chemical potential, while k represents Boltzmann's constant. The probability of r electrons being trapped is given by

$$P_{ro} = \frac{1}{\boxed{Z}} Z_r \exp(r\bar{\mu}/kT) = \frac{Z_r \exp(r\,\bar{\mu}/kT)}{\sum_{r=0}^{M} Z_r \exp(r\,\bar{\mu}/kT)} \quad . \qquad (5.2.3)$$

If g_{ri} represents the degeneracy of the energy level E_{ri} then we may rewrite (5.2.2) as

$$Z_r = \sum_{i} g_{ri} \exp(-E_{ri}/kT) \quad , \qquad (5.2.4)$$

where the sum here, is over all the energy levels of a defect having trapped r electrons.

An important special case occurs when the defect, like most donors is capable of trapping at most one electron i.e. $r = 0$ or 1, and $M = 1$. So, if a donor trap state is unoccupied, in which case it is ionized, then (for an ionized hydrogen-like donor impurity) there is only one

quantum state at the ground state energy. Therefore if g_o represents the degeneracy of the ground state energy level for the unoccupied ($r = 0$) defect then $g_o = 1$. Similarly, if the defect is singly occupied by an electron (in which case it is neutral $r = 1$), then the degeneracy g_1 of the ground state energy level equals 2. This is because two possible spin states exist for a neutral hydrogen like impurity, there being only one electron, (of either spin up or spin down) which is unpaired and loosely bound to the atom.

Furthermore if we neglect the excited states in the calculation of the partition functions Z_o and Z_1 we obtain for the ratio Z_o/Z_1, the expression

$$\frac{Z_o}{Z_1} = \frac{\sum_i g_{oi}\, e^{-E_{oi}/kT}}{\sum_i g_{1i} e^{(-E_{di}-E_{oi})/kT}} \xrightarrow[\text{excited states}]{\text{Neglecting}} \frac{g_o}{g_1}\, e^{eE_d/kT}, \qquad (5.2.5)$$

where E_d represents the energy of an electron at the donor level, and is measured in units of electron volts. Another simplification has been made, in that the defect with no electrons has energy levels E_{oi}, with degeneracy g_{oi}, while the defect with only one electron has energy levels $E_{oi} + E_{di}$, with degeneracy g_{1i}, so that E_{di} can reasonably be associated with the energy levels of the trapped electron. So by assuming that a donor trap state is either unoccupied (ionized) or singly occupied we find that the occupation probability is given by

$$P_{to} = \frac{Z_1 \exp(\bar{\mu}/kT)}{Z_o + Z_1 \exp(\bar{\mu}/kT)} = \left[1 + \frac{Z_o}{Z_1} \exp(-\bar{\mu}/kT)\right]^{-1}, \qquad (5.2.6)$$

where we have used equation (5.2.3) for $M = 1$. Now, by using equation

(5.2.5) together with $g_o = 1$ and $g_1 = 2$, as discussed above, the occupation probability P_{to} in thermodynamic equilibrium is given by

$$P_{to} = \frac{1}{1 + \frac{1}{2} \exp(e(E_d - E_{FM})/kT)} \quad , \qquad (5.2.7)$$

where we have replaced $\bar{\mu}$ (the electro-chemical potential) by $e\,E_{FM}$, and E_{FM} is the Fermi level measured in units of electron volts.

Let the total concentration of donors be $N_D(m^{-3})$, and let $N^+_{Do}(x)$ represent the concentration of ionized donors in thermodynamic equilibrium (denoted by suffix o) at some position x in the semiconductor. In general the semiconductor's energy bands bend when a Schottky barrier contact is formed. Therefore one expects the donor levels to follow the curvature of the bands. Consequently, the energy of these donor levels will have a functional dependence on the position x in the semiconductor substrate, similar to that of the band edge. In actual fact, the doping levels remain below the semiconductor's conduction band by a constant amount of energy. This energy separation is known as the ionization energy, and will be denoted by E_{DI}, which will be measured in units of electron volts.

The donor state occupation probability in thermodynamic equilibrium, can also be represented as the ratio of the occupied donor state concentration to the total donor state concentration.

$$\text{So} \qquad \frac{N_D - N^+_{D_o}(x)}{N_D} = P_{to} \quad , \qquad (5.2.8)$$

where we again point out that an unoccupied donor state corresponds to an ionized donor state, which must of course have a positive charge e. Hence the concentration of ionized donors in thermodynamic equilibrium,

as a function of position x, is given by

$$N_{Do}^{+}(x) = \frac{N_D}{1 + 2\exp((E_{FM} - E_d(x))/kT)} \quad , \qquad (5.2.9)$$

with E_d (the energy of the donor level) replaced by its position dependent counterpart $E_d(x)$.

We will now construct relations governing the ionized donor concentration $N_D^+(x)$ for non equilibrium conditions, by applying the results of Evans and Landsberg (1963) to a single level of donor trap states. Following the procedure used in chapter 2 to obtain the net electron and hole trapping rates at a localized trapping level, the net electron trapping rate U_e is

$$U_e = (T_1^s + T_1 n + T_2 p)(n\, p_{td} - \bar{n}_1\, n_{td}) \quad , \qquad (5.2.10)$$

and the net hole trapping rate U_h is given by

$$U_h = (T_2^s + T_3 n + T_{4p})(p\, n_{td} - \bar{p}_1\, p_{td}) \quad , \qquad (5.2.11)$$

with T_1^s, T_2^s, T_1, T_2, T_3 and T_4 as the appropriate reaction constants, see figure 2.3 and equations (2.4.13) and (2.4.14). Here, n_{td} and p_{td} are the concentrations of occupied and unoccupied donors respectively. So, we see that p_{td} represents the concentration of ionized donors $N_D^+(x)$ at some position x. Therefore $N_D^+(x) + n_{td} = N_D$. The parameters $\bar{n}_1$ and $\bar{p}_1$ are given by the principle of detailed balance to be

$$\bar{n}_1 = n_o\, p_{tdo}/n_{tdo} = n_o(1 - p_{tdo})/p_{tdo} = \tfrac{1}{2}\, n_o \exp(e(E_d - E_{FM})/kT) \quad ,$$

$$\text{and} \quad \bar{p}_1 = p_o\, n_{tdo}/p_{tdo} = 2\, p_o \exp(e(E_{FM} - E_d)/kT) \quad , \qquad (5.2.12)$$

where, as usual n_o and p_o respectively, represent the thermodynamic equilibrium electron and hole concentrations at some position x in the semiconductor .

As our attention will be confined to the steady state, one must have $U_e = U_h$ in order that the number of trapped electrons remains constant. Hence the steady state concentration of trapped electrons, and the steady state recombination rate U_d (due to the donor traps) are given by

$$n_{td} = \frac{\bar{G}n + \bar{H}\,\bar{p}_1}{\bar{G}(n + \bar{n}_1) + \bar{H}(p + \bar{p}_1)}\, N_D \quad , \tag{5.2.14}$$

and

$$U_d = U_e = U_h = \frac{(np - n_i^2)\,\bar{G}\,\bar{H}\,N_D}{\bar{G}(n + \bar{n}_1) + \bar{H}(p + \bar{p}_1)} \quad , \tag{5.2.15}$$

where $\bar{G} = T_1^{\,s} + T_1 n + T_2 p$ and $\bar{H} = T_2^{\,s} + T_3 n + T_4 p$. Therefore the concentration of unoccupied donors gives the ionized doping concentration as

$$N_D^+(x) = \frac{(\bar{G}\bar{n}_1 + \bar{H}p)N_D}{\bar{G}(n + \bar{n}_1) + \bar{H}(p + \bar{p}_1)} \quad , \tag{5.2.16}$$

for non-equilibrium situations remaining in a steady state.

In general the electron and hole concentrations n and p will be functions of position x in the semiconductor. Also, the equilibrium electron and hole concentrations n_o and p_o , and consequently $\bar{n}_1$ and $\bar{p}_1$, will be functionally dependent on the position x . The results (5.2.15) and (5.2.16) will be used in the next chapter, which will deal with the non-equilibrium situations encountered when a Schottky barrier solar cell is forward biased either with or without illumination.

5.3 The separation between the Fermi level and the bottom of the conduction band at the ohmic (back) contact.

For our purposes we shall assume that an ohmic contact has the following main properties (as mentioned in section (3.4)): (a) it can always supply more carriers than the bulk material can carry under given applied potential, and (b) it produces an almost insignificant amount of semiconductor band bending in the vicinity of the ohmic contact.

We shall assume that such an ohmic contact to the n-type semiconductor region $(0 \leqslant x \leqslant L)$ is always possible. Then if there is no band bending near the ohmic contact, at the position $x = L$ in the semiconductor, we shall set the volume charge density $\rho(x)$ equal to zero at this point. The situation is depicted in figure 5.1, where the thermodynamic equilibrium band diagram of an n-type S.B.S.C. is represented schematically. In connection with this band diagram we note the following:

(a) the substrate is of finite thickness L,

(b) image force lowering effects have been neglected,

(c) a uniform doping concentration $N_D(m^{-3})$ has been assumed,

(d) the interfacial surface states, of density $D_S(m^{-2}e\ V^{-1})$, are assumed to be distributed evenly over the energy gap of the semiconductor at position $x = 0$ (the interfacial layer/semiconductor interface).

One further note regarding ohmic contacts should be made. Because an ohmic contact can always supply more carriers than the bulk semiconductor can carry, and if we further assume a large surface recombination velocity at $x = L$, we see that the ohmic contact maintains the carrier concentrations just inside the semiconductor (away from the ohmic contact) at their respective equilibrium values. Therefore the electron and hole concentrations at the position $x = L$ in the semiconductor, remain pinned at their respective equilibrium concentrations, irrespective of illumination and operating voltage.

If $\rho(x)$ represents the volume charge density in the semiconductor, then it is given by

$$\rho(x) = e\left[p - n + N_D^+(x)\right] \text{ , out of equlibrium ,} \qquad (5.3.1)$$

and $$\rho_o(x) = e\left[p_o - n_o + N_{Do}^+(x)\right], \text{ in thermodynamic equilibrium,}$$

where a suffix o denotes a thermodynamic equilibrium quantity. Now at position $x = L$ we have zero volume charge density, so

$$0 = p(L) - n(L) + N_D^+(L) \quad \text{and} \quad 0 = p_o(L) - n_o(L) + N_{D_o}^+(L), \qquad (5.3.2)$$

together with $n(L) = n_o(L)$, $p(L) = p_o(L)$ and $N_D^+(L) = N_{D_o}^+(L)$. We will consider a non-degenerate semiconductor with a constant doping profile N_D across the semiconductor region $(0 \leqslant x \leqslant L)$. Let the separation between the bottom of the semiconductors conduction band and the Fermi level at the ohmic contact be V_n electron volts.

The relation $E_c(x) - E_d(x) = E_{DI}$, indicates that the energy of the donor levels $E_d(x)$ remains at a constant energy E_{DI} below the bottom of the semiconductors conduction band $E_c(x)$ as we move through the semiconductor $(0 \leqslant x \leqslant L)$. However, if $E_{Fn}(x)$ and $E_{Fp}(x)$ respectively, represent the electron and hole quasi Fermi levels variation with position, then (according to the above discussion) at the ohmic contact $(x = L)$ $E_{Fn}(L)$ and $E_{Fp}(L)$ are pinned to the Fermi level of ohmic contact. Therefore we can write $E_{Fn}(L) = E_{Fp}(L) = E_c(L) - V_n$. Now from equations (2.2.12) and (2.2.13) $n(L)$ and $p(L)$, the electron and hole concentrations at the ohmic contact, are given by

$$n_o(L) = n(L) = N_c \exp(- e V_n/kT) \quad , \qquad (5.3.3)$$

and $$p_o(L) = p(L) = N_v \exp(e(V_n - E_g)/kT) \quad , \qquad (5.3.4)$$

where E_g is the energy gap of the semiconductor and is measured in units of electron volts. By using equation (5.3.2) together with (5.2.9), (5.3.3) and (5.3.4), we find an implicit relation for the separation V_n, it is

$$0 = N_v \exp(+ e(V_n - E_g)/kT) - N_c \exp(- eV_n/kT) + N_D/(1 + 2\exp(e(E_{DI} - V_n)/kT), \qquad (5.3.5)$$

where we have used $E_c(x) - E_d(x) = E_{DI}$ and $E_{Fn}(L) = E_{Fp}(L) = E_c(L) - V_n$. Equation (5.3.5) holds true for all possible operating conditions of an n-type Schottky barrier solar cell provided that the semiconducting region remains non-degenerate .

5.4 The differential equations predicting the thermodynamic equilibrium behaviour of an n-type Schottky barrier solar cell with a thin insulating interfacial layer.

Firstly, we shall construct the differential equation covering the thermodynamic equilibrium barrier height of an n-type S.B.S.C., assuming a continuous distribution of interfacial surface states of density D_S ($m^{-2} e\ V^{-1}$) over the energy gap at position $x = 0$. Secondly, we shall set up Poisson's equation for the equilibrium electrostatic potential and field. The fundamental equation for the thermodynamic equilibrium barrier height of an n-type S.B.S.C., whose derivation will be deferred until section 6.3 of the next chapter (for exposition purposes), is given by

$$\left(\varepsilon_{i/\delta}\right) \Delta = \frac{1}{2} \delta \rho_o + Q_{io} + Q_{sco} + (- \varepsilon_s E_s^o(L)), \qquad (5.4.1)$$

where ε_s is the permittivity of the semiconductor and $E_s^o(L)$ is the equilibrium electrostatic field in the semiconductor adjacent to the ohmic contact at $x = L$. $(- \varepsilon_s E_s^o(L))$ represents the small amount of charge contained in the surface of the metal forming the ohmic contact to semiconductor substrate (however, see chapter 6 below). Here $\phi_B = \phi_M - \chi - \Delta$, is the thermodynamic equilibrium barrier height, ϕ_M is the barrier metals work function (see figure 5.1), χ is the semiconductors electron affinity and ρ_o is the equilibrium volume charge density inside the interfacial layer. Again ε_i is the permittivity of the insulating interfacial layer, while δ is the thickness of this layer.

The interfacial surface state charge density (Qm^{-2}) is given by equation (2.4.33) as

$$Q_{io} = D_S \, kT \left\{ \ln \left\{ \frac{1 + \exp(e\phi_B/kT)}{1 + \exp(e(\phi_B - E_g)/kT)} \right\} - e \, E_g/kT \right\} + e \, D_S \phi_o \quad , \qquad (5.4.2)$$

in thermodynamic equilibrium with ϕ_o (see chapter 2) as the neutral level. (In thermodynamic equilibrium the Fermi level is constant throughout the cell, so correction of the equilibrium surface state charge density due to tunneling from the metal, is not required). However, the thermodynamic equilibrium space charge density in the semiconductor region is now given by

$$Q_{sco} = \int_0^L \rho_o(x)dx = e \int_0^L (p_o - n_o + N_{Do}^+(x)) \, dx \quad , \qquad (5.4.3)$$

due to the removal of the depletion approximation. Now by using equation (5.4.1) in conjunction with (5.4.2) and (5.4.3),

$$\phi_B = \phi_M - \chi - \frac{\delta^2 \rho_o}{2\varepsilon_i} + D_S \frac{\delta}{\varepsilon_i} \left\{ e\, E_g - kT \ln \left\{ \frac{1 + \exp(e\phi_B/kT)}{1 + \exp(e(\phi_B - E_g)/kT)} \right\} \right\}$$

$$- e \frac{\delta}{\varepsilon_i} D_S \phi_o - \frac{\delta}{\varepsilon_i} e \int_0^L (p_o(x) - n_o(x) + N_{Do}^+(x))dx + \frac{\delta}{\varepsilon_i} \varepsilon_s E_s{}^o(L), \qquad (5.4.4)$$

where ϕ_B has been used to denote the thermodynamic equilibrium barrier height of an n-type Schottky barrier solar cell.

Let us now define a position dependent barrier height function $\phi_B(x)$ through equation (5.4.4). We replace ϕ_B by $\phi_B(x)$, and the lower limit of the integral is replaced by x. We will transform this new integral equation into a first order non-linear differential equation with a boundary condition at $x = L$ i.e. at the back contact (ohmic contact). Therefore $\phi_B(x = L)$ is the required boundary condition and is given by the solution to the equation

$$\phi_B(L) = \phi_M - \chi - \frac{\delta^2 \rho_o}{2\varepsilon_i} + \frac{D_S \delta}{\varepsilon_i} \left\{ e\, E_g - kT \ln \left\{ \frac{1 + \exp(e\phi_B(L)/kT)}{1 + \exp(e(\phi_B(L) - E_g)/kT)} \right\} \right\}$$

$$- \frac{\delta}{\varepsilon_i} e\, D_S\, \phi_o + \frac{\delta}{\varepsilon_i} \varepsilon_s\, E_s{}^o(L). \qquad (5.4.5)$$

This boundary condition yields a numerical value for $\phi_B(L)$ when $E_s{}^o(L)$ is specified together with the parameters given in table 2. The value of $\phi_B(x)$ at $x = 0$ represents the thermodynamic equilibrium barrier height. So, using equation (5.4.4), having replaced ϕ_B by $\phi_B(x)$, with x replacing the lower limit of the integral, and differentiating with

Table 2

Data adopted for an Au - SiO_2/n-type Si S.B.S.C. in thermodynamic equilibrium

parameter	numerical value	dimensions	references and notes
D_S	1.0×10^{16}	$m^{-2}\ eV^{-1}$	Lane (1968)
$m_{e/m}$	1.1	-	Effective mass ratio for electrons *
$m_{h/m}$	0.59	-	Effective mass ratio for holes *
E_g	1.1	eV	* [an asterisk refers to Sreedhar er al (1969)]
χ	4.01	eV	*
T	300	K	-
ϕ_M	4.7 (Au)	eV	Riviere (1957), Sze (1969)
ε_s	$11.8\ \varepsilon_o$	Farad m^{-1}	} ε_o permittivity of free space
ε_i	$3.9\ \varepsilon_o$	Farad m^{-1}	} ε_o permittivity of free space
N_D	1.0×10^{21}	m^{-3}	-
E_{DI}	0.049	eV	As dopant, Bonch-Bruevich and Landsberg (1968)
ρ_o	0	Q m^{-3}	-
δ	19	$\mathring{A}$	-
L	3.6	μm	-

with respect to position x, we obtain the required differential equation as

$$\frac{d\phi_B(x)}{dx} = \frac{e\,\delta/\varepsilon_i \left[p_o(x) - n_o(x) + N_{Do}^+(x)\right]}{\left\{1 + e\frac{D_S\delta}{\varepsilon_i}\left\{\frac{1}{1 + \exp(e(\phi_B(x) - E_g)/kT} - \frac{1}{1 + \exp(e\phi_B(x)/kT)}\right\}\right\}} \quad . \tag{5.4.6}$$

This equation has $\phi_B(x)$ as a solution, subject to the boundary condition $\phi_B(L)$ given by equation (5.4.5). The value of $\phi_B(x)$ at $x = 0$ represents the thermodynamic equilibrium barrier height ϕ_B ($= \phi_B(x = 0)$) for an n-type S.B.S.C. This differential equation does not have any singularities due to the facts that the energy gap E_g is greater than zero, and that the electron and hole concentrations are well behaved functions of position. Incidentally the electron and hole concentrations will be functions of ϕ_B, since the potential distribution throughout the semiconductor region will in general depend upon $\phi_B(= \phi_B(0))$. This means that equation (5.4.6) must be solved simultaneously with Poisson's equation for the potential distribution.

In the n-type semiconductor, Poisson's equation for the thermodynamic equilibrium electrostatic potential $\phi_s^{\,o}(x)$ is given by

$$\frac{d^2\phi_s^{\,o}(x)}{dx^2} = -\frac{dE_s^{\,o}(x)}{dx} = -\frac{e}{\varepsilon_s}\left[p_o(x) - n_o(x) + N_{Do}^+(x)\right] , \tag{5.4.7}$$

where $E_s^{\,o}(x)$ is the thermodynamic equilibrium electrostatic field at some point x in the semiconductor. Again ε_s is the permittivity of the semiconductor and e is the electron's charge. The Poisson equation (5.4.7) is a second order non-linear differential equation and therefore requires two boundary conditions.

It is convenient to take the origin of the electrostatic potential at the barrier metal's Fermi level E_{FM}. We will use the bottom of the equilibrium conduction band to represent the equilibrium electrostatic potential at any point x in the semiconductor, however see figure 5.1. Therefore the thermodynamic equilibrium electrostatic potential, takes the following values at the edges of the semiconducting region.

(i) at $x = L$, $\phi_s^{o}(L) = - V_n$,

and (ii) at $x = 0$, $\phi_s^{o}(0) = - \phi_B$. (5.4.8)

As the equilibrium electrostatic potential is being measured from the barrier metal's Fermi level E_{FM} in thermodynamic equilibrium, the Fermi level being constant throughout the Schottky barrier solar cell, we can easily deduce relations connecting the electron, hole and ionized doping concentrations with the equilibrium electrostatic potential.
So, for a non-degenerate n-type Schottky barrier solar cell, the thermodynamic equilibrium electron, hole and ionized doping concentrations represented by $n_o(x)$, $p_o(x)$ and $N_{Do}^{+}(x)$ respectively, are given by

$$n_o(x) = N_c \exp(e\,\phi_s^{o}(x)/kT) \quad , \qquad (5.4.9)$$

$$p_o(x) = N_v \exp(-\,e\,(E_g + \phi_s^{o}(x))/kT) \quad , \qquad (5.4.10)$$

and

$$N_{Do}^{+}(x) = 1/\left\{1 + 2\exp(e(E_{DI} + \phi_s^{o}(x))/kT\right\} \quad . \qquad (5.4.11)$$

Here we have used equations (2.2.12), (2.2.13) in thermodynamic equilibrium and (5.2.9) together with $E_c(x) - E_d(x) = E_{DI}$ (from section 5.3), and $E_{co}(x) - E_{FM} = - \phi_s^{o}(x)$[which is just the statement that we are measuring the equilibrium electrostatic potential relative to the Fermi level in the barrier metal] .

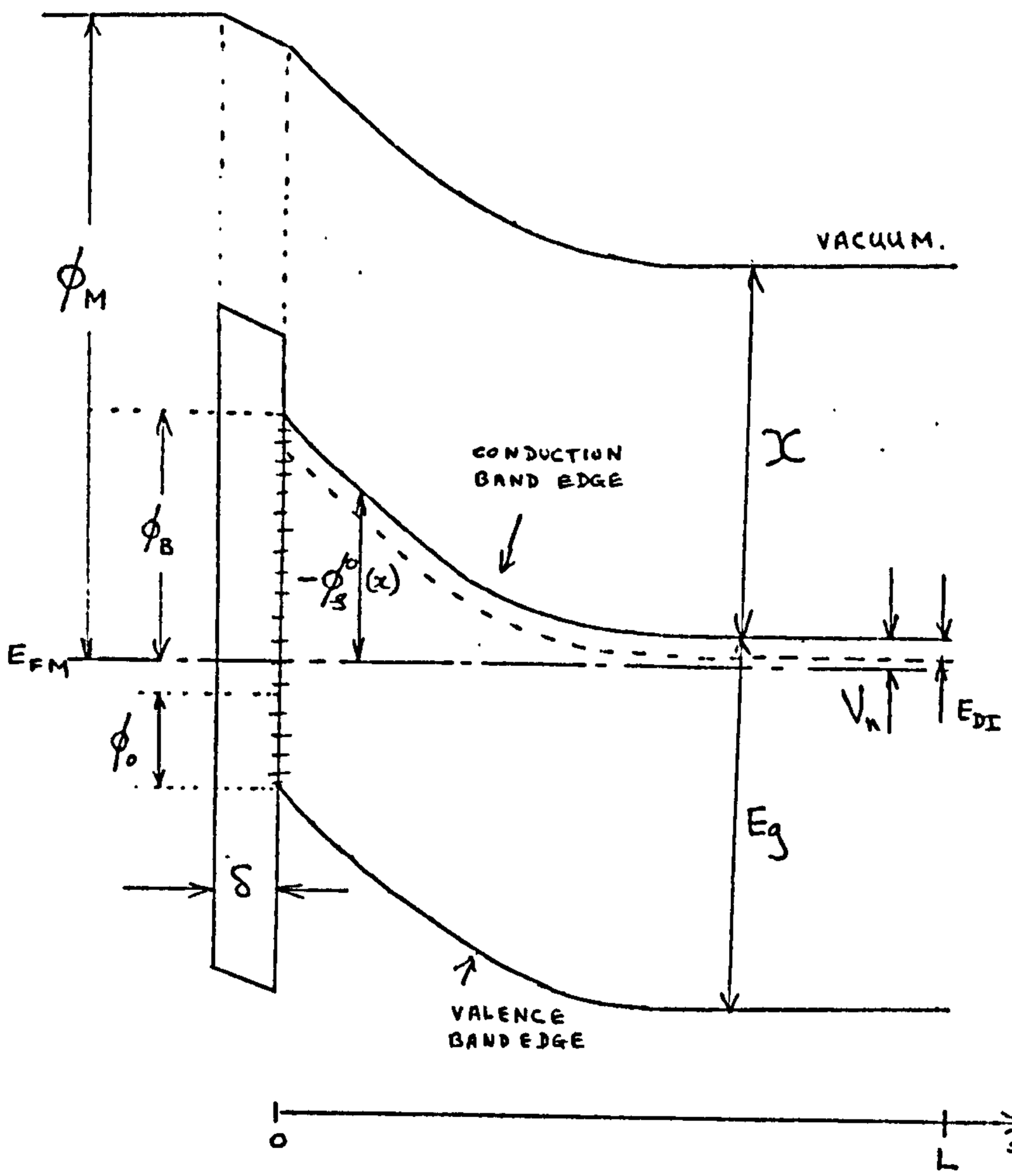

Figure 5.1 Band diagram of an n-type S.B.S.C. in thermodynamic equilibrium.

The thermodynamic equilibrium problem can be formulated as a system of three simultaneous first order non-linear differential equations together with their appropriate boundary conditions. Therefore the thermodynamic equilibrium barrier height, band edge(electrostatic potential) and electrostatic field are given by the solution of

$$\frac{d\,\phi_B(x)}{dx} = \frac{\frac{e\delta}{\varepsilon_i}\,(p_o(x) - n_o(x) + N_{Do}^{+}(x))}{\left[1 + \frac{eD_S\delta}{\varepsilon_i}\,\left\{\frac{1}{1+\exp(e(\phi_B(x) - E_g)/kT} - \frac{1}{1+\exp(e\phi_B(x)/kT)}\right\}\right]} ,$$

$$\frac{d\,\phi_s^o(x)}{dx} = -\,E_s^o(x) \quad .$$

and
$$\frac{d\,E_s^o(x)}{dx} = \frac{e}{\varepsilon_s}\left[p_o(x) - n_o(x) + N_{Do}^{+}(x)\right] \quad . \qquad (5.4.12)$$

The boundary conditions are given by

$$\left.\begin{aligned} &\text{(a)}\quad \text{at}\quad x = 0,\quad \phi_B(0) = -\,\phi_s^o(0),\quad \text{this represents the thermodynamic}\\ &\qquad\qquad\qquad\qquad\qquad\qquad\qquad\qquad\qquad\qquad \text{equilibrium barrier height}\ \ \phi_B\ ,\\ &\text{(b)}\quad \text{at}\quad x = L,\quad \phi_B(L)\ \ \text{is given by the solution to equation (5.4.5),}\\ &\text{(c)}\quad \text{at}\quad x = L\ ,\ \phi_s^o(L) = -\,V_n\ . \end{aligned}\right\} \qquad (5.4.13)$$

The functions $p_o(x)$, $n_o(x)$ and $N_{Do}^{+}(x)$ are given in terms of the equilibrium potential distribution $\phi_s^o(x)$ by equations (5.4.9), (5.4.10), and (5.4.11). We therefore have a system of three first order differential equations with three boundary conditions. These boundary conditions are of mixed type, thus making the problem of the n-type Schottky barrier solar cell in thermodynamic equilibrium of the two point boundary value type.

These equations, when solved, give the variation of the equilibrium electrostatic field and potential with position in the semiconducting region ($0 \leqslant x \leqslant L$) of the S.B.S.C., together with the thermodynamic equilibrium barrier height ϕ_B. The solution to this system of equations can only be obtained by numerical procedures.

The method used will now be discussed briefly. To start with, the parameters of table 2 are used in conjunction with equation (5.4.5), so that $\phi_B(L)$ can be found in terms of the field $E_s^o(L)$ at the ohmic contact by an iterative procedure. The separation V_n, being determined from equation (5.3.5) (also by an iterative method), gives us the other boundary condition (in a numerical form) at the back contact ($x = L$). Now, as two boundary conditions (one for the electrostatic potential and the other for the barrier height function $\phi_B(x)$) are known at position $x = L$, then if the electrostatic field were also known at $x = L$, we would be able to treat this system of equations as an initial value problem. Unfortunately, we do not know the electrostatic field at $x = L$. However, we only have one boundary condition at $x = 0$ to satisfy. If we 'guess' a value for the equilibrium electrostatic field at $x = L$, and integrate towards the barrier from the ohmic contact, as if we were dealing with an initial value problem, then by comparing the calculated value of $\phi_B(0) + \phi_s^o(0)$ with zero, we can adjust our estimate of the field at $x = L$ to improve the accuracy of the calculated boundary condition at $x = 0$. Ultimately we will find the value of the field at $x = L$, such that the calculated boundary condition at $x = 0$ is satisfied.

In effect this solution procedure corresponds to a minimization problem in one variable, such that the function value is zero at the minimum point. Here the variable is just the thermodynamic equilibrium electrostatic field $E_s^o(L)$ at the ohmic contact ($x = L$). Integration

of the system of equations, towards the rectifying contact yields the numerical values of $\phi_B(0)$ and $\phi_s^o(0)$ as functions of $E_s^o(L)$. Using these values we construct the required function as $(\phi_B(0) + \phi_s^o(0))^2$. This function is only dependent upon the equilibrium electrostatic field $E_s^o(L)$ at the ohmic contact, and can therefore be minimized.

Of course, when we have found a value for $E_s^o(L)$ such that $(\phi_B(0) + \phi_s^o(0))^2 = 0$, then we have also found the solution of the thermodynamic equilibrium problem. The integrations can be performed by various means, but the one chosen for use here was the Runge Kutta method of fourth order. The step length was continuously monitored and adjusted in an attempt to control the rounding errors when the solution curves varied rapidly. A few numerical solutions will be presented in the next section.

5.5 Results and discussion

Some results of this theory for the thermodynamic equilibrium properties of an Au - SiO_2 - n-type single crystal Si Schottky barrier solar cell are presented in figures 5.2 and 5.3. The system of equations (5.4.12) have been solved subject to the boundary conditions of (5.4.13) by the method outlined above. Everything has been calculated on the basis of the data presented in table 2. Before we proceed with the explanation of the results, it is important to remember that the effect of image force lowering of the barrier has been neglected.

Figure 5.2 shows the variation of the thermodynamic equilibrium electrostatic field with position in the semiconducting region of the n-type Schottky barrier solar cell. The thermodynamic equilibrium electrostatic field $E_s^o(x)$ is seen to vary approximately exponentially with position, in the semiconductor region ($0 \leq x \leq L$). In particular we note that the equilibrium electrostatic field $E_s^o(x)$, in the semiconducting region at position $x = L$, has a negative non-zero value. At position $x = L$ (the ohmic contact, see figure 5.1) the volume charge

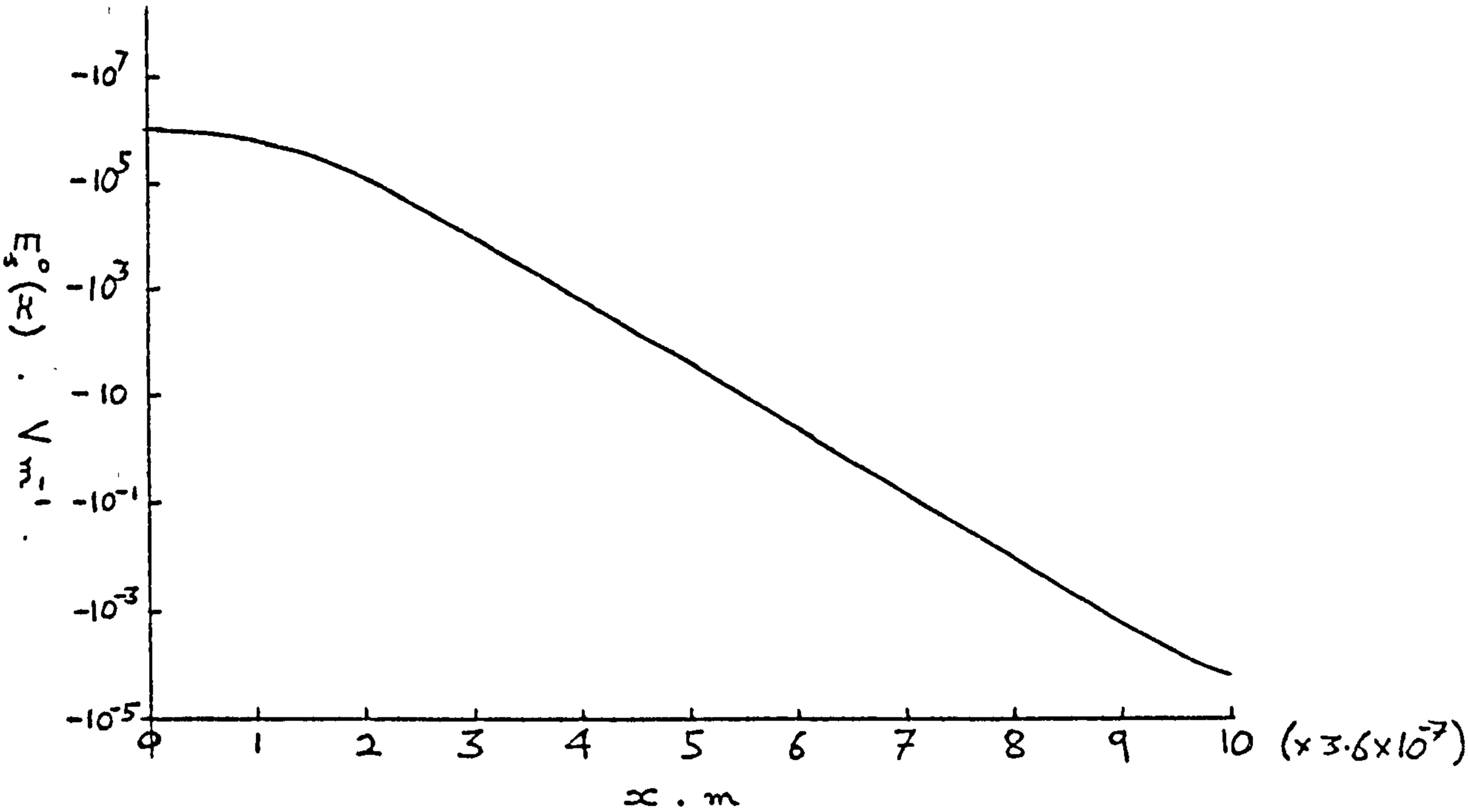

Figure 5.2 The thermodynamic equilibrium electrostatic field $E_s^o(x)$ as a function of position x. The parameters of table 2 have been used.

density has been set equal to zero in accordance with section 5.3. As we move through the semiconductor towards the barrier at $x = 0$, the equilibrium volume charge density $\rho_o(x)$ increases with decreasing x. This is caused by the reduction in the equilibrium electron concentration as we approach the barrier from the ohmic contact, due to the fact that with a negative equilibrium electrostatic field $E_s^o(x)$ in the semiconducting region, the thermodynamic equilibrium potential $\phi_s^o(x)$ decreases with decreasing x.

Eventually, as we move much closer to the position $x = 0$, say to within 0.5 μm of the interface , the effect of the decreasing equilibrium electron concentration with decreasing x becomes less important. Here, in this region the volume charge density $\rho_o(x)$ almost equals the equilibrium ionized doping concentration multiplied by e (the electronic charge), the effect of the increase in the equilibrium hole concentration with decreasing x having a minor role. Therefore, for x less than about 0.5μm, the volume charge density remains almost constant. Conse quently because $\rho_o(x)$ is no longer increasing rapidly with decreasing x (when x is near $x = 0$), the thermodynamic equilibrium electrostatic field $E_s^o(x)$ near $x = 0$ deceases approximately linearly, and therefore less rapidly than exponentially, with decreasing x. Thus the thermodynamic equilibrium electrostatic field $E_s^o(x)$ tends to level off as the position $x = 0$ is approached. These results show that the depletion approximation, even when used under thermodynamic equilibrium conditions, does not apply throughout the semiconducting region of the Schottky barrier solar cell.

Turning to figure 5.3, the variation of the thermodynamic equilibrium electrostatic potential $\phi_s^o(x)$ with position x in the semiconductor is shown. The modulus of the equilibrium electrostatic potential at the interface between the semiconductor and the insulating interfacial layer ($x = 0$), represents the thermodynamic equilibrium barrier height ϕ_B.

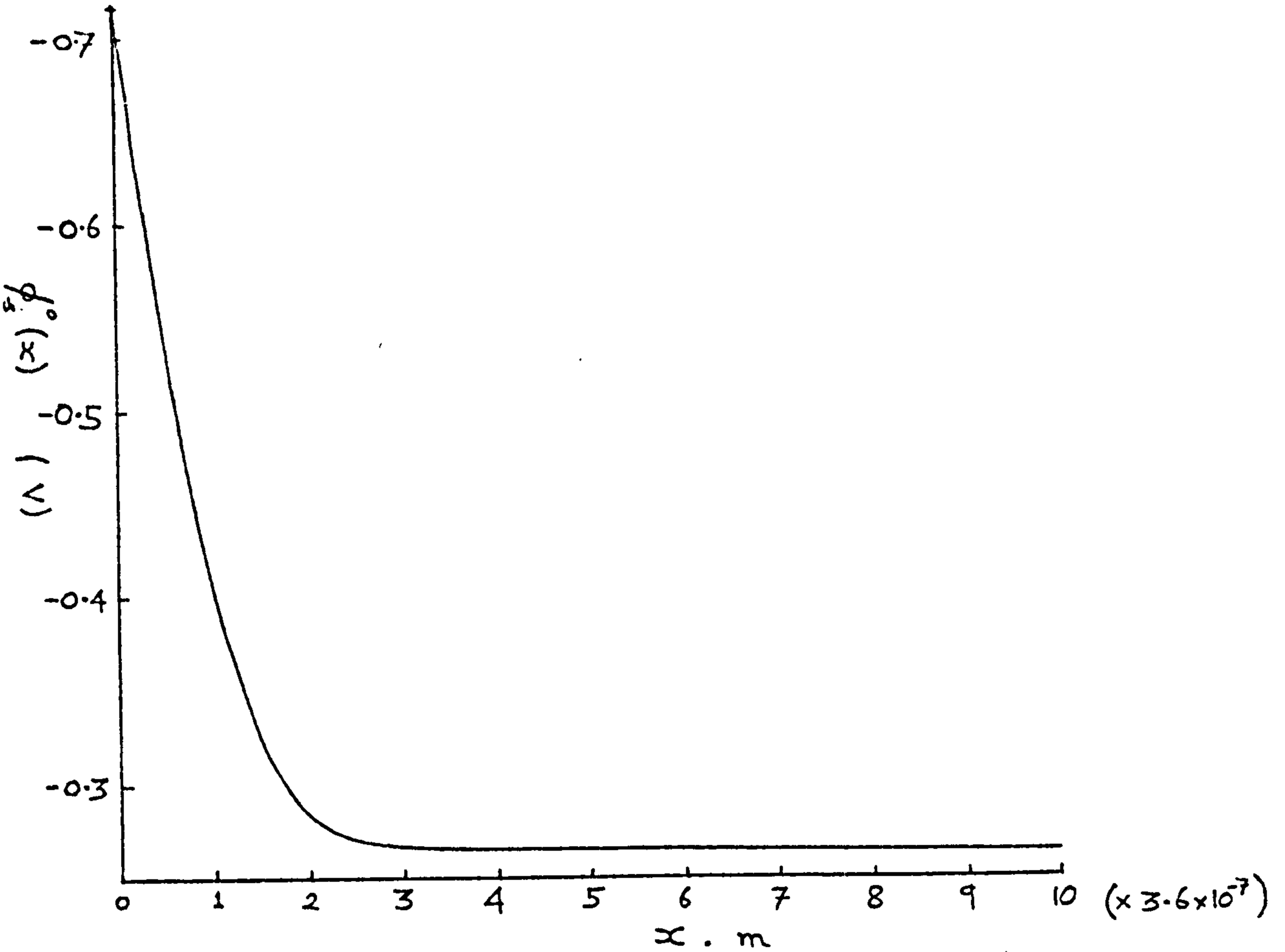

Figure 5.3 The thermodynamic equilibrium electrostatic potential as a function of the position x in the substrate. The parameters of table 2 have been used, and from the figure the thermodynamic equilibrium barrier height, ϕ_B = 0.717 eV.

From the figure, ϕ_B is given as 0.718 eV. The thermodynamic equilibrium electrostatic potential $\phi_s^o(x)$ is seen to remain <u>almost</u> constant when $x > 1$ μm, due tc the relatively low value of the equilibrium volume charge density $\rho_o(x)$ for x greater than 1μm. For x less than about 1 μm the thermodynamic equilibrium electrostatic potential is seen to decrease rapidly with decreasing x .

In principle we could find the thermodynamic equilibrium properties of any n-type Schottky barrier using the above formalism. In practice, the use of this theory is restricted in the sense that, we cannot perform the calculations directly on cells having very large substrate thickness L . For if $x(< L)$, the position in the semiconductor, were near the ohmic contact at $x = L$ and if L were very large then we would expect the thermodynamic equilibrium electrostatic field in the semiconductor at $x = L$ to be extremely small. Therefore small variations in this equilibrium electrostatic field would produce large variations in the equilibrium electrostatic potential at the interface between the semiconductor and the interfacial layer $(x = 0)$. Hence for large substrate thicknesses L , one cannot accurately relate the value of $\phi_s^o(x)$ at $x = 0$ to the equilibrium electrostatic field $E_s^o(x)$ at position $x = L$ (i.e. at the ohmic contact), because of the rounding errors occuring when equations (5.4.12) are numerically integrated from the ohmic contact at $x = L$ to the interface at $x = 0$.

In all of our work so far the effects of the image force lowering potential have been ignored. The effect of the image force potential is to round off the corners, and reduce the thickness of the tunneling barrier. Therefore the image force potential tends to increase the communication between the barrier metal and both the semiconductor's bands and the interfacial surface states. The approximate effect of including image forces into the insulating interfacial layer is to reduce the effective thickness of the insulating interfacial layer by about

5 Å (see for example Simmons (1963)). Therefore our calculations for an interfacial layer thickness δ correspond to a geometrical interfacial layer thickness of $(\delta + 5)$Å . The effect of including image forces in the semiconductor's substrate is likely to cause a slight reduction in the thermodynamic equilibrium barrier height ϕ_B. In view of the large tunneling barriers present to both electrons in the semiconductor's conduction band and holes in the valence band (see chapter 6 below), the inclusion of image force lowering of the barrier is likely to cause only slight variations in the characteristics. Therefore in all of the numerical results, both those already presented and those yet to be given, we have neglected <u>all</u> image force lowering effects.

CHAPTER 6

THE MORE COMPLETE FORMALISM OF THE n-TYPE SCHOTTKY BARRIER SOLAR CELL

6.1 Introduction.

This chapter will be devoted to the construction of the system of equations, governing the properties of an n-type Schottky barrier solar cell with a thin insulating interfacial layer, separating the metal from the semiconductor substrate. In the model, to be presented later in this chapter, the semiconductor's substrate having thickness L (assumed to be finite), is composed of single crystal material. The interfacial surface state population model of chapter 2, will be adapted to include the effect of the interfacial surface state's communication with the barrier metal. To do this, we require knowledge of the interfacial surface state tunneling time constant τ. Using the improved expression for the interfacial surface state occupation probability, and by removing the depletion approximation entirely together with the usual assumptions regarding the quasi-Fermi levels in the semiconductor region ($0 \leqslant x \leqslant L$), we will develop an improved relation covering the interfacial voltage V_i developed across the insulating layer.

The theory of Chapter 5 is a special case of the more general formalism presented in this chapter. The phenomenological current density equations, Poisson's equation (out of thermodynamic equilibrium) and the two continuity equations (one for electrons in the semiconductor's conduction band and the other for holes in the semiconductor's valence band) are

subsequently introduced. The corresponding boundary conditions for the equations are introduced where appropriate. These boundary conditions, being of mixed type, characterise the study of the n-type Schottky barrier solar cell as a two point boundary value problem.

Also, in this chapter we shall present some of the results following calculations made for an Au - SiO_2-n-type single crystal Si Schottky barrier solar cell, for both illuminated and unilluminated operating conditions, using the numerical data summarized in table 3. For each operating condition, the illumination and output voltage being specified, we obtain one set of solar cell properties. Therefore at each point on the relevant current density-voltage characteristic, according to the nature of the illumination, we may calculate the variation of the semiconductor's band edges with position x in the semiconductor. Also, the variations of the electron and hole quasi-Fermi levels with the position x in the semiconductor, have been calculated. The electron and hole current densities are given as functions of x and furthermore, it is found that these current densities remain reasonably constant with respect to the position x in the substrate ($0 \leqslant x \leqslant \bar{L}$), when the cell is under forward bias in the dark (no illumination). However, if the solar cell is illuminated reasonably strongly (say AM1 intensity) then the electron and hole current densities show a marked dependence on x, the position in the semiconductor. This particular result is, of course, expected from the simpler theories of S.B.S.C.'s.

The voltage V_i developed across the interfacial layer may be calculated at any operating condition; specifying the illumination and output voltage. Firstly, with the n-type Schottky barrier solar cell in the dark under an applied forward voltage $V(> 0)$ we have that V_i the portion of the applied voltage existing across the insulating inter-

facial layer, is always positive, or zero only when either $V = 0$ or $\delta = 0$. Secondly, for the illuminated n-type Schottky barrier solar cell under short circuit conditions $(V = 0)$, the interfacial voltage V_i developed across the insulating layer has been found to be negative. As the operating voltage V is increased, the interfacial voltage V_i also increases, and will eventually become positive for the larger output voltages. The negative value of V_i obtained for the short circuited n-type S.B.S.C. receiving illumination has been attributed to a change in the occupancy of the interfacial surface states and is caused, we believe, by the accumulation of photo-generated holes in the semiconductor's valence band near the interfacial layer. In fact simple arguments of electrostatics and charge conservation clearly show that V_i is of negative sign when the cell is short circuited in the presence of illumination This argument will be presented at the end of the chapter.

6.2 Tunneling effects on the population of interfacial surface states.

In this section we consider the interfacial surface trap states, each of which can only trap one electron, having a continuous sheet distribution $D_S(m^{-2}\ eV^{-1})$ across the energy gap of the semiconductor at $x = 0$. The influence on the surface state population, due to the proximity of the metal will be taken into consideration. The situation is depicted in figure 6.1. Using the notation adopted in chapter 2, and by neglecting all trap to trap transitions, the total electron and hole trapping rates $d\,U_e^{ifr}$ and $d\,U_h^{ifr}$, due to the interfacial surface states (within the energy range $(E_t, E_t + dE_t)$) communication with the bands of the semi - conductor, are by equations (2.4.15) and, (2.4.16) given as

$$d\,U_e^{ifr} = G\left[n(0)\ D_S\ dE_t - (n(0) + n_1(0))dn_t\right] \qquad (6.2.1)$$

and $$d\,U_h^{ifr} = H\left[(p(0) + p_1(0))dn_t - p_1(0)D_S\ dE_t\right] \quad , \qquad (6.2.2)$$

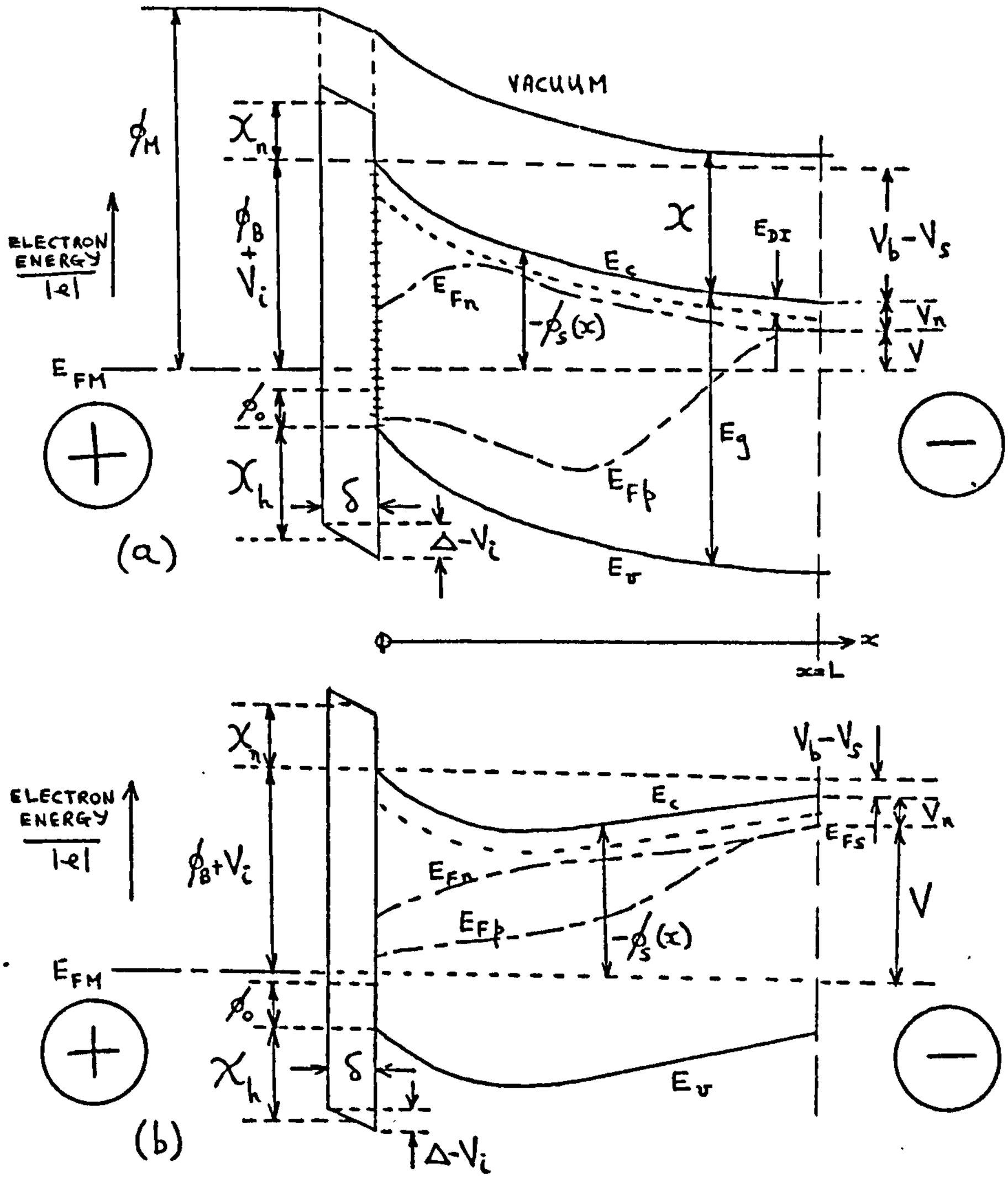

Figure 6.1 Band diagrams for an n-type Schottky barrier solar cell. (a) Under illumination, delivering power and (b) in the dark with a forward bias V applied.

where dn_t is the concentration of electrons trapped at the interfacial surface trap states within the energy range $(E_t, E_t + dE_t)$, [measured in electron volts]. Therefore dn_t may be written in the form

$$dn_t = f_t D_S dE_t \quad , \qquad (6.2.3)$$

where f_t represents the occupation probability of an interfacial surface state at the energy E_t.

We will now examine the transport of carriers between the barrier metal and the interfacial surface states, by using the tunneling time constant. Suppose that f_m represents the occupation probability of a state at an energy E_t in the metal. Then f_m will be given by

$$f_m = 1/(\exp(e(E_t - E_{FM})/kT + 1) \quad , \qquad (6.2.4)$$

with k as Boltzmanns constant and T as the absolute temperature. Consider the interfacial surface states within the energy range $(E_t, E_t + dE_t)$ eV as being in communication with the barrier metal via carriers tunneling, through the insulating interfacial layer, at an energy E_t. Then the number of surface states per unit area in the energy range $(E_t, E_t + dE_t)$ is $D_S dE_t$. Now τ is the net tunnel time constant, which physically represents the average time a carrier takes to tunnel through the insulating interfacial layer to or from an interfacial state, (see Chapter 4) . So, using equation (4.4.50), the net charge transition rate from the metal to one interfacial surface state is $e(f_t - f_m)/\tau$. Therefore the net charge transition rate due to tunneling between the barrier metal and the <u>interfacial surface states</u> having energies in the range $(E_t, E_t + dE_t)$ is given by

$$edU_{ht}^{ifr} = \frac{e}{\tau}(f_t - f_m)\, D_S\, dE_t \quad , \qquad (6.2.5)$$

where dU_{ht}^{ifr} represents an apparent hole capture rate, due to tunneling between the barrier metal and the interfacial surface states in the energy range $(E_t, E_t + dE_t)$ eV's.

As our attention will be confined to the steady state, one must have $dU_e^{ifr} = dU_h^{ifr} + dU_{ht}^{ifr}$ in order that the number of electrons trapped at the interfacial surface states, in the energy range $(E_t, E_t + dE_t)$, remains constant. Hence, by equations (6.2.1), (6.2.2), (6.2.3) and (6.2.5) the steady state concentration (m^{-2}) of trapped electrons dn_t and, the steady state recombination rates, dU_e^{ifr} and dU_h^{ifr}, due to the interfacial surface states within the energy range $(E_t, E_t + dE_t)$ are given by

$$dn_t = \frac{\tau G n(o) + \tau H p_1(o) + f_m}{\{\tau G(n(o) + n_1(o)) + \tau H(p(o) + p_1(o)) + 1\}}\, D_S dE_t \quad ,$$

$$\equiv f_t\, D_S dE_t \qquad (6.2.6)$$

$$dU_e^{ifr} = \frac{G\{\tau H(n(o)\, p(o) - n_i^2) - (n(o) + n_1(o))f_m + n(o)\}}{\tau G(n(o) + n_1(o)) + \tau H(p(o) + p_1(o)) + 1}\, D_S\, dE_t \quad , \qquad (6.2.7)$$

and $$dU_h^{ifr} = \frac{H\{\tau G(n(o)\, p(o) - n_i^2) + (p(o) + p_1(o))f_m - p_1(o)\}}{\tau G(n(o) + n_1(o) + \tau H(p(o) + p_1(o)) + 1}\, D_S\, dE_t . \qquad (6.2.8)$$

Also dU_e^{ifr} and dU_h^{ifr} respectively, represent the recombination rates of electrons and holes in the semiconductor's conduction and valence bands, at the interface $x = o$, due to the interfacial surface states within the energy range $(E_t, E_t + dE_t)$.

If we examine the above equations as the tunnel time constant τ tends towards zero we find that the population of the interfacial surface states is governed by the metal, as expected. So $f_t = f_m$ when $\tau \to o$. Also, as τ tends towards zero dU_e^{ifr} and dU_h^{ifr} are given by

$$dU_e^{ifr} = G\{n(o)\ (1 - f_m) - n_1(o)f_m\}\ D_S dE_t \qquad (6.2.9)$$

$$\text{and} \quad dU_h^{ifr} = H\{p(o)f_m - p_1(o)\ (1 - f_m)\}\ D_S dE_r. \qquad (6.2.10)$$

As expected $dU_{ht}^{ifr} = dU_e^{ifr} - dU_h^{ifr} \not\to o$ as $\tau \to o$ unless thermodynamic equilibrium conditions prevail. Conversely, if the interfacial layer is so thick as to increase the tunneling time constant τ to a very large value then, from equation (6.2.6), the population of the interfacial surface states is governed by the carrier concentrations in the semiconductor's conduction and valence bands at position $x = o$. In this case the barrier metal has no direct influence over the interfacial surface state population, and the recombination rates dU_e^{ifr} and dU_h^{ifr} reduce to the form given by equation (2.4.18). If conditions of thermodynamic equilibrium are applied to equations (6.2.6), (6.2.7) and (6.2.8) then $f_t \to f_{to} = \left[1 + \exp(e(E_{to} - E_{FM})/kT\right]^{-1}$ and $dU_e^{ifr} = dU_h^{ifr} = o$.

In the above relations G, H, and the Shockley-Read parameters $n_1(o)$, $p_1(o)$ are as given in chapter 2. We shall require the total number of occupied interfacial surface states n_t, as well as the total interfacial surface state electron and hole trapping rates, $\int dU_e^{ifr}$ and $\int dU_h^{ifr}$ respectively. As noted in chapter 2 the integrations should be performed over the equilibrium interfacial surface state energies $E_{to}(eV)$. Thus E_{to} ranges between

$E_{FM} + \phi_B - E_g$ (= $E_{vo}(o)$) and $E_{FM} + \phi_B$ (= $E_{co}(o)$), where ϕ_B is the thermodynamic equilibrium barrier height, E_g is the energy gap of the semiconductor.

Now an interfacial surface state of energy E_{to}, in thermodynamic equilibrium, has energy $E_t (= E_{to} + V_i)$ measured relative to the barrier metal when non-equilibrium conditions apply. This is because the semiconductor's conduction and valence bands at the interface x = o rise by an amount equal to V_i when non-equilibrium conditions apply. Therefore, if all the integrations concerning the interfacial surface states are to be performed over the thermodynamic equilibrium surface state energies, in accordance with chapter 2, then we must modify the expression for f_m (the occupation probability in the barrier metal). Thus f_m, given by equation (6.2.4), is written as

$$f_m = 1/(1 + \exp (e (E_{to} + V_i - E_{FM})/kT)). \qquad (6.2.11)$$

The Shockley-Read parameters $n_1(o)$ and $p_1(o)$ are given by (2.4.24) as

$$\frac{n_1(o)}{n_o(o)} = \frac{p_o(o)}{p_1(o)} = \exp (e (E_{to} - E_{FM}) /kT), \qquad (6.2.12)$$

with $n_o(o)$ and $p_o(o)$ respectively, as the equilibrium electron and hole concentrations at the interface x = o. Hence the total number of occupied interfacial surface states n_t, and the total steady state recombination rates $\int dU_e^{ifr}$, $\int dU_h^{ifr}$ due to the interfacial surface states in the energy gap of the semiconductor, at position x = o, are given by integrating equations (6.2.6), (6.2.7), (6.2.8) over the thermodynamic equilibrium interfacial surface state energies E_{to}. [Note that because $E_t = E_{to} + V_i$

we have $dE_t = dE_{to}$]. The relations (6.2.11) and (6.2.12) have been used to give the integrands their equilibrium surface state energy dependence. Consequently, the interfacial surface state parameters n_t, $\int dU_e^{ifr}$ and $\int dU_h^{ifr}$, representing the steady state surface concentration of trapped electrons, the electron and hole recombination rates (in the semiconductors conduction and valence bands respectively), are given by

$$n_t = \int_{E_{FM} + \phi_B - E_g}^{E_{FM} + \phi_B} \frac{\tau G n(o) + \tau H p_1(o) + f_m}{\{\tau G(n(o) + n_1(o)) + \tau H(p(o) + p_1(o)) + 1\}} \cdot D_S dE_{to}$$

$$= \int_{E_{FM} + \phi_B - E_g}^{E_{FM} + \phi_B} f_t D_S dE_{to} , \qquad (6.2.13)$$

$$\int dU_e^{ifr} = \int_{E_{FM} + \phi_B - E_g}^{E_{FM} + \phi_B} \frac{G\{\tau H(p(o)n(o) - n_i^2) - (n(o) + n_1(o))f_m + n(o)\}}{\{\tau G(n(o) + n_1(o)) + \tau H(p(o) + p_1(o)) + 1\}} D_S dE_{to},$$

(6.2.14)

and

$$\int dU_h^{ifr} = \int_{E_{FM} + \phi_B - E_g}^{E_{FM} + \phi_B} \frac{H\{\tau G(n(o)p(o) - n_i^2) + (p(o) + p_1(o))f_m - p_1(o)\}}{\{\tau G(n(o) + n_1(o)) + \tau H(p(o) + p_1(o)) + 1\}} D_S dE_{to}.$$

(6.2.15)

6.3 The differential equations predicting the non-equilibrium behaviour of an n-type Schottky barrier solar cell with a thin insulating interfacial layer.

In this section we continue the theme of removing the usual assumptions regarding the quasi-Fermi levels together with the removal of the depletion approximation. To begin with, we shall find an expression for the voltage V_i developed across the insulating interfacial layer of an n-type Schottky barrier solar cell. The figures 6.1(a) and (b) represent, schemat·icaly, the band diagrams of an n-type Schottky barrier solar cell with and without illumination respectively. In each case a forward voltage V(>o) exists across the device. In figure 6.1(a) the total conventional current density is flowing from right to left across the diagram, therefore indicating that the solar cell is delivering power to some external system. On the other hand, see figure 6.1(b), when the solar cell is unilluminated while under a forward bias voltage V(>o) the total conventional current density flows from left to right across the diagram. The notation of chapter 2 is used together with the assumption that the semiconductor is non degenerate. In this study we shall assume that the semiconductor's substrate thickness L is finite, and that the interfacial surface states are distributed evenly, with density $D_S(m^{-2}\ eV^{-1})$, over the semiconductor's energy gap at position x = o.

From the theory of chapter 2, the field $E_i(x)$ in the interfacial layer $(-\delta \leq x < o)$, sandwiched between the barrier metal and the semiconductor substrate $(o \leq x \leq L)$, is given by

$$\frac{dE_i}{dx} = \rho/\varepsilon_i \quad , \tag{6.3.1}$$

where ε_i is the permittivity of the interfacial layer, ρ is the charge density in the interfacial layer and is independent of position. Now in the semiconductor region, Poisson's equation for the electrostatic field is given by

$$\frac{dE_s(x)}{dx} = \rho(x)/\varepsilon_s = \frac{e}{\varepsilon_s}\left[p(x) - n(x) + N_D^{+}(x)\right] , \tag{6.3.2}$$

where ε_s is the permittivity of the semiconductor. $n(x)$, $p(x)$ and $N_D^{+}(x)$ are respectively, the electron, hole and ionized doping concentrations at some position x in the semiconductor substrate. Equation (6.3.2) gives

$$E_s(L) - E_s(o) = \frac{1}{\varepsilon_s}\int_o^L e(p(x) - n(x) + N_D^{+}(x))\,dx = \frac{Q_{sc}}{\varepsilon_s} \quad ,$$

which when used in conjunction with the boundary condition $(\underset{\sim}{D}_s - \underset{\sim}{D}_i).\hat{\underset{\sim}{n}} = Q_i$ at $x = o$ (here $\hat{\underset{\sim}{n}}$ is the unit normal to the plane of the junction, $\underset{\sim}{D}$ is the displacement vector and Q_i is the charge density (Qm^{-2}) at the interfacial surface states) together with equation (6.3.1), gives the electrostatic field $E_i(x)$ in the insulating layer as

$$E_i(x) = \frac{1}{\varepsilon_i}\left(\rho x - (Q_{sc} + Q_i - \varepsilon_s E_s(L)\right), \; x\varepsilon\,[-\delta, o]. \tag{6.3.3}$$

Here Q_{sc} represents the charge density (Q_m^{-2}) in the semiconductor's substrate ($o \leq x \leq L$).

Suppose we now apply the Gauss flux theorem to a surface enclosing the barrier metal/interfacial layer boundary, then the charge Q_M in the surface of the barrier metal is given by

$$Q_M = \varepsilon_i \lim_{x \to -\delta_+} E_i(x),$$

By using the expression for $E_i(x)$ given by (6.3.3) we find that

$$Q_M = -Q_{int} - Q_{sc} - Q_i + \varepsilon_s E_s(L)$$

which gives

$$Q_M + Q_{int} + Q_{sc} + Q_i + (-\varepsilon_s E_s(L)) = o, \qquad (6.3.4)$$

where Q_{int} $(=\rho\delta)$ is the charge density (Qm^{-2}) in the interfacial layer.

Application of the Gauss flux theorem to a surface including the semiconductor substrate/ohmic contact metal boundary (x=L), leads us to deduce that $(-\varepsilon_s E_s(L))$ represents the charge density (Qm^{-2}) in the surface (x=L) of the ohmic contact metal. Therefore (6.3.4) represents the equation for the conservation of charge. In general we would expect the electrostatic field $E_s(L)$ at the ohmic contact to be very small, compared to the field near the interface x = o.

From figures 6.1(a) and (b) the voltage drop across the whole cell is $V = V_i + V_s$, where V_i and V_s are the parts of the output voltage developed across the interfacial layer and semiconductor substrate respectively. Let $\Delta - V_i$ and $V_b - V_s$ be the potential

drops across the interfacial layer and semiconductor substrate respectively. In thermodynamic equilibrium $V = V_i = V_s = o$, therefore Δ becomes the thermodynamic equilibrium potential drop across the interfacial layer. Now from the figure, with ϕ_M as the barrier metals work function, χ the semiconductor's electron affinity and V_n as the separation between the bottom of the conduction band and the semiconductor's Fermi level at the ohmic contact (see section 5.3),

$$\phi_M = V + V_n + (V_b - V_s) + \chi + (\Delta - V_i) = \phi_B + \chi + \Delta. \qquad (6.3.5)$$

The potential drop $\Delta - V_i$ across the interfacial layer is given under illumination by

$$\Delta - V_i = -\int_{-\delta}^{o} E_i(x) = \frac{\rho\delta^2}{2\varepsilon_i} + (Q_i + Q_{sc} - \varepsilon_s E_s(L))\,{}^{\delta}/_{\varepsilon_i}$$

$$\text{thus} \quad ({}^{\varepsilon_i}/_{\delta})\ (\Delta - V_i) = \tfrac{1}{2}\ \delta\rho + Q_i + Q_{sc} - \varepsilon_s E_s(L) \qquad (6.3.6)$$

becomes in equilibrium

$$({}^{\varepsilon_i}/_{\delta})\ \Delta = \tfrac{1}{2}\ \delta\rho_o + Q_{io} + Q_{sco} - \varepsilon_s E_s^o(L)\ . \qquad (6.3.7)$$

Subtracting

$$-({}^{\varepsilon_i}/_{\delta})\ V_i = \tfrac{1}{2}\ (\rho - \rho_o) + (Q_i - Q_{io}) + (Q_{sc} - Q_{sco}) - \varepsilon_s(E_s(L) - E_s^o(L)), \qquad (6.3.8)$$

where both suffix o, and superfix o denote thermodynamic equilibrium quantities. Relation (6.3.7) is the fundamental equation, predicting the thermodynamic equilibrium barrier height ϕ_B through equation (6.3.5). Equation (6.3.7) was presented (without derivation) earlier in chapter 5 (see equation (5.4.1)).

The integral equation yielding the interfacial voltage V_i developed across the interfacial layer, is given by using equation (6.3.8) together with the integral expressions for Q_{sco} and Q_{sc}, representing respectively the charge densities (Qm^{-2}) in the semiconductor substrate ($o \leqslant x \leqslant L$) both in and out of thermodynamic equilibrium. Therefore Q_{sco} and Q_{sc} are given by

$$Q_{sco} = e \int_o^L (p_o(x) - n_o(x) + N_{Do}^{+}(x))\, dx \qquad (6.3.9)$$

$$\text{and} \quad Q_{sc} = e \int_o^L (p(x) - n(x) + N_D^{+}(x))\, dx \,, \qquad (6.3.10)$$

where $n(x)$, $p(x)$ and $N_D^{+}(x)$ respectively, represent the electron, hole and ionized doping concentrations at some position x in the semiconductors substrate ($o \leqslant x \leqslant L$). A suffix o indicates a thermodynamic equilibrium quantity. Using an analogous argument to that of section (2.4), the interfacial surface state charge densities Q_{io} and Q_i respectively, in and out of thermodynamic equilibrium are given by

$$Q_{io} = eD_S\phi_o - eD_S \int_{E_{FM} + \phi_B - E_g}^{E_{FM} + \phi_B} f_{to}\, dE_{to}$$

$$= eD_S \phi_o - eD_S \int_{E_{FM}+\phi_B-E_g}^{E_{FM}+\phi_B} (1+\exp(e(E_{to}-E_{FM})/kT)^{-1} \, dE_{to}, \qquad (6.3.11)$$

$$\text{and } Q_i = eD_S \phi_o - eD_S \int_{E_{FM}+\phi_B-E_g}^{E_{FM}+\phi_B} f_t \, dE_{to} = eD_S \phi_o - e\, n_t, \qquad (6.3.12)$$

where we have used equation (6.2.13) and f_t is given in (6.2.6).

The next step is to convert the integral equation (6.3.8), for the interfacial voltage V_i, into a first order non-linear differential equation with an appropriate boundary condition. Let us therefore define a functional interfacial voltage $V_i(x)$ by the above equation (6.3.8) with V_i replaced by $V_i(x)$, and with the lower limits of the integrals for Q_{sc} and Q_{sco} replaced by x, (the position in the semiconductor substrate). Therefore one observes that when x=o, $V_i(x)$ represents the interfacial voltage V_i developed across the insulating layer. The expressions for Q_{io} and Q_i , given by equations (6.3.11) and (6.3.12) respectively, are calculated as functions of V_i ($=V_i(x=o)$) and ϕ_B (which is known from the equilibrium problem of chapter 5). Consequently, Q_i and Q_{io} have no direct x dependence. Hence from equation (6.3.8) the differential equation for $V_i(x)$, and its associated boundary condition are given by

$$-(\varepsilon_i/\delta)\frac{dV_i(x)}{dx} = -e(p(x) - n(x) + N_D^+(x)) + e(p_o(x) - n_o(x) + N_{Do}^+(x))$$

which becomes

$$\frac{dV_i(x)}{dx} = \frac{\delta e}{\varepsilon_i} \{(p(x) - p_o(x)) - (n(x) - n_o(x)) + N_D^+(x) - N_{Do}^+(x)\}, \tag{6.3.13}$$

and

$$-(\varepsilon_i/\delta)\, V_i(x=L) = (\frac{\delta}{2})\, (\rho-\rho_o) + (Q_i-Q_{io}) - \varepsilon_s(E_s(L) - E_s^o(L)). \tag{6.3.14}$$

In principle, the boundary condition (6.3.14) relates $V_i(x)$ at $x = L$ to $V_i(x=o)$ (implicit in expressions for Q_i and Q_{io}) and the electrostatic fields $E_s^o(x)$, $E_s(x)$ both at $x = L$. However, we should remember that the differential equation (6.3.13) is coupled to the position dependent quasi-Fermi levels $E_{Fn}(x)$ and $E_{Fp}(x)$, governing the concentration of electrons and holes in the semiconductors conduction and valence bands respectively. Therefore equation (6.3.13) must be solved simultaneously with the equations predicting the band edge and quasi-Fermi level variations with the position x in the semiconductor substrate. The interfacial voltage V_i developed (as a result of the operating conditions) across the interfacial layer of an n-type Schottky barrier solar cell is represented by $V_i(x=o)$, and can only be obtained numerically, when the voltage V is specified together with the parameters of table 3, through a complete solution to the system of equations governing the properties of the solar cell. We will now set up the remaining differential equations and their associated boundary conditions.

In the n-type semiconductor, Poisson's equation for the electrostatic field is given by

Table 3

Data adopted for an Au - SiO_2/n-type Si S.B.S.C.

parameter	numerical value	dimensions	references and notes
A_e^*	120	$Acm^{-2}K^{-2}$	Pulfrey & McOuat 1974
A_h^*	120	$Acm^{-2}K^{-2}$	—
D_S	1.0×10^{16}	$m^{-2}\ eV^{-1}$	Lane (1968)
$m_{e/m}$	1.1	-	Effective mass ratio for electrons.*
$m_{h/m}$	0.59	-	Effective mass ratio for holes.*
μ_e	1900	$cm^2V^{-1}s^{-1}$	* [An asterisk refers to Sreedhar et al (1969)]
μ_h	425	$cm^2V^{-1}s^{-1}$	*
E_g	1.1	eV	*
χ	4.01	eV	*
T	300	K	-
ε_s	$11.8\ \varepsilon_o$	Farad m^{-1}	ε_o permittivity of free space
ε_i	$43.9\ \varepsilon_o$	Farad m^{-1}	ε_o permittivity of free space
ϕ_M	4.7	eV	Riviere (1957), Sze (1969)
N_D	1.0×10^{21}	m^{-3}	-
E_{DI}	0.049	eV	As dopant, Bonch-Bruevich & Landsberg (1968)
ρ_o	0	$Q\ m^{-3}$	-
δ	19	Å	-
L	3.6	μm	-
P_{in}	0.1	$W\ cm^{-2}$	incident power, using an AM1 spectrum.
χ_n	0.93	eV	Buxo. et al 1976
χ_h	0.88	eV	Buxo. et al 1976

Table 3 continued

parameter	numerical value	dimensions	references and notes
τ_{oe}	6.6×10^{-14}	s	Lundstrom & Svensson (1972)
τ_{oh}	6.6×10^{-14}	s	-
B^s	1×10^{-11}	$cm^3\ s^{-1}$	Landsberg 1967
B_1	1.2×10^{-32}	$cm^6\ s^{-1}$	D. Hill & P.T. Landsberg (1976)
B_2	1.2×10^{-32}	$cm^6\ s^{-1}$	D. Hill & P.T. Landsberg (1976)
$T_1^s = T_2^s$	1.12×10^{-8}	$cm^3 s^{-1}$	from capture cross-section x thermal velocity (Barret & Vapaille 1975)
$T_{1\,i}^{\ s} = T_{2\,i}^{\ s}$	1.12×10^{-8}	$cm^3 s^{-1}$	from capture cross-section x thermal velocity (Barret & Vapaille 1975)
$T_1=T_2=T_3=T_4$	3.66×10^{-25}	$cm^6 s^{-1}$	$T_1 = T_1^s \times (5 \times 10^{-7})/n_i$ (Evans & Landsberg (1963))
$T_{1i}=T_{2i}=T_{3i}=T_{4i}$	3.66×10^{-25}	$cm^6 s^{-1}$	$T_1 = T_1^s \times (5 \times 10^{-7})/n_i$ (Evans & Landsberg (1963))

The values of the recombination coefficients T_i are needed only in the calculations of the interfacial surface state current densities, and are there taken as independent of the trap energy E_t. The recombination coefficients T are needed only to calculate the recombination occuring within the substrate. It is hoped however, that the simplifications implied by the last four lines of table 3 will yield the correct orders of magnitude of these current densities.

The electron/hole tunnel time constants (τ_{oe} and τ_{oh} respectively) of an interfacial surface state, have been assumed to be equal and furthermore the weak dependence on the surface state energy has been ignored in the calculations. Also, the electron and hole tunneling barriers between each interfacial surface state and the barrier metal are assumed to be the same as the respective tunneling barriers between the barrier metal and the semiconductors conduction and valence bands. Therefore by equation (4.4.51), the net tunnel time constant τ is given by

$$\frac{1}{\tau} \simeq \frac{1}{\tau_{oe}} \exp\left(-\bar{\delta}\, \chi_n^{\frac{1}{2}}\right) + \frac{1}{\tau_{oh}} \exp\left(-\bar{\delta}\, \chi_h^{\frac{1}{2}}\right) .$$

$$\frac{dE_s(x)}{dx} = \frac{e}{\varepsilon_s}\left[p(x) - n(x) + N_D^+(x)\right] \quad . \qquad (6.3.15)$$

The electrostatic potential $\phi_s(x)$ is therefore given by

$$\frac{d\phi_s(x)}{dx} = -E_s(x) \quad . \qquad (6.3.16)$$

We shall take the origin of the electrostatic potential $\phi_s(x)$ at the barrier metal Fermi level E_{FM} (see figure 6.1). Clearly with $E_{FM} - \phi_s(x)$ as the electrons potential energy (eV) in the semiconductor's conduction band, we see that the electrostatic potential is measured in an opposite sense to the electron's potential energy (the electron's potential energy increases upwards in figure 6.1 while the electrostatic potential increases downwards in the figure). We measure the electron's energy in units of electron volts, therefore the steady state electron, hole and ionized doping concentrations, represented by n(x), p(x) and $N_D^+(x)$ respectively, are given by

$$n(x) = N_c \exp\left(e(\phi_s(x) + E_{Fn}(x) - E_{FM})/kT\right), \qquad (6.3.17)$$

$$p(x) = N_v \exp\left(e(-E_{Fp}(x) - \phi_s(x) - E_g + E_{FM})/kT\right), \qquad (6.3.18)$$

and

$$N_D^+(x) = \frac{(\bar{G}\,\bar{n}_1(x) + \bar{H}p(x))\,N_D}{\bar{G}(n(x) + \bar{n}_1(x)) + \bar{H}(p(x) + \bar{p}_1(x))} \qquad (6.3.19)$$

where we have used equations (2.2.12), (2.2.13) and (5.2.16) together with $E_c(x) - E_{FM} = -\phi_s(x)$ and $E_c(x) - E_v(x) = E_g$. [$E_{Fn}(x)$ and $E_{Fp}(x)$ represent the position dependent quasi-Fermi levels.] Also $\bar{G}$, $\bar{H}$ and the Schockley-Read parameters $\bar{n}_1(x)$ and $\bar{p}_1(x)$ from

(5.2.12) are given by

$$\overline{G} = T_1^s + T_1 n(x) + T_2 p(x) \text{ and } \overline{H} = T_2^s + T_3 n(x) + T_4 p(x), \quad (6.3.20)$$

with

$$\frac{\bar{n}_1(x)}{n_o(x)} = \frac{p_o(x)}{\bar{p}_1(x)} = \tfrac{1}{2} \exp\left(-e\left(E_{DI} + \phi_s^o(x)\right)/kT\right), \quad (6.3.21)$$

where $n_o(x)$ and $p_o(x)$ are as given in equations (5.4.9) and (5.4.10). The reaction constants T_1^s, T_1, T_2, T_2^s, T_3, T_4 are defined through figure 2.4 and equations (2.4.13) and (2.4.14). N_D is of course, the total (ionized + unionized) doping concentration.

The two continuity equations, one for electrons in the semiconductor's conduction band and the other for holes in the semiconductor's valence band, are given by equations (2.5.5) and (2.5.6) as

$$\frac{dJ_e}{dx}(x) = e(U - F), \quad (6.3.22)$$

$$\text{and} \quad \frac{dJ_h}{dx}(x) = -e(U - F), \quad (6.3.23)$$

where F is the photogeneration rate, which is a function of position x in the semiconductor's substrate, given by (2.5.17), while U represents the total recombination rate at some position x in the semiconductor. We therefore write U as the sum of two components: U_{unav} for band-band transitions, and U_{avoid} for transitions involving intermediate trapping levels (i.e. donor levels). Thus

$$U = U_{unav} + U_{avoid}$$

$$= \overline{F}(n(x)p(x)-n_i^2) + \frac{(n(x)p(x)-n_i^2)\ \overline{G}\ \overline{H}\ N_D}{\overline{G}(n(x)+\overline{n}_1(x)) + \overline{H}(p(x)+\overline{p}_1(x))}\ , \quad (6.3.24)$$

where we have obtained expressions for U_{unav} and U_{avoid} from equations (2.5.1) and (5.2.15) respectively. Here we have written U_d, the steady state recombination rate due to the donor traps, as U_{avoid}.

Two more equations are required before the system of differential equations is complete, they are the phenomenological current density equations for electron and hole flow in the semiconductor's conduction and valence bands respectively. From equations (2.2.15) and (2.2.16) they are, in a one dimensional setting, given by

$$J_e(x) = e\mu_n\ n(x)\ \frac{d}{dx}\ E_{Fn}(x), \quad (6.3.25)$$

$$\text{and}\quad J_h(x) = e\mu_p\ p(x)\ \frac{d}{dx}\ E_{Fp}(x), \quad (6.3.26)$$

where μ_n and μ_p are respectively, the mobilities of electrons in the semiconductor's conduction band and holes in the semiconductor's valence band. In fact both μ_n and μ_p have been assumed to be independent of position in the calculations performed later. The equations (6.3.13), (6.3.15), (6.3.16), (6.3.22), (6.3.23), (6.3.25) and (6.3.26) together with the differential equations (5.4.12), for the thermodynamic equilibrium problem, give the complete system of differential equations, which when used in conjunction with appropriate boundary conditions, predict the

behaviour of the n-type Schottky barrier solar cell (with a thin insulating interfacial layer).

We will now establish the remaining boundary conditions for the above system of equations. The boundary condition for equation (6.3.13) has already been found and is given in (6.3.14). Let us consider an n-type Schottky barrier solar cell having a finite semiconductor substrate thickness L. We assume that an ohmic contact is formed at x = L, and that figures 6.1(a) and (b) represent the n-type S.B.S.C.'s band diagram, when the cell is illuminated and unilluminated respectively. A voltage V exists across the device in such a way that it is forward biased when V>o. Then for an n-type S.B.S.C. the Fermi-level at the ohmic contact x = L (which incidentially equals the quasi-Fermi levels E_{Fn} and E_{Fp} just inside the semiconductor at x = L, see chapter 5, section 3) is raised above the barrier metal's Fermi level E_{FM} by an amount equal to V. Therefore at the ohmic contact (x = L) we have the following conditions:

$$\phi_s(L) = -(V_n + V), \quad E_{Fn}(L) = E_{FM} + V \qquad (6.3.27)$$

and $E_{Fp}(L) = E_{FM} + V$,

where V_n is determined from equation (5.3.5) (i.e. charge neutral ity at the ohmic contact). However, at the other end of the semiconductor substrate (x = o) we have a condition on the electrostatic potential $\phi_s(x = o)$. This is deduced by observing (from figure 6.1) that the bottom of the semiconductor's conduction band at the interface x = o is above E_{FM} by an amount equal to ϕ_B in thermo-

dynamic equilibrium, and an additional amount V_i for non-equilibrium conditions. Therefore at x = o we have a relation between the electrostatic potential, the thermodynamic equilibrium barrier height ϕ_B and the interfacial voltage V_i developed across the interfacial layer. Thus

$$\phi_s(o) = -(\phi_B + V_i), \text{ at } x = o. \qquad (6.3.28)$$

We shall now establish two more boundary conditions at the interface x = o. These boundary conditions will connect the thermionic emission tunnel current densities and the interfacial surface state recombination current densities to the quasi-Fermi levels $E_{Fn}(x)$ and $E_{Fp}(x)$ at the position x = o. Here, the thermionic emission tunnel current density, and the interfacial surface state recombination current density, represent the two components of the current density in the semiconductor's substrate just away from x = o. Let J_e^t be the electron thermionic emission current density, due to electrons tunneling through the insulating layer $x\varepsilon(-\delta,o)$ between the barrier metal and the semiconductors conduction band and let J_h^t be the hole thermionic emission current density, due to holes tunneling through the insulating layer between the barrier metal and the semiconductor's valence band. Finally, we let J_t represent the interfacial surface state tunnel current density, due to carriers communicating between the barrier metal and the interfacial surface states.

Consider a small region of semiconductor $x\varepsilon(o,\varepsilon)$ where ε is small and greater than zero, see figure 6.2. We shall assume that this region of the semiconductor contains all the interfacial

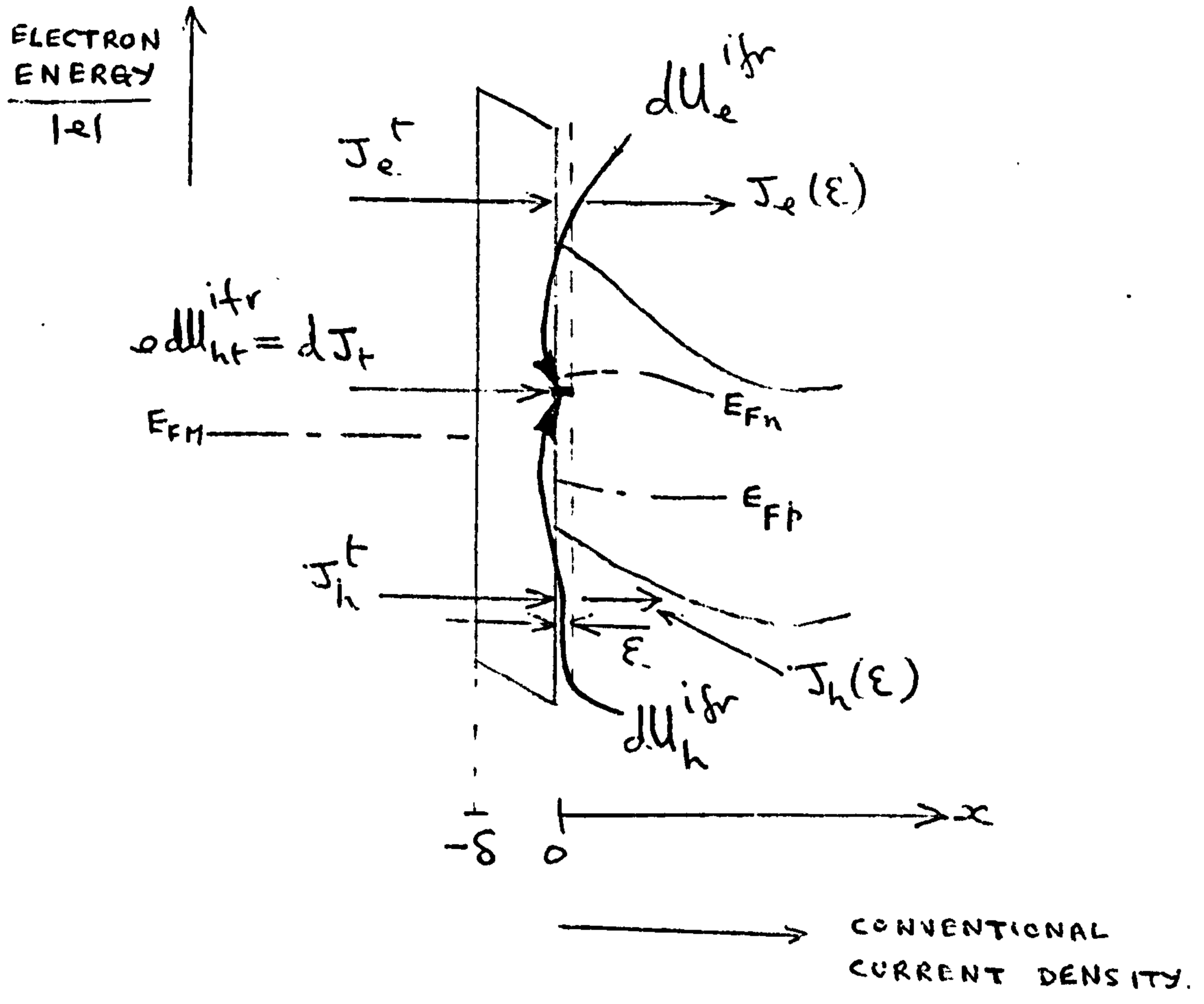

Figure 6.2 Band diagram of an n-type S.B.S.C. illustrating the tunnel currents between the metal and both the interfacial surface states and the bands of the semiconductor.

surface states. Invoking the conservation of charge in the semiconductor's conduction band near x = o, one has for the electron current densities

$$J_e{}^t/_e + \int dU_e{}^{ifr} = J_e(\varepsilon)/_e \,, \tag{6.3.29}$$

where $J_e(\varepsilon)$ represents the electron current density just inside the semiconductor region, while $\int dU_e{}^{ifr}$ represents the total net electron recombination rate due to the interfacial surface states and is given by (6.2.14).

Similarly for holes in the semiconductor's valence band, we obtain

$$J_h{}^t/_e = \int dU_h{}^{ifr} + J_h(\varepsilon)/_e \,, \tag{6.3.30}$$

where $J_h(\varepsilon)$ represents the hole current density just inside the semiconducting region, while $\int dU_h{}^{ifr}$ represents the total net hole recombination rate due to the interfacial surface states and is given by equation (6.2.15). Now we let $\varepsilon \to o_+$ so that the interfacial surface states become confined to a sheet distribution. Assuming that the quasi-Fermi levels remain virtually unchanged (over the interval $[o,\varepsilon)$) as they meet the interfacial layer at x = o we identify $J_e(\varepsilon)$ and $J_h(\varepsilon)$ as $\varepsilon \to o_+$ with $J_e(o)$ and $J_h(o)$ respectively. Also the two thermionic emission tunnel current densities $J_e{}^t$ and $J_h{}^t$, representing the thermionic emission tunnel current densities due to electron and hole tunneling between the barrier metal and the semiconductor's conduction and valence bands respectively, are constructed in (A.11) and (A.16) of Appendix A, and are given as

$$J_e{}^t = A_e^* T^2 \exp(-\chi_n{}^{\frac{1}{2}} \bar{\delta}) \exp(-e(\phi_B+V_i)/kT)\{\exp(e(E_{Fn}(o)-E_{FM})/kT)-1\}, \quad (6.3.31)$$

and

$$J_h{}^t = A_h^* T^2 \exp(-\chi_h{}^{\frac{1}{2}} \bar{\delta}) \exp(-e(E_g-\phi_B-V_i)/kT)\{1-\exp(-e(E_{Fp}(o)-E_{FM})/kT)\}, \quad (6.3.32)$$

where A_e^* and A_h^* represent the effective Richardsons constants for the thermionic emission of electrons and holes repectively. χ_n and χ_h represent the effective tunnel barrier heights (eV) present against tunneling electrons and holes respectively. $\bar{\delta}$ in this case represents the thickness of the interfacial layer measured in $\mathring{A}$, see for example J. Buxo et.al. (1976). The interfacial voltage V_i developed (as a result of the illumination) across the insulating interfacial layer is of course, coupled to equation (6.3.13) where it was stated that $V_i = V_i(x=o)$. From equations (6.3.29) and (6.3.30) we construct the two final boundary conditions as

$$J_e(o) = J_e{}^t + e\int dU_e{}^{ifr}, \quad (6.3.33)$$

$$\text{and} \quad J_h(o) = J_h{}^t - e\int dU_h{}^{ifr}, \quad (6.3.34)$$

where $J_e{}^t$, $J_h{}^t$, $\int dU_e{}^{ifr}$ and $\int dU_h{}^{ifr}$ are given by the equations (6.3.31), (6.3.32), (6.2.14) and (6.2.15) respectively.

So, we have seven boundary conditions (6.3.14), (6.3.27), (6.3.28), (6.3.33) and (6.3.34) which match the seven first order non-linear differential equations given in this chapter. In fact, because of the dependence of equations (6.3.19) and (6.3.24) on

the equilibrium electron and hole concentrations, we introduce the equations established in chapter 5 to the above mentioned system. Therefore the system of equations covering the behaviour of the n-type Schottky barrier solar cell with a thin insulating interfacial layer, is composed of ten simultaneous first order non-linear coupled differential equations, with ten boundary conditions, some of which are of the mixed type.

A solution to this system, for a particular operating voltage, yields the semiconductor's band edges, the quasi-Fermi levels ($E_{Fn}(x)$ for electrons in the c.b. and $E_{Fp}(x)$ for holes in the v.b), the electrostatic field $E_s(x)$, the electron and hole current densities $J_e(x)$ and $J_h(x)$, all as functions of position x in the semiconductor substrate $x\varepsilon(o,L)$. Also, the thermodynamic equilibrium barrier height ϕ_B is found using the procedure of chapter 5, and the interfacial voltage V_i developed across the insulating layer is given by the value of $V_i(x)$ at $x = o$.

In all of the work presented in this chapter the image force lowering effect has been neglected. This causes the total current density J ($=J_e(x)+J_h(x)$), which is independent of x by virtue of equations (6.3.22) and (6.3.23), to be slightly underestimated . Note that when the n-type Schottky barrier solar cell is delivering power J is less than zero, while on the other hand when it is forward biased in the dark J is greater than zero. A few remarks concerning the method of solution will be given in the next section, also numerical results for calculations performed for an Au - SiO_2 n-type Si Schottky barrier solar cell will be presented and discussed.

6.4 Discussion of results

Some results of the theory are presented in figures 6.3 - 6.9. They were calculated by assuming that a total voltage V exists across the Au - SiO_2 - n-type Si Schottky barrier solar cell, and that the parameters of table 3 are given. The neutral level ϕ_o is assumed to be independent of applied voltage and illumination and has been estimated to lie at about 0.3± 0.36 eV (Cowley and Sze 1965), and it has been taken as zero for the present calculation. In the numerical work we have assumed that the volume charge density ρ is independent of illumination and output voltage, $s\sigma\ \rho=\rho_o$.

Briefly, the method of solving the equations of section 6.3, is as follows: (a) The thermodynamic equilibrium problem of chapter 5 is solved, according to the algorithm presented in section 5.4. This gives us the thermodynamic equilibrium barrier height ϕ_B, and the variation of the equilibrium electrostatic potential and field with the position x in the semiconductor. (b) The boundary condition (6.3.14) is restructured by defining a new function $\bar{V}_i(x)$ given by

$$\bar{V}_i(x) = V_i(x) - V_i(x=L). \qquad (6.4.1)$$

It is clear that $\bar{V}_i(x)$ must satisfy equation (6.3.13) because $V_i(x=L)$ has no x dependence. Therefore we replace the differential equation (6.3.13) for the functional interfacial voltage by

$$\frac{d\bar{V}_i}{dx}(x) = \left(\frac{\delta e}{\varepsilon_i}\right)\{(p(x)-p_o(x))-(n(x)-n_o(x))+(N_D^+(x)-N_{Do}^+(x))\}, \qquad (6.4.2)$$

where we have the corresponding boundary condition as

$$\bar{V}_i(x) = o \quad \text{at } x = L \text{ (i.e. at the ohmic contact).} \qquad (6.4.3)$$

Now as

$V_i(x) = V_i$ when $x = o$, we observe that

$$V_i = \bar{V}_i\ (x = o) + V_i(x = L). \qquad (6.4.4)$$

(c) The next step is to introduce the parameters $J_e(L)$, $J_h(L)$ and $E_s(L)$ which represent respectively the electron current density, the hole current density and the electrostatic field, all at the ohmic contact ($x = L$). These parameters, if known, would complete the set of boundary conditions at $x = L$.

Treating the problem of an n-type Schottky barrier solar cell as an initial value problem we integrate the system of differential equations from $x = L$ to $x = o$. Having <u>assumed</u> specific values for the parameters $J_e(L)$, $J_h(L)$, $E_s(L)$ and V_i, we then use the calculated function values ($E_{Fn}(o)$, $E_{Fp}(o)$, $\phi_s(o)$, $J_e(o)$, $J_h(o)$ and $\bar{V}_i(o)$) to estimate the accuracy of the boundary conditions at $x = o$. Therefore we construct the following error function

$$f(J_e(L),J_h(L),E_s(L),V_i) = (\phi_s(o) + \phi_B + V_i)^2 + (J_e(o) - J_e^t - e\int dU_e^{ifr})^2$$

$$+(J_h(o) - J_h^t + e\int dU_h^{ifr})^2 + (\bar{V}_i(o) + V_i(x=L) - V_i)^2, \qquad (6.4.5)$$

where we must stress that $\phi_s(o)$, $J_e(o)$, $J_h(o)$ and $\bar{V}_i(o)$ have been obtained as a result of integrating the differential equations from $x=L$ to $x=o$. Hence these calculated function values at position $x=o$ are themselves functions of the three unknown parameters $J_e(L)$, $J_h(L)$ and $E_s(L)$. The interfacial voltage V_i developed across the insulating layer has been introduced as a

parameter to facilitate the formation of the error function (6.4.5). We see that $f(J_e(L), J_h(L), E_s(L), V_i)$ is always greater than or equal to zero. Thus by minimizing the function of (6.4.5) with respect to the four variables $J_e(L)$, $J_h(L)$, $E_s(L)$ and V_i, together with the constraint that at the required minimum the value of f is zero, the boundary conditions at the interface x=o will therefore be satisfied at the minimum point. The values of the four variables $J_e(L)$, $J_h(L)$, $E_s(L)$ and V_i at the minimum point determine the solution (at a particular voltage V) completely. This basic numerical procedure has been applied to both the illuminated and unilluminated Au - SiO_2 - n-type Si Schottky barrier solar cell, for various operating voltages V(>o, forward bias).

Figure 6.3 shows the variation of the electrostatic field $E_s(x)$ with the position x in the semiconductors substrate ($o \leq x \leq L$). The thermodynamic equilibrium electrostatic field's variation with position is shown for comparison purposes. The electrostatic field $E_s(x)$, for the illuminated n-type Schottky barrier solar cell, is seen to have a negative non-zero value for all $x \in [o,L]$ when the solar cell is short circuited. As the output voltage V is increased the hole and electron current densities at the ohmic contact (x=L) increase, thereby reducing the magnitude of the output current density. (When the n-type S.B.S.C. is delivering power the total current density $J = J_e(x) + J_n(x)$ is of negative sign). Therefore we expect the electrostatic field $E_s(L)$ at the ohmic contact (x=L) to increase with increasing output voltage V. In fact the elestrostatic field $E_s(L)$ changes, from being of negative sign at shortcircuit conditions, to be of positive sign at the output voltage of 0.2 volts.

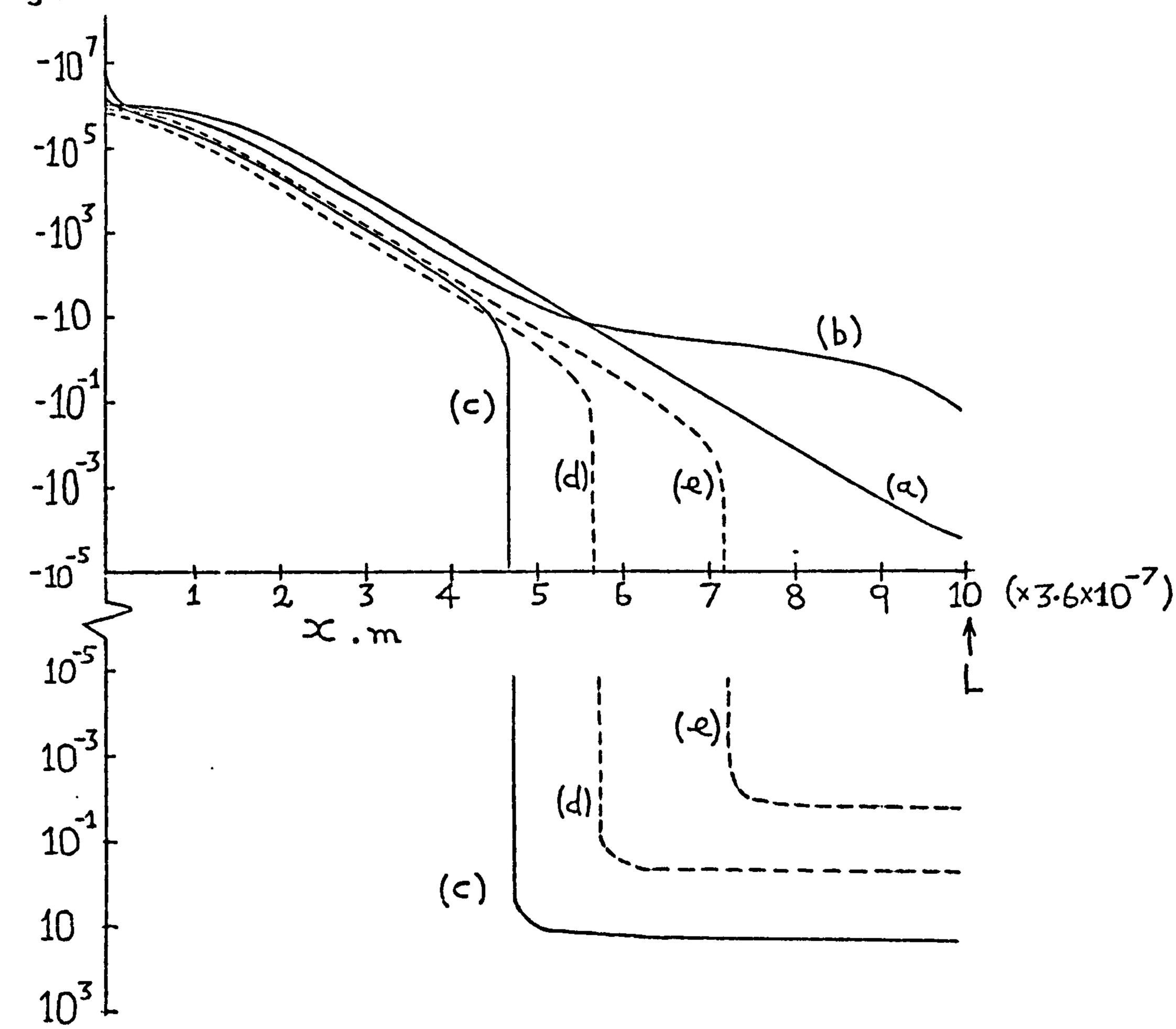

Figure 6.3 The electrostatic field $E_s(x)$ as a function of the position x in the semiconductor substrate. The parameters of table 3 have been used. (a) The thermodynamic equilibrium electrostatic field, (b) the electrostatic field of the illuminated and short-circuited cell, (c) the electrostatic field of the illuminated cell operating at an output voltage of 0.2 volts, (d) the electrostatic field of the unilluminated cell at a forward potential of 0.3 volts, (e) the electrostatic field of the unilluminated cell at a forward potential of 0.2 v.

As we move towards the barrier region the electrostatic field $E_s(x)$ eventually settles down to follow an exponential type of variation with the position x in the semiconductors substrate. However, as we move a little closer to the interface at x=o, the volume charge density in the semiconductor tends to approach a constant value (this is because the electron concentration n(x) then becomes small when compared with $N_D^+(x)$, and so far the hole concentration p(x) has had a negligible effect on the volume charge density). Consequently the electrostatic field $E_s(x)$ therefore begins to decrease approximately linearly with decreasing x, so the electrostatic field in figure 6.3 appears to start leveling off.

Since the solar cell is being illuminated and is delivering power (J<o), there is an increase in the hole concentration near the interface x=o, due to the imperfect communication between the barrier metal and the semiconductor's valence band (see below). If the interfacial layer is thick enough (say 20 Å) and also if the tunneling barrier against hole flow between the barrier metal and the semiconductor's valence band is large enough (say an effective tunneling barrier of 0.9 eV), then the hole concentration which builds up at the interface x=o, (because of the influx of photogenerated holes) may have a magnitude somewhat similar to that of the ionized doping concentration $N_D^+(x)$. Therefore in considering the electrostatic field's variation close to the interface, one sees that as we move closer towards the interface the volume charge density becomes extremely sensitive to the hole concentration near the interface.

Hence, as we move away from the region of near constant volume charge density ($=eN_D^+(x)$) towards the interface, the contribution to

the volume charge density from the build-up of photo-generated holes becomes pronounced. Consequently, for x very near zero(say to within 0.15μm)the volume charge density increases rapidly as x decreases. Thus the electrostatic field $E_s(x)$ decreases strongly with decreasing x (when x is less than 0.15μm say).

Also shown in figure 6.3 are the variations of the electrostatic field $E_s(x)$ for the <u>unilluminated</u> n-type Schottky barrier solar cells. For any appreciable forward voltage, greater than 0.05 volts say, the electrostatic field in the semiconductor at the ohmic contact x=L is positive. Note that for all forward voltages (V>o), the total current density J flowing is also positive. Again, as the barrier region is approached the electrostatic field takes an exponential variation with the position x in the semiconductor. This is caused by the increase in the volume charge density, due to the decrease in the electron concentration n(x), as x decreases. The increase in the hole concentration p(x), in the expression for the volume charge density, never becomes important when the n-type S.B.S.C. is forward biased in the dark. Eventually, as we move closer still to the interface x=o, say to within 0.5μm of the interface, the effect of the decreasing electron concentration n(x) with decreasing x becomes relatively unimportant. Hence in this region the volume charge density ρ(x) almost equals the ionized donor charge concentration $eN_D^+(x)$. Therefore for x less than about 0.5μm, the volume charge density remains almost constant for a forward bias voltage V. Consequently because ρ(x) is no longer increasing rapidly with decreasing x (when x is near x=o), the electrostatic field $E_s(x)$ for the unilluminated n-type S.B.S.C. under a forward bias V, decreases approximately linearly with decreasing x. Therefore(for various forward voltages) the

electrostatic field $E_s(x)$ in the substrate of the unilluminated n-type S.B.S.C., shown in figure 6.3, appears to level off near x=o.

In figure 6.4, the variation of the electrostatic potential as a function of the position x in the semiconductor substrate ($o \leq x \leq L = 3.6\mu m$) is shown for various operating conditions. The electostatic potential $\phi_s(x)$ is measured from an origin at the barrier metal's Fermi level E_{FM} such that $E_c(x) - E_{FM} = -\phi_s(x)$. Here $E_c(x)$ represents the variation of the bottom of the semiconductor's conduction band with x. Also $E_v(x)$, representing the top of the semiconductor's valence band, is related to the potential distribution $\phi_s(x)$ by $E_v(x) = -E_g + E_c(x) = -E_g - \phi_s(x) + E_{FM}$, so we see that the band edges are parallel to $-\phi_s(x)$. In particular we note that at the interface $E_c(x=o) - E_{FM}$ ($= -\phi_s(o)$), represents the thermodynamic equilibrium barrier height ϕ_B plus the interfacial voltage V_i developed across the insulating interfacial layer. The thermodynamic equilibrium electrostatic potential $\phi_s^o(x)$ is, from chapter 5, shown for comparison purposes.

The illuminated n-type Schottky barrier solar cell under short circuit conditions has an electrostatic potential distribution $\phi_s(x)$ in the semiconductor's substrate, and has the following properties: The short circuit electrostatic potential remains almost constant for $x > 1.5\mu m$, being virtually the same as $\phi_s^o(x)$ for the larger x values. In fact when $x > 1.5\mu m$, $\phi_s(x)$ is just less than $\phi_s^o(x)$, so that the conduction band edge of the short circuited n-type S.B.S.C. is just above the thermodynamic equilibrium conduction band edge. As we move towards

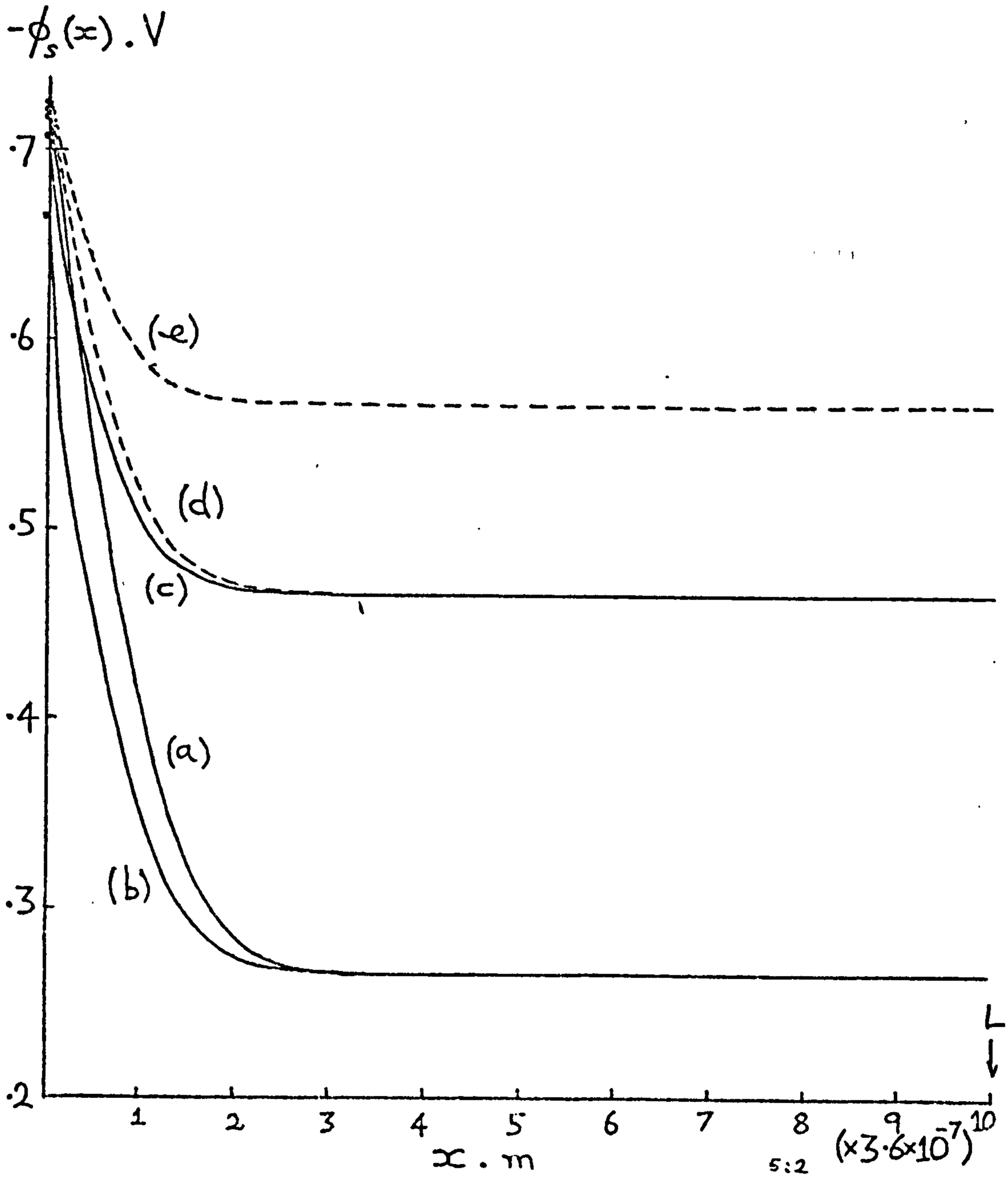

Figure 6.4 The electrostatic potential $\phi_s(x)$ as a function of the position x in the substrate. The parameters of table 3 have been used. (a) the thermodynamic equilibrium electrostatic potential distribution, (b) the electrostatic potential distribution for the illuminated and short-circuited cell (V_i = - 0.054v), (c) the electrostatic potential distribution for the illuminated cell operating at an output voltage of 0.2 volts (V_i = - 0.01v), (d) the electrostatic potential distribution of the unilluminated cell at a forward potential of 0.2 volts (V_i = 0.0019v), (e) the electrostatic potential distribution of the unilluminated cell at a forward potential of 0.3v (V_i = 0.0069v).

the interface x=o, the semiconductor's conduction band edge corresponding to the short-circuited n-type S.B.S.C. moves below the thermodynamic equilibrium conduction band edge. Eventually when the interface x=o is reached, the conduction band edge (at x=o) is below the thermodynamic equilibrium conduction band edge (at x=o) by an amount equal to $(-V_i)$. This gives the interfacial voltage V_i developed across the insulating interfacial layer (as a result of the illumination) as -0.054 volts, when the n-type Schottky barrier solar cell is short circuited. [An explanation of negative interfacial voltages will be given in the next section].

Figure 6.4, also shows the semiconductor's conduction band edge variation with position in the n-type S.B.S.C., at a forward bias voltage of 0.2 volts, with and without illumination. Here the semiconductor's conduction band edge under illumination always remains below that of the unilluminated cell. This is due to the fact that the electrostatic field in the semiconducting region of the illuminated cell (at an output voltage of 0.2V) is always greater than the electrostatic field of the unilluminated cell (at a forward bias of 0.2V), except when x is very close to zero, in which case the converse will be true. Therefore by invoking the relation $E_s(x) = \frac{-d}{dx} \phi_s(x)$ we deduce the above statements, by asserting that within the region very close to the interface, the sudden decrease in the electrostatic field in the semiconducting region of the illuminated n-type S.B.S.C. does not have a very marked effect on the position of the illuminated semiconductor's conduction band edge at the interface x=o. The interfacial voltage V_i for the illuminated n-type S.B.S.C., which is delivering power at an output potential of

0.2 volts, is given as -0.01 volts. However, in the case of the n-type S.B.S.C. forward biased at 0.2 volts in the dark, the interfacial voltage V_i is given as 0.0019 volts. The interfacial voltage V_i developed across the interfacial layer is seen to increase with the operating (forward bias) voltage V, for both the illuminated and unilluminated n-type Schottky barrier solar cells.

Turning now to figure 6.5, the increase in the electron quasi-Fermi level, of the illuminated n-type S.B.S.C. under short circuit conditions, with decreasing x is due to the electron current density at the ohmic contact having a negative sign. As the electron concentration near the ohmic contact is large, the electron quasi-Fermi level tends to increase slowly with decreasing x (this is clear from equation (6.3.25)). Now when we approach the barrier region, the electron current density remains of negative sign, but the semiconductor conduction band edge increases in energy (i.e. the potential $\phi_s(x)$ reduces with decreasing x in the barrier region). Hence the slope of the electron's quasi-Fermi level becomes much more negative as we approach the interface, because of the rapidly decreasing electron concentration in the barrier region. Thus as the position x, in the semiconductor's substrate, decreases the electron quasi-Fermi level increases rapidly in the barrier region.

For the short circuited and illuminated n-type Schottky barrier solar cell, the electron current density $J_e(x)$ tends to increase from its large negative value at the ohmic contact (x=L) to some positive value at the interface x=o. In the illuminated S.B.S.C. the electron current density will have a strong functional dependence on the position x, because of the strong x-dependence

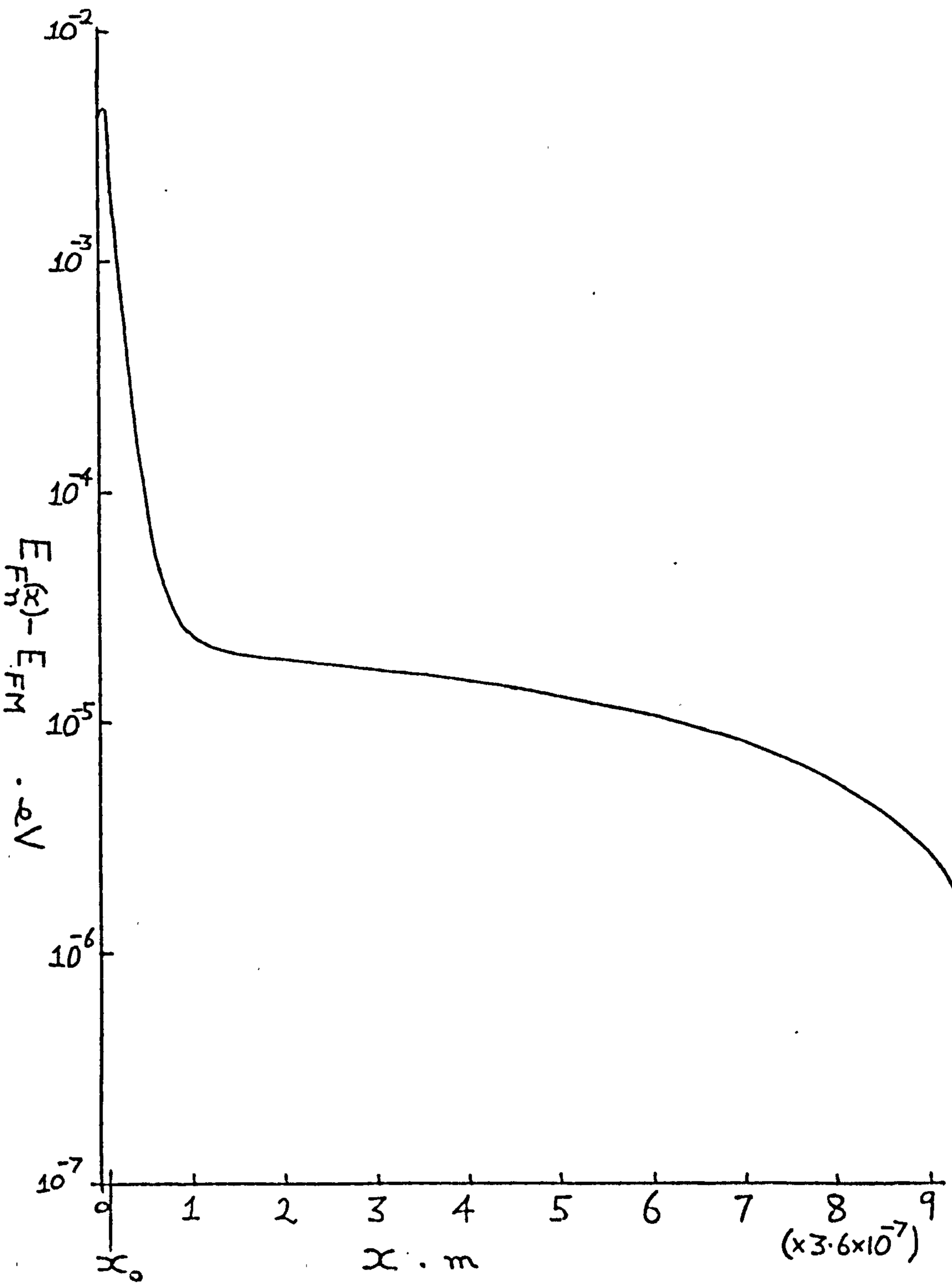

Figure 6.5 The electron quasi-Fermi level as a function of the position x in the substrate. The solar cell is being illuminated (100 mW cm^{-2} of direct radiation) under short-circuit conditions. The parameters of table 3 have been used.

of the photogeneration rate F(x) (see equations (6.3.22) and (2.5.17)). The electron current density is seen to be of positive sign at the interface, thus indicating that some emission of the photogenerated majority carriers (electrons) into the metal is occurring together with some interfacial surface state recombination (see, for example Lavagna et al 1977).

The electron current density is therefore seen to have a zero value at some point, x_o say, very close to the interface. When x is decreased to below x_o, the electron current density takes a positive value and because the electron concentration is low in this region, the electron quasi-Fermi level decreases as $x(<x_o)$ decreases. Hence we observe a maximum in the electron quasi-Fermi level at x_o as shown in the figure.

Figure 6.6 shows the variation of the hole quasi-Fermi level with the position x in the semiconductors substrate. The n-type S.B.S.C. is illuminated under short circuit conditions. At the ohmic contact x=L the hole diffusion current is large and positive because of the thin substrate used in the calculations. Consequently, the hole quasi-Fermi level drops rapidly with decreasing x,because of the very low hole concentration in the semiconductor's substrate at x=L. As we move towards the barrier region, the hole current density decreases in accordance with (6.3.23) and the hole concentration increases as the hole quasi-Fermi level decreases, therefore the hole quasi-Fermi level begins to level off as observed in the figure.

Eventually, as we continue to move towards the barrier region, the hole current density changes its sign (i.e. for x near the interface J_h is negative), and the hole quasi-Fermi level then begins to increase with decreasing x. Note that the hole concentration is still increasing with decreasing x (because of the rapidly

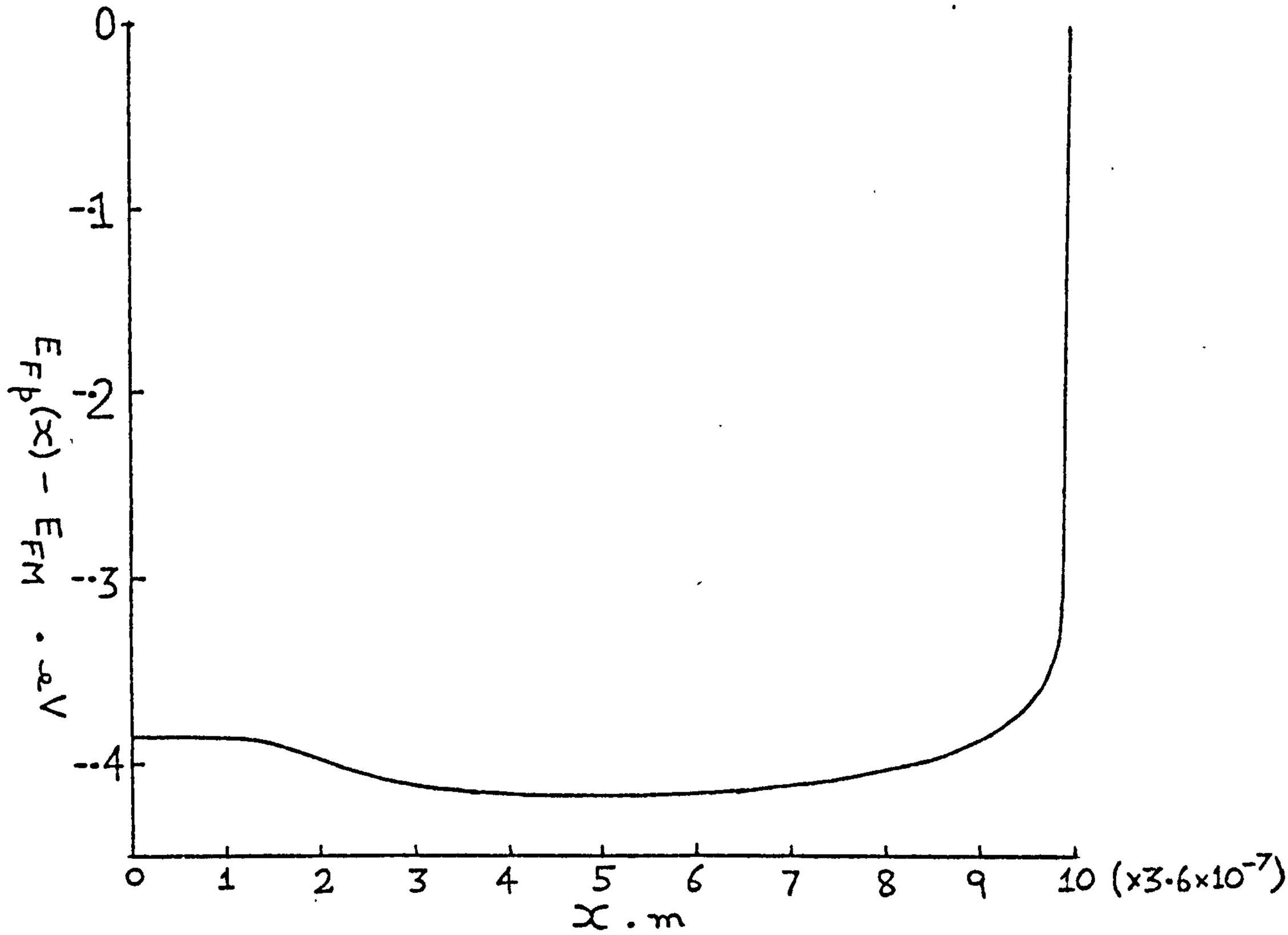

Figure 6.6 The hole quasi-Fermi level as a function of the position x in the substrate. The cell is being illuminated under short-circuit conditions. The parameters of table 3 have been used.

decreasing potential), but the dominant effect at the moment is the rapid decrease in the hole current density as we move closer to the interface. Ultimately, as we approach the interface x=o, the hole current density becomes increasingly negative and the hole concentration is seen to increase dramatically as the valence band edge becomes closer to the hole quasi-Fermi level. Therefore, according to (6.3.26), the hole quasi Fermi level is seen (from the figure) to level off as the interface x=o is approached. In fact the hole quasi-Fermi level at the interface x=o is below the barrier metal's Fermi level E_{FM} by an amount equal to 0.385 (eV). This indicates that the communication between the barrier metal and the semiconductor's valence band is rather poor. Therefore some of the photo-generated holes, which have accumulated in the semiconductor's valence band near the interface x=o, will be lost to recombination both at the interface and within the semiconductor. If the interfacial layer were made much thicker, then the above mentioned recombination effects would play a dominant role in the device characteristics, because the separation between the barrier metal Fermi level E_{FM} and the hole quasi-Fermi level $E_{Fp}(o)$ at the interface x=o is likely to become much larger for the thicker interfacial layers.

In figure 6.7 the electron and hole quasi-Fermi levels are shown as functions of the position x in the semiconductor's substrate, for the illuminated n-type Schottky barrier solar cell delivering power at a voltage of 0.2 volts. Here the major feature of interest is the increased magnitude of the hole diffusion current at the ohmic contact (x=L). This means that for the thin film S.B.S.C. studied, the hole diffusion current density $J_h(L)$ at x=L can be a very important loss mechanism

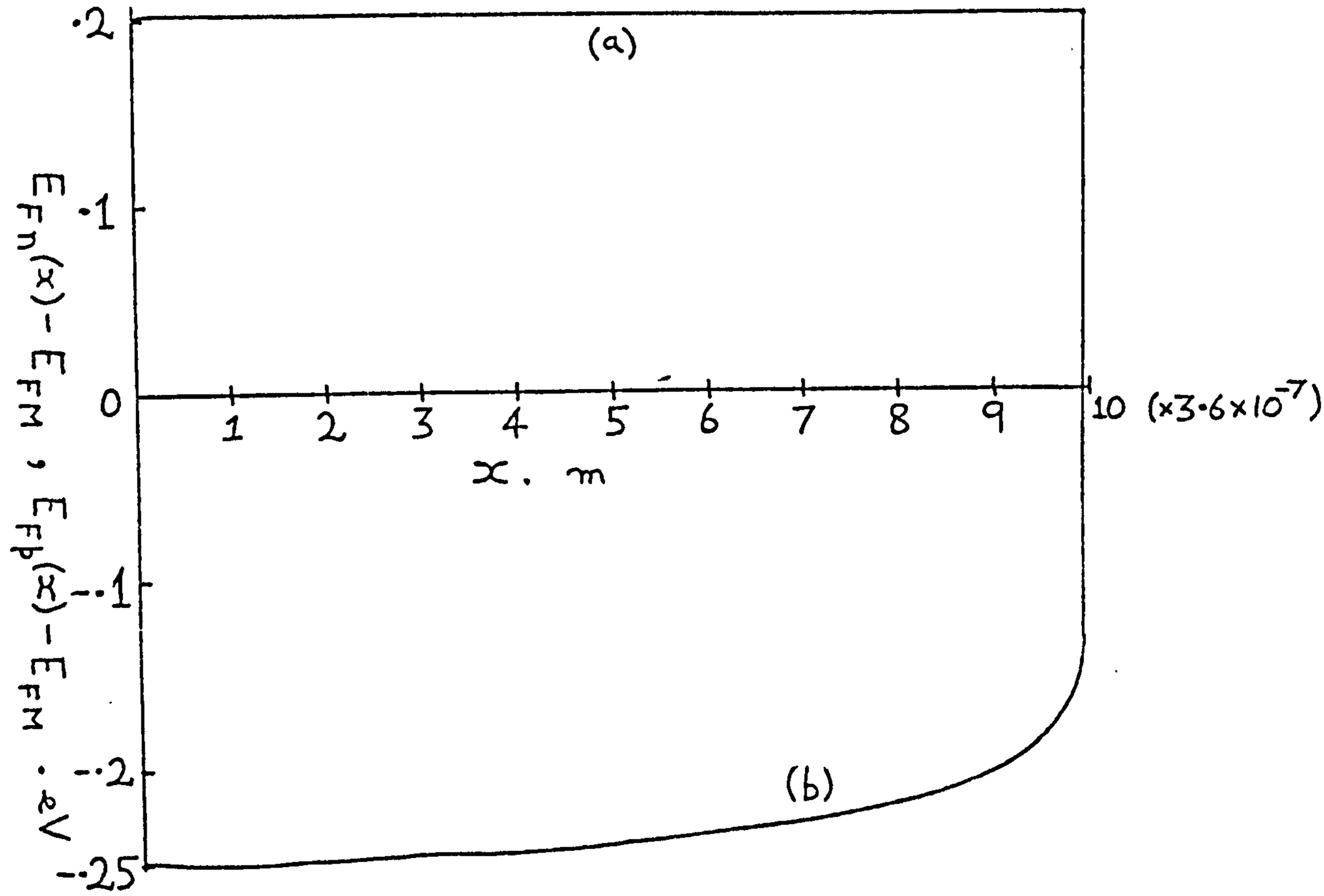

Figure 6.7 The electron and hole quasi-Fermi levels (E_{Fn} and E_{Fp} respectively) as functions of the position x in the substrate The cell is being illuminated and is delivering power at an output voltage of 0.2v. The parameters of table 3 have been used. Curve (a) represents the variation of the electron quasi-Fermi level whereas curve (b) represents the variation of the hole quasi-Fermi level.

(i.e. $J_h(L)$ being large and positive reduces the magnitude of the total current density flowing when the device is delivering power). The behaviour of the electron and hole quasi-Fermi levels as functions of the position x in the semiconductors substrate, are similar to those discussed for the short circuited n-type S.B.S.C. under illumination. However, we remark that, for the illuminated n-type S.B.S.C. at V=0.2 volts,the quasi-Fermi levels near the interface do not have such marked variations (with position), as the quasi-Fermi levels corresponding to the short circuited cell. In actual fact the electron quasi-Fermi level appears to be <u>almost</u> flat when compared to the variation of the hole quasi-Fermi level,with the position x,in the semiconductors substrate.

Figure 6.8 shows the variation, with position x, of the electron and hole quasi-Fermi levels for an unilluminated n-type Schottky barrier solar cell for various operating voltages V. When the device is forward biased in the dark, the electron and hole current densities remain positive and '<u>almost</u>' constant throughout the substrate. Therefore the electron quasi-Fermi level decreases slightly as x decreases. In fact when we approach the interface, the electron quasi-Fermi level tends to decrease a little faster, due to the reduction in the electron concentration near the interface x=o. This reduction in the electron quasi-Fermi level with decreasing x near x=o is not very pronounced because of the relatively low electron current density. If this electron current density were increased by applying a higher forward bias, then the electron concentration in the barrier region would also be increased, and consequently the electron quasi-Fermi level would only decrease (with position x) marginally faster than before.

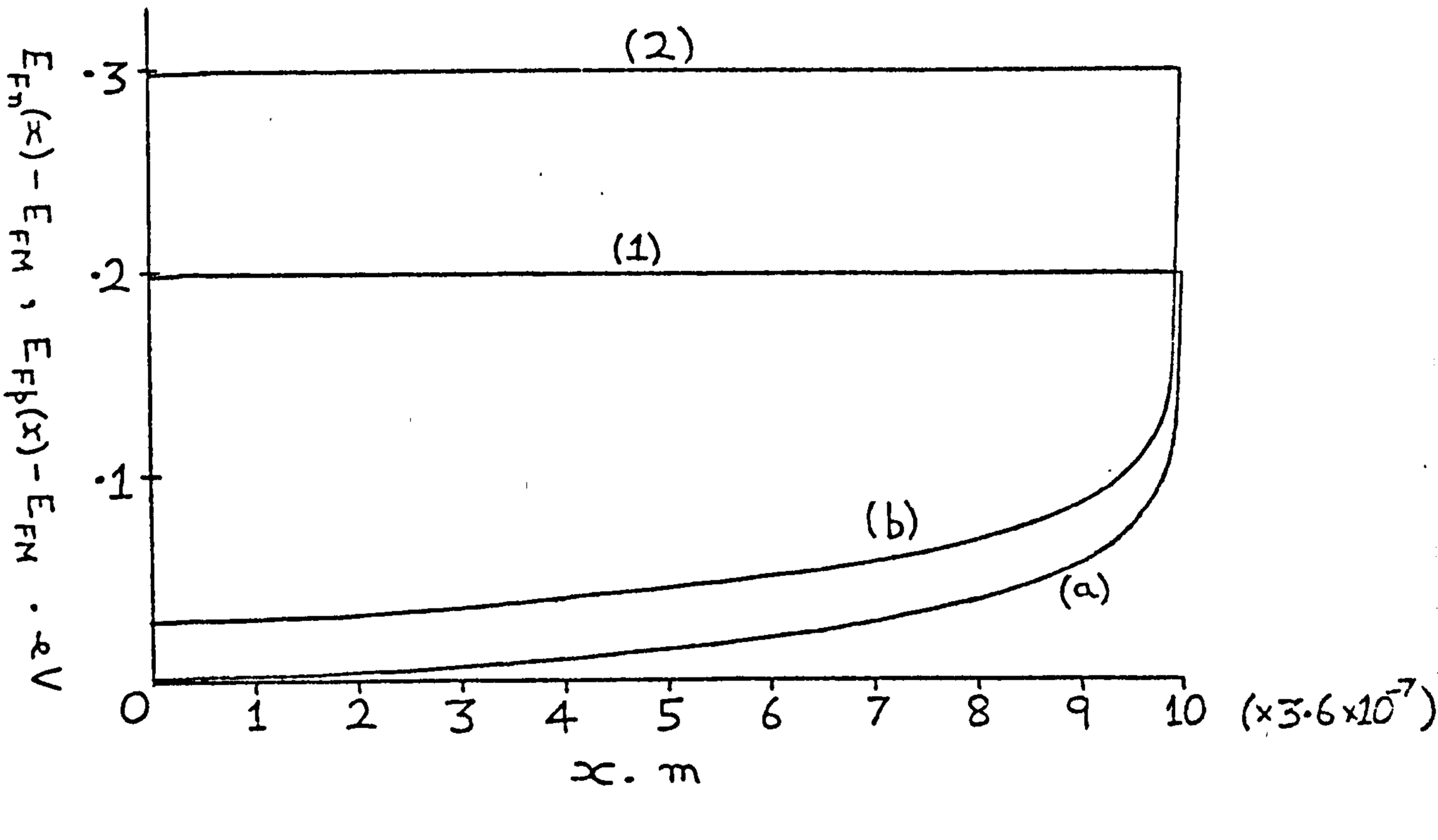

Figure 6.8 The electron and hole quasi-Fermi levels (E_{Fn}(curves 1,2)and E_{Fp} (curves a,b) respectively), as functions of the position x in the substrate. The cell is unilluminated, at a forward bias of 0.2 volts (curves 1 and a) and at a forward bias of of 0.3 volts (curves 2 and b). The parameters of table 3 have been used.

Turning our attention now to the hole quasi-Fermi level we see that (because of the low hole concentration at the ohmic contact (x=L), and as the hole current density at the ohmic contact is positive) the hole quasi-Fermi level decreases rapidly as we move away from the ohmic contact towards the barrier region. As we proceed in this direction, the hole quasi-Fermi level begins to level off because of the increase in the hole concentration, caused by the valence band edge becoming closer to the hole quasi-Fermi level. Ultimately when we reach the interface x=o, the hole quasi-Fermi level is slightly above the barrier metals Fermi level. Therefore we deduce that the separation between the quasi-Fermi levels at the interface x=o is always less than the forward voltage applied to an n-type S.B.S.C. in the dark.

Finally, in turning to figures 6.9 (a) and (b), the electron and hole current densities as functions of position x, in the semiconductors substrate, are given for both the unilluminated and illuminated n-type Schottky barrier solar cell, at various operating voltages V. The electron and hole current densities for the unilluminated n-type S.B.S.C. under a forward bias V, are seen (figure 6.9(a)) to remain almost constant across the semiconductor's substrate. This indicates that, for the unilluminated device, recombination in the semiconductor region is not a very important process. However, this is not the case for the interfacial surface state recombination effects. In fact the communication of the interfacial surface states with the barrier metal and the bands (at x=o), are observed to be very important processes when compared to the thermionic emission tunnel current densities. Therefore a substantial part of the total current density flowing through the device passes through

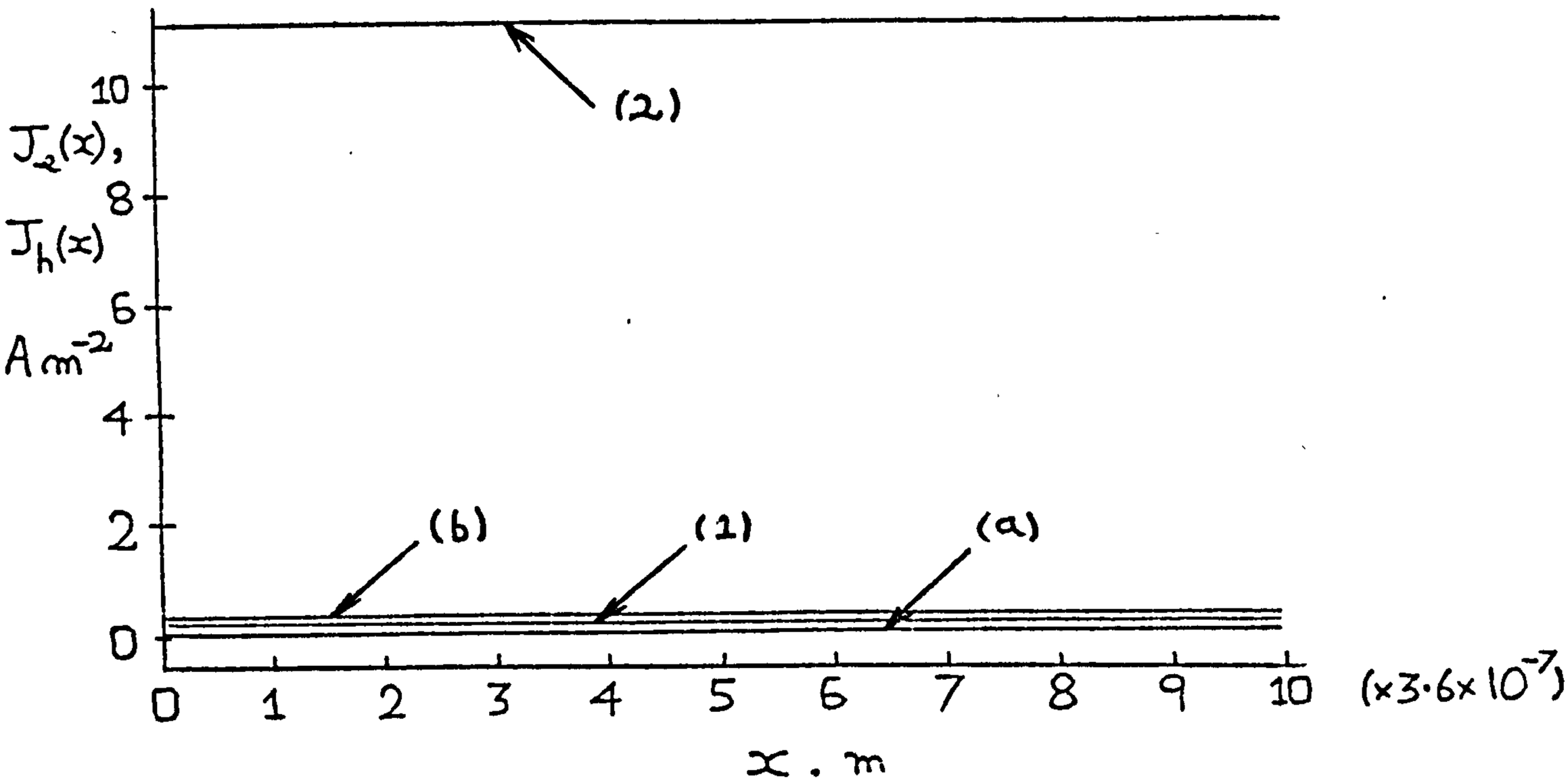

Figure 6.9(a) The electron and hole current densities (J_e (curves 1,2) and J_h(curves a,b) respectively) as functions of the position x in the substrate. The cell is unilluminated, at a forward bias of 0.2 volts (curves 1 and a) and at a forward bias of 0.3 volts (curves 2 and b). The parameters of table 3 have been used.

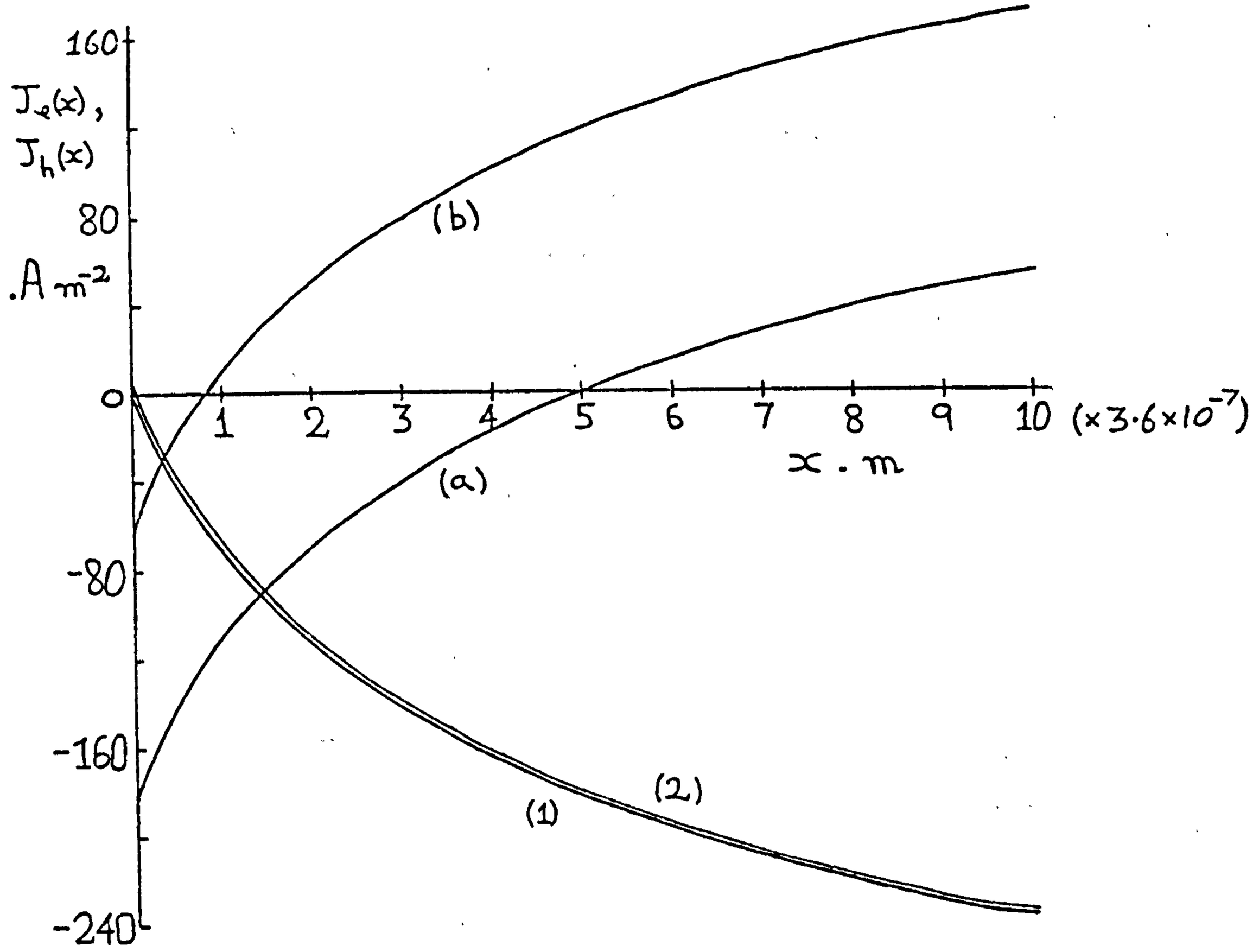

Figure 6.9(b) The electron and hole current densities (J_e (curves 1,2) and J_h(curves a,b) respectively) as functions of the position x in the substrate. The cell is illuminated (100 mW cm^{-2} of direct radiation), under short-circuit conditions (curves 1 and a), and at an output voltage of 0.2 volts (curves 2 and b). The parameters of table 3 have been used.

the interfacial surface states. Hence the tunneling of carriers between the barrier metal and the interfacial surface states, has been shown to be an important effect.

On the other hand, for the illuminated n-type S.B.S.C. delivering a total current density J<o, the electron and hole current densities are shown to be strong functions of the position x in the semiconductors substrate. The hole diffusion current density at the ohmic contact (x=L) is seen to be relatively large and positive, this is a consequence of the very thin substrate thickness used in the calculations. [If the calculations were performed for larger values of the substrate thickness, we would expect the magnitude of the hole diffusion current density, at the ohmic contact, to be very much reduced.] The hole current density at the interface x=o is large and negative (see equation (6.3.23)). This hole current density (at x=o) is formed from two components, one due to interfacial surface state recombination, and the other is due to the thermionic emission of holes, tunneling through the interfacial layer into the barrier metal. These two processes have effects of approximately the same magnitude.

The variation of the electron current density with position x in the semiconductor substrate of an illuminated n-type S.B.S.C. is given in figure 6.9(b). Again there is a strong functional dependence on x, and in particular we note that at the interface (x=o) $J_e(x=o)$ takes its maximum positive value. Conversely when x is large $J_e(x)$ is, of course, negative. The positive value of $J_e(x=o)$ represents the current density due to the emission of photo-generated electrons from the semiconductors conduction band into the barrier metal, plus the current density flowing between the conduction band and the interfacial surface states.

To sum up, we have shown that the depletion approximation seems to be invalid and the influence of the interfacial surface states upon the device characteristics is important, not only in understanding the nature of the currents involved at the interface, but also in understanding the electrostatics of the junction. In the next section we will give a simple argument to show that the sign of V_i, the voltage developed (by the illumination) across the interfacial layer, is negative when the n-type S.B.S.C. is illuminated under short circuit conditions.

6.5 Negative interfacial voltages

In this section we shall show, by simple arguments, that the interfacial voltage V_i developed (as a result of the illumination) across the insulating interfacial layer is negative when the n-type S.B.S.C. is being illuminated under short circuit conditions. These arguments will be qualitative, and serve only as an indicator for the expectation of negative interfacial voltages V_i. We shall approach this problem from two viewpoints: (a) electrostatic and (b) charge conservation considerations.

We examine an n-type Schottky barrier solar cell with a thin insulating interfacial layer, which is being illuminated under short-circuit conditions. The photo-generated holes tend to build up in the semiconductor's valence band near the interface x=o. This is due to the poor communication existing between the barrier metal and the semiconductors valence band. In order that a short circuit current is to flow, the hole quasi-Fermi level moves below the barrier metals Fermi level, thereby taking account of the increased hole concentration at the interface x=o, due to the accumulation of the photo-generated holes. It is expected that the electron quasi-Fermi level (at the interface x=o) will move

upwards (i.e. above the metals Fermi level) by a small amount, so that the increase in the electron concentration at the interface is also catered for.

One therefore expects the charge density Q_i (Qm^{-2}) on the interfacial surface states, to increase to a value greater than the thermodynamic equilibrium surface state charge density Q_{io}. This is because the number of occupied interfacial surface states n_t, would decrease when the hole quasi-Fermi level at the interface moves far below the metal Fermi level (the interfacial surface state quasi-Fermi levels then tend to lie below F_{FM}), while in contrast the electron quasi-Fermi level remains almost static. Therefore, illumination of the n-type S.B.S.C. causes the interfacial surface state charge density Q_i to increase. Hence $(Q_i - Q_{io}) > o$ for the illuminated n-type S.B.S.C. under short circuit conditions.

The electrostatic interpretation (a) of this result will now be given. We consider the additional potential, in the semiconducting region, produced by an additional positive charge at the interface. This electrostatic potential is positive everywhere and tends towards zero as x tends to infinity. Hence we would expect the increase in the charge density at the interfacial surface states, to cause an increase in the potential near the interface, the effect of this additional potential dying away at large distances. Therefore we deduce that for a short-circuited n-type S.B.S.C. receiving illumination, the interfacial voltage V_i developed across the insulating interfacial layer, by the illumination, is of negative sign.

Similarly, the interpretation via charge conservation (b) is made as follows: We make the assumption that $\rho=\rho_o=o$ i.e. the

interfacial volume charge densities are set to zero. Now by appealing to equation (6.3.8), and by neglecting the electrostatic fields at the ohmic contact (x=L), we write the charge conservation equation as

$$-(\varepsilon_i/\delta)V_i + (Q_{sco} - Q_{sc}) = Q_i - Q_{io} > o, \qquad (6.5.1)$$

for the short circuited n-type S.B.S.C. under illumination. If we now invoke the depletion approximation to enable us to calculate the space charge densities Q_{sco} and Q_{sc} (see equations (2.4.9) and (2.4.11)), then by using the fact that $V_i = -V_s$ (at the short circuit point) we observe that when V_i is negative, both the first and second terms on the L.H.S. of (6.5.1) are positive. Therefore a value of $V_i(<o)$ exists, for which equation (6.5.1) is satisfied. Hence we again deduce that V_i, the voltage developed across the insulating interfacial layer, is negative when the illuminated S.B.S.C. is short circuited.

In the next chapter we shall go on to present a simplified model for the p-type S.B.S.C., based on the system of equations given in this chapter.

CHAPTER 7

THE THEORY OF THE P-TYPE SCHOTTKY BARRIER SOLAR CELL

7.1 Introduction

In this chapter a simplified model of a p-type Schottky barrier solar cell with a thin insulating interfacial layer is constructed. Whilst retaining the more important features of the more general formalism covering the n-type Schottky barrier solar cell, developed in chapters 5 and 6, the usual assumptions regarding the quasi-Fermi levels and potential drop across the bulk region are carefully reintroduced. Again we assume a constant and uniform distribution of interfacial surface states over the energy gap of the semiconductor. The theory of the n-type S.B.S.C. presented in Chapter 2 is extended to cover the p-type case with the following four improvements: (i) The electron quasi-Fermi level E_{Fn} at the interface x=o is allowed to rise by V_{ph} above the Fermi level E_{FM} in the metal. This takes account of the imperfect communication between the semiconductor's conduction band and the metal. (ii) Tunneling between the metal and both the interfacial surface states and the bands of the semiconductor is taken into account. (iii) Recombination (avoidable and unavoidable) of the photogenerated carriers in the depletion layer, which was neglected in the formalism of Chapter 2, is also accounted for. (iv) The unavoidable recombination is also considered in the bulk semiconductor.

The model neglects the slopes of the quasi-Fermi levels in the depletion layer and it neglects the slope of the majority carrier (hole) quasi-Fermi level E_{Fp} in the bulk semiconductor. The shape

of the band edge is calculated using the depletion approximation. The results of the calculations made show that the J - V characteristics of the p-type Schottky barrier solar cell are strongly controlled by the parameters of the interfacial layer, which in effect determine the extent of the recombination within the solar cell. The voltage V_i, developed across the insulating interfacial layer when the device is illuminated, is found to be negative when short-circuit conditions apply, and becomes positive when the solar cell is operating at large output voltages. This is a new effect which has not appeared previously in the literature.

Recombination in the semiconductor's bulk and depletion layers are shown to be of great importance. In particular, for some thicker interfacial layers >25Å say, these recombination currents in the semiconductors depletion layer and bulk region can dominate. Degeneracy effects are seen to become very important when studying the degraded characteristics of p-type Schottky barrier solar cells. [The degradation is due to chemical changes occurring after encapsulation, and not to particle irradiation damage to the semiconductor (Lillington and Townsend 1978)]. Reasonable agreement between the experimental and theoretical J - V degraded characteristics is obtained.

We believe that the degradation of the p-type Al - SiO_2 - Si Schottky barrier solar cell is due to the presence of water vapour when the cell is being fabricated (especially as no degradation is observed when care is taken to ensure that water vapour is <u>not</u> present during the fabrication of the solar cell). It is suggested that, after a period of time the water vapour (traped at the interface during fabrication) reacts chemically with the Al barrier

metal to give an additional interfacial layer. The additional insulating interfacial layer sandwiched between the barrier metal and the already existing interfacial layer (oxide layer) is thought to cause the Schottky barrier solar cells degradation.

7.2 The electrostatics of the junction

The following assumptions will be made: (a) in the depletion region $o<x<w$ of the semiconductor the quasi-Fermi levels are taken to be of negligible slope. (b) The potential drop across the bulk semiconductor $w<x$ is regarded as negligible and the hole quasi-Fermi level has negligible slope in this region. (c) The band diagram is as shown in figure 7.1 for the illuminated p-type Schottky barrier solar cell delivering power at an output voltage V.

With these assumptions the electrostatics of the junction will be studied in this section. Let D_S be the density of interfacial surface states ($m^{-2}eV^{-1}$) and let δ be the thickness of the insulating interfacial layer. Also let Q_M, Q_{int}, Q_i, Q_{sc} be the charges per unit area in the surface of the metal, interfacial layer, interfacial states and depletion region respectively. The notation of figure 7.1 is used, $V(= V_i+V_s)$ being the output voltage developed across the S.B.S.C. Here V_i and V_s are the parts of the output voltage developed (as a result of the illumination) across the interfacial and depletion layers respectively. Again let the suffix S denote a surface quantity and a suffix s denote a quantity in the interior of the semiconductor. Now by figure 7.1, the Fermi level in the interior of the semiconductor is $E_{Fs} = E_{FM} - V = E_{Fp}$. Also the separation between the electron and hole quasi-Fermi levels in the depletion layer, is given as

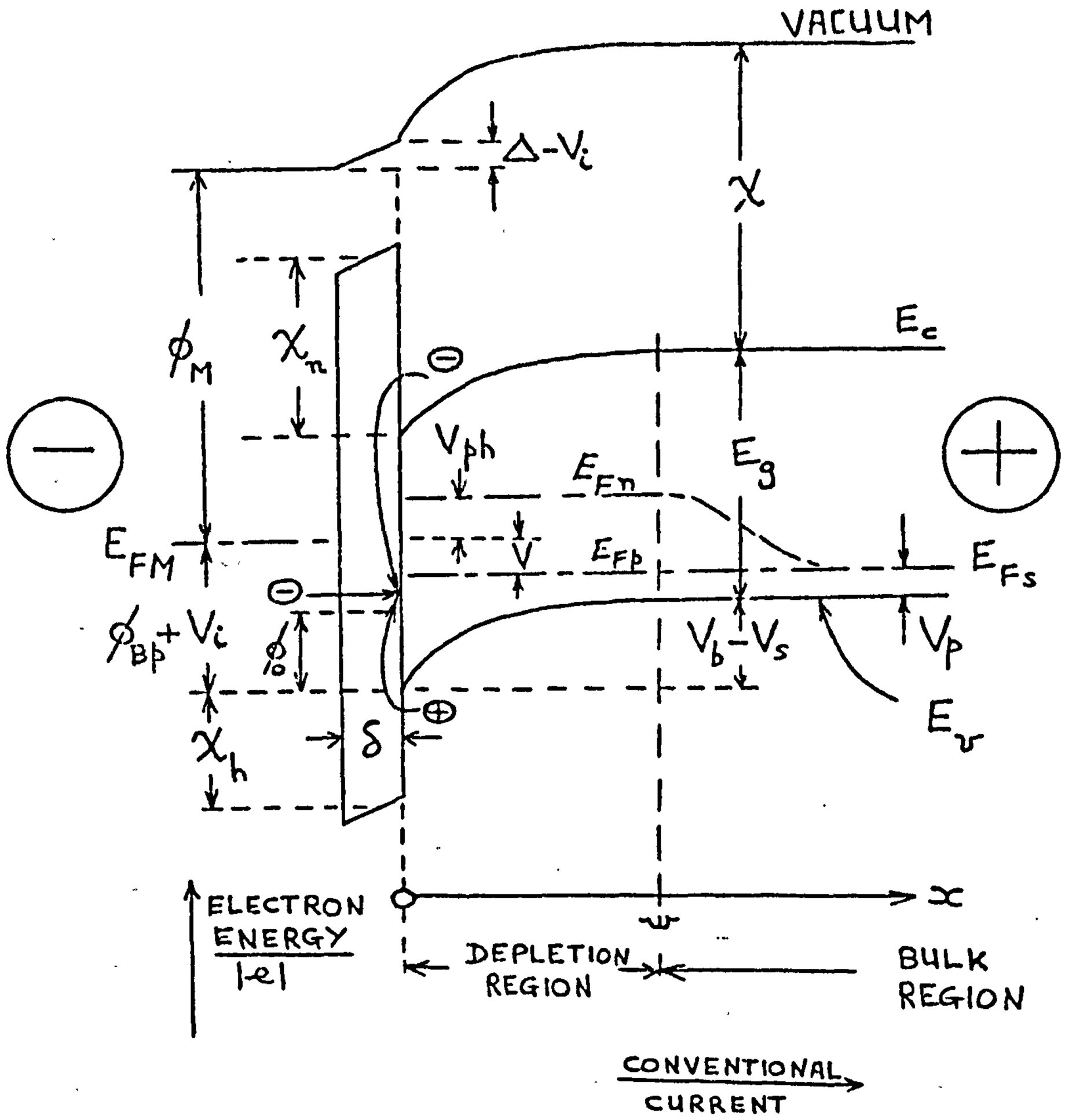

Figure 7.1 Band diagram of the illuminated p-type Schottky barrier solar cell, with an insulating layer, delivering power at an output voltage V.

$$E_{Fn} - E_{Fp} = V + V_{ph} , \quad o<x<w , \tag{7.2.1}$$

where V_{ph} represents the photo-induced voltage i.e. the amount by which the electron quasi-Fermi level, at the interface x=o, rises above the Fermi level E_{FM} in the metal. Therefore we may write

$$E_{FM} = E_{Fn} - V_{ph} , \quad o<x<w . \tag{7.2.2}$$

Let ϕ_{Bp}^{*} be the barrier height, $V_b - V_s$ the potential drop across the depletion layer, and $\Delta - V_i$ the potential drop across the insulating interfacial layer, each under illumination. Under zero illumination and applied potential $V = V_i = V_s = 0$; Δ is thus the equilibrium potential drop across the interfacial layer and ϕ_{Bp}^{*} becomes ϕ_{Bp} (the thermodynamic equilibrium barrier height). Under illumination and short circuit conditions, the photo-induced voltage $V_{ph} > o$ and $V_i = -V_s \neq o$. Now from the figure, with ϕ_M as the metal work function, χ the electron affinity of the semiconductor, and V_p as the separation between the Fermi level E_{Fs} in the interior of the semiconductor and the semiconductors valence band edge deep in the semiconductor substrate,

$$\phi_M = E_g - (V_b - V_s) + \chi - (\Delta - V_i) - V - V_p$$

$$= -V_p - V_b + \chi - \Delta + E_g = -\phi_{Bp} + \chi - \Delta + E_g . \tag{7.2.3}$$

By the depletion approximation with $E_s(x)$ as the electrostatic field in the semiconductors depletion layer ($o<x<w$) and ε_s as the permittivity of the semiconductor, we have from the Poisson equation

$$E_s(x) = (eN_A/\varepsilon_s)\ (w - x)\ , \qquad (7.2.4)$$

where the boundary condition $E_s(w) = o$ has been used, and the ionized doping concentration is N_A (here we have assumed that all the acceptors are ionized). The potential distribution $\phi_s(x)$ in the depletion layer is given by

$$\phi_s(x) = C + (eN_A/2\varepsilon_s)\ (w - x)^2\ , \qquad (7.2.5)$$

where C is a constant and $x\varepsilon(o,w]$. Let $\rho(V)$ be the charge density in the interfacial layer at an output voltage V, then equation (2.4.7) gives the electrostatic field $E_i(x)$ inside the interfacial layer as

$$E_i(x) = (^1/_{\varepsilon_i})\ [\rho x - (Q_i + Q_{sc})],\ (-\delta<x<o) \qquad (7.2.6)$$

where Q_i and Q_{sc} are the charges per unit area in the interfacial surface states (at x=o) and depletion layer respectively.

The space charge density in the depletion layer Q_{sc} is

$$Q_{sc} = -eN_A w = -\left[2e\ N_A\ \varepsilon_s(V_b - V_s)\right]^{\frac{1}{2}}\ , \qquad (7.2.7)$$

where we have invoked the depletion approximation. In thermodynamic equilibrium, denoted by a suffix o, the space charge density becomes

$$Q_{sco} = -\left[2\varepsilon_s\ e\ N_A\ V_b\right]^{\frac{1}{2}}\ . \qquad (7.2.8)$$

The analysis of the interfacial surface states presented in sections (6.2) and (6.3), is applicable to the present problem of the p-type Schottky barrier solar cell provided that all trap to trap transitions are neglected. In chapter 6, all integrations concerning the interfacial surface states were performed over the thermodynamic equilibrium surface state energy distribution. Hence in applying the results concerning the interfacial surface states (obtained in chapter 6) to the present problem, we must repace ϕ_B by $E_g - \phi_{Bp}$. This is because the range of the integration over the thermodynamic equilibrium surface state energies is from $E_{FM} + \phi_B - E_g(=E_{vo}(o))$ to $E_{FM} + \phi_B(=E_{co}(o))$ for the n-type S.B.S.C, and from $E_{FM} - \phi_{Bp}(=E_{vo}(o))$ to $E_{FM} - \phi_{Bp} + E_g(=E_{co}(o))$ for the p-type S.B.S.C. Here ϕ_B and ϕ_{Bp} respectively represent the thermodynamic equilibrium barrier heights for the n-type and p-type Schottky barrier solar cells. The thermodynamic equilibrium barrier height ϕ_{Bp} for the p-type S.B.S.C. is the energy difference, measured in units of electron volts, between the Fermi level E_{FM} in the metal and the top of the semiconductors valence band at the interface x = o, in thermodynamic equilibrium.

For the p-type Schottky barrier solar cell, an interfacial surface state of thermodynamic equilibrium energy E_{to} has a non equilibrium energy of $E_{to} - V_i$, measured relative to the metal, when the device is operating. The probability of a state of energy $(E_{to} - V_i)$ in the barrier metal, being occupied by an electron is given by

$$f_m = 1/(\exp(e(E_{to} - V_i - E_{FM})/kT) + 1) \quad . \qquad (7.2.9)$$

Using equations (6.3.11) and (6.3.12), the interfacial surface state charge densities (Qm^{-2}) in and out of thermodynamic equilibrium are given by

$$Q_{io} = eD_S\phi_o - eD_S \int_{E_{FM}-\phi_{Bp}}^{E_{FM}-\phi_{Bp}+E_g} (1+\exp(e(E_{to}-E_{FM})/kT))^{-1}\, dE_{to}$$

$$= eD_S\phi_o + D_S kT \left\{ \ln \left[\frac{(1+\exp(e(E_g-\phi_{Bp})/kT))}{(1+\exp(-e\phi_{Bp}/kT))} \right] - \frac{eE_g}{kT} \right\}, \quad (7.2.10)$$

and

$$Q_i = eD_S\phi_o - eD_S \int_{E_{FM}-\phi_{Bp}}^{E_{FM}-\phi_{Bp}+E_g} f_t\, dE_{to}\ , \quad (7.2.11)$$

where ϕ_o is the usual neutral level (see section 2.4) and f_t, the occupation probability of an interfacial surface trap state (of thermodynamic equilibrium energy E_{to}), is given by equation (6.2.6) as

$$f_t = \frac{\tau G n(o) + \tau H p_1(o) + f_m}{\{\tau G(n(o)+n_1(o)) + \tau H(p(o)+p_1(o)) + 1\}}\ . \quad (7.2.12)$$

Expressions for the carrier concentrations will be given in section 7.4 below. The Shockley-Read parameters $n_1(o)$ and $p_1(o)$ are given by equation (6.2.12). The recombination data G and H are as given in section 2.4, and the net tunneling time constant τ is given by equation (4.4.51). The occupation probability f_t in

equation (7.2.12) includes the effect of tunneling between the metal and the interfacial surface states.

The potential drop $V_b - V_s$ across the depletion layer is given under illumination by

$$(V_b - V_s) = \int_0^w E_s(x)\, dx = \frac{eN_A}{2\varepsilon_s} w^2 \quad . \qquad (7.2.13)$$

This yields the depletion layer thickness w.

The potential drop across the insulating interfacial layer is given, under illumination, by

$$-(\Delta - V_i) = -\int_{-\delta}^{0} E_i(x)\, dx = \frac{\rho\delta^2}{2\varepsilon_i} + (Q_i + Q_{sc}) \frac{\delta}{\varepsilon_i} \quad , \qquad (7.2.14)$$

thus

$$-(\varepsilon_i/\delta)(\Delta - V_i) = \frac{1}{2}\delta\rho + Q_i + Q_{sc} \qquad (7.2.15)$$

becomes in equilibrium

$$-(\varepsilon_i/\delta)\,\Delta = \frac{1}{2}\delta_{\rho o} + Q_{io} + Q_{sco} \qquad (7.2.16)$$

subtracting,

$$(\varepsilon_i/\delta)\, V_i = \frac{1}{2}\delta(\rho - \rho_o) + (Q_i - Q_{io}) + (Q_{sc} - Q_{sco}) \quad . \qquad (7.2.17)$$

Now from (7.2.3) $\phi_{Bp} (= E_g + \chi - \Delta - \phi_M)$, the thermodynamic equilibrium barrier height of the p-type Schottky barrier solar cell, is given by the solution of

$$\phi_{Bp} = \chi + E_g - \phi_M + \frac{\delta^2}{2\varepsilon_i}\rho_o + \frac{\delta}{\varepsilon_i} D_S kT \left\{ \ln\left(\frac{(1+\exp(e(E_g - \phi_{Bp})/kT))}{(1+\exp(-e\phi_{Bp}/kT))} \right) - eE_g/kT \right\} + \frac{\delta}{\varepsilon_i} eD_S \phi_o - \frac{\delta}{\varepsilon_i} eN_A \left\{ \frac{2\varepsilon_s}{eN_A} (\phi_{Bp} - V_p) \right\}^{\frac{1}{2}} \quad . \qquad (7.2.18)$$

This is an implicit relation for ϕ_{Bp} in terms only of the parameters given in table 4, and can be solved by iterative procedures. Relation (7.2.17) is an implicit relation for V_i, the voltage developed across the interfacial layer, in terms of known parameters including V, but depends also on the photo-induced voltage V_{ph}.

7.3 Junction currents

For the moment we shall consider only non-degenerate semiconductor substrates, and we will take the conventional current density through the cell as positive when flowing to the right. When the p-type Schottky barrier solar cell is illuminated and delivers power, to some external load, the device appears to be forward biased and the current flows in the reverse direction i.e. to the right in figure 7.1.

The continuity equations for electrons and holes, in the semiconductors conduction and valence bands respectively, are given by equations (2.5.5) and (2.5.6) as

$$\frac{dJ_e(x)}{dx} = -\frac{dJ_h(x)}{dx} = e(U - F) \quad , \tag{7.3.1}$$

with F as the photo-generation rate given by equation (2.5.17) and U as the total recombination rate (unavoidable + avoidable) occurring at some position x within the semiconductor substrate.

We therefore write U as the sum of two components: U_{unav} for band-band transitions, and U_{avoid} for transitions involving intermediate trapping levels (i.e. acceptor levels). Hence by using equations (2.5.1) and (2.5.3) with N replaced by N_A (the concentration of acceptor levels),the total recombination rate U is given by

Table 4

Data adopted for an In doped Al - SiO_2 /p-type Si Schottky barrier solar cell

parameter	numerical value	dimensions	references and notes
A_e^*	120	$Acm^{-2}K^{-2}$	Pulfrey & McOuat (1974)
A_h^*	120	$Acm^{-2}K^{-2}$	—
D_S	$10^{15} \rightarrow 10^{17}$	$m^{-2}\ eV^{-1}$	Lane (1968)
δ	$4 \rightarrow 30$	Å	-
ϕ_M	4.2	eV	Riviere (1957)
$m_{e/m}$	1.1	-	Effective mass ratio for electrons *
$m_{h/m}$	0.59	-	Effective mass ratio for holes *
μ_e	1900	$cm^2V^{-1}s^{-1}$	*
μ_h	425	$cm^2V^{-1}s^{-1}$	* [an asterisk refers to Sreedhar et al (1969)]
E_g	1.1	eV	*
χ	4.01	eV	*
T	300	K	-
ε_s	11.8 ε_o	Farad m^{-1}	ε_o permittivity of free space
ε_i	3.9 ε_o	Farad m^{-1}	
P_{in}	0.1	W cm^{-2}	incident power, using an AM1 spectrum.
N_A	10^{16}	cm^{-3}	-
E_A	E_v + 0.16	eV	Bonch-Bruevich & Landsberg 1968.
V_p	0.18	eV	-
ρ_o	0.0	Q m^{-3}	-
χ_n	0.5	eV	-

Table 4 continued

parameter	numerical value	dimensions	reference and notes
χ_h	0.5	eV	-
τ_{oe}	6.6×10^{-14}	s	Lundstrom & Svensson (1972)
τ_{oh}	6.6×10^{-14}	s	-
B^s	1×10^{-11}	$cm^3\ s^{-1}$	Landsberg 1967
T_1^s	4.4×10^{-16}	$m^3\ s^{-1}$	from capture cross section x thermal velocity (Bonch-Bruevich & Landsberg 1968)
T_2^s	3×10^{-13}	$m^3\ s^{-1}$	
$T_{1\,i}^s$	4.4×10^{-15}	$m^3\ s^{-1}$	-
$T_{2\,i}^s$	3×10^{-14}	$m^3\ s^{-1}$	-

The values of the recombination coefficients T_i are needed only in the calculations of the interfacial surface state current densities, and are there taken as independent of the trap energy E_t. It is hoped that the last two lines of table 4 yield the correct orders of magnitude of these current densities.

The electron/hole tunnel time constants (τ_{oe} and τ_{oh} respectively) of an interfacial surface state, have been assumed equal and furthermore the weak dependence on the surface states energy has been ignored in the calculations. Also, the electron and hole tunneling barriers, between each interfacial surface state and the barrier metal, are assumed to be the same as the respective tunneling barriers between the barrier metal and the semiconductors conduction and valence bands. Therefore by equation (4.4.51), the net tunnel time constant τ is given by

$$\frac{1}{\tau} \simeq \frac{1}{\tau_{oe}} \exp(-\bar{\delta}\chi_n^{\frac{1}{2}}) + \frac{1}{\tau_{oh}} \exp(-\bar{\delta}\chi_h^{\frac{1}{2}}) \quad .$$

$$U = (np - n_i^2) \left\{ \overline{F} + \frac{\overline{G}\,\overline{H}\,N_A}{\overline{G}\,(n+n_1) + \overline{H}\,(p+p_1)} \right\} \qquad (7.3.2)$$

where $\overline{G}$ and $\overline{H}$ are as given in equation (2.5.4). n_1 and p_1 are respectively, the electron and hole concentrations at some position $x \geq o$, when the Fermi level is at the effective acceptor state energy level E_A in thermodynamic equilibrium.

Equations (7.3.1) give the total current density J flowing through the junction under illumination as

$$J = J_e(o) + J_h(o) , \qquad (7.3.3)$$

$$\text{with} \quad J_e(o) = J_e(w) - e \int_o^w (U - F)\, dx. \qquad (7.3.4)$$

Here $J_h(o)$ represents the net hole current density just inside the semiconductor at $x = o$. It is composed of two basic current densities. Firstly, there is a hole thermionic emission tunnel current over the semiconductor barrier and through the insulating interfacial layer. Secondly, there is an interfacial surface state recombination effect. By replacing ϕ_B by $E_g - \phi_{Bp}$, V_i by $-V_i$, and $E_{FM} - E_{Fp}(o)$ by V, equations (6.3.34) and (6.3.32) give $J_h(o)$ as

$$J_h(o) = A_h^* T^2 e^{-\chi_h^{\frac{1}{2}}\delta} \exp(-e(\phi_{Bp}+V_i)/kT)\ (1-\exp(eV/kT)) - e \int_{E_{FM}-\phi_{Bp}}^{E_{FM}-\phi_{Bp}+E_g} dU_h^{ifr} , \qquad (7.3.5)$$

where we have integrated over the thermodynamic equilibrium surface state energy range (see section 7.2) and dU_h^{ifr} is as given in equation (6.2.8) with the Shockley-Read parameters given by (6.2.12).

Similarly, for the electron current density $J_e(o)$ just inside the semiconductor at x = o, equations (6.3.33) and (6.3.31) together become

$$J_e(o) = A_e^* T^2 \exp\left(-\chi_n^{\frac{1}{2}}\,\overline{\delta}\right) \exp(-e(E_g-\phi_{Bp}-V_i)/kT\ \{\exp(eV_{ph}/kT)-1\} + e\int_{E_{FM}-\phi_{Bp}}^{E_{FM}-\phi_{Bp}+E_g} dU_e^{ifr}, \quad (7.3.6)$$

where dU_e^{ifr} is as given in equation (6.2.7). The communication of the semiconductors conduction and valence bands with the metal, via the interfacial surface states, has been included in the expressions for dU_e^{ifr} and dU_h^{ifr} by modifying the surface state occupation model to encompass the effects of metal/interfacial surface state tunneling (see, for example section 6.2).

In the expressions for the electron and hole current densities in the semiconductor at the interface x = o, A_e^* and A_h^* respectively, represent the effective Richardsons constants for thermionically emitting electrons and holes, while χ_n and χ_h represent the effective tunnel barrier heights, measured in units of electron volts, present against tunneling electrons and holes respectively. In this case $\overline{\delta}$ represents the thickness of the insulating interfacial layer measured in angstroms ($\overline{\delta} = 1.0 \times 10^{10}\delta$).

Turning next to the bulk region, the net electron current density at x = w is given by

$$J_e(w) = eD_n \left.\frac{dn}{dx}\right|_{x=w} , \qquad (7.3.7)$$

from equation (2.2.9) with the neglect of the drift component, in accordance with assumption (b) of section (7.2). Now by the continuity equation (7.3.1) for electrons in the semiconductors conduction band, and by expressing the recombination rate U, in the bulk semiconductor, in terms of a minority carrier (electron) lifetime τ_n (see chapter 2, for the analogous derivation of the hole lifetime), we easily deduce that the electron concentration n(x), in the bulk semiconductors conduction band, is given by:

$$D_n \frac{d^2n}{dx^2} - \frac{n - n_o}{\tau_n} + F = o , \qquad (7.3.8)$$

where D_n is the electron diffusion constant, and the photo-generation rate F is given in equation (2.5.17) as

$$F = \int_{\lambda_o}^{\lambda_1} \alpha \Phi e^{-\alpha x} \, d\lambda \quad (s^{-1} m^{-3}) , \qquad (7.3.9)$$

where λ_o, $\lambda_1 = hc/(eEg)$ indicate the wavelength limits for the indicent solar spectrum, h is Planck's constant and c is the velocity of light. Φ represents the photon flux ($m^{-2} s^{-1}$) incident to the semiconductor from the metal, while α represents the absorption coefficient as a function of wavelength.

The net electron current density at the edge of the depletion layer (i.e. at x = w) is obtained by solving the differential equation for n:

$$J_e(w) = -en_o \frac{D_n}{L_n} (\exp(e(V+V_{ph})/kT)-1) + \int_{\lambda_o}^{\lambda_1} \frac{e\alpha\Phi L_n}{1+L_n\alpha} \exp(-\alpha w) d\lambda , \qquad (7.3.10)$$

where $L_n(=(D_n\tau_n)^{\frac{1}{2}})$ is the diffusion length of electrons in the semiconductors conduction band, and the following boundary conditions have been used:

(1) $n(x) \to n_o$, the unilluminated electron concentration far from the junction as $x \to \infty$.

(2) $n(w) = n_o \exp(e(V+V_{ph})/kT)$ and is a consequence of assumptions (a) and (c).

The electron current density in the semiconductor at position $x = o$ is given by equation (7.3.4) to be

$$J_e(o) = J_e(w) - e\left[\int_o^w Udx + \int_{\lambda_o}^{\lambda_1} e\Phi\ (1-\exp(-\alpha w))d\lambda\right], \qquad (7.3.11)$$

which becomes

$$J_e(o) = e\int_{\lambda_o}^{\lambda_1} \left(\frac{\Phi-\Phi\ \exp(-\alpha w)}{1+L_n\alpha}\right) d\lambda - e\int_o^w Udx - \frac{en_oD_n}{L_n}\left[\exp\left(\frac{e(V_{ph}+V)}{kT}\right)-1\right]$$

$$\equiv J_L - J^D_{rec} - J^o_e\ , \qquad (7.3.12)$$

by the use of equation (7.3.10). J_L is the photo-generated current density. This will not be equal to the short circuit current density (given by $V = o$) because the photo-induced voltage V_{ph} will in general be greater than zero, due to the imperfect communication between the metal and the semiconductors conduction band. Therefore J^D_{rec} and J^o_e, the recombination current densities in the depletion layer and bulk semiconductor respectively, will have non-zero contributions to the total current density even at the short circuit point ($V = o$).

7.4 Recombination in the depletion layer and degeneracy effects

The current density due to recombination (both unavoidable and avoidable) processes in the depletion layer is given by

$$J^{D}_{rec} = e\int_{o}^{w} U dx \ , \qquad (7.4.1)$$

where U is the recombination rate and is given by equation (7.3.2).

The electron concentration n in the semiconductor's conduction band, and the hole concentration p in the semiconductor's valence band are, from equations (2.2.12) and (2.2.13) for a non-degenerate semiconductor,

$$n = N_c \exp(e(E_{Fn}-E_c)/kT) \qquad (7.4.2)$$

$$\text{and} \quad p = N_v \exp(e(E_v-E_{Fp})/kT) \ . \qquad (7.4.3)$$

If we use the potential distribution $\phi_s(x)$ from equation (7.2.5) then

$$(E_{Fn} - E_c) = \frac{eN_A}{2\varepsilon_s} (w - x)^2 - E_g + V_p + V_{ph} + V \qquad (7.4.4)$$

$$\text{and} \quad (E_v - E_{Fp}) = -\frac{eN_A}{2\varepsilon_s} (w - x)^2 - V_p \qquad (7.4.5)$$

in the depletion layer. Thus n and p become for $x\varepsilon[o,w]$

$$n(x) = N_c \exp\left[e\left(\frac{eN_A}{2\varepsilon_s} (w-x)^2 - E_g + V_p + V_{ph} + V\right)/kT\right] \qquad (7.4.6)$$

$$\text{and} \quad p(x) = N_v \exp\left[-e\left(\frac{eN_A}{2\varepsilon_s} (w-x)^2 + V_p\right)/kT\right] \ . \qquad (7.4.7)$$

Therefore the thermodynamic equilibrium carrier concentrations $n_o(x)$ and $p_o(x)$ in the depletion layer ($o \leqslant x \leqslant w$) become

$$n_o(x) = N_c \exp\left[e\left(\frac{eN_A}{2\varepsilon_s}(w-x)^2 - E_g + V_p\right)/kT\right] \qquad (7.4.8)$$

$$\text{and} \quad p_o(x) = N_v \exp\left[-e\left(\frac{eN_A}{2\varepsilon_s}(w-x)^2 + V_p\right)/kT\right] . \qquad (7.4.9)$$

Owing to assumptions (a) and (b), there are two special cases for the carrier concentrations:

(1) At the interface x=o the thermodynamic equilibrium and non-equilibrium electron and hole concentrations are given by

$$n_o(o) = N_c \exp(e(\phi_{Bp}-E_g)/kT), \; n(o) = N_c \exp(e(\phi_{Bp}+V_i-E_g+V_{ph})/kT)$$

(7.4.10)

$$\text{and } p_o(o) = N_v \exp(-e\phi_{Bp}/kT), \; p(o) = N_v \exp(-e(\phi_{Bp}+V_i-V)/kT) .$$

Here we have used relation (7.2.13) for the depletion layer thickness w together with the fact that $\phi_{Bp} = V_b+V_p$ (see figure 7.1).

(2) In the bulk region ($x \geqslant w$), the majority carrier (hole) concentration remains virtually constant, both in and out of thermodynamic equilibrium, while only the thermodynamic equilibrium minority carrier (electron) concentration remains constant with respect to the position in the bulk region of the semiconductor. These carrier concentrations are given respectively as

$$p_o(x \geqslant w) = p(x \geqslant w) = N_v \exp(-eV_p/kT)$$

$$\text{and} \quad n_o(x \geqslant w) = N_c \exp(-e(E_g - V_p)/kT). \qquad (7.4.11)$$

The carrier concentrations, as given by equations (7.4.10), are used in the analysis of the interfacial surface state occupation probability and recombination rates. Also, the thermodynamic equilibrium electron concentration ($n_o(x \geq w)$ of (7.4.11))within the bulk region is used in the determination of J^o_e(the recombination current density in the bulk semiconductor).

A further relationship between the photo-induced voltage V_{ph} and the interfacial voltage V_i can be constructed, now that all the current densities in equation (7.3.12) have been fully explained. So, using equations (7.3.12) and (7.3.6) we have

$$J_L - J^D_{rec} - J^o_e = A^*_e T^2 \exp(-\chi_n^{\frac{1}{2}}\delta) \exp(-e(E_g - \phi_{Bp} - V_i)/kT) \times$$

$$\left[\exp(eV_{ph}/kT)-1\right] + e\int_{E_{FM}-\phi_{Bp}}^{E_{FM}-\phi_{Bp}+E_g} dU_e^{ifr} \qquad (7.4.12)$$

This equation when used in conjunction with the expressions for J_L, J^D_{rec}, J^o_e and dU_e^{ifr}, yields an implicit relation connecting the interfacial voltage V_i with the photo-induced voltage V_{ph}. The two equations (7.2.17) and (7.4.12) represent two simultaneous non-linear equations in V_i and V_{ph}. Assuming that the barrier height ϕ_{Bp} has been determined from (7.2.18), and that the output voltage V is specified together with the other relevant physical parameters, then the solution to the pair of equations (7.2.17) and (7.4.12) yields V_i and V_{ph}. Substitution of these voltages together with the output voltage V, back into equations (7.3.5) and (7.3.6) enables us to form the complete J - V characteristics. It should be noted, however, that for each output voltage V both V_i and V_{ph} must be recalculated.

In our work so far we have assumed that the semiconductor remains non-degenerate, whilst the solar cell is operating. If however, we endeavour to examine the current density-voltage characteristics of water vapour degraded p-type Schottky barrier solar cells, then it becomes apparent that the non-degenerate model, as given above, is not adequate. The presence of water vapour, during the fabrication of the cell, causes some water to be trapped at the barrier metal/interfacial layer interface, and this trapped water then reacts chemically with the barrier metal to give an additional insulating layer which is sandwiched between the barrier metal and the already existing interfacial layer (oxide layer). The increased thickness and different effective tunneling barriers, caused by the trapped water, gives rise to the so called water vapour degradation of p-type Schottky barrier solar cells. As a direct consequence of increased tunneling attenuation, brought about by the additional insulating layer, the communication between the metal and the semiconductors conduction band becomes very difficult. For this reason the photo-induced voltage V_{ph} tends to become large (see, for example (7.3.6)) so that some of the photo-generated electrons may pass through the insulating layers to the metal. In fact, V_{ph} tends to become so large that the electron quasi-Fermi level E_{Fn}, at the interface $x = o$, approaches the conduction band edge. Therefore we must make allowances for degeneracy effects in the above theory.

Because of the increased interfacial layer thickness, the semiconductors conduction band, near the interface $x = o$, becomes degenerate. This throws up two important points to be considered:

(a) The degenerate electron thermionic emission tunnel current

density and (b) degenerate recombination effects. We shall consider each of these points in turn.

(a) The degenerate electron thermionic emission tunnel current may easily be identified, using appendix A, to be

$$A_e^* T^2 \exp(-\chi_n^{\frac{1}{2}}\delta) \int_{e(E_g-\phi_{Bp}-V_i)/kT}^{\infty} \ln\left[\frac{(1+\exp(eV_{ph}/kT-g))}{(1+\exp(-g))}\right] dg \; . \qquad (7.4.13)$$

Therefore, when examining degraded p-type S.B.S.C.'s, the electron thermionic emission tunnel current density (7.4.13) for degenerate conditions, replaces the first term on the R.H.S. of equations (7.3.5) and (7.4.12).

(b) Degenerate recombination effects are, however, not quite so clear cut. In order to accurately allow for degeneracy effects in the recombination processes we need to know the dependence of the reaction coefficients upon the electron and hole energies (see, for example, Landsberg (1957)). For the present work we shall restrict ourselves to the case where the reaction coefficients are constants. Then following Landsberg (1957) we observe that the recombination rates reduce to their usual forms, dependent upon the degenerate electron and hole concentrations. Hence, as the semiconductors conduction band, near the interface x = o, is the only region where degeneracy effects become apparent, we must replace the electron concentration n, in the expressions for the depletion layer and interfacial surface state recombination rates (U, dU_e^{ifr} and dU_h^{ifr}, respectively), by its corresponding degenerate form. The degenerate electron concentration is given by Landsberg (1969) to be

$$n = N_c \int_{eE_c/kT}^{\infty} \frac{\sqrt{(x - eE_c/kT)}}{1+\exp(x-eE_{Fn}/kT)}\, dx \,, \qquad (7.4.13)$$

where E_{Fn} is the electron quasi-Fermi level.

With the degenerate form of the electron thermionic emission tunnel current density, together with approximate forms of the electron interfacial surface state and depletion layer recombination rates (the approximation being due to the assumed constant value for the functional reaction constants appropriate to degenerate recombination), we can examine the characteristics of degraded p-type S.B.S.C.'s by using the above theory.

In the next section we shall present the results of calculations made for an In-doped Al-SiO_2-Si p-type Schottky barrier solar cell.

7.5 Results and discussion

Some results of the theory are presented in figures 7.2 - 7.10 They were calculated for an In-doped Al-SiO_2- p-type Si Schottky barrier solar cell. In the numerical work we have assumed that the interfacial layer's volume charge density ρ is independent of illumination and output voltage, so $\rho=\rho_o$ (see table 4). Turning to the neutral level ϕ_o, this is independent of illumination and output voltage and has been estimated to lie at about 0.30± 0.36eV (Cowley and Sze 1965), and it has been taken as zero for the present calculation. A positive value of ϕ_o would however lead to an increased thermodynamic equilibrium hole barrier height ϕ_{Bp}. The results were calculated, on the lines suggested in the last section, by assuming that a total output voltage V is developed by the cell and that the parameters of table 4 are given.

Consider a p-type Schottky barrier solar cell, illuminated under AM1 conditions. The size of both recombination current densities

(1 to 4, below) and thermionic emission tunnel current densities (5 and 6, below) will be discussed for various conditions.

1. Recombination in (a) the depletion and (b) the bulk layers of the semiconductor. In (a) the unavoidable, i.e. band-band, processes by single electron transitions are considered together with the corresponding avoidable processes, i.e. processes proceeding via traps. For (b) an effective minority carrier lifetime has been used. The total current density due to recombination within the semiconductor substrate is given by $(J^{D}_{rec} + J^{o}_{e})$.

2. Band-band recombination via interfacial states.

3. Metal-conduction band recombination via interfacial states.

4. Metal-valence band recombination via interfacial states.

The three processes 2, 3 and 4 are effectively lumped together in the two terms $\int dU_e^{ifr}$ and $\int dU_h^{ifr}$ (see, for example equations (7.3.5), (7.3.6), (6.2.7) and (6.2.8)). In both 3. and 4. there are cases when an interfacial surface state quasi-Fermi level lies above the metal Fermi level E_{FM} and cases when it lies below E_{FM}. The electron flow is to the left in the first case in both 3. and 4., and it is to the right in the second case (figure 7.1). The potential drop Δ across the insulating interfacial layer in thermodynamic equilibrium is decreased to $\Delta - V_i$ in the illuminated cell. The above reversal of direction is therefore accompanied by a decrease in this potential drop from a valve above to a value below that corresponding to thermodynamic equilibrium.

5. Thermionic emission of electrons from the semiconductors conduction band to the metal. This is the first term in equation (7.3.6).

6. Thermionic emission of holes from the semiconductors valence band to the metal. This is represented by the first term in

equation (7.3.5). In fact the thermionic emission tunnel current density between the metal and the semiconductors valence band is rarely important (when compared with processes 2 and 4) for the range of interfacial layer thicknesses δ considered. On the one hand, with a low value of δ, one can show that the thermionic equilibrium barrier height has a large value, thereby making thermionic emission over the barrier difficult. On the other hand, if δ is large then a large tunneling barrier exists to hole flow between the metal and the semiconductors valence band.

Let us examine a p-type S.B.S.C., which is being illuminated under AM1 conditions, having a low interfacial surface state density D_S ($\lesssim 10^{15}$ m^{-2} eV^{-1}) and a large interfacial layer thickness δ (~ 25 Å). While the photo-generated holes move into the semiconductor, the photo-generated electrons tend to accumulate in the semiconductors conduction band near the interface $x = o$ because of the large tunneling barrier. Therefore the electron quasi-Fermi level E_{Fn} rises and the photo-induced voltage V_{ph} becomes greater than zero. This encourages an important contribution from process 5. The electron concentration in the bulk is increased over its equilibrium value by virtue of the bunching of electrons near $x = o$. This encourages considerable recombination in the substrate (bulk and depletion layers i.e. process 1). Because of the low value of D_S and as the hole concentration near $x = o$ is small, process 2 is rather weak. In addition, processes 3 and 4 are also relatively weak because of the thickness of the barrier.

A strong internal electrostatic field, causing holes to be swept away from the region $x = o$, while electrons are bunched up there is expected at short circuit. This leads to minimal recombination mainly from process 1 (figure 7.2), maximal V_{ph}

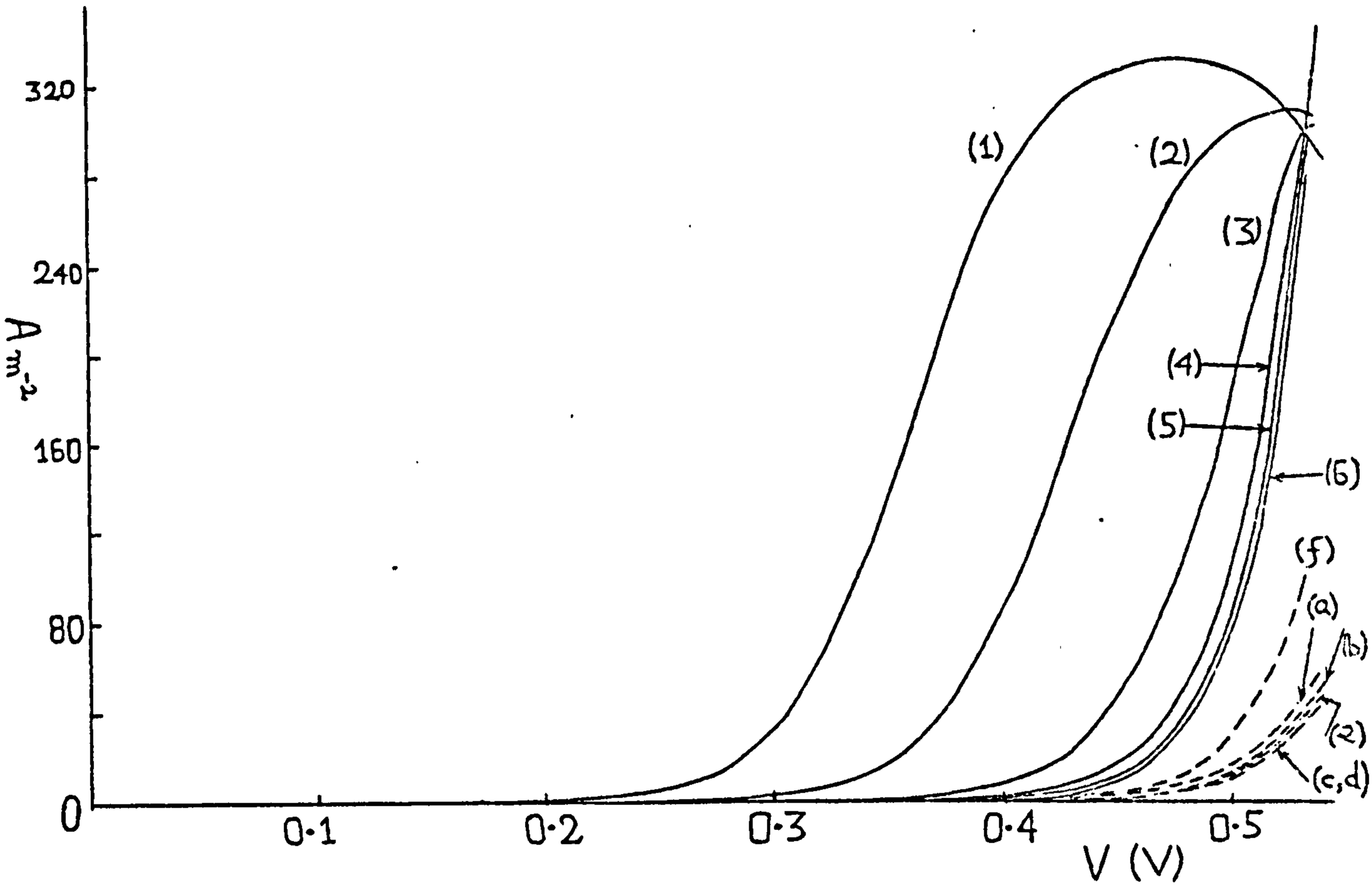

Figure 7.2 The substrate (full lines) and interfacial hole (dashed lines) recombination current densities as a function of output voltage V, for various interfacial layer thicknesses δ. The parameters of table 4 have been used together with $D_S = 10^{15}\ m^{-2}\ eV^{-1}$

(a,1) $\delta = 25\mathring{A}$: (b,2) $\delta = 22\mathring{A}$: (c,3) $\delta = 19\mathring{A}$:

(d,4) $\delta = 16\mathring{A}$: (e,5) $\delta = 13\mathring{A}$: (f,6) $\delta = 10\mathring{A}$.

(figure 7.3), and most of the photogenerated electrons are carried by process 5. Minimal recombination can also be recognised from the maximal output current J in figure 7.4.

For relatively low interfacial surface state densities D_S and large interfacial layer thickness δ we do not expect processes 2, 3 and 4 to be important unless the internal electrostatic field is reduced sufficiently, by an increased output voltage V, to allow a significant concentration of holes near x = o (see figure 7.2). The increased output voltage V enhances process 1 even more (see, for example curve 1 of figure 7.2) until the switch-over noted under point 4 takes place. Hence process 3 is no longer able to transmit photo-generated electrons to the metal via the interfacial surface states, but instead the interfacial surface states tend to receive electrons from the metal. Meanwhile, by virtue of processes 2 and 4 and the increased hole concentration, the hole interfacial surface state recombination current density ($e \int dU_h^{ifr}$) becomes significant. It causes a rapid decrease in the photo-induced voltage V_{ph} and a switching of recombination from the semiconductors substrate (process 1) to recombination via the interfacial states (process 2). This decrease in V_{ph} is sufficiently rapid to bring the quasi-Fermi levels closer together even though V increases. The increased level of recombination can also be seen from the drop in curve a of figure 7.4, and the recombination switching-over effect is clearly seen in curve a of figure 7.2.

Keeping the density of the interfacial surface states D_S at a low value ($\sim 10^{15}$ m^{-2} eV^{-1}), and by decreasing the thickness δ of the insulating interfacial layer (say to about 16 Å), communication between the metal and the semiconductors conduction band (processes 3 and 5) becomes much easier for all output voltages. Thus the

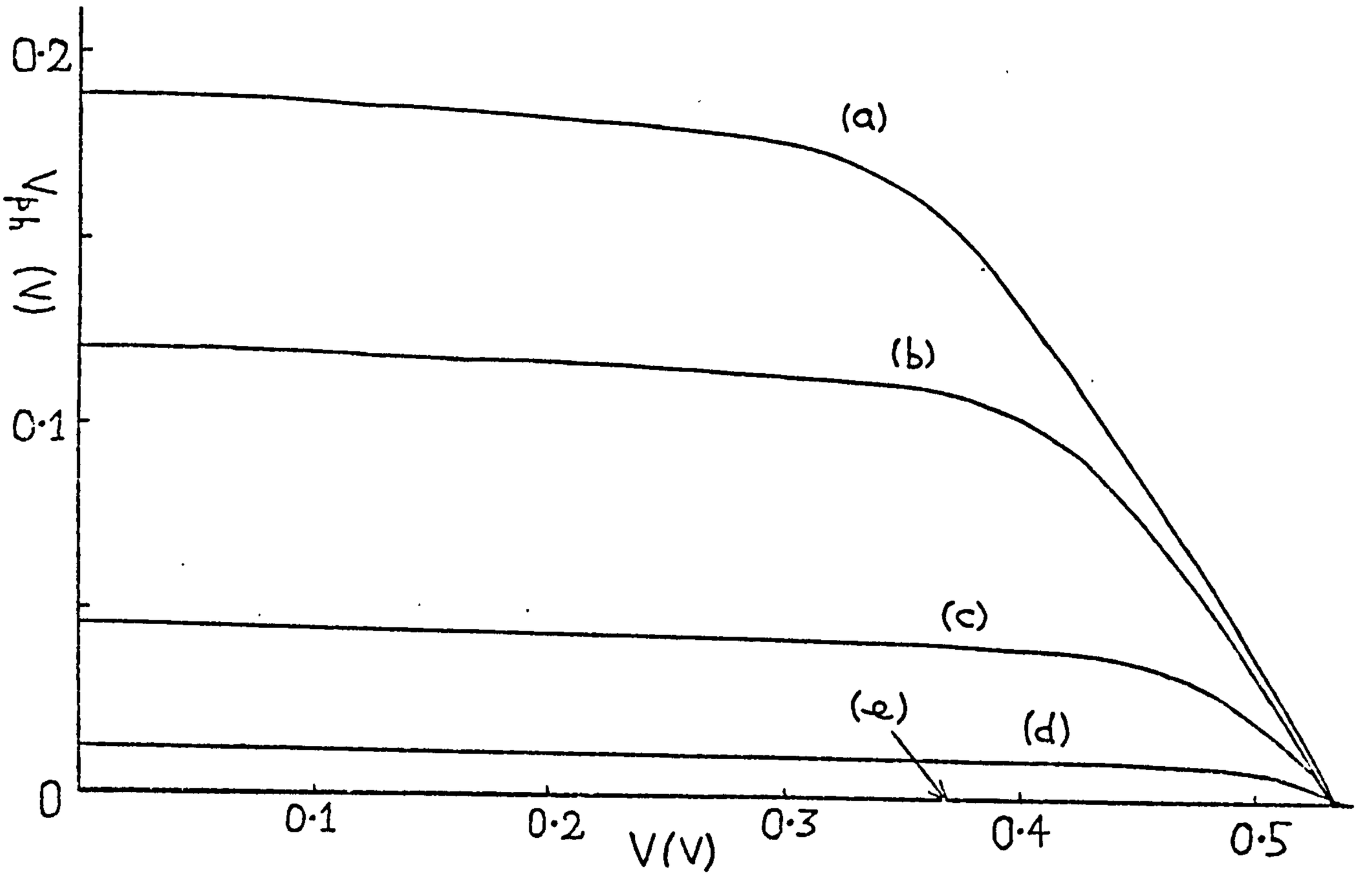

Figure 7.3 The photo-induced voltage V_{ph} as a function of output voltage V for various interfacial layer thicknesses δ. The parameters of table 4 have been used together with $D_S = 10^{15}\ m^{-2}\ eV^{-1}$

(a) $\delta = 25\mathring{A}$: (b) $\delta = 22\mathring{A}$: (c) $\delta = 19\mathring{A}$

(d) $\delta = 13\mathring{A}$: (e) $\delta = 13,10,7\mathring{A}$.

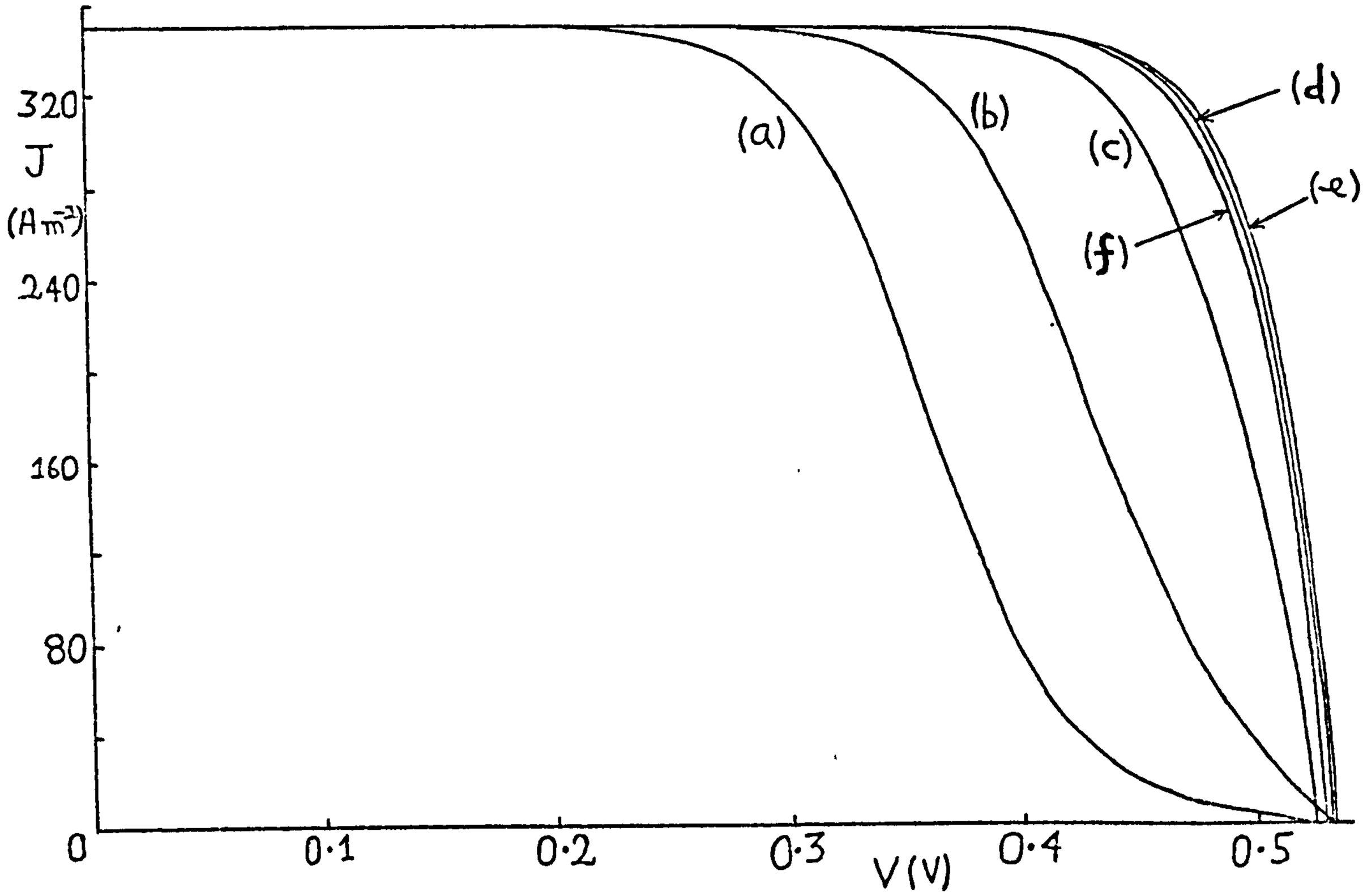

Figure 7.4 The current density-voltage characteristics of the p-S.B.S.C. for various interfacial layer thicknesses δ. The parameters of table 4 have been used together with $D_S = 10^{15}\ m^{-2}\ eV^{-1}$. (a) $\delta = 25\text{Å}$: (b) $\delta = 22\text{Å}$ (c) $\delta = 19\text{Å}$: (d) $\delta = 16\text{Å}$: (e) $\delta = 13\text{Å}$ (f) $\delta = 10\text{Å}$.

photo-generated electrons encounter smaller tunneling barriers, and consequently the photo-induced voltage V_{ph} reduces (see figure 7.3), because fewer photo-generated electrons accumulate in the semiconductor near x = o. This tends to give less recombination via process 1, in the substrate (see for example, figure 7.2, curve 4) and, because D_S is low, slightly reduced recombination by process 2 (figure 7.2, curve d). Recombination process 4 increases slightly because of the reduced δ, but still remains a lower order effect. Hence, by decreasing δ to some moderate value, the power output of the p-type S.B.S.C. is improved as shown in figure 7.4, curve d.

If the thickness δ of the insulating interfacial layer is reduced still further, say to about 10 Å, then the communication between the metal and the interfacial surface states improves to such an extent that, even though the photo-induced voltage V_{ph} is very small (see figure 7.3, curve e) because of the very much reduced tunneling barriers, the metal readily communicates with the valence band of the semiconductor via the interfacial surface states. The interfacial surface states' quasi-Fermi levels now tend to lie below E_{FM} and electrons from the metal will contribute to the recombination current via process 4 rather than process 3. Some of the photo-generated electrons are carried by the important process 5, and the rest recombine via processes 1 and 2. Hence the hole recombination current via processes 2 and 4 becomes more important for the very small values of δ, particularly for the higher output voltages V, when the hole concentration is large. The increased hole recombination (figure 7.2, curve f) drags down the power output somewhat (figure 7.4, curve f).

Turning now to the voltage V_i developed across the insulating

interfacial layer (having a large thickness $\delta(\sim 25\ \mathring{A})$) as a result of the illumination, it is expected that the photo-voltage V_{ph} is positive at the short circuit point. The interfacial surface states' quasi-Fermi levels then tend to lie above E_{FM}, and consequently the interfacial surface state charge density reduces from its thermo-dynamic equilibrium value. If we invoke ideas of charge conservation (see section 6.5 for an analogous discussion), remembering that the space charge in a p-type semiconductor is of negative sign, then we are lead to the conclusion that V_i must be negative for the short-circuited and illuminated p-type S.B.S.C.

As the operating voltage V is increased the hole quasi-Fermi level E_{Fp} moves below E_{FM} by an amount equal to V. This tends to pull the quasi-Fermi levels for the interfacial surface states downwards, and V_{ph} decreases (figure 7.3). Therefore, the inter-facial surface state charge density then increases from its value under short circuit conditions, and as a result V_i increases. In fact for the larger operating voltages, V_i eventually increases to become positive (see figure 7.5).

Again, for a low value of the density of interfacial surface states D_S ($\sim 10^{15}\ m^{-2}\ eV^{-1}$) at the short-circuit point, the photo-voltage V_{ph} decreases with decreasing thickness δ of the insulating interfacial layer. Therefore the voltage V_i tends to approach zero because decreasing V_{ph} causes an increase in the interfacial surface state charge density as above. As the thickness of the insulating layer is reduced this layer becomes increasingly unable to support a potential drop, so that in the limit as $\delta \to o$ we would expect both Δ and V_i to be zero.

If we now consider the situation of an illuminated p-type S.B.S.C., having a moderate interfacial surface state density

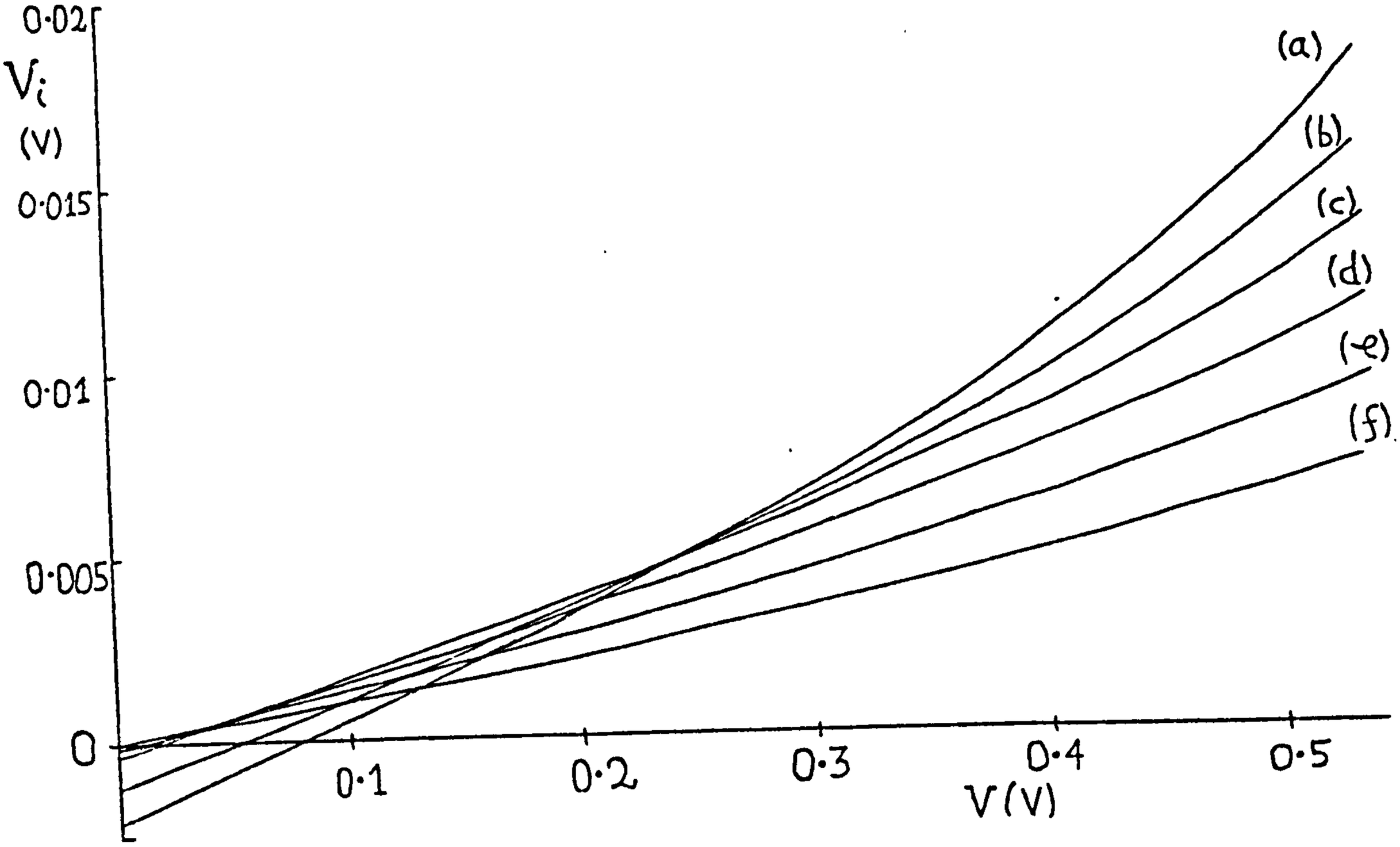

Figure 7.5 The voltage V_i, resulting from the illumination, developed across the insulating interfacial layer as a function of the output voltage V, for various interfacial layer thicknesses δ. The parameters of table 4 have been used together with $D_S = 10^{15}\ m^{-2}\ eV^{-1}$.

(a) $\delta = 25\mathring{A}$: (b) $\delta = 22\mathring{A}$: (c) $\delta = 19\mathring{A}$: (d) $\delta = 16\mathring{A}$

(e) $\delta = 13\mathring{A}$: (f) $\delta = 10\mathring{A}$.

D_S ($\sim 10^{16}$ m^{-2} eV^{-1}), and a large interfacial layer thickness δ($\sim$ 25 Å), then we would expect a much reduced thermodynamic equilibrium barrier height ϕ_{Bp} because of the reduction in the interfacial surface state charge density (if ϕ_o = o). Hence the electron quasi-Fermi level E_{Fn} rises, and V_{ph} (figure 7.6) tends to become larger than for the corresponding situation with the lower interfacial surface state density. The large value of the photo-voltage V_{ph} encourages an important contribution from process 5. Hence the electron concentration in the bulk is therefore increased over its equilibrium value by virtue of the bunching of electrons near x = o. This encourages pronounced recombination in the substrate (process 1), and because of the moderate value of D_S, process 2 is significant. The large thickness of the interfacial layer makes processes 3 and 4 relatively weak. Increased output voltage V enhances process 1 even more (curve 1 of figure 7.7) until the switch-over,noted under point 4 of paragraph 2 in section 7.5,takes place. At this stage the hole interfacial surface state recombination current becomes extremely important. It causes a rapid decrease in V_{ph} and a switching of recombination from the semiconductor substrate (process 1) to recombination via the interfacial surface states (process 2). Again, this decrease in V_{ph} is sufficiently rapid to bring the quasi-Fermi levels closer together even though V increases. The increased level of recombination may also be seen from the drop in curve a of figure 7.8.

As δ is decreased (say to about 16 Å), and holding the density of interfacial surface states D_S at a moderate value ($\sim 10^{16} m^{-2} eV^{-1}$), the communication between the metal and the semiconductors conduction band (processes 3 and 5) becomes much easier. Consequently the

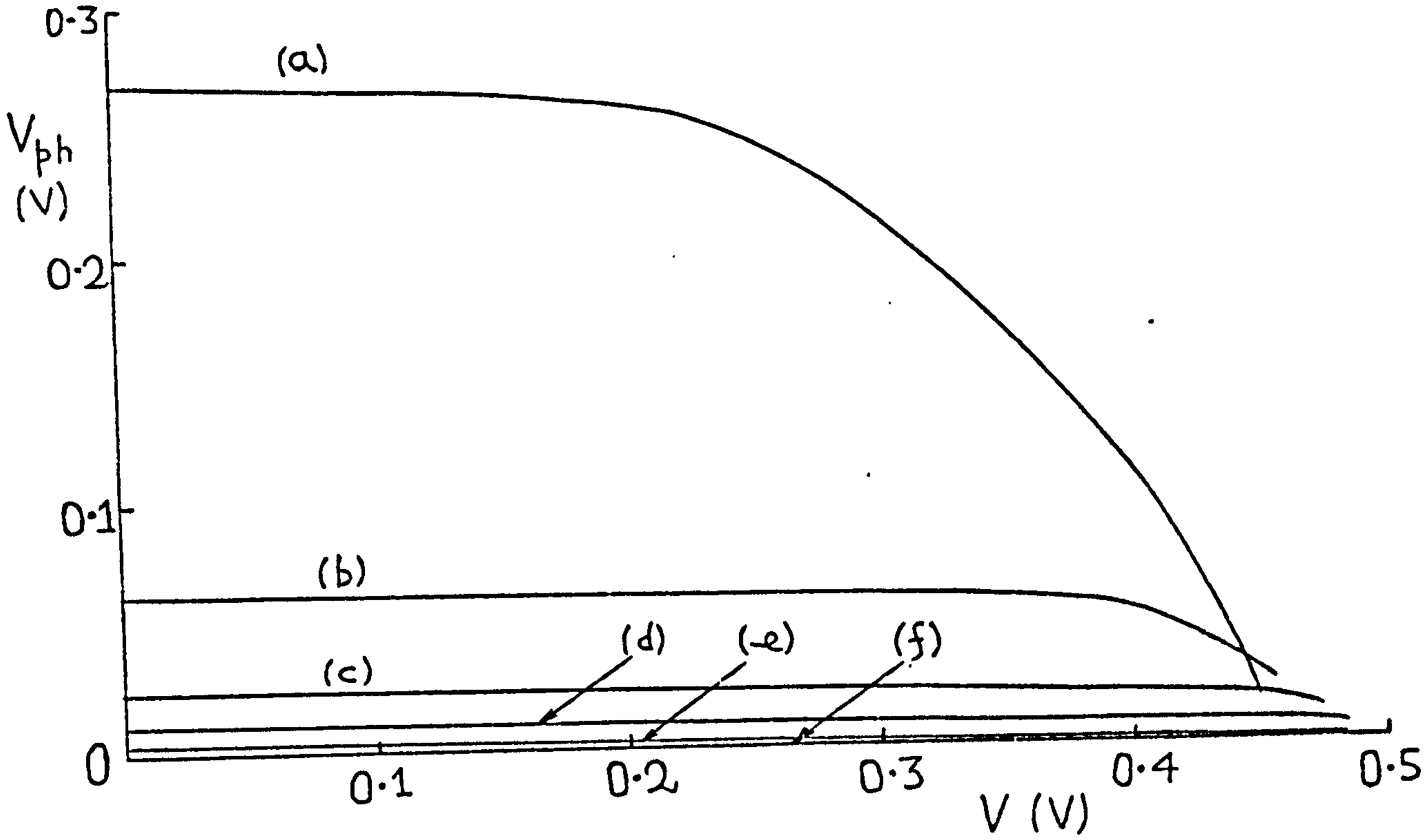

Figure 7.6 The photo-induced voltage V_{ph} as a function of the output voltage V, for various interfacial layer thicknesses δ. The parameters of table 4 have been used together with $D_S = 10^{16}\ m^{-2}\ eV^{-1}$. (a) $\delta = 25\mathring{A}$: (b) $\delta = 22\mathring{A}$: (c) $\delta = 19\mathring{A}$: (d) $\delta = 16\mathring{A}$: (e) $\delta = 13\mathring{A}$: (f) δ = 10, 7, 4A.

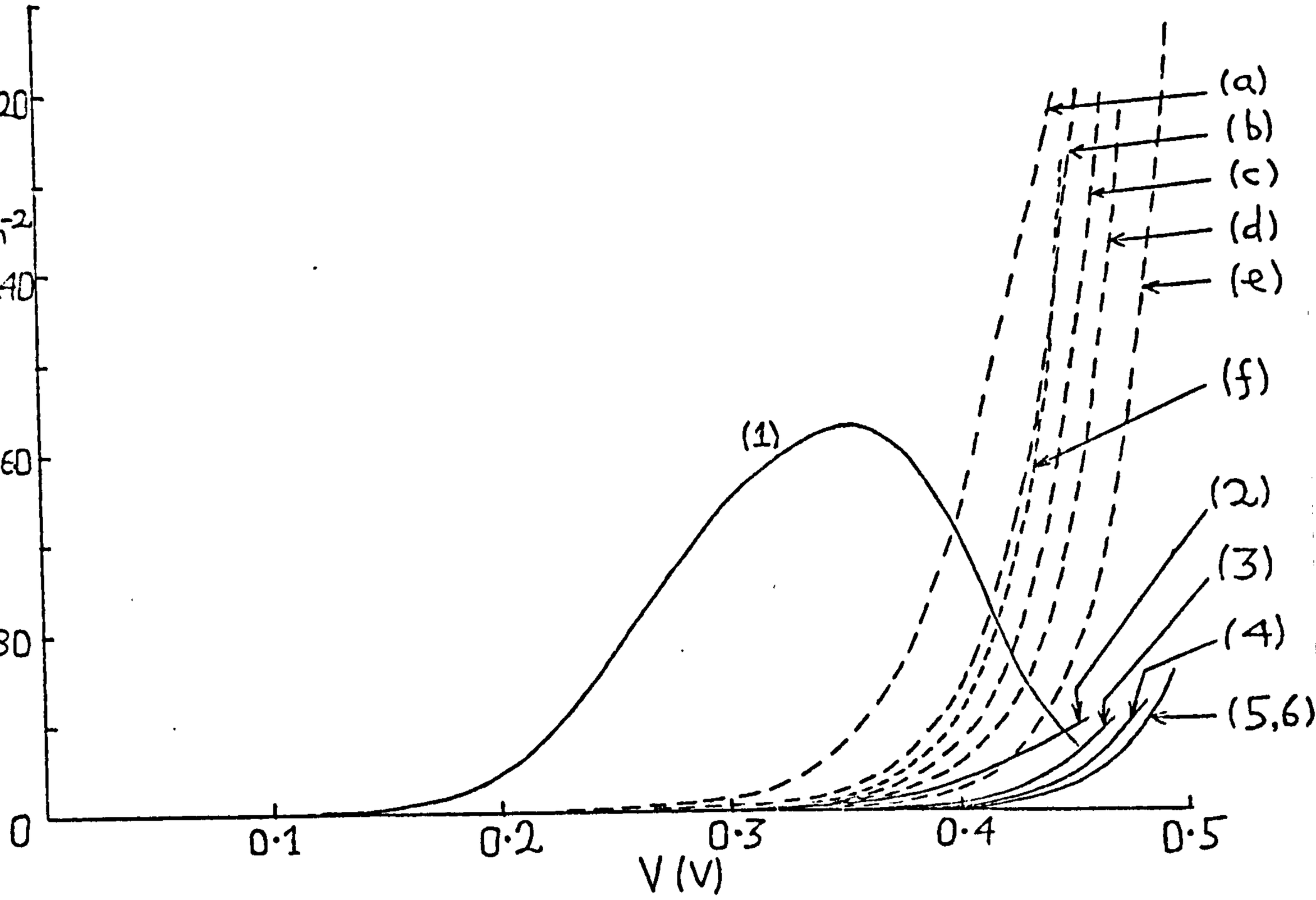

Figure 7.7 The substrate (full lines) and interfacial hole (dashed lines) recombination current densities as a function of output voltage V, for various interfacial layer thicknesses δ. The parameters of table 4 have been used together with $D_S = 10^{16}\ m^{-2}\ eV^{-1}$.

(a,1) $\delta = 25\mathring{A}$: (b,2) $\delta = 22\mathring{A}$: (c,3) $\delta = 19\mathring{A}$:

(d,4) $\delta = 16\mathring{A}$: (e,5) $\delta = 10\mathring{A}$: (f,6) $\delta = 4\mathring{A}$.

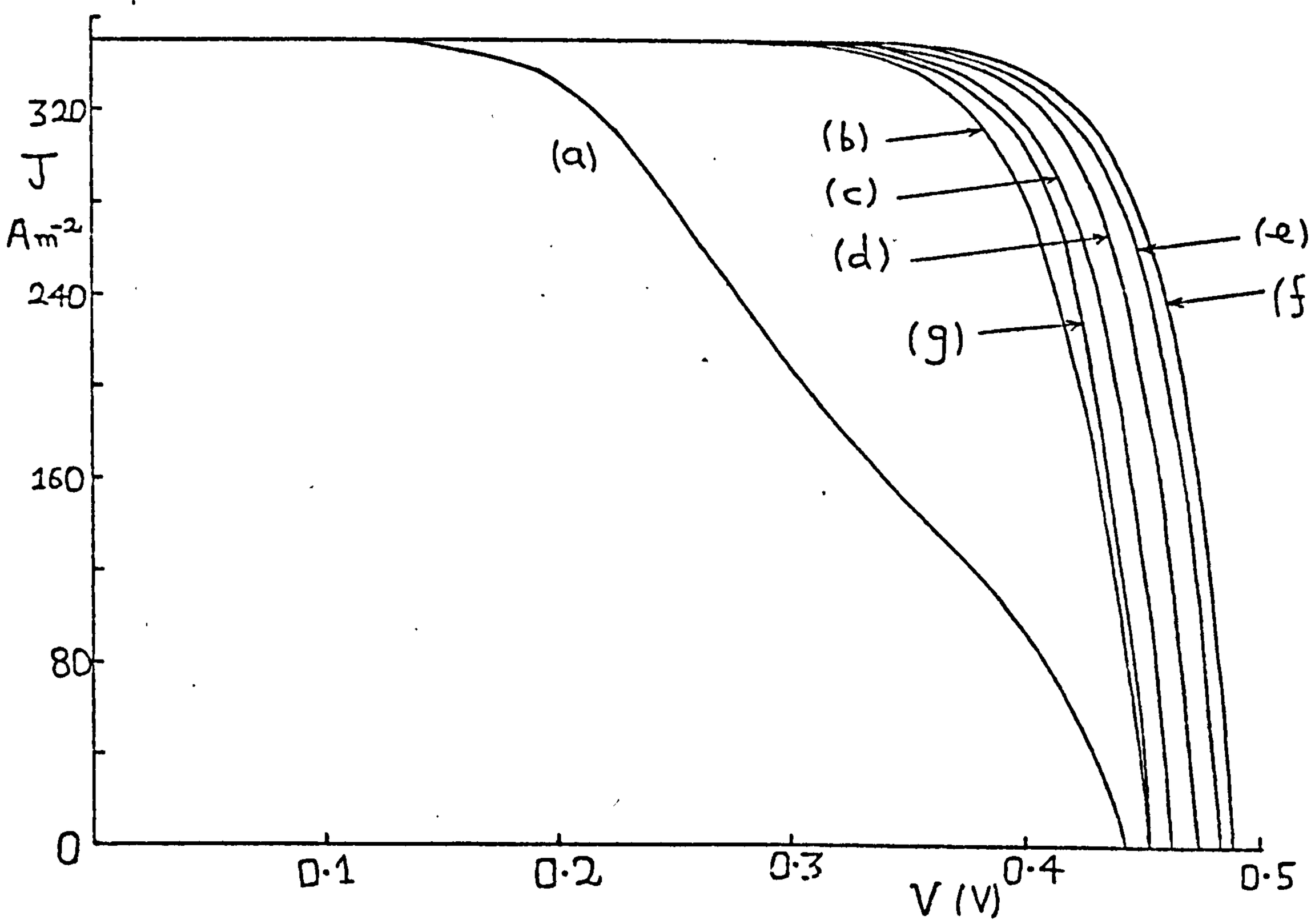

Figure 7.8 The current density-voltage characteristics of the p-S.B.S.C. for various interfacial layer thicknesses δ. The parameters of table 4 have been used together with $D_S = 10^{16}\ m^{-2}\ eV^{-1}$.

(a) $\delta = 25\mathring{A}$: (b) $\delta = 22\mathring{A}$: (c) $\delta = 19\mathring{A}$

(d) $\delta = 16\mathring{A}$: (e) $\delta = 13\mathring{A}$: (f) $\delta = 10\mathring{A}$

(g) $\delta = 4\mathring{A}$.

photo-induced voltage V_{ph} reduces (see figure 7.6) because fewer photo-generated electrons accumulate in the semiconductors conduction band near x = o. This tends to give less recombination via process 1 in the substrate, and slightly reduced recombination by process 2 (figure 7.7, curve d). Recombination process 4 increases slightly because of the reduced thickness δ, but still remains a lower order effect. Hence, by decreasing δ to some moderate value the power output of the p-type S.B.S.C. is improved as shown in curve d of figure 7.8.

If δ is reduced still further, say to about 4 $\mathring{A}$, then the communication between the metal and the interfacial surface states improves to such an extent that, even though the photo-induced voltage V_{ph} is very small (see figure 7.6, curve f) because of the very much reduced tunneling barriers, the metal <u>readily</u> communicates with the valence band of the semiconductor via the interfacial surface states. The interfacial surface states quasi-Fermi levels now tend to lie below E_{FM} and electrons from the metal will contribute to the recombination current density via process 4 rather than process 3. Some of the photo-generated electrons are carried by the important process 5 and the rest recombine via processes 1 and 2. Hence the hole recombination via process 2 and the now important process 4 becomes more dominant than for the situation corresponding to the case of moderate D_S, particularly for the higher output voltages V (see, for example curve f of figure 7.7). The increased hole recombination tends to drag down the power outputs somewhat (figure 7.8, curve g).

For moderate interfacial surface state densities D_S ($\sim 10^{16} m^{-2} eV^{-1}$) and a large interfacial layer thickness δ ($\gtrsim$ 25 $\mathring{A}$), it is expected that at short circuit, the photo-induced voltage V_{ph} is positive

and greater than that corresponding to the equivalent situation of low D_S. Therefore by the same charge conservation argument as was used before, we would expect the voltage V_i developed across the insulating interfacial layer, as a result of the illumination, to be negative at short circuit. Again, for the larger operating voltages V the voltage V_i eventually increases to become positive (see figure 7.9).

Turning now to the situation of large interfacial surface state densities $D_S \sim 10^{17}$ m^{-2} eV^{-1}, the interfacial surface state recombination processes dominate, while recombination in the substrate (process 1) plays only a secondary role. In fact for large interfacial layer thicknesses δ processes 2 and 5 dominate the characteristics, whereas for small δ, the recombination processes 2, 3 and 4 are most important.

After making the necessary adjustments for the transmission coefficient (for light passing through the Al film), and by allowing for a series resistance (by using an equivalent circuit) of $\sim 3\Omega$ for a cell of area 1 cm^2, the calculated J - V characteristics (for a moderate density of interfacial surface states $D_S \sim 0.6 \times 10^{16}$ m^{-2} eV^{-1}) agree reasonably well with experimental data (Lillington and Townsend 1978) (see figure 7.10). It is therefore hoped that the numerical values of the reaction constants, given in table 4, are reasonably realistic. The calculated and experimental characteristics, for both the degraded and undegraded cells, are shown in figure 7.10. The theoretical calculations for water vapour degraded p-type Schottky barrier solar cells, have been performed on the basis of, a large interfacial layer thickness $\delta (= 29\ \text{Å})$, a moderate interfacial surface state density D_S ($\sim 0.6 \times 10^{16}$ m^{-2} eV^{-1}), and a slightly different electron tunneling barrier height χ_n (~ 0.7 eV).

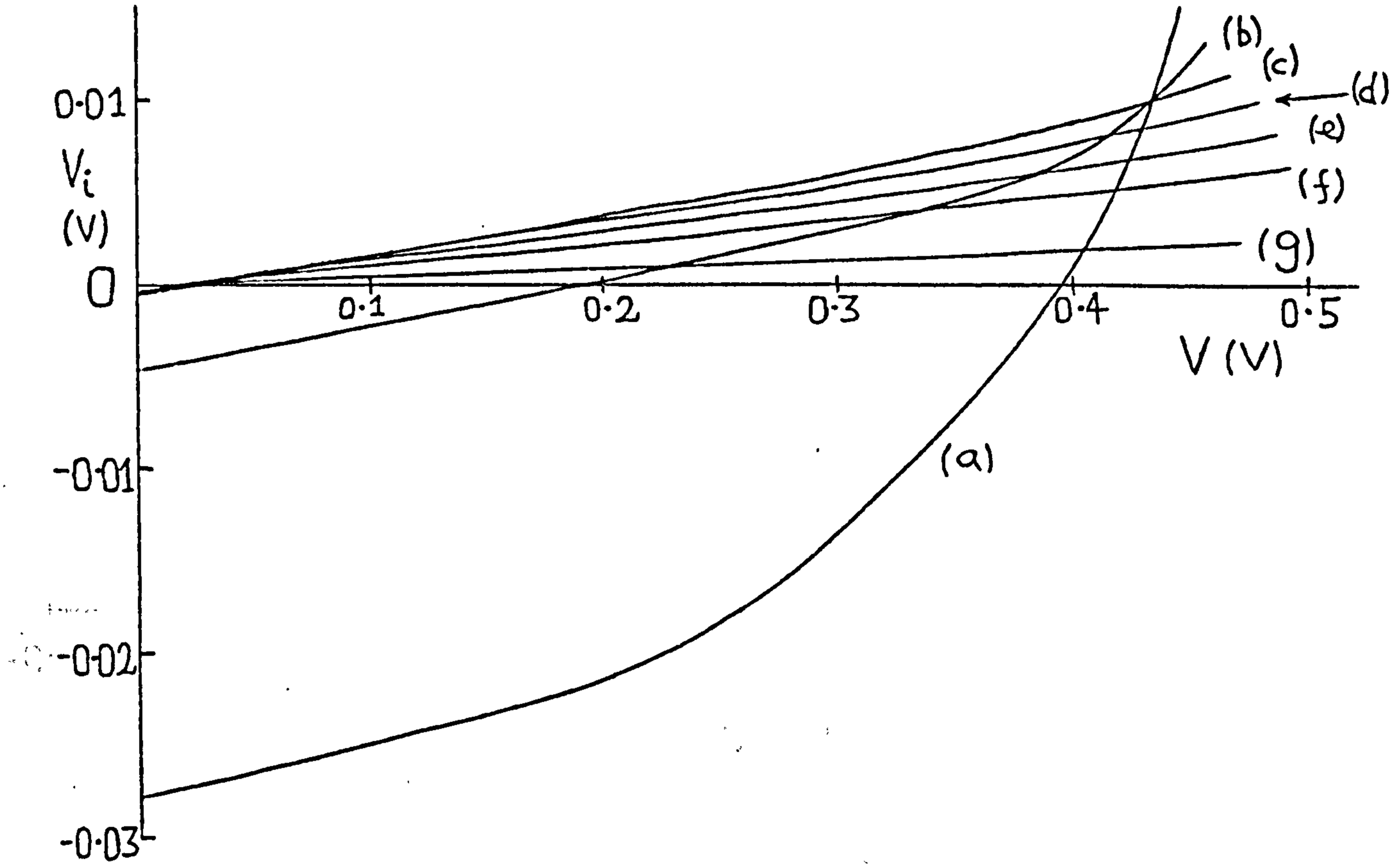

Figure 7.9 The voltage V_i, resulting from the illumination, developed across the insulating interfacial layer as a function of the output voltage V, for various interfacial layer thicknesses δ. The parameter of table 4 have been used together with $D_S = 10^{16}\ m^{-2}\ eV^{-1}$.

(a) $\delta = 25\mathring{A}$: (b) $\delta = 22\mathring{A}$: (c) $\delta = 19\mathring{A}$:

(d) $\delta = 16\mathring{A}$: (e) $\delta = 13\mathring{A}$: (f) $\delta = 10\mathring{A}$:

(g) $\delta = 4\mathring{A}$.

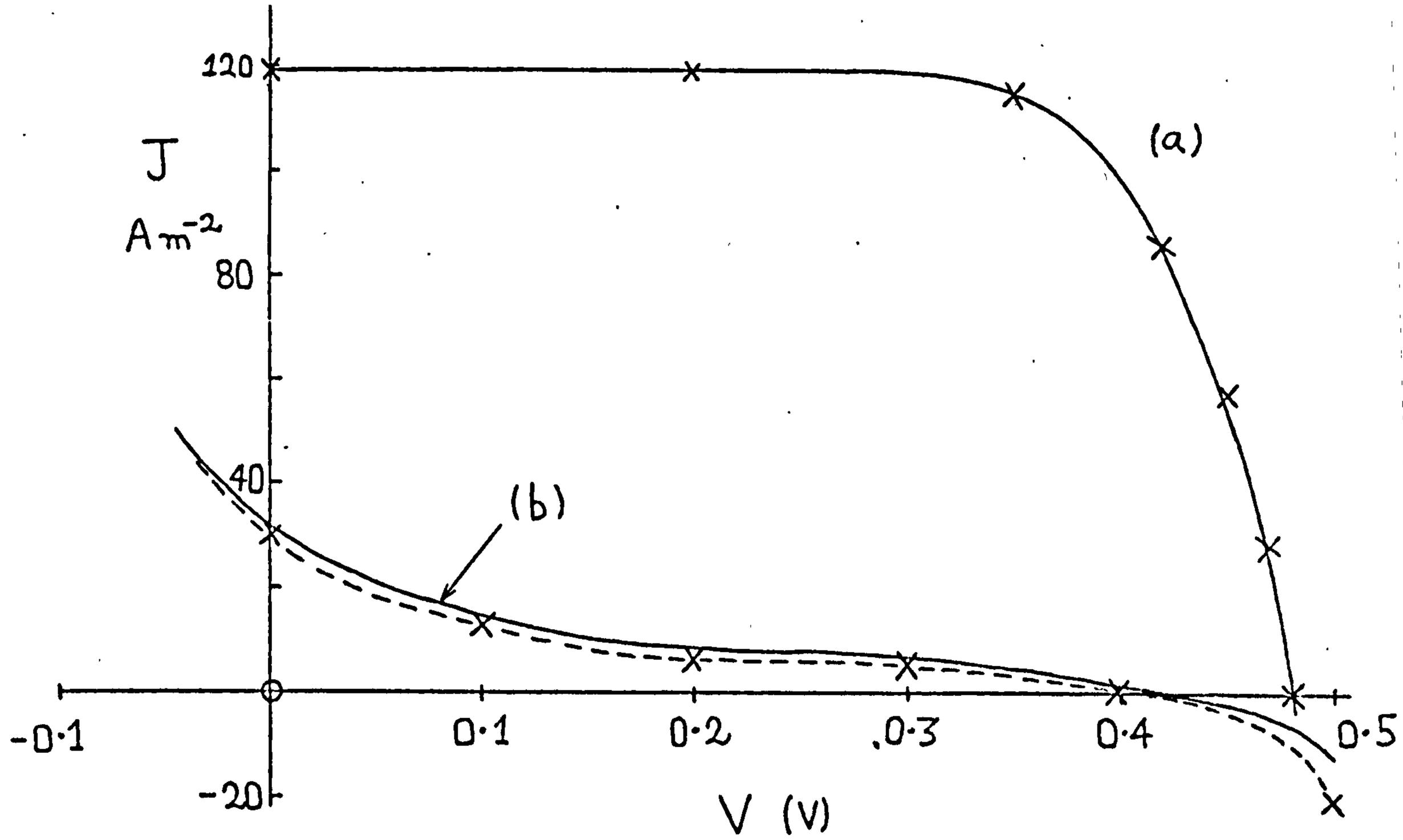

Figure 7.10 The undegraded and degraded current density-voltage characteristics of the p-type S.B.S.C. The parameters of table 4 have been used together with $D_S = 0.6 \times 10^{16} m^{-2} eV^{-1}$ and a series resistance (by the use of an equivalent circuit) of 3.2 Ω for a cell of area 1 cm^2.

(a) Cell before degradation, $\delta = 13\text{Å}$, $\chi_n = \chi_h = 0.5$ eV

(b) Cell after degradation, $\delta = 29\text{Å}$, $\chi_n = 0.7$ eV, $\chi_h = 0.5$ eV.

x - experimental points (Lillington and Townsend 1978).

The description, given earlier, for the case of moderate D_S and large interfacial layer thickness δ applies equaly well to the situation under consideration here. In particular we point out that, due to the large tunneling barrier, the photo-generated electrons tend to accumulate in great numbers within the semi-conductors conduction band, near x = o. Therefore the photo-induced voltage V_{ph} becomes so large that, the electron quasi-Fermi level E_{Fn} rises to such an extent that the semiconductors conduction band, near x = o, becomes degenerate. This encourages considerable recombination in the semiconductors substrate (depletion and bulk layers, process 1), even at the short circuit point (see, curve b of figure 7.10, at V = o).

The next chapter goes on to present the conclusions, and discusses some of the limitations of the present theory together with some ideas for its improvement.

CHAPTER 8

CONCLUSIONS AND FUTURE TOPICS OF INTEREST

8.1 The conclusions

A theory of Schottky barrier solar cells, with a thin insulating interfacial layer sandwiched between the barrier metal and the semiconductors substrate, has been presented. The effects of varying the density of interfacial surface states and the thickness of the interfacial layer have been studied.

For an n-type Schottky barrier solar cell, having a low to moderately valued interfacial surface state density D_S (say of the order 10^{16} m^{-2} eV^{-1}, distributed evenly over the semiconductors energy gap), the conversion efficiency η increases with increasing D_S. But as D_S is further increased (say to some large value) the recombination traffic through the interfacial surface states begins to dominate the J-V characteristics, thereby pulling the efficiency down. Thus, as the conversion efficiency goes through a maximum, we deduce that an optimum value of D_S exists for each interfacial layer thickness δ. Further to this, the value of optimum density of interfacial surface states decreases with increasing δ (see Chapter 2 or Landsberg and Klimpke (1977) and Klimpke and Landsberg (1976)).

The effect of the direct (dashed) as against the diffuse (solid lines) spectra is exhibited in Figures 3.3 - 3.5. The obvious disadvantage of diffuse radiation is its low intensity. However, the diffuse spectrum being more compact enables one to make better use of this radiation. In figures 3.3 - 3.5 we have standardised on one

incident intensity (30m W cm^{-2}), thereby shielding the results from the first disadvantage. This must be borne in mind when studying figures (3.3 - 3.5). For given incident power the power output and conversion efficiency are greater for diffuse rather than direct radiation. Apart from this, one observes that the conversion efficiency depends on cell parameters in much the same way for both incident spectra. [See Chapter 3 or Klimpke and Landsberg 1978a].

The more complete formalism of the n-type Schottky barrier solar cell, presented in chapters 5 and 6, shows that the depletion approximation is never in fact strictly valid. Also, the separation between the quasi-Fermi levels in the illuminated cell is greater than the output voltage. This suggests that recombination within the semiconductor substrate and through the interfacial surface states will be important loss mechanisms. The hole diffusion current density (near the ohmic contact) is shown to be of great importance, especially for thin substrate thicknesses. For the forward biased, unilluminated n-type Schottky barrier solar cell the separation between the quasi-Fermi levels in the substrate tends to be less than the bias voltage. This leads to slightly reduced recombination in the substrate and through the interfacial surface states. Perhaps one of the more interesting results is that, when the cell is being illuminated under short circuit conditions, the interfacial voltage V_i developed across the insulator (as a result of the illumination) is negative, whereas with the device forward biased without illumination V_i always positive (or zero when the bias voltage equals zero).

Turning to the theory of the illuminated p-type Schottky barrier solar cell developed in chapter 7 (see Klimpke and Landsberg 1978 b), we observe that for the density of interfacial surface states D_S lying within the range (10^{15} - 10^{17} m^{-2} e V^{-1}), the conversion efficiency

η decreases with increasing D_S provided that the other cell parameters are held constant. This is in contrast to the behaviour of the n-type cell because, unlike the n-type S.B.S.C., the thermodynamic equilibrium barrier height ϕ_{Bp} of the p-type S.B.S.C. decreases with increasing D_S, thereby increasing the hole concentration at the interface between the semiconductor and the interfacial layer. Again, the voltage V_i, developed across the insulating interfacial layer as a result of the illumination, is negative for low output voltages, thus increasing the potential drop across this layer relative to that of thermodynamic equilibrium conditions. This is contrary to what is usually assumed. V_i eventually becomes positive for the larger operating voltages of the illuminated p-S.B.S.C. The photo-induced voltage V_{ph} (i.e. the amount by which the electron quasi-Fermi level E_{Fn} at the interface, rises above the Fermi level E_{FM} in the metal),is usually assumed to be zero, but in our model of the p-type S.B.S.C. it is always positive when the cell delivers power. This shows, rather clearly, that recombination is a more important constraint of cell efficiencies than has been thought heretofore.

A general remark is that the theory, for both the n and p-type cells, seems to correlate the inter-dependence of the parameters in a way which can be understood by physical reasoning.

8.2 Future topics of interest.

The overall aim of continued research is to produce a comprehensive theory of one-dimensional photovoltaic devices such as Schottky barrier cells. As many experimentalists (e.g. - Townsend and Lillington 1977) have turned their attention to p-type cells, the theory of the n-type Schottky barrier solar cell, as given in chapters 5 and 6 above, should be extended to that of the p-type case, paying particular attention to the

numerical difficulties arising when large substrate thicknesses are considered. In order to make accurate correlations between the theoretical and the experimental curves we must include the effects of,(a) the variation of the mobilities as functions of the electrostatic field and ionized doping concentration (Caughey and Thomas 1967),and (b) degeneracy. Degeneracy effects have, to some extent been examined in Chapter 7, and are seen to become very important when studying the degraded characteristics of p-type S.B.S.C.'s. [The degradation is due to chemical changes occuring after encapsulation, and not to particle irradiation damage to the semiconductor.] The inclusion of degeneracy effects throws up another important question regarding recombination. Following earlier work (Landsberg 1957), we require to know how the reaction constants vary as functions of energy in the semiconductors bands.

Using the theory of chapters 5 and 6, the capacitance of the Schottky barrier, under illumination or in the dark could also be studied theoretically, thereby yielding a more detailed model for the semiconductor and oxide capacitance than those used to date. The influence of the interfacial surface states on the capacitance should also yield to theoretical analysis.

Our work to date has tended to concentrate on substrates made of single crystal materials, but we believe that it could be ammended to cover thin film devices such as those made from a-Si or polycrystalline silicon. From the calculated variation of the quasi-Fermi levels and the semiconductors band edge with position x in the substrate, we would expect to improve our understanding of these solar cells with a view to enhancing their performance.

In principle the same type of calculations may be performed on n-p or p-n homojunction and heterojunction solar cells, having either single crystal or poly-crystalline or amorphous substrates. In the case of the heterojunction solar cell, the influence of the interfacial surface states on both the current density-voltage and capacitance-voltage characteristics may be studied extensively. Tunnel communication of the semiconductors conduction and valence bands, with the interfacial surface states could also be investigated. Also the same basic types of calculations may be performed on photo-chemical diodes (see, for example Nozik 1977, and Williams and Nozik 1978), since these structures utilise semiconductor substrates forming Schottky type contacts and p - n type junctions.

APPENDIX A

The electron supply function

Let the number of electrons per sec per unit area, having energies (electron volts) within the range $(E_x, E_x + dE_x)$, incident on the surface barrier be denoted by $N(T, E_F, E_x)dE_x$. Here E_F is the Fermi energy and E_x is that part of the energy for motion normal to the surface.

The Fowler-Nordheim equation (see, Fowler and Nordheim (1928) or Good and Muller (1956)), is obtained:

$$N(T, E_F, E_x) = \frac{4\pi\, m_e k\, Te}{h^3} \ln \left\{1 + \exp(-\, e(E_x - E_F)/kT)\right\} , \qquad (A.1)$$

$$\text{Here} \quad eE_x = e\varepsilon - (p_y^{\,2} + p_z^{\,2})/2m_e = p_x^{\,2}/2m_e + V(x) \quad , \qquad (A.2)$$

where $V(x)$ is the effective electron potential energy, ε is the total energy, p_x, p_y, p_z are respectively the components of the the electron momentum in the three coordinate directions, and m_e is the electrons effective mass.

The hole supply function

For the sake of clarity of exposition, we will derive the analogous hole supply function. This is the number of holes per sec per unit area, having hole energies within the range $(E_x^{\,h}, E_x^{\,h} + dE_x^{\,h})$, incident on the surface barrier and is denoted by $N^h(T, E_F^h, E_x^{\,h})dE_x^{\,h}$. Here $E_F^{\,h}$ is the Fermi energy measured on the hole energy scale and $E_x^{\,h}$, the part of the energy for motion normal to surface, is given by

$$eE_x^h = e\varepsilon^h - \left(p_y^{h_2} + p_z^{h_2}\right)/\,2m_h = p_x^{h_2}/2m_h + V^h(x) \qquad (A.3)$$

where $V^h(x)$ is the effective hole potential energy, ε^h is the total energy on the hole energy scale, p_x^h, p_y^h, p_z^h are respectively the three components of the hole momentum, and m_h is the hole effective mass.

The number of states, having momenta in $(p_x^h, p_x^h + dp_x^h)$,$(p_y^h, p_y^h + dp_y^h)$. $(p_z^h, p_z^h + dp_z^h)$, per unit volume (real space) is $\frac{2}{h^3}\, d^3\, \underline{p}^h$.

If this density of states function is multiplied by the hole occupation probability (i.e. the probability that a state is not occupied by an electron) then the concentration of holes, with momenta in the range $(p_x^h, p_x^h + dp_x^h)$, $(p_y^h, p_y^h + dp_y^h)$, $(p_z^h, p_z^h + dp_z^h)$, follows. The concentration of holes is now multiplied by the hole x-velocity p_x^h/m_h. Hence the number of holes crossing unit area perpendicular to the x axis per unit time, with momentum p_x^h in the range $(p_x^h, p_x^h + dp_x^h)$, is given by

$$\frac{2}{h^3}\; p_x^h/m_h \; dp_x^h \int_{-\infty}^{\infty}\!\!\int \left(1 + \exp(-e(eE_F^h - \varepsilon^h)/kT\right)^{-1} dp_y^h\, dp_z^h$$

But at some fixed point, x say, $e\, dE_x^h = \frac{p_x^h}{m_h}\, d\, p_x^h$. Hence the flux of holes incident to the barrier, with the x-component of energy lying within the range $(E_x^h, E_x^h + dE_x^h)$, is given by

$$N^h(T, E_F^h, E_x^h)\; dE_x^h = \frac{2}{h^3}\, e\, dE_x^h \int_{-\infty}^{\infty}\!\!\int \frac{dp_y^h\, dp_z^h}{1 + \exp(-e(E_F^h - E_x^h)/kT)\exp\left[\dfrac{p_y^{h_2} + p_z^{h_2}}{2m_h kT}\right]}.$$

A change of variables: $p_y^h = \xi\cos\theta$, $p_z^h = \xi\sin\theta$ with $y = \frac{\xi^2}{2m_h KT}$, gives

$$N^h(T, E_F{}^h, E_x{}^h) = \frac{2}{h^3} \quad 2\pi\, m_h\, kTe \int_0^\infty \frac{dy}{1 + \exp(-e(E_F{}^h - E_x{}^h)/kT)\exp y}$$

$$\text{So} \quad N^h(T, E_F{}^h, E_x{}^h) = \frac{4\pi\, m_h\, kTe}{h^3} \quad \ln\left\{1 + \exp(-e(E_x{}^h - E_F{}^h)/kT\right\}, \qquad (A.4)$$

where both $E_x{}^h$ and $E_F{}^h$ are measured on the hole energy scale (see Chapter 4), and T is of course, the absolute temperature. The above results hold true irrespective of degeneracy conditions.

The thermionic emission tunnel current density between the barrier metal and the semiconductors' conduction band.

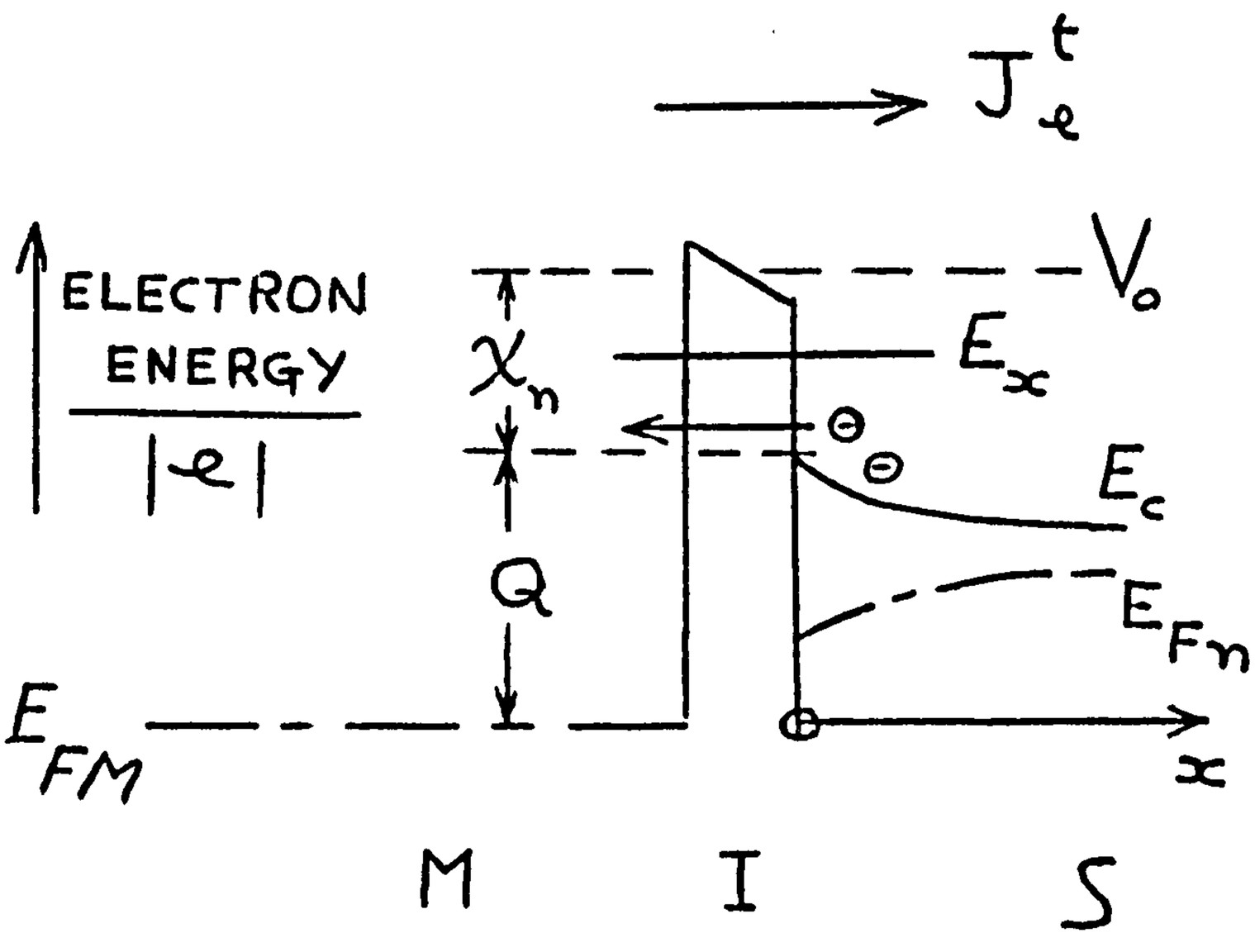

Figure A.1 Band diagram illustrating the communication between the barrier metal and the semiconductors' conduction band.

Following Penley (1962), the current density J_{sm}^e due to electrons entering the metal from the semiconductors' conduction band, and the current density J_{ms}^e due to electrons entering the semiconductors' conduction band from the metal are given by

$$J^{e}_{sm} = e \int_{Q + E_{FM}}^{\infty} T(E_x)\, N(T, E_{Fn}(0), E_x)\, dE_x \quad , \qquad (A.5)$$

and $$J^{e}_{ms} = e \int_{Q + E_{FM}}^{\infty} T(E_x)\, N(T, E_{FM}, E_x)\, dE_x \quad , \qquad (A.6)$$

where $T(E_x)$ is the tunnel transmission coefficient for an electron tunneling through the insulator (see fig. A1). Now by the W.K.B. approximation, and by assuming a rectangular barrier of height V_o and thickness δ, the tunnel transmission coefficient is given by

$$T(E_x) = \exp \left\{ - 2\delta \frac{(2m)^{\frac{1}{2}}}{\hbar} (V_o - eE_x)^{\frac{1}{2}} \right\} \quad .$$

Further to this, if we also assume that the tunneling barrier is the same for all electrons at energies above $E_x = Q + E_{FM}$ (electron volts), we make the usual approximation (see for example, Card and Rhoderick 1971).

$$T(E_x) \approx \exp \left(- \bar{\delta}\, \chi_n^{\frac{1}{2}} \right) , \qquad (A.7)$$

where χ_n represents the effective energy difference, measured in units of electron volts, between the conduction band edge of the insulator and that of the semiconductor (see figure A.1). Also $\bar{\delta}$ is the thickness of the insulating layer measured in angstroms.

The total thermionic emission tunnel current between the barrier metal and the semiconductors conduction band is given by

$$J_e^t = J_{sm}^e - J_{ms}^e = e\int_{Q+E_{FM}}^{\infty} \exp(-\bar{\delta}\,\chi_n^{\frac{1}{2}})\,\frac{4\pi\, m_e\, kTe}{h^3}\left\{\ln\left(1+e^{-e(E_x-E_{Fn}(0))/kT}\right)\right.$$

$$\left. - \ln\left(1+e^{-e(E_x-E_{FM})/kT}\right)\right\} dE_x \,. \qquad (A.7)$$

In this result we have assumed the same electron effective mass in both the metal and the semiconductors conduction band.

Result (A.7) holds for degenerate situations. If we now make the assumption that $E_x >> E_{FM}, E_{Fn}(0)$ (i.e. non-degeneracy) thenequation (A.7) is easily reduced to

$$J_e^t = \frac{4\pi\, m_e\, kT\, e^2}{h^3}\exp(-\bar{\delta}\,\chi_n^{\frac{1}{2}})\int_{Q+E_{FM}}^{\infty}\left(e^{-e(E_x-E_{Fn}(0))/kT} - e^{-e(E_x-E_{FM})/kT}\right)dE_x$$

$$= A_e^* T^2 \exp(-\bar{\delta}\,\chi_n^{\frac{1}{2}})\exp(-eQ/kT)\left\{\exp(-e(E_{FM}-E_{Fn}(0))/kT) - 1\right\} \qquad (A.8)$$

where $A_e^* = 4\pi\, m_e\, k^2 e/h^3$ is the effective Richardsons constant for thermionically emitting electrons and Q is as given in figure A.1.

There are three special applications for equation (A.8), we will deal with each of them in turn.

(1) The thermionic emission current densities J_{sm}^e and J_{ms}^e, for the case of negligible tunneling attenuation, are required in chapter 2. In chapter 2, the quasi-Fermi levels have been assumed to have negligible slope and therefore $E_{Fn}(0) - E_{FM} = V$ and $Q = \phi_B + V_i$ (see chapter 2). Thus J_{sm}^e and J_{ms}^e, in this case, are given by

$$J_{sm}^e = A_e^* T^2 \exp(-e(\phi_B + V_i)/kT)\exp(eV/kT), \qquad (A.9)$$

and $$J_{ms}^{e} = A_e^{*} T^2 \exp(-e(\phi_B + V_i)/kT) \quad . \qquad (A.10)$$

(2) The electron thermionic emission tunnel current density, as used in chapter 6 for the n-type Schottky barrier solar cell, is given by equation (A.8) to be

$$J_e{}^{t} = A_e^{*} T^2 \exp(-\bar{\delta}\, \chi_n^{\frac{1}{2}}) \exp(-e(\phi_B + V_i)/kT)\left\{\exp(-e(E_{FM} - E_{Fn}(O))/kT)-1\right\} \qquad (A.11)$$

where Q in figure A.1 is given by $Q = \phi_B + V_i$ (see Chapter 6).

(3) The electron thermionic emission tunnel current density for the p-type S.B.S.C. (chapter 7) is determined from equation A.8, by writing Q in figure A.1 as $Q = E_g - \phi_{Bp} - V_i$, and $E_{Fn}(O) - E_{FM} = V_{ph}$ (see chapter 7). Hence the electron thermionic emission tunnel current density may be written as

$$J_e{}^{t} = A_e^{*} T^2 \exp(-\bar{\delta}\, \chi_n^{\frac{1}{2}}) \exp\,(-e(E_g - \phi_{Bp} - V_i)/kT)\left\{\exp(eV_{ph}/kT)-1\right\}. \qquad (A.12)$$

This result agrees with that of Buxo et al (1976).

The degenerate form of the electron thermionic emission tunnel current density, required in the analysis of the degraded p-type S.B.S.C. in chapter 7 (see equation (7.4.13)), is found by using equation (A.7) together with $Q = E_g - \phi_{Bp} - V_i$ and $E_{Fn}(O) - E_{FM} = V_{ph}$. Therefore we write, for degenerate conditions

$$J_e{}^{t} = \frac{4\pi\, m_e\, kT\, e^2}{h^3} \exp(-\bar{\delta}\, \chi_n^{\frac{1}{2}}) \int_{E_g - \phi_{Bp} - V_i + E_{FM}}^{\infty} \left\{\ln(1 + e^{-e(E_x - E_{Fn}(O))/kT}) - \ln\,(1 + e^{-e(E_x - E_{FM})/kT})\right\} dE_x \quad .$$

Thus, by a change of variables to $y = \frac{e}{kT}(E_x - E_{FM})$, and by setting $A_e^* = 4\pi m_e k^2 e/h^3$ we deduce that

$$J_e^t = A_e^* T^2 \exp(-\bar{\delta}\chi_n^{\frac{1}{2}}) \int_{e(E_g - \phi_{Bp} - V_i)/kT}^{\infty} \ln\left\{\frac{1 + e^{(-y + eV_{ph}/kT)}}{1 + e^{-y}}\right\} dy. \quad (A.13)$$

The hole thermionic emission tunnel current density between the barrier metal and the semiconductor's valence band.

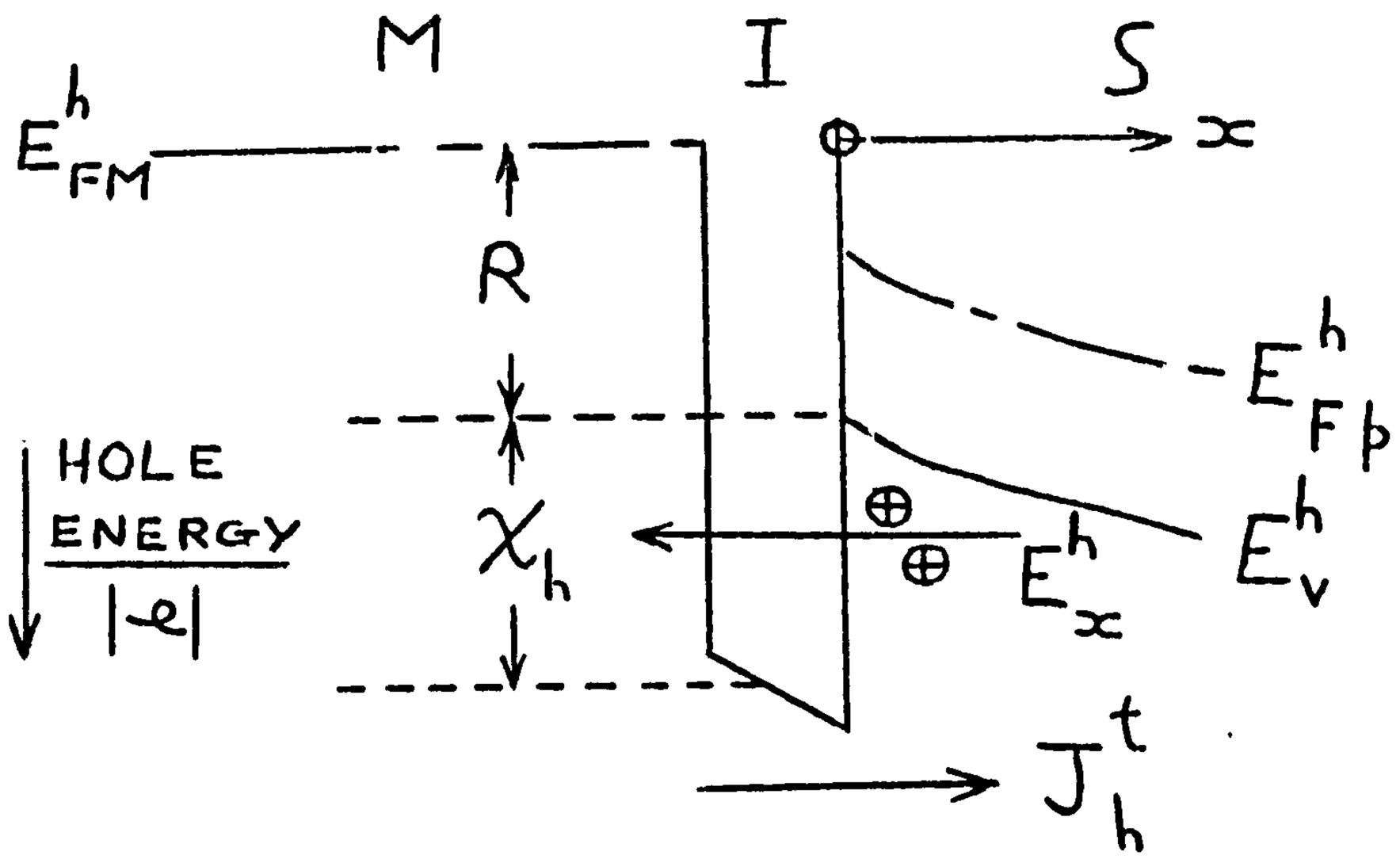

Figure A.2 Band diagram illustrating the communication between the barrier metal and the semiconductor's valence band.

Figure A.2 shows the situation for hole thermionic emission analogous to that of the electron thermionic emission. By making similar assumptions for the transmission coefficient $T(E_x^h)$, we write the total hole thermionic emission tunnel current density, between the barrier metal and the semiconductor's valence band, as

$$J_h^t = \frac{4\pi\, m_h\, kT\, e^2}{h^3}\; e^{-\bar{\delta}\,\chi_h^{\frac{1}{2}}} \int_{E_{FM}^h + R}^{\infty} \left\{ \ln\left(1 + e^{-e(E_x^h - E_{FM}^h)/kT}\right) - \ln\left(1 + e^{-e(E_x^h - E_{Fp}^h(0))/kT}\right) \right\} d\,E_x^h \,, \qquad (A.14)$$

where we have used the hole supply function given in equation (A.4). Also, χ_h is the effective energy difference, measured in units of electron volts, between the valence band edge of the insulator and that of the semiconductor (see figure A.2). Application of non-degenerate conditions (i.e. $E_x^h >> E_{FM}^h, E_{Fp}^h(0)$) yields the following result,

$$J_h^t = \frac{4\pi\, m_h\, e(kT)^2}{h^3}\; \exp(-\bar{\delta}\,\chi_h^{\frac{1}{2}})\, \exp(-e\,R/kT)\left\{1 - \exp(e(E_{Fp}^h(0) - E_{FM})/kT)\right\}. \qquad (A.15)$$

Here $E_{Fp}^h(0)$ and E_{FM}^h are measured on the hole energy scale, and R is as given in figure A.2. In fact, $E_{Fp}^h(0) - E_{FM}^h = E_{FM} - E_{Fp}(0)$, where E_{FM} and $E_{Fp}(0)$ are measured on the electronic energy scale (in units of electron volts).

There are two special cases of equation (A.15), we will examine each of these in turn.

(a) The hole thermionic emission tunnel current density for the n-type Schottky barrier solar cell is obtained by using (A.15) in conjunction with $R = E_g - \phi_B - V_i$ (see Chapter 6), and is given by

$$J_h^t = A_h^* T^2 \exp(-\bar{\delta}\,\chi_h^{\frac{1}{2}})\, \exp(-e(E_g - \phi_B - V_i)/kT)\left\{1 - \exp(e(E_{FM} - E_{Fp}(0))/kT)\right\}, \qquad (A.16)$$

where $A_h^* = 4\pi\, m_h\, ek^2/h^3$ is the effective Richardson's constant for

thermionically emitting holes. This result is used in chapter 6.

(b) The hole thermionic emission tunnel current density, for the p-type Schottky barrier solar cell, is obtained by using equation (A.15) in conjunction with $R = \phi_{Bp} + V_i$ and $E_{FM} - E_{Fp}(0) = V$ (see chapter 7), and is therefore given by

$$J_h^t = A_h^* T^2 \exp(-\bar{\delta} \chi_h^{\frac{1}{2}}) \exp(- e(\phi_{Bp} + V_i)/kT) \{1 - \exp(eV/kT)\} . \quad (A.17)$$

A similar result for the hole thermionic emission tunnel current has been given by Buxo et al (1976).

References

Anderson, W.A., Milano, R.A., Delahoy, A.E., and Vernon, S., 1974 Extended abstracts, Electrochemical Soc., Fall meeting. New York, 621.

Barret, C. and Vapaille, A. 1975 Solid State el. 19, 73.

Bonch-Bruevich, V.L. 1965 Sov. Phys. Solid State 6, 1615.

Bonch-Bruevich, V.L. and Landsberg, E.G. 1968 Phys. Stat. Sol 29,9.

Buxo, J., Esteve, D. and Sarrabayrouse, G. 1976 Phys. Stat. Sol. (a) 37, K105.

Card, H.C. and Rhoderick, E.H. 1971 J. Phys. D. 4 1589.

Card, H.C. and Rhoderick, E.H. 1972 Solid State el. 15, 993.

Caughey, D.M. and Thomas, R.E. 1967 Proc. I.E.E.E. 55, 2192.

Cowley, A. and Sze, S. 1965 J. Appl. Phys. 36, 3212.

Delahoy, A.E., Anderson, W.A. and Kim, J.K. 1977. In Proc. E.E.C., Photovoltaic Solar Energy Conference, held at Luxembourg, p. 308, Boston:Reidel.

Evans, D.A. and Landsberg, P.T. 1963 Solid State el. 6. 169.

Fonash, S.J. 1975a J. Appl. Phys. 46, 1286.

Fonash, S.J. 1975b In 11th I.E.E.E. Photovoltaic Specialist Conference, p.376. New York:I.E.E.E.

Fowler, R.H. and Nordheim, L. 1928 Proc. Roy. Soc. Lond. A.119, 173.

Freeman, L.B. and Dahlke, W.E. 1970 Solid State el. 13, 1483.

Good, R.H. and Muller, E.W. 1956 In Handbuch der Physik (edited by S. Flugge). Vol.21, p.176, Springer, Berlin.

Hill, D.J. 1976 J. Phys. C.9, 3527.

Hill, D.J. and Landsberg, P.T. 1976 Proc. R. Soc. Land. A.347, 547.

Hovel, H.J. 1975 Semiconductors and semimetals, Vol.11. New York: Academic Press.

Kane, E.O. 1969 In Tunneling Phenomena in Solids, edited by E. Burstein and S. Lundqvist (Plenum, New York) Chapt. 1, p.5.

Klimpke, C.M. and Landsberg, P.T. 1976 In 12th I.E.E.E. Photovoltaic Specialist Conference, p.868. New York:I.E.E.E.

Klimpke, C.M. and Landsberg, P.T. 1978a Solid State el. devices 2, S20, special issue.

Klimpke, C.M. and Landsberg, P.T. 1978b Solid State el. (To be published).

Landsberg, P.T. 1957 Proc. Phys. Soc. 70, 282.

Landsberg, P.T. 1967 In Festkörperprobleme VI (ed. O. Madelung). Braunschweig:Vieweg.

Landsberg, P.T. 1969 Solid State Theory, New York: Wiley.

Landsberg, P.T. and Klimpke, C.M. 1977 Proc. R. Soc. Lond. A.354, 101.

Lane, C.H. 1968 I.E.E.E. Trans. el. devices 15, 998.

Lavagna, M., Pique, J.P. and Marfaing, Y. 1977 Solid State el.20, 235.

Lillington, D.R. and Townsend, W.G. 1976 Appl. Phys. Lett. 28, 97.

Lillington, D.R. and Townsend, W.G. 1978 Private communication.

Lundstrom, I. and Svensson, C. 1972 J. Appl. Phys. 43, 5045.

Mallinson, J.R. and Landsberg, P.T. 1977 Proc. R. Soc. Lond. A.355, 115.

Mead, C.A. 1966 Solid State el. 9, 1023.

Merzbacher, E. 1961 Quantum Mechanics. New York:Wiley, Chapt.11, p.209.

McKelvey, J.P. 1966 Solid State and Semiconductor Physics. New York: Harper and Row.

McOuat, R.F. and Pulfrey, D.L. 1975 In 11th I.E.E.E. Photovoltaic Specialist Conference, p.371. New York:I.E.E.E.

Nozik, A.J. 1977 Appl. Phys. Lett. 30, 567.

Penley, J.C. 1962 Phys. Rev. 128, 596.

Pulfrey, D.L. and McOuat, R.F. 1974 Appl. Phys. Lett. 24, 167.

Riviere, C.R. 1957 Proc. Phys. Soc. B 70, 676.

Roger, J.A., Pivot, J. and Dupuy, C.H.S. 1976 In Colloque international 'Electricite Solaire,' 1976 (Toulouse:C.E.N.E.S. 1976).

Shockley, W.and Read, W.T. 1952 Phys. Rev. 87, 835.

Simmons, J.G. 1963 J. Appl. Phys. 34,2581.

Sreedhar, A.K., Sharma, B.L. and Purohit, R.K. 1969 I.E.E.E. Trans. el. devices 16, 309.

Stirn, R.J. and Yeh, Y.C.M. 1973 In 10th I.E.E.E. Photovoltaic Specialist Conference, p.15. New York:I.E.E.E.

Sze, S.M. 1969 Physics of semiconductor devices. New York:Wiley.

Townsend, W.G. and Lillington, D.R. 1977 In Proc. E.E.C. Photovoltaic Solar Energy Conference, held at Luxembourg, p.207, Boston:Reidel.

Varshni, Y.P. 1967 Phys. Stat. Sol. 19,459, Table 2.

Williams, F. and Nozik, A.J. 1978 Nature 271, 137.